University of Tennessee, Knoxville

TRACE: Tennessee Research and Creative Exchange

Doctoral Dissertations

Graduate School

5-2017

Ion Separations: Achieving Selectivity Through Rational Design in Solvent Extraction and Crystallization Systems

Neil Justin Williams
University of Tennessee, Knoxville, nwilli47@vols.utk.edu

Follow this and additional works at: https://trace.tennessee.edu/utk_graddiss

Part of the Inorganic Chemistry Commons, Organic Chemistry Commons, and the Radiochemistry Commons

Recommended Citation

Williams, Neil Justin, "Ion Separations: Achieving Selectivity Through Rational Design in Solvent Extraction and Crystallization Systems. " PhD diss., University of Tennessee, 2017.
https://trace.tennessee.edu/utk_graddiss/4509

This Dissertation is brought to you for free and open access by the Graduate School at TRACE: Tennessee Research and Creative Exchange. It has been accepted for inclusion in Doctoral Dissertations by an authorized administrator of TRACE: Tennessee Research and Creative Exchange. For more information, please contact trace@utk.edu.

To the Graduate Council:

I am submitting herewith a dissertation written by Neil Justin Williams entitled "Ion Separations: Achieving Selectivity Through Rational Design in Solvent Extraction and Crystallization Systems." I have examined the final electronic copy of this dissertation for form and content and recommend that it be accepted in partial fulfillment of the requirements for the degree of Doctor of Philosophy, with a major in Chemistry.

Sheng Dai, Major Professor

We have read this dissertation and recommend its acceptance:

Craig Barnes, Bin Zhao, Hong Guo

Accepted for the Council:

Dixie L. Thompson

Vice Provost and Dean of the Graduate School

(Original signatures are on file with official student records.)

Ion Separations: Achieving Selectivity Through Rational Design in Solvent Extraction and Crystallization Systems

A Dissertation Presented for the
Doctor of Philosophy
Degree
The University of Tennessee, Knoxville

Neil Justin Williams
May 2017

Copyright © 2017 by Neil Justin Williams
All rights reserved.

DEDICATION

This work is dedicated to my mother Twoey, father Kent, sister Jenny, brother Alexander and the rest of my extended family. Without your constant support and encouragement, I would never have reached this point.

One additional person I must give credit to as an inspiration and would therefore like to also dedicate this work to is Walt Disney, who once said; “Around here, however, we don’t look backwards for very long. We keep moving forward opening new doors, and doing new things, because we’re curious and curiosity keeps leading us down new paths” this quote can not only explain why I do sciences but can be an anthem in life.

ACKNOWLEDGEMENTS

During my whole time as a student in college and later the various graduate schools I have attended I learned that the most important thing you can have is a good support system consisting of family and friends. The best friend you can have is one how is honest and unafraid to tell you the truth even when the truth is the last thing you want to hear. Therefore, I would like to acknowledge my close friends Ronald Burton Jr., Janos Nadas, Charles Seipp, Benjamin Roach without your advice of matters of science in addition to other things, I might still be lost in the woods.

I would like to kindly offer my thanks to my advisors Dr. Sheng Dai who has allowed me the freedom to pursue my own ideas and Dr. Bruce Moyer who has taught me more about the sciences and the importance of good grammar than can be truly be expressed.

My sincere thanks to Dr. Radu Custelcean, Dr. Ross Ellis, Dr. Richard Mayes, Dr. Carter Abney, Dr. Lætitia Delmau, and Frederick Sloop for their immense help, instruction, meaningful discussion, and collaboration on multiple projects as well as the camaraderie.

I would also like to thank my first scientific advisors Dr. Robert Hancock. His love of science and discovery was so infectious that after doing research as an undergraduate, I decided to continue for my Masters with him. Without his help and guidance, I would never have arrived at Oak Ridge National Laboratory and most likely this work would never have come about.

Additionally, I would like to the Department of Energy, Office of Science, Basic Energy Sciences Program for funding this research and work.

ABSTRACT

The selective separation of ions from aqueous solutions has been a difficult challenge to address in the separation sciences. The difficulties associated with selective separations of ions are due to a multitude of chemical and physical differences between them. Additionally, the term ions encompass both positively charged cations and their counter parts the negatively charge anions. The work covered in this dissertation discusses the difficulties encountered during the selective separation of both oxoanions and cations. Apart from the Introduction **Chapter 1** and Conclusion **Chapter 10**, the selective separations oxoanions and cations will be discussed separately with the dissertation being divided into two sets of chapters. While the overarching theme of this dissertation is the selective separations of ions, the means and methods utilized to achieve these separations are divergent, to the point that it is necessary to divide them into individual sets of chapters in order to reduce the chance of confusion. The selective separation of oxoanions will be covered from **Chapter 2-6**, while the selective separation of cations particularly the *f*-block elements the actinides and lanthanides is discussed in **Chapter 7-9**. In this work, much focus is given to the use of the techniques of solvent extraction and crystallization which are used as a means of achieving a selective separation of either anions or cations.

TABLE OF CONTENTS

Chapter 1 : Introduction 1

1.1 Ions 1

1.2 Anion Receptors 3

1.3 Cation Receptors 12

1.4 References 19

1.5 Appendix 1A Figures and Tables for Chapter 1 28

Chapter 2 : $\alpha, \alpha', \alpha'', \alpha'''$-*meso*-Tetrahexyltetramethyl-calix[4]pyrrole: An easy-to-prepare, isomerically pure anion extractant with enhanced solubility in organic solvents 46

Publication Statement for Chapter 2 47

Abstract 49

2.1 Introduction 50

2.2 Results and Discussion 53

2.2.1 NMR Titrations 55

2.2.2 Extraction Results 56

2.2.3 Crystal Structures 60

2.2.4 Computational Studies 60

2.3 Conclusion 66

2.4 Experimental 67

2.4.1 General Methods 67

2.4.2 Materials 67

2.4.3 Preparations of Calix[4]pyrroles 68

2.4.4 Distribution Experiments 69

2.4.5 ^{1}H-NMR titrations 70

2.4.6 Solubility of 1 and 2 in organic solvents 71

2.4.7 Crystal Structures of 2, Free ligand, and $TMA^{+}Cl^{-}$ Complex 71

2.4.8 Computational Details 72

2.5 References 74

2.6 Appendix 2A Supplemental Information for Chapter 2 80

2.6.1 Determination of Binding Constants via Solvent Extraction 80

2.6.2 Determination of Binding Constants by ^{1}H–NMR 81

2.6.3 Data for Greasy C[4]P 83

2.6.4 Representative NMRs for greasy C[4]P showing effect of increasing amounts of chloride 84

2.6.5 Data for C[4]P 85

2.6.6 Representative NMRs for C[4]P showing effect of increasing amounts of chloride 86

2.7 Appendix 2B Figures and Tables for Chapter 2 87

Chapter 3 : Selective Separation of Sulfate Via Implementation of a New Highly Soluble Diiminoguanidinium in Solvent Extraction Systems 100

Abstract 101

3.1 Introduction 101

3.2 Experimental 105

3.2.1 Synthesis of the Diiminoguanidinium Receptor 105

3.2.2 Synthesis of 3,7-dimethyl-1-iodooctane 106

3.2.3 Synthesis of 3,4-bis((3,7-dimethyloctyl)oxy)benzaldehyde 107

3.2.4 Synthesis of TABEDIG Cl..... 109

3.2.5 Liquid-liquid Extraction Studies of Sulfate Removal Using TABEDIG.. 109

3.2.6 Karl Fischer Titrations of Pre- and Post Contacting Isopar L Solutions 111

3.3 Results and Discussion 112

3.3.1 Removal of Sulfate Using TABEDIG 112

3.4 Conclusion 116

3.5 References 117

3.6 Appendix 3A Supplemental Information for Chapter 3 119

3.6.1 Attempts at Guanylation Reactions in Mixed Urea-Guanidinium Anion Receptors 119

3.7 Appendix References 122

3.8 Appendix 3B Figures and Tables for Chapter 3 123

Chapter 4 : Aqueous Sulfate Separation by Crystallization of Sulfate-Water Clusters 135

Publication Statement for Chapter 4 136

Abstract..... 142

4.1 Introduction 143

4.2 References 151

4.3 Appendix 4A Supplemental Information for Chapter 4 154

4.3.1 Supporting Information 154

4.3.2 Synthesis and Crystallization of Glyoxal bis(amidinohydrazone) Sulfate (A), Nitrate (C), and Perchlorate (D) 154
4.3.3 Single-Crystal X-Ray Structural Determination 156
4.3.4 Solubility Measurements of the GBAH Salts A-D 157
4.3.5 Solubility Measurements of the Guanidinium and Aminoguanidinium Salts 159
4.3.6 Competitive Crystallizations 159
4.4 Appendix References 163
4.5 Appendix 4B Figures and Tables for Chapter 4 164
Chapter 5 : Aqueous Sulfate Separation by Sequestration of $[(SO_4)_2(H_2O)_4]^{4-}$ Clusters within Highly Insoluble Imine-Linked Bis-Guanidinium Crystals 187
Publication Statement for Chapter 5 188
Abstract 194
5.1 Introduction 195
5.2 Results and Discussion 197
5.3 Conclusion 201
5.4 Experimental 202
5.4.1 Synthesis and crystallization of 1,4-benzene-bis(iminoguandinium) sulfate (BBIG-SO_4) and nitrate (BBIG-NO_3) 203
5.4.2 Solubility measurements of BBIG-Cl, BBIG-SO_4, and BBIG-NO_3 204
5.4.3 Variable-temperature solubility measurements of BBIG-SO_4 206

5.4.4 Competitive crystallization of BBIG-SO_4 from an aqueous mixture of sulfate, nitrate, and chloride 206
5.4.5 Recovery of the BBIG ligand 207
5.4.6 Sulfate separation from seawater 208
5.4.7 Analysis of sulfate concentration by β liquid scintillation counting 208
5.4.8 Single-crystal X-ray structural determination 209
5.5 References 211
5.6 Appendix 5A Supplemental Information for Chapter 5 214
5.6.1 Electronic-Structure Calculations 214
5.7 Appendix References 215
5.8 Appendix 5B Figures and Tables for Chapter 5 217
Chapter 6 : CO_2 Capture from Ambient Air by Crystallization with a Guanidinie Sorbent 240
Publication Statement for Chapter 6 241
Abstract 247
6.1 Introduction 248
6.2 References 257
6.3 Appendix 6A Supplemental Information for Chapter 6 259
6.4 Appendix 6B Figures and Tables for Chapter 6 264
Chapter 7 : Extraction of lanthanides using 1-hydroxy-6-N-octylcarboxamido-2(1H)-pyridinone as an extractant via competitive ligand complexatios between aqueous and organic phases 274

Publication Statement for Chapter 7 275

Abstract 277

7.1 Introduction 278

7.2 References 282

7.3 Appendix 7A Supplemental Information for Chapter 7 286

7.3.1 Experimental Details 286

7.4 Appendix References 291

7.5 Appendix 7B Figures and Tables for Chapter 7 292

Chapter 8 : Selective Separation of Americium from Europium Using 2,9-Bis(triazine)-1,10-phenanthrolines in Ionic Liquids: A New Twist on an Old Story 298

Publication Statement for Chapter 8 299

Abstract 301

8.1 Introduction 302

8.2 Conclusions 309

8.3 References 310

8.4 Appendix 8A Supplemental Information for Chapter 8 313

8.4.1 Materials and Synthetic Methods 313

8.4.2 Determination of distribution ratios 314

8.4.3 Slope Analysis 316

8.4.4 Quantification of Extracted Nitrate 317

8.4.5 Computational Methods 317

8.4.6 X-ray Absorption Fine Structure Spectroscopy 318

8.4.7 Principal Component Analysis 321
8.5 Appendix References 322
8.6 Appendix 8B Figures and Tables for Chapter 8 325
Chapter 9 : Selective separation of trivalent f-ions using 1,10-phenanthroline-2,9-dicarboxamide ligands in ionic liquids 343
Publication Statement for Chapter 9 344
Abstract 346
9.1 Introduction 347
9.2 Conclusion 353
9.3 References 355
9.4 Appendix Supplemental Information for Chapter 9 359
9.4.1 Materials and synthetic methods 359
9.4.2 Determination of distribution ratios 366
9.4.3 Computational approach 368
9.5 Appendix References 370
9.6 Appendix 9B Figures and Tables for Chapter 9 371
Chapter 10 : Conclusion 402
Vita 406

LIST OF TABLES

Table 1.1. Anion radii, valence charge, and hydration energies 28

Table 1.2. Dielectric constants and Hildebrand Constants for various solvents arranged in order of decreasing ε 31

Table 2.1. Solubilities of **1** and **2** in various neat solvents 88

Table 2.2. Determined equilibrium constants 91

Table 2.3. Complexation energies for reactions (7) and (8) obtained at the M06-2X/6-31+G(d) and B3LYP-D3/6-31+G(d) levels of theory (kcal/mol). Solvent corrections (ΔG_{solv}) are included using the SMD model for chloroform 99

Table 3.1. List of distribution values (*D*values) obtained with TABEDIG in various solvents during the sulfate extraction experiments 128

Table 4.1. Aqueous solubilities of A to D at 25 °C. [a] Measured by UV spectroscopy. [b] Determined gravimetrically 167

Table 4.2. Competitive crystallization experiments 168

Table 4.3. Solubilities of GBAH salts at 25 °C, determined via UV spectroscopy. Absorbance and dilution factors are also given for each compound. The reported solubility for each salt is the average of three different measurements, with the standard deviation representing the uncertainty 174

Table 4.4. Aqueous solubilities of the guanidinium salts determined gravimetrically ... 175

Table 4.5 Aqueous solubilities of the aminoguanidinium salts determined gravimetrically 176

Table 5.1. Aqueous solubilities of different BBIG salts at 25 °C 220

Table 5.2. Sulfate separation from seawater 224

Table 5.3. Aqueous solubilities of BBIG-SO_4 in the 15-35 °C temperature range 229

Table 5.4. Bader charge analysis for the BBIG-SO4 crystal. Charges on atoms are tabulated and shown for the asymmetric unit 233

Table 5.5. Bader charge analysis for the BBIG-NO3 crystal. Charges on atoms are tabulated and shown for the asymmetric unit. 236

Table 5.6. Bader charge analysis for the BBIG·$2H_2O$ crystal. Charge on atoms are tabulated and shown for the asymmetric unit 239

Table 7.1. Comparison of distribution ratios for octyl-HOPO and DEHPA utilizing TALSPEAK conditions 295

Table 8.1. Extraction value (*D*), separation factor (*SF*), and percent recovery of Am and Eu by 4 mM Me-BTPhen for various nitric acid concentrations 326

Table 8.2. Data for EXAFS fit with $[Eu(Me\text{-}BTPhen)_2(H_2O)]^{2+}$ structure model 329

Table 8.3. Eu/Am-Ligand bond distances in Å for geometrically optimized molecules as determined by DFT Calculations 334

Table 9.1. Distribution ratios (D) between IL and aqueous phases and separation factors (SFAm/Eu) for Am(III) and Eu(III) ions in 1 M nitric acid solutions. The extraction concentration in $[C_n mim][NTf_2]$ was 4 mM (1:1 v/v extraction) 373

Table 9.2. Distribution ratios (D_{Am} and D_{Eu}) and separation factors ($SF_{Am/Eu}$) for Am(III) and Eu(III) ions in nitric acid solutions. The extractant (L) concentration in $[C_n mim][NTF_2]$ was 4 mM (1:1 v/v/ extraction) 378

Table 9.3. Distribution ratios D_{Ln} for Ln(III) ions for extraction from aqueous solution (pH 3.25) using 4 mM 1 in different imidazolium ILs (n is the carbon number for the alkyl arm of the IL cation) and *n*-dodecane 379

Table 9.4. Distribution ratios D_{Ln} for Ln(III) ions for extraction from aqueous solution (pH 3.25) using 4 mM 3 in different imidazolium ILs (n is the carbon number for the alkyl arm of the IL cation) 380

LIST OF FIGURES

Figure 1.1. Typical geometries of Anions. (1) Spherical (Halide), (2) Trigonal Planar (Carbonate, Nitrate, etc…), (3) Tetrahedral (Sulfate, Phosphate, etc.) 29

Figure 1.2. Delocalization of charge across oxoanions. Electrostatic potential and Mulliken partial charge for sulfate (Reproduced with permission from Journal) [12] is shown on the left and a contour map of the electrostatic potential for a nitrate[13] is shown on the right 30

Figure 1.3. Structure of one of the first anion receptors reported by Simmons and Park in the 1960s. On the left is the receptor deprotonated and therefore will not interact favorable with anions, while the structure of the right can interact with anions because it has become protonated in acidity media 32

Figure 1.4. Series of anion receptors with hydrogen bonding donors 33

Figure 1.5. Conformations of C4P the unbound 1,3-alt conformation (left) and bound cone conformation (right). The hydrogens have been removed from the eight methyl groups in the C4P to make it easier to see the core of the structure 34

Figure 1.6. Structure of a unbound strapped C4P and crystal structure of a strapped C4P bound to sulfate 35

Figure 1.7. On the right: Crystal structure of urea bound along the edge of a nitrate by coordinating to two of the oxygens of nitrate. On the left: Crystal Structure of C4P bound to a single oxygen of a sulfate is an example of axial binding 36

Figure 1.8. Multi-urea/thiourea receptors 37

Figure 1.9. Top: Crystal structure of a hexaurea tripodal based anion receptor bound to sulfate, not shown are two quaternary ammoniums present in the crystal structure to offset the -2 charge of the sulfate. Bottom: Chemdraw representation showing how the six ureas are bound to the sulfate and their arrangement around the sulfate (red NH's of urea are bound along the axial region, while blue NHs are bound equatorial region of the sulfate) 38

Figure 1.10. Examples of polyguanidiniums synthesized by Lehn and co-workers[38] in the late 1970s. The anion counter balancing the guanidiniums have not been shown in the figure above 39

Figure 1.11. Conformations of a substituted –NH guaindiums 40

Figure 1.12. Structures of Preorganized guanidinium receptors 41

Figure 1.13. Pathways for the production of ^{241}Am, ^{243}Am, and ^{242}Cm. Not listed in the figure are the half-life of the isotopes for the beta decays ($\boldsymbol{\beta}^{-}$), the neutron and gamma absorption $(\boldsymbol{n}, \boldsymbol{\gamma})$ by the isotopes occur instantaneously 42

Figure 1.14. TALSPEAK chemical components 43

Figure 1.15. Donor Groups for minor actinides 44

Figure 1.16. Series of ligands used to demonstrate the how increasing levels of both preorganization and number of donor groups can be obtains using pyridine based ligands as an example 45

Figure 2.1. Structure of the *meso*-octamethylcalix[4]pyrrole (1) and the $\boldsymbol{\alpha}, \boldsymbol{\alpha}', \boldsymbol{\alpha}'', \boldsymbol{\alpha}'''$-*meso*-tetrahexyltetramethyl-calix[4]pyrroles (2) 87

Figure 2.2. Results of the liquid−liquid extraction experiment in which 10 mM solutions of 1 or 2 in chloroform were equilibrated at 25 °C with equal volumes of aqueous solutions of 0.001–0.1 M $TBMA^{+}Cl^{-}$ traced with $^{36}Cl^{-}$. Data for a blank without calixpyrrole show weak, though noticeable extraction of $TBMA^{+}Cl^{-}$ by chloroform alone 89

Figure 2.3. Slope analysis of the extraction of $TBMA^{+}Cl^{-}$ from aqueous solution into chloroform using calixpyrroles 1 and 2 at 10 mM. Also shown is the blank extraction of $TBMA^{+}Cl^{-}$ into chloroform alone. Data were taken from Figure 18 and treated as discussed in the text 90

Figure 2.4. Crystal Structure of unbound 2, side view (left) and top view (right) 92

Figure 2.5. Crystal Structure of 2 bound to $TMA^{+}Cl^{-}$, side view (left) and top view (right) 93

Figure 2.6. Structures and relative energies of 2a $(\alpha,\alpha,\alpha,\alpha)$ and 2b$(\alpha,\beta,\alpha,\beta)$ in the unbound free state obtained after geometry optimization at the M06-2X/6-31+G(d) level of theory. Solvent corrections are included using the SMD model for chloroform). Relative energies in the gas phase are shown in parentheses 94

Figure 2.7. Structures and relative energies of 1:1 chloride – ligand 3 complexes obtained after geometry optimization at the M06-2X/6-31+G(d) level of theory. Solvent corrections are included using the SMD model for chloroform. Relative energies in the gas phase are shown in parentheses. Thin lines indicate hydrogen bonds and dashed lines indicate close contacts between the C–H groups of alkyl chains and the chloride anion 95

Figure 2.8. Structures (side and bottom views) and relative energies of 1:1 chloride – ligand 2 complexes obtained after geometry optimization at the M06-2X/6-31+G(d) level

of theory. Solvent corrections are included using the SMD model for chloroform. Relative energies in the gas phase are shown in parentheses. Thin lines indicate hydrogen bonds and dashed lines indicate close contacts between the C–H groups of alkyl chains and the chloride anion 96

Figure 2.9. M06-2X/6-31+G(d) optimized structures of 1:1 chloride – ligand complexes indicating that chloride can accommodate up to four chloroform molecules in the first solvation shell when bound to ligand 1 and two chloroform molecules when bound to ligand 2. Thin lines indicate hydrogen bonds and dashed lines indicate close contacts between the alkyl C-H groups and the chloride anion 97

Figure 2.10. Structures and relative energies of ion-pairs formed with ligand 1 obtained after geometry optimization at the M06-2X/6-31+G(d) level of theory. Solvent corrections are included using the SMD model for chloroform. Relative energies in the gas phase are shown in parentheses. Thin lines indicate hydrogen bonds and dashed lines indicate close contacts between the alkyl C–H groups and the chloride anion 98

Figure 3.1. Structures of iminoguaniginium chloride and diiminoguanidnium chloride. 123

Figure 3.2. Synthetic route for TABEDIG Cl. a.) I_2, imidazole, PPh_3, DCM, 0 °C→ RT b.) 3,4-dihydroxybenzaldehyde, K_2CO_3, acetone, 65 °C c.) diaminoguanidinium chloride, E*t*OH, 65 °C, overnight 124

Figure 3.3. Structures of the simple guanidiniums and TABEDIG 125

Figure 3.4. Comparison of simple guanidinium sulfate extraction versus TABEDIG's sulfate extraction 126

Figure 3.5. TABEDIG performance for sulfate extraction in various solvents. The axis and values are shown as in log form 127

Figure 3.6. Possible conformations of TABEDIG in the reversed micelles 129

Figure 3.7. Initial target oxoanion receptors of the selective recognition sulfate and phosphate via shape and charge complementarity 130

Figure 3.8. Urea-thiourea precursors for the mixed urea-guanidinium oxoanion receptors 131

Figure 3.9. General two-step procedure used to convert thioureas to guanidiniums ... 132

Figure 3.10. Proposed synthetic route for the mixed urea-guanidinium receptors 133

Figure 3.11. Isolated products for the guanylation reaction, cyclic guanidinium and corresponding amine 134

Figure 4.1. Preparation of the GBAH salts A to D by hydrazine condensation in water 164

Figure 4.2. X-ray crystal structure of A. a) ORTEP representation showing the GBAH cation and the anionic $SO_4(H_2O)_5^{2-}$ cluster. b) Hydrogen-bonded $[SO_4(H_2O)_5^{2-}]_n$ clusters. c) Stacking of the GBAH cations. d) Hydrogen bonding of the sulfate–water clusters by the cationic GBAH stacks, viewed down the crystallographic b axis. e) Space-filling representation of the crystal packing viewed down the crystallographic b axis 165

Figure 4.3. X-ray crystal structures of C (a) and D (b). Top: ORTEP representations; middle: hydrogen-bonded layers; bottom: packing of the layers 166

Figure 4.4. PXRD patterns for A·5H2O. Red: simulated pattern from the single-crystal; Blue: experimental pattern from the bulk crystalline powder 169

Figure 4.5. PXRD patterns for C. Red: simulated pattern from the single-crystal; Blue: experimental pattern from the bulk crystalline powder 170

Figure 4.6. PXRD patterns for D. Red: simulated pattern from the single-crystal; Blue: experimental pattern from the bulk crystalline powder 171

Figure 4.7. UV calibration spectra obtained using the chloride salt B. The concentrations of the GBAH cation ranged from a minimum of 1 Å~ 10^{-6} to a maximum of 1 Å~ 10^{-4} M..... 172

Figure 4.8. UV calibration curve obtained using the absorbance of GBAH at 286 nm. 173

Figure 4.9. PXRD patterns for A·5H2O (red) and the product of the SO_4^{2-}/ClO_4^- competitive crystallization (blue) 177

Figure 4.10. FTIR spectra of A·5H2O (blue) and the product of the SO_4^{2-}/ClO_4^- competitive crystallization (red) 178

Figure 4.11. PXRD patterns for A·5H2O (red) and the product of the SO_4^{2-}/Cl^- competitive crystallization (blue) 179

Figure 4.12. FTIR spectra of A·5H2O (red) and the product of the SO_4^{2-}/Cl^- competitive crystallization (green) 180

Figure 4.13. PXRD patterns for A·$5H_2O$ (red), C (green) and the product of the SO_4^{2-}/NO_3^- competitive crystallization (blue) 181

Figure 4.14. FTIR spectra of A·$5H_2O$ (red), C (green) and the product of the SO_4^{2-}/NO_3^- competitive crystallization (blue) 182

Figure 4.15. PXRD patterns for C (red) and the product of the NO_3^-/ClO_4^- competitive crystallization (blue)..... 183

Figure 4.16. FTIR spectra of C (blue) and the product of the NO_3^-/ClO_4^- competitive crystallization (red) 184

Figure 4.17. PXRD patterns for A·5H2O (red), C (green) and the product of the $SO_4^{2-}/NO_3^-/Cl^-/ClO_4^-$ competitive crystallization (blue) 185

Figure 4.18. FTIR spectra of A·5H2O (green), C (blue) and the product of the $SO_4^{2-}/NO_3^-/Cl^-/ClO_4^-$ competitive crystallization (red) 186

Figure 5.1. Synthesis of BBIG-SO_4 and BBIG-NO_3 by imine condensation in water ... 217

Figure 5.2. X-ray crystal structure of BBIG-SO_4. a) ORTEP representation showing the planar BBIG cation and the sulfate with the two water molecules of hydration. b) $[(SO_4)_2(H_2O)_4]^{4-}$ cluster. c) Stacking of the BBIG cations, with the black and red dashed lines corresponding to the C=N(imine)···Ph and H_2N···C=N(imine) intermolecular contacts. d) Hydrogen bonding of the sulfate–water clusters by the guanidinium groups of the BBIG stacks, viewed down the crystallographic a axis 218

Figure 5.3. X-ray crystal structure of BBIG-NO_3. a) ORTEP representation. b) Stacking of the BBIG cations. c) Hydrogen bonding of the nitrate anions by the guanidinium groups of the BBIG cations 219

Figure 5.4. Van't Hoff plot for dissolution of BBIG-SO_4 in the 15-35 °C temperature range 221

Figure 5.5. Results from DFT calculations. a) Electrostatic potential map (0.24 e/a_0^3 isovalue) for the BBIG-SO_4 crystal, obtained from periodic calculations. b) Electrostatic potential map (0.11 e/a_0^3 isovalue) for the isolated BBIG cation, obtained from non-

periodic calculations. c) Atomic charges for the BBIG cation in the BBIG-SO_4 crystal, calculated using the Bader scheme 222

Figure 5.6. Complete separation cycle for sulfate removal by crystallization of BBIG-SO_4. A) In situ synthesis of BBIG dichloride salt from aqueous aminoguanidinium chloride and terephthalaldehyde. B) Selective crystallization of BBIG-SO_4. C) Filtration of BBIG-SO_4. D) Ligand recovery by neutralization of BBIG-SO_4 with NaOH and crystallization of neutral BBIG; sulfate is removed as aqueous Na_2SO_4. E) Regeneration of the BBIG dichloride salt, which can be recycled for another separation cycle 223

Figure 5.7. PXRD patterns for BBIG-SO_4. Red: simulated pattern from the single-crystal; Blue: experimental pattern from the bulk crystalline powder 225

Figure 5.8. PXRD patterns for BBIG-NO_3. Red: simulated pattern from the singlecrystal; Blue: experimental pattern from the bulk crystalline powder 226

Figure 5.9. UV calibration spectra obtained using the BBIG-Cl salt. The concentrations of the GBAH cation ranged from a minimum of 5×10^{-7} to a maximum of 1×10^{-5} M 227

Figure 5.10. UV calibration curve obtained using the absorbance of the BBIG dication at 322 nm 228

Figure 5.11. Experimental PXRD pattern of the crystalline solid obtained from the competitive crystallization experiment (blue) overlaid over the simulated PXRD pattern from the single-crystal X-ray structure of BBIG-SO_4 (red) 230

Figure 5.12. Overlay of the FTIR spectra for BBIG-SO_4 (blue) and the product of the competitive crystallization experiment (green) 231

Figure 5.13. X-Ray crystal structure of BBIG $\cdot$ $2H_2O$ 232

Figure 5.14. Electron density isosurfaces colorized according to the values of the electrostatic potentials for (a) BBIG-NO_3 crystal, (b) isolated BBIG$(NO_3)_2$ complex. Positive and negative regions are shown in blue and red, respectively. The isovalues are 0.24 e/a_0^3 for (a) and 0.14 e/a_0^3 for (b), where a_0 is the Bohr radius 235

Figure 5.15. Electron density isosurfaces colorized according to the values of the electrostatic potentials for (a) BBIG$\cdot 2H_2O$ crystal, (b) isolated BBIG ligand. Positive and negative regions are shown in blue and red, respectively. The isovalues are 0.19 e/a_0^3 for (a) and 0.11 e/a_0^3 for (b), where a_0 is the Bohr radius 238

Figure 6.1. Atmospheric CO_2 capture via crystalline PyBIG$H_2(CO_3)(H_2O)_4$. a) Reaction of aqueous PyBIG (ChemDraw structure on the left) with CO_2 to form PyBIG$H_2(CO_3)(H_2O)_4$ (X-ray crystal structure on the right). b) Hydrogen-bonded $[CO_3(H_2O)_4^{2-}]_n$ cluster formed in the crystal. c) CO_3^{2-} binding site, with the anion accepting 4 water and 5 guanidinium hydrogen bonds. d) Hydrogen bonding of the $[CO_3(H_2O)_4^{2-}]_n$ cluster by the cationic stacks. e) Overlay of the experimental PXRD pattern of the bulk crystalline product (red) and the simulated PXRD pattern from the single-crystal X-ray data (blue) 264

Figure 6.2. Thermal decomposition of PyBIG$H_2(CO_3)(H_2O)_4$ crystals and regeneration of the PyBIG sorbent. a), b) Micrographs of the initial crystals (a) and after heating in air at 120 °C for one hour (b); scale bar: 100 μm. c), d) TGA plots from temperature-ramped (c) and isothermal (d) measurements. e) Overlaid FTIR spectra of the carbonate crystals (red) and the recovered PyBIG ligand (blue). f) ^{1}H NMR spectra (in DMSO-d_6) of the initial (red) and regenerated (blue) PyBIG 265

Figure 6.3. Atmospheric CO_2 capture combining CO_2 sorption by an alkali carbonate solution (Eq. 1) and carbonate crystallization with PyBIG (Eq. 2). The overall CO_2 separation cycle is shown in the schematic diagram 266

Figure 6.4. ^{1}H-NMR Spectrum of PyBIG in DMSO-d_6 267

Figure 6.5. ^{13}C-NMR Spectrum of PyBIG in DMSO-d_6 268

Figure 6.6. Single-crystal X-ray structure of PyBIG.2.5H_2O 269

Figure 6.7. TGA-MS of PyBIG$H_2(CO_3)(H_2O)_4$. Overlay of the molecular peaks in the MS, corresponding to CO_2 (m/z 44, teal) and H_2O (m/z 18, blue), and the weight loss from the TGA (red), as a function of time. Fragmentation peaks in the MS are omitted for clarity 270

Figure 6.8. PXRD pattern of crystalline solid isolated from the slurry reaction of PyBIG with aqueous sodium bicarbonate (red) overlaid over the simulated PXRD pattern from the single-crystal X-ray structure of PyBIG$H_2(CO_3)(H_2O)_4$ (blue) 271

Figure 6.9. Comparative FTIR spectra of the solids isolated from the slurry reaction of PyBIG with aqueous sodium bicarbonate. a) Products from the first two cycles (green, red) overlaid over the reference spectrum of PyBIG$H_2(CO_3)(H_2O)_4$ (black); virtually no PyBIG ligand is observed. b) Product from the third cycle (blue), overlaid over the reference spectrum of PyBIG$H_2(CO_3)(H_2O)_4$ (black), indicating a mixture of carbonate and PyBIG 272

Figure 6.10. Comparative FTIR spectra of the recovered PyBIG ligand from the slurry reaction with aqueous sodium bicarbonate. The regenerated ligand matches the spectra of the as synthesized PyBIG. The only difference is the water peaks in the 3100-3600

region (O–H stretch) and at 1640 (H–O–H bend), present in the as synthesized PyBIG.2.5H_2O (black), and absent in the recovered anhydrous PyBIG (green, red) ... 273
Figure 7.1. Structure of DEHPA and its proposed replacement octyl-HOPO 292
Figure 7.2. Reaction scheme for 1-Hydroxy-6-N-octylcarboxamido-2(1H)-pyridinone (Octyl-HOPO) 293
Figure 7.3. Extraction results of the solvent extractions under TALSPEAK conditions (DTPA holdback and citric acid buffer). For extraction 20 mmol of octyl-HOPO was dissolved in diisopropylbenzene (DIPB). An organic–to–aqueous phase ratio (O:A) of 1 was used and the samples were mixed for 3 hrs. at 25 °C 294
Figure 7.4. Extraction results for the lanthanides in a citric acid buffer in the absence of the DTPA holdback reagent. For the extraction experiments 20 mmol of either octyl-HOPO or DEHPA dissolved in DIPB was used. An O:A of 1 was used and samples were mixed for 3 hrs. at 25 °C 296
Figure 7.5. Synthesis scheme for 1-hydroxy-6-N-octylcarboxamido-2(1H)-pyridinone (octyl-HOPO, 2) 297
Figure 8.1. Structures of bis-triazine heterocycles 325
Figure 8.2. Geometry optimized Eu-Me-BTPhen complexes obtained from DFT calculations. The name of the complex is provided below the corresponding structure. Eu is turquoise, C grey, O red, S yellow, and H white 327
Figure 8.3. Fourier transform of the Eu LIII-edge EXAFS spectrum in *R*-space (black line), with accompanying fit afforded by the $[Eu(BTPhen)_2(H_2O)]^{2+}$ model. The imaginary

component (grey line) and fit are offset beneath. Grey dashed lines denote the fit window 328

Figure 8.4. Synthetic route for the preparation of Me-BTPhen 330

Figure 8.5. ^{1}H NMR of Me_2-BTPhen in $CDCl_3$ 331

Figure 8.6. ^{13}C NMR of Me_2-BTPhen in $CDCl_3$ 332

Figure 8.7. Slope Analysis of Me-BTPhen with Eu extracted from 0.1 M HNO_3. The y-axis represents the logD_{Eu} and the x-axis is the log[Me-BTPhen] 333

Figure 8.8. The first six principal components derived from nine Eu L_{III}-edge k^2-weighted EXAFS spectra of a Eu solution with 7.5 mM Me-BTPhen in an ionic liquid solvent. Components 7-9 (not shown) are similar to components 2 – 6. These data reveal only one mathematical component in the EXAFS spectra, indicating an adequate fit should be achievable from a single appropriate structure model 335

Figure 8.9. Single scattering paths for potential structure models compared against experimental EXAFS data, ordered by increasing coordination number and first-shell bond length. Representative DFT-calculated structures are provided in the upper corner of their corresponding spectrum. Top row, left to right: No anion, H^-; second row, left to right: H_2O, NTf_2 (monodentate); third row, left to right: NO_3 (chelate), NTf_2 (chelate); bottom row: $Eu_2(Phen)_2(OH)_2$ dimer 336

Figure 8.10. Assignment of ΔR and σ^2 parameters for the Me-BTPhen ligands 337

Figure 8.11. (Left) Rejected XAFS fit from structure model $[Eu(Me\text{-}BTPhen)_2]^{3+}$. (Right) DFT-optimized structure model used for preparation of the structure model 338

Figure 8.12. (Left) Rejected XAFS fit from structure model $[Eu(Me\text{-}BTPhen)_2NO_3]^{2+}$. (Right) DFT-optimized structure model used for preparation of the structure model ... 339

Figure 8.13. (Left) Rejected XAFS fit from structure model $[Eu(Me\text{-}BTPhen)_2OH]^{2+}$. (Right) DFT-optimized structure model used for preparation of the structure model ... 340

Figure 8.14. (Left) Rejected XAFS fit from structure model $[Eu(Me\text{-}BTPhen)_2NTf_2]^{2+}$. (Right) DFT-optimized structure model used for preparation of the structure model ... 341

Figure 8.15. k^2-weighted $\chi(k)$ EXAFS data and fit for $[Eu(Me\text{-}BTPhen)_2(H_2O)]^{3+}$ 342

Figure 9.1. Chemical structures for 1,10-phenanthroline-2,9-dicarboxamidecomplexants **1** to **4** 371

Figure 9.2. Influence of the alkyl chain length in IL cation on the distribution ratios for Eu(III) (squares) and Am(III) (circles) ions in 1 M nitric acid (4 mM **3** or **4** in Cnmim NTf_2). For $[C_6mim][NTf_2]$, the conditions are optimum for efficient Am/Eu separations 372

Figure 9.3. Distribution ratios D_{Ln} for Ln(III) ions across the lanthanide period for 4mM **1** in $[C_6mim][NTf_2]$ (open squares) and 4 mM **3** in $[C_4mim][NTf_2]$ (filled circles). D_{Ln} are plotted vs. the atomic number Z of the lanthanide 374

Figure 9.4. Molecular structure of **3** interacting with four NTf_2^- anions (taken from the optimized geometry gas phase $[Gd^{III}L_2](NTf_2^-)_8$ complex shown in Figure 9.5). The arrows indicate hydrogen bonds between the amide group in **3** and the sulfuryl groups in the IL anion 375

Figure 9.5. Optimized geometry $[Gd^{III}L_2(NO_3^-)_x](NTf_2^-)_8$ complexes for ligand **3** with (a) x = 0 and (b) x = 1 (the outer anions not shown) 376

Figure 9.6. Synthetic scheme for extractants **1** to **4** 377

Figure 9.7. Extraction of Ln(III) ions from 1 mM nitric acid using 4 mM **1** (a) or **3** (b) for different imidazolium ILs ([Cnmim] [NTf_2], *n*=2-8) and *n*-dodecane (in panel a). The distribution ratios D_{Ln} are plotted vs. 1/*r*, where *r* is the ionic radius for coordination number 8. In panel a, the complex dependencies observed for [C_2mim] [NTf_2] and [C_4mim] [NTf_2] are likely to arise due to interference of cation exchange, which is entirely suppressed for more hydrophobic cations 381

Figure 9.8. Space filling renditions of optimized geometry axisymmetric [$Gd^{III}L_2(NO_3^-)_x](NTf_2)_8$ complexes for ligand **3**: (a) x=0 and (b) x=1 complexes. The arrows indicate the nitrate ligand. Top views and side views of these helical complexes are given side by side 382

Figure 9.9. Ionic radius dependences for Ln-X distances in optimized geometry $[Ln^{III}L_2(NO_3)_x](NTf_2^-)_8$ complexes for ligand **3** assuming x=0 (filled symbols) and x=1 (open symbols). Panel a is for O and N atoms in ligand **3**, panel b is for the nitrate ligand. X=O corresponds to the circles and X=N corresponds to the squares. The ionic radii (across the lanthanide period) are for the coordination number of eight. As the ionic radius increases for lighter lanthanide ions, the ligands move away from the metal ion, making it more accessible to nitrate addition 383

Figure 9.10. (a) Energy profile for the axisymmetric $[Ln^{III}L_2(NO_3^-)](NTf_2^-)_8$ complex (for La, Gd, Er and Lu) as a function of Ln-N distance for the NO_3^- nitrogen (all other degrees of freedom optimized). The arrow indicates a local potential minimum for the nitrate anion in between the two imidazolium cations in this complex, as shown in panel b. As the ionic radius increases, the energy barrier to NO_3^- addition systematically decreases, and so

does the enthalpy of this addition. Zero energy corresponds to the nitrate anion removed from the complex 384

Figure 9.11. Simulated R-space k3-weighted EXAFS (extended X-ray absorption fine structure) patterns for $[Gd^{III}L_2(NO_3^-)_x](NTf_2^-)_8$ complexes for x=0 and x=1 (see the legend in the plot) juxtaposed onto the electron density distribution in these two complexes. The large amplitude in the first peak due to the presence of the bound nitrate ligand makes it easy to quantify the degree of nitrate involvement by means of X-ray absorption spectroscopy 385

Figure 9.12. ^{1}H NMR of compound **1** in $CDCl_3$ 386

Figure 9.13. ^{1}H NMR of compound **2** in $CDCl_3$ 387

Figure 9.14. ^{1}H NMR of compound **3** in DMSO-d_6 388

Figure 9.15. ^{1}H NMR of compound **4** in DMSO-d_6 389

Figure 9.16. ^{1}H NMR of compound **8** in DMSO-d_6 390

Figure 9.17. ^{1}H NMR of compound **9** in DMSO-d_6 391

Figure 9.18. ^{1}H NMR of compound **10** in $CDCl_3$ 392

Figure 9.19. ^{1}H NMR of compound **11** in DMSO-d_6 393

Figure 9.20. ^{13}C NMR of compound **1** in $CDCl_3$ 394

Figure 9.21. ^{13}C NMR of compound **2** in $CDCl_3$ 395

Figure 9.22. ^{13}C NMR of compound **3** in DMSO-d_6 396

Figure 9.23. ^{13}C NMR of compound **4** in DMSO-d_6 397

Figure 9.24. ^{13}C NMR of compound **8** in DMSO-d_6 398

Figure 9.25. ^{13}C NMR of compound **9** in DMSO-d_6 399

Figure 9.26. ^{13}C NMR of compound **10** in $CDCl_3$ 400

Figure 9.27. ^{13}C NMR of compound **11** in $CDCl_3$ 401

Chapter 1 : Introduction

1.1 Ions

Currently with ever increasing demands for materials for globalized markets, there is a dire need to develop new methods to increased production and recover of raw materials (e.g. lithium, lanthanides, etc.). Separation science has been heavily relied upon in the last few centuries to develop new processes for extracting and recovering materials. To fulfill the demands for materials by industries and societies in general, major technological improvements and innovations were made, allowing for the development of new methods and equipment for separations (e.g. centrifuges, gas diffusion, etc.). With these new methods and equipment, it was possible to provide the specific materials necessary for the development of nations into industrial superpowers. However, with the industrialization of a nation comes the concern over the increases in the release of harmful materials into the environment.

Many of the harmful materials and compounds (e.g. chromate, nitrate, phosphates, carbon dioxide, etc.) present in the environment must be removed to lower their concentrations to manageable levels to reduce the chance of their build up to toxic levels. Additionally, the prevention of their release during industrial processes and development are key to creating stable and safe process that can benefit countries and population worldwide. Separation technologies currently in use and in development represents some of the major methods and tools that could be used and implemented to combat and

prevent the release of the hazardous and toxic materials and compounds into the surrounding environment. This work focuses on the development and testing of new materials and techniques that could led to the future development of new technologies to reduce the impact of man on his surrounding environment. Many issues of increased interest are addressed in this work, these issues arise in the course of the production of energy and fuels for power production. These issues range from the removing minor actinides from radioactive waste generated in reactors in the nuclear power industry, to the removal of sulfate from seawater using in offshore oil drilling rigs, and the reduction in atmospheric carbon dioxide (CO_2) concentrations whose rises coincides with the observed increase in global temperatures.

The development of new separation technologies for the selective removal of minor actinides from nuclear waste can led to the closing of the nuclear fuel cycle and the use of nuclear reactors of the production of power. By selectively removing the minor actinides and other harmful transuranics in radioactive waste, the radiotoxicity of the waste is greatly reduced and the costs of long term storage of the waste is greatly reduced.[1] The selective removal of sulfate from seawater can save the off-shore drilling industry millions of dollars associated with the costs of replacing pipes clogged with barium sulfate scale[2] which results from the mixing of sulfate in seawater and barium present in the pipes. Separations technologies developed for direct capture of carbon dioxide (CO_2) from the air would allow for a reversal of the harmful build-up of CO_2 in the environment, which has been linked to climate change. Every day, throughout the developed world, people

take for granted all the technologies and products at their fingertips without a single thought of how many of these appliances, and the energies used to power them are made possible by separation processes and technologies development using the accumulated knowledge of generations scientists and engineers.

In this introduction, key concepts pertaining to the selective separation of anions (negative ions) and cations (positive ions) will be introduced in form of two sections one on anions and the next on cations. By subdividing the ions by their respective charge it is hoped that a clearer picture can be gained of the individual problems and challenges addressed by my research presented in the following eight chapters. The five chapters which follow this introduction are aimed at the selective separation of anions particularly oxoanions like sulfate and carbonate. The three chapters which follow those target the selective separation of cations, in particular the selective separation of *f*-block elements for example actinides from lanthanides.

1.2 Anion Receptors

In this section of the introduction and succeeding chapters (**Chapters 2-6**) I will discuss the work done by myself, in collaboration with my colleagues in the Chemical Separations Group at Oak Ridge National Laboratory. My research focused on the selective separation of oxoanions (particularly sulfate) using two methods liquid-liquid extraction (solvent extraction) and crystallization. In **Chapters 2-3** work on the development of organic soluble anion receptors for using in solvent extraction systems are discussed.

Chapters 4-6 discusses the use of aqueous soluble guanidines and guanidiniums for the selective crystallization of oxoanions from aqueous solutions. Both crystallization and solvent extraction proved to be effective methods for selectively removing oxoanions when the new ligands/extractants were used in these systems. While both were shown to be effective, each method has different challenges and hurdles which must be overcome to develop practical systems. To understand the challenges and difficulties associated with selectively separating oxoanions, it is necessary to understand why the targets are difficult to remove and the prior research that has been done in the fields of anion coordination and separations.

Selective separations of oxoanions from aqueous solutions represent a difficult and technologically important challenge in separation science. Oxoanions are targets of interest due to their environmental and industrial impact.[2-5] Many oxoanions are known to have a major impact in both industrialized and developing societies worldwide. For example, the presence of chromate salts in drinking water, a problem mainly in developing third-world nations, has been linked to heavy metal poisoning.[6-7] If new materials are developed to effectively remove this toxic anion from ground water millions of people around the world will have access to potable sources of water.

Two other oxoanions, nitrate and phosphate, are closely associated with red tide and algae blooms which have become more prevalent in the past decades.[8-10] Nitrate and phosphate are introduced into both fresh water and salt-water marine ecosystems due to

excessive use of artificial fertilizers in farmer fields worldwide. When these over fertilized fields are over-watered or excessive rainfall occurs, the resulting run-off drains directly into streams eventually making its way to larger bodies of water acting as a major food sources for micro-organisms. If these oxoanions can be captured and removed from the run-off prior to draining into streams then the blooms can be avoided. Additionally, the captured nitrate and phosphate can be stripped from the materials and reused by the farmers.

Another oxoanion that has become a nuisance to industry is sulfate. This anion is problematic in both the energy and fuel industries. Sulfate is responsible for the formation and build-up of scale in the pipes used to transport seawater in off-sea drilling rigs.[2] In the nuclear waste industry, the presence of sulfate in the vitrified glass reduces the stability and lifetimes of the glass logs used for the long–term storage and sequestration of nuclear waste in the United States. When the sulfate is removed from the liquid nuclear waste prior to undergoing the vitrification process,[3] the leachability of the radionuclides from the glass logs is greatly reduced. However, the selective recognition and removal of these oxoanions is not simple due to the presence of competing anions (e.g. chloride and nitrate) in the solutions.

The selective recognition and separation of oxoanions is a challenging problem to address because of the variation in their geometries, highly charged nature and their high

energies of hydration. In **Table 1.1**, a few oxoanions are listed along with their charge, radii and energies of hydrations.

The geometries of oxoanions have discrete geometric shapes and are not spherical like simple anions. Nitrate and carbonate have a trigonal planar geometry and sulfate, chromate, and phosphate have a tetrahedral geometry. These variations in the shapes of the anions shown in **Figure 1.1**, make it necessary to design hosts/ligands which can bind in a complimentary fashion giving rise to the concept of shape complementarity.

In addition to increasing complexity caused by the change in geometries, is the issue that the charges of the oxoanions are not simple point charges seen in simple spherical anions. The oxygens of the oxoanions allow the charge to be spread throughout the molecule with the charge being distributed across the atoms of the oxoanion. The delocalization of charge across the oxoanions can be seen in **Figure 1.2** which shows the electrostatic potentials of sulfate and nitrate.

The larger the charge density of an anion, the stronger its energy of hydration is shown in **Table 1.1**. To effectively coordinate and extract anions, complexants must be able to replace the waters of solvation associated with the anion and form a charge neutral species by offsetting the negative charge of the anion. These two criteria are of utmost importance since organic solvents are typically immiscible with water. Additionally, the presence of highly charged species are not favorable in organic solvents with low

dielectric constants as these solvents cannot help with charge stabilization. In **Table 1.2**, the dielectric constants(ε) and Hildebrand solubility parameter(δ) for multiple solvents are shown.

The properties of oxoanions listed and described in the previous paragraphs represent some of the major hurdles which make the selective coordination, binding, and separation of oxoanions so challenging. Despite these challenges the field of anion coordination has developed and grown in the past few decades. To gain a more complete picture of the work that is discussed in the first few chapters of this dissertation it is necessary to have a firm understanding of what has been done in the field and see the progression of how previous scientist and groups have addressed some of the challenges associated with achieving selectivity.

Anion coordination chemistry is a broad and diverse field of supramolecular chemistry.[4-5, 18-21] Attempting to describe all the developments and improvements that have occurred during the past 40 years since the first literature reported occurrence of anion binding would be a true herculean effort. For reasons of brevity, I will only focus on a couple of examples of oxoanion receptors from the history of anion coordination. The examples that are covered herein are used to give a better understanding of what was done and how my research represents the next logical progression for oxoanion coordination and separation.

The first synthetic anion receptor was reported in the literature in 1968 by Simmons and Park[22], they reported that a macrobicyclic receptor when protonated would bind to halide anions. The structure of this receptor is shown in **Figure 1.3**.

Since Simmons' and Park's discovery of anion binding, the amount of knowledge surrounding these receptors has exploded. In recent years, it has even become possible to rationally design receptors to selectively bind one particular oxoanion over another. All the research and development since the first reported case of anion binding has resulted in the publication of multiple books and reviews specifically on anion coordination.[4-5, 18-19] Some of the well-known examples of anions receptors that I will discuss in the following couple of pages of this introduction are shown in **Figure 1.4**, below.

A well-known anion receptor from the literature is calix[4]pyrrole (C4Ps).[23-25] Calix[4]pyrroles are known to be exceptional halide receptors coordinating to spherical anions through four hydrogen bonds by adopting a cone shape conformation.[23-28] This characteristic of forming a cone conformation allows the C4P to form strong complexes with halides and allows for the balancing or partially balancing of the charge because it is possible for a cation to bind on the opposite side of the receptor across from the halide, resting inside of the cup of the calix(**Figure 1.5**).

The strong binding interaction C4Ps have had with halides has also led to studies looking at their use for bind oxoanions like nitrate and sulfate.[23-24, 26-28] Even with the strong

interactions of the C4Ps with anions there are still a couple of disadvantages for selectively binding and extraction oxoanions. One drawback to C4Ps is that they can only coordinate strongly to single oxygen or weakly to two oxygens of the oxoanions. This means that the remaining oxygens which are uncoordinated will still be solvated making separations via extraction more difficult. Modified versions of C4P have been synthesized to coordinate to additional oxygens of the oxoanions. The variations of C4Ps utilized straps to incorporate additional H-bonding groups (**Figure 1.6**) into their structures, however these have only been moderately effective at improving the selectivity and extractability of oxoanions.

One additional factor that limits the effectiveness of the C4Ps and their derivatives is their limited solubility in most of the common organic solvents used in solvent extraction processes and their insolubility in aqueous solutions for effective crystallization of oxoanions. In this dissertation, **Chapter 2** will be devoted to looking at a method for enhancing the solubility of C4Ps in common organic solvents using in liquid-liquid separation processes.

Two classic yet similar, functional groups used as neutral anion receptors are ureas and thioureas. The binding motifs for both types of receptors differ from that of C4P, since these receptors have two H-bonding amines that point in the same direction and coordinate along the edges of oxoanions. C4Ps bind along the axis of the oxoanion making them less effective for oxoanions since all the H-bonding donors point toward a

single point. The examples for edge binding compared to axial binding is shown in **Figure 1.7**, below. By coordination along the edges of oxoanions, ureas and thioureas form stronger bonds compared to axial binding.[5, 18-19] Additionally, binding along the edge of the anions aids the replacement of the waters of hydration associated with the highly charged oxoanions.[13, 30]

Recent literature examples have shown that multiple ureas and thioureas can be combined into single receptors for oxoanions.[31-33] In one case six ureas were used in a single molecule on a tripodal scaffold.[31] This receptor exhibited very strong binding to sulfate encapsulating the oxoanions by binding along all six edges of the sulfate. The structures of the various multi-urea/thiourea receptors are shown in **Figure 1.8**. The crystal structure for the hexaurea bound to sulfate is shown in **Figure 1.9** as well.

Although ureas and thioureas exhibited strong binding with oxoanions there are a couple of issue which make their use in solvent extraction problematic. One problematic issue with these classes of receptor are their low solubilities in various organic solvents.[4, 19] Another issue is that ureas are unable to accommodate a cation into their structure making it even more difficult to affect an extraction of oxoanions into organic solvents. One solution to the inability of the ureas and thioureas to balance the negative charge of the anions is the addition of lipophilic quaternary amines in the organic solvent.[31] However, when more components are added to an extraction system the more complex the chemistry of that system becomes making it less attractive for oxoanion separations.

A simple solution to this lack of charge can be found in guanidiniums.[34-37] Guanidiniums take the favorable geometry of ureas and thioureas, and add to it a delocalized positive charge. This charge serves to create charge neutral complexes and an additional source of attraction (through favorable coulombic forces). The reported first use of guanidiniums as anion receptors was done by Lehn and co-works in the late 1970s.[38] In their work, Lehn and his co-works observed and measured the binding of phosphates and carboxylates with polyguanidiniums.[38] The structures of these early guanidinium based anion receptors are shown in **Figure 1.10**.

Since Lehn's first reported use of guanidiniums in the late 1970s there have been multiple groups who have use guanidiniums for anion binding.[35-37] Much of the work that followed in the 1990s and early 2000s was done looking at binding to anionic biomolecules[35-37, 39-40] mostly enzymes, responsible for phosphodiester cleavage in biological systems. Attempting to increase the selectivity of their receptors for anionic biocatalyst multiple groups developed ways to preorganize guanidinium receptors.[41-42] One issue that is encountered with guanidinium based receptors which doesn't occur with ureas and thioureas are the various conformers which the NHs of the guanidiniums can adopt. The various conformations of the guanidiniums are shown in Figure 11. In Figure 11, the guanidinium shown is a simple di-substituted guanidinium, with two NHs and one NH_2^+.

Multiple groups have developed strategies to preorganize guanidiniums into the complementary conformation for binding to oxoanions.[41, 43-44] By preorganizing the guanidiniums the cost associated with rearranging into the correct conformation is

removed thereby increasing the likelihood of a stronger and more favorable interaction between receptor and anion. In their initial follow-on work to Lehn, Hamilton and co-workers[27-28] used systems where one of the NHs of the guanidiniums could H-bond with a carbonyl (CO). Ariga and Anslyn then developed more rigid linkers to lock the guanidiniums in complementary conformations for specific biomolecules.[43-44] Schmidtchen and co-workers[41, 45] developed conformationally rigid guanidiniums which locked the central nitrogen of the guanidinium in place by making it quaternary, ensuring the receptor was always in the correct conformation for binding to oxoanions. The structures of some of the receptors used by the three groups to preorganized the guanidiniums are shown in **Figure 1.12** below.

Most of the guanidiniums reported in the literature had limited solubility in water and in traditional organic solvents used for liquid-liquid separations. This limited solubility is a handicap which must be overcome to develop systems capable of extracting and separating oxoanions from complex mixtures.

1.3 Cation Receptors

The selective removal of minor actinides (e.g. curium, americium, etc.) from nuclear waste represents one of the more complex challenges in nuclear chemistry and the separation sciences.[1, 46-48] Minor actinides (MAs) present in nuclear waste are a by-product produced in the fuel rods of nuclear reactors during the lifetime of the fuel in the reactor.[48-49] The concentrations of MAs present in the waste increases over time as the uranium in the fuel

of the reactors are bombarded by neutrons. The ^{238}U present in the fuel rods undergo a series of neutron absorptions and beta decays eventually producing mixtures of MAs. Two of the most well-known MAs generated in nuclear reactors are americium-241 (^{241}Am) and curium-242 (^{242}Cm)[48]. The pathways for reactions which eventually lead to the production of these elements and their isotopes are shown in **Figure 1.13**.

The plutonium (Pu) and MAs present in the nuclear waste are responsible for the radiotoxicity and heat generation associated with radioactive waste. These two deleterious characteristics are cause by alpha decay from the Pu and MAs isotopes. While the Plutonium Uranium Redox Extraction(PUREX)[50] process can be used to easily remove the Pu and U present in the waste it is much more difficult to remove the MAs due to the nature of their chemistry and their similarities to the lanthanide elements also produced as by-products in the reactors.[48, 50] To remove the MAs from the nuclear waste it is necessary to design new ligands/extractants which will selectively bind MAs, while rejecting the other *f*-block elements (e.g. lanthanides(Ln)).

There are two proposed solvent extraction pathways for separating the MAs from the Ln. Both have been investigated with the latter being the preferable option. The first pathway involves the selective extraction and removal of the Ln from the nuclear waste leaving the MAs in the nitric acid. The second pathway involves selectively extracting the MAs from the nuclear waste leaving the Ln behind. In this dissertation one of my three chapters on *f*-block separations will look at the possible use of a new organic soluble ligands in a

modified TALSPEAK process.[46-47, 51-54] **Chapters 8** and **9** will discuss the use of phenanthroline based ligands for the selective extraction and separation of MAs.

Until the development and use of triazine based ligands by French scientists in the 1980s the selective extraction of MAs over Ln was not possible because no ligands had shown promise for selectively binding to MAs. Prior to this discovery, the first method of extraction of Ln was the main pathway proposed for separating the Ln from the MAs. The most well-known process using the first method was the TALSPEAK[46-47, 54-55] (Trivalent Actinide Lanthanide Separation with Phosphorus-Reagent Extraction from Aqueous Komplexes) process which was complex and required the use of complexants in both the organic and aqueous phases. Additionally, the process was pH sensitive requiring the aqueous solutions to be buffered using lactic acid and later citric acid which was more robust causing less problems in the process. The complexants used in the TALSPEAK process are an alkylated phosphate (di-2-ethylhexylphosphate (DEHPA)) in the organic phases and diethylenetriaminepentacarboxylic acid (DTPA) in the aqueous phase. The chemical structures of the TALSPEAK components are shown in **Figure 1.14**.

The DTPA acts as a hold-back reagent in the aqueous phase selectively binding the MAs leaving the Ln free to be extracted by the DEHPA. The TALSPEAK process was originally developed and studied at Oak Ridge National Laboratory in the 1960s[55] and since then has been modified and changed countless times generating multiple reviews discussing the improvement and changes to this process. As stated previously the second method of selectively extracting the MAs is preferred over methods such as the TALSPEAK

process due in part to the complexity and the costs associated with it because of the need to modify the aqueous feed (waste) in the process. These modifications can add up. Even through DTPA and citric acid are relatively inexpensive, the amounts needed to achieve the desired level of separation of Ln from MAs drives the costs up making it less desirable. If the process could be modified to an extent that the holdback reagent and/or buffer could be removed than this method could become viable for Ln/MAs separations.

The second pathway where the MAs are extracted preferentially over the Ln requires an understanding of the principles of ligand design.[56-57] An understanding of the principles of ligand design is necessary since the goal of the second pathway utilizies a solvent extraction method which only employs a single highly selective ligand in the organic solvent to extract the MA without buffers and hold-back reagents. Achieving the selectivity for the MAs over Ln is difficult because of their similar chemical properties; charge (+3) and size (~1.00 Å).[58-59] The MAs and Ln only differ with regard to the preferred bonding type with MAs having a covalent nature giving them softer character compared to the Ln series which prefer to form more ionic type bonds.[60-64] For this reason, special attention was paid to the donor groups that were selected for use in the ligands which were designed and synthesized to selectively separate MAs from nuclear waste. In **Figure 1.15**, possible donor groups are shown the donors are shown arranged from left to right in terms of increasing covalence/hard and soft donors.

From the donor groups shown in **Figure 1.15**, two donors were more appealing than the other because of their characteristics. These donors were amides and N-type heterocycles (pyridines) because prior research has shown that they possessed greater affinity for softer more covalent metals.[56-57, 65-67] Additionally, these donors are more robust compared to other known softer donors (e.g. thiols, thiophosphates, etc.). While the choice of donor type is important, of equal importance is the number of donor atoms in the ligands.[56, 68-69] This is due to the coordination number of the MAs and Ln varying between eight and nine. The coordination number is an important factor in the design of the ligands in regards to the number of donors and the arrangement/geometry of the atoms around the MAs.[59] Because of the high coordination number of the MAs (n = 9) it is necessary to have ligands which can bind in a 2:1 conformation (2 ligands: 1 MA) to ensure the coordination sites of the MAs are filled. Binding the metals in a 2-to-1 (L:MA) fashion is preferable to designing and synthesizing a single ligand that can completely coordinate to all the coordination sites as the ligand would be very complex with a high likelihood that the ligand will form complex species binding to multiple metals instead of just one.

To ensure the ligands binds as strongly as possible all the donors much be aligned in the most thermodynamically favorable arrangement for complexing to a metal. When the ligand has been designed to achieve this arrangement, the ligands is said to be preorganized for complexing to metals. This correlation of donor atoms and the amount of preorganization are shown in **Figure 1.16**.[67]

The ligands discussed in the **Chapters 8** and **9**, utilize a rigid 1,10-phenanthroline scaffold on additional donor atoms have been attached to increase the effective binding of the ligands to the MAs. The phenanthroline scaffold was selected because it allows for the preorganization of the two central pyridines in the phenanthrolines, ensuring that the two nitrogen donors are already arranged in a favorable binding motif, unlike BIPY which must undergo a conformational change to form a complex. Preorganization of the donors removes entropic penalty incurred by flexible less conformationally rigid ligands such as BIPY which must pay an energetic penalty for rearranging their donors to bind to metals.

Although the phenanthroline based ligands have been shown to bind more strongly and have more stable complexes with MAs, their use in solvent extraction is limited by the number of solvents which they are soluble in.[70-72] Most of the research done on the phenathrolines required the use of exotic solvents that are difficult to obtain. Additionally, the performance of the ligands in these solvents required the use of cation exchangers to enable the formation of charge neutral species in the organic phase. One possible solution to the issue of solubility in organics is using ionic liquids in place of the exotic solvents. Ionic liquids (ILs) have been shown in multiple examples in the literature to solubilize ligands which have had very limited solubility in most organic solvents. The ligands once dissolved in ILs have also shown to have enhanced performance compared to their use in traditional solvents, this could be attributed to the ability off the ILs itself to also function as a cation exchanger. This added characteristic of the ILs to be both a solvent and cation exchanger makes their use more appealing compared to more

complex system which utilize separate modifiers to enhance solubility, and cation exchangers to balance the charge.

1.4 References

1.Tracy, C. L.; Dustin, M. K.; Ewing, R. C., Reassess New Mexico's nuclear–waste repository. *Nature* **2016,** *529*, 149-151.

2.Crabtree, M.; Eslinger, D.; Fletcher, P.; Miller, M.; King, G., Fighting Scale–Removal and Prevention. *Oilfield Reveiw* **1999,** *11* (3), 30-45.

3.Moyer, B. A.; Custelcean, R.; Hay, B. P.; Sessler, J. L.; Bowman-James, K.; Day, V. W.; Kang, S. O., A Case for Molecular Recognition in Nuclear Separations: Sulfate Separation from Nuclear Wastes. *Inorganic Chemistry* **2013,** *52* (7), 3473-3490.

4.Gale, Philip A.; Howe, Ethan N. W.; Wu, X., Anion Receptor Chemistry. *Chem* **2016,** *1* (3), 351-422.

5.Jonathan L Sessler, P. A. G., Won-Seob Cho, *Anion Receptor Chemistry*. The Royal Society of Chemistry: 2006; p 413.

6.Korngold, E.; Belayev, N.; Aronov, L., Removal of chromates from drinking water by anion exchangers. *Separation and Purification Technology* **2003,** *33* (2), 179-187.

7.WHO, Chromium in Drinking-water. 2nd ed.; WHO, Ed. Guidelines for drinking-water quality, 2003.

8.Vries, W. d.; Hettelingh, J.-P.; Posch, M., *Critical Loads and Dynamic Risk Assessments: Nitrogen, Acidity and Metals in Terrestrial and Aquatic Ecosystems*. Springer: New York, 2015; Vol. 25.

9.Prescott, G. W., *The Algae: A Review*. Houghton Mifflin Company: New York, 1968.

10.Andrews, W. A., *Investigating Aquatic Ecosystems*. Prentice-Hall Canada Inc.: Scarborough, 1987.

11.Marcus, Y., *Ion Properties*. Marcel Dekker, Inc.: New York, 1997.

12.Shim, H.-M.; Kim, J.-W.; Koo, K.-K., Molecular interaction of solvent with crystal surfaces in the crystallization of ammonium sulfate. *Journal of Crystal Growth* **2013,** *373*, 64-68.

13.Hay, B. P.; Gutowski, M.; Dixon, D. A.; Garcza, J.; Vargas, R.; Moyer, B. A., Structural Criteria for the Rational Design of Selective Ligands: Convergent Hydrogen Bonding Sites for the Nitrate Anion. *JACS* **2004,** *126*, 7925-7934.

14.Riddick, J. A.; Bunger, W. B., *Techniques of Chemistry: Organic Solvents*. Wiley & Sons: New York, 1970; Vol. 2.

15.Barton, A. F. M., *Handbook of Solubility Parameters and Other Cohesion Parameters*. 2 ed.; CRC: Boca Raton, 1991.

16.Bermudez, A.; Foco, G.; Bottini, S. B., Infintie Dilution Activity Coefficients in Tributyl Phosphate and Triacetin. *J. Chem. Eng. Data* **2000,** *45*, 1105-1007.

17.Durkee, J. B., *Cleaning with Solvents*. Elsevier: New York, 2014.

18.Wenzel, M.; Hiscock, J. R.; Gale, P. A., Anion receptor chemistry: highlights from 2010. *Chem Soc Rev* **2012,** *41* (1), 480-520.

19.Gale, P. A.; Busschaert, N.; Haynes, C. J.; Karagiannidis, L. E.; Kirby, I. L., Anion receptor chemistry: highlights from 2011 and 2012. *Chem Soc Rev* **2014,** *43* (1), 205-41.

20.Bowman-James, K.; Bianchi, A.; Garcia-Espana, E., *Anion Coordination Chemistry* Wiley-VCH: New York, 2011.

21.Steed, J. W.; Atwood, J. L., *Supramolecular Chemistry*. 2nd ed.; Wiley-VCH: New York, 2009.

22.Park, C. H.; Simmons, H. E., Macrobicyclic Amines .3. Encapsulation of Halide Ions by in,in-1,(K+2)-Diazabicyclo[K.L.M]Alkane-Ammonium Ions. *Journal of the American Chemical Society* **1968,** *90* (9), 2431-2432.

23.Allen, W. E.; Gale, P. A.; Brown, C. T.; Lynch, V. M.; Sessler, J. L., Binding of Neutral Substrates by Calix[4]pyrroles. *Journal of the American Chemical Society* **1996,** *118* (49), 12471-12472.

24.Custelcean, R.; Delmau, L. H.; Moyer, B. A.; Sessler, J. L.; Cho, W. S.; Gross, D.; Bates, G. W.; Brooks, S. J.; Light, M. E.; Gale, P. A., Calix 4 pyrrole: An old yet new ion-pair receptor. *Angew Chem Int Edit* **2005,** *44* (17), 2537-2542.

25.Wintergerst, M. P.; Levitskaia, T. G.; Moyer, B. A.; Sessler, J. L.; Delmau, L. H., Calix 4 pyrrole: A new ion-pair receptor as demonstrated by liquid-liquid extraction. *Journal of the American Chemical Society* **2008,** *130* (12), 4129-4139.

26.Moyer, B. A.; Sloop, F. V.; Fowler, C. J.; Haverlock, T. J.; Kang, H. A.; Delmau, L. H.; Bau, D. M.; Hossain, M. A.; Bowman-James, K.; Shriver, J. A.; Bill, N. L.; Gross, D. E.; Marquez, M.; Lynch, V. M.; Sessler, J. L., Enhanced liquid-liquid anion exchange using macrocyclic anion receptors: effect of receptor structure on sulphate-nitrate exchange selectivity. *Supramolecular Chemistry* **2010,** *22* (11-12), 653-671.

27.Borman, C. J.; Custelcean, R.; Hay, B. P.; Bill, N. L.; Sessler, J. L.; Moyer, B. A., Supramolecular organization of calix[4]pyrrole with a methyl-trialkylammonium anion exchanger leads to remarkable reversal of selectivity for sulfate extraction vs. nitrate. *Chem Commun (Camb)* **2011,** *47* (27), 7611-3.

28.Borman, C. J.; Bonnesen, P. V.; Moyer, B. A., Selectivity control in synergistic liquid-liquid anion exchange of univalent anions via structure-specific cooperativity between quaternary ammonium cations and anion receptors. *Anal Chem* **2012,** *84* (19), 8214-21.

29.Kim, S. K.; Lee, J.; Williams, N. J.; Lynch, V. M.; Hay, B. P.; Moyer, B. A.; Sessler, J. L., Bipyrrole-strapped calix[4]pyrroles: strong anion receptors that extract the sulfate anion. *J Am Chem Soc* **2014,** *136* (42), 15079-85.

30.Bryantsev, V. S.; Hay, B. P., De novo structure-based design of bisurea hosts for tetrahedral oxoanion guests. *Journal of the American Chemical Society* **2006,** *128* (6), 2035-2042.

31.Jia, C. D.; Wu, B. A.; Li, S. G.; Huang, X. J.; Zhao, Q. L.; Li, Q. S.; Yang, X. J., Highly Efficient Extraction of Sulfate Ions with a Tripodal Hexaurea Receptor. *Angew Chem Int Edit* **2011,** *50* (2), 486-490.

32.Kadam, S. A.; Martin, K.; Haav, K.; Toom, L.; Mayeux, C.; Pung, A.; Gale, P. A.; Hiscock, J. R.; Brooks, S. J.; Kirby, I. L.; Busschaert, N.; Leito, I., Towards the discrimination of carboxylates by hydrogen-bond donor anion receptors. *Chemistry* **2015,** *21* (13), 5145-60.

33.Zhang, Y.; Zhang, R.; Zhao, Y.; Ji, L.; Jia, C.; Wu, B., Anion binding of tris-(thio)urea ligands. *New Journal of Chemistry* **2013,** *37* (8), 2266.

34.Dietrich, B.; Fyles, D. L.; Fyles, T. M.; Lehn, J.-M., 280. Anion Coordination Chemistry: Polyguanidinium Salts as Anion Complexones. *Helv. Chim. Acta* **1979,** *62* (8), 2763-2787.

35.Dixon, R. P.; Gieib, S. J.; Hamilton, A. D., Molecular Recognition: Bis-Acylguanidiniums Provide a Simple Family of Receptors for Phosphodiesters. *J Am Chem Soc* **1992,** *114*, 365-366.

36.Fan, E.; Van Arman, S. A.; Kincaid, S.; Hamilton, A. D., Molecular Recognition: Hydrogen-Bonding ReceptorsThat Function in Highly Competitive Solvents. *J Am Chem Soc* **1993,** *115*, 369-370.

37.Linton, B. R.; Goodman, M. S.; Fan, E.; van Arman, S. A.; Hamilton, A. D., Thermodynamic Aspects of Dicarboxylate Recognition by Simple Artificial Receptors. *The Journal of Organic Chemistry* **2001,** *66* (22), 7313-7319.

38.Dietrich, B.; Fyles, D. L.; Fyles, T. M.; Lehn, J. M., Anion Coordination Chemistry - Polyguanidinium Salts as Anion Complexones. *Helv Chim Acta* **1979,** *62* (8), 2763-2787.

39.Gross, R.; Durner, G.; Gobel, M. W., Beschleunigung von Substitutionsreaktionen eines Phosphorsaurediesters durch Bis(g uanidinium)-Verbindung en. *Liebigs Ann. Chem.* **1994**, 49-58.

40.Jubian, V.; Dixon, R. P.; Hamilton, A. D., Molecular Recognition and Catalysis. Acceleration of Phosphodiester Cleavage by a Simple Hydrogen-Bonding Receptor *J Am Chem Soc* **1992,** *114*, 1120-1121.

41.Schmidtchen, F. P., Synthese symmetrisch substituierter bicyclischer Guanidine. *Chemische Berichte* **1980,** *113* (6), 2175-2182.

42.Schmidtchen, F. P., Synthese makrotricyclischer Amine. *Chem. Ber.* **1980,** *113*, 864-874.

43.Ariga, K.; Anslyn, E. V., Manipulating the Stoichiometry and Strength of Phosphodiester Binding to a Bisguanidine Cleft in DMSO/Water Solutions *J. Org. Chem.* **1992,** *57*, 417-419.

44.Kneeland, D. M.; Ariga, K.; Lynch, V. M.; Huang, C.-Y.; Anslyn, E. V., Bis(alkylguanidinium) Receptors for Phosphodiesters: Effect of Counterions, Solvent Mixtures, and Cavity Flexibility on Complexation *J Am Chem Soc* **1993,** *115*, 10042-10055.

45.Kurzmeier, H.; Schmidtchen, F. P., Abiotic Anion Receptor Functions. A Facile and Dependable Access to Chiral Guanidinium Anchor Groups *J. Org. Chem.* **1990,** *55*, 3749-3755.

46.Nilsson, M.; Nash, K. L., Review Article: A Review of the Development and Operational Characteristics of the TALSPEAK Process. *Solvent Extraction and Ion Exchange* **2007,** *25* (6), 665-701.

47.Nilsson, M.; Nash, K. L., Trans-Lanthanide Extraction Studies in the TALSPEAK System: Investigating the Effect of Acidity and Temperature. *Solvent Extraction and Ion Exchange* **2009,** *27* (3), 354-377.

48.Cotton, S., *Lanthanide and Actinide Chemistry*. John Wiley & Sons, Ltd: West Sussex, 2006.

49.Cotton, F. A.; Wilkinson, G., *Advanced Inorganic Chemistry*. fifth Edition ed.; John Wiley & Sons, Inc.: New York, 1988; p 1455.

50.Choppin, G. R.; Lilijenzin, J.-O.; Rydberg, J.; Ekberg, C., *Radiochemistry and Nuclear Chemistry*. Academic Press: New York, 2013.

51.Leggett, C. J.; Liu, G.; Jensen, M. P., Do Aqueous Ternary Complexes Influence the TALSPEAK Process? *Solvent Extraction and Ion Exchange* **2010,** *28* (3), 313-334.

52.Braley, J. C.; Grimes, T. S.; Nash, K. L., Alternatives to HDEHP and DTPA for Simplified TALSPEAK Separations. *Industrial & Engineering Chemistry Research* **2012,** *51* (2), 629-638.

53.Braley, J. C.; McAlister, D. R.; Philip Horwitz, E.; Nash, K. L., Explorations Of Talspeak Chemistry In Extraction Chromatography: Comparisons of TTHA with DTPA and HDEHP with HEH[EHP]. *Solvent Extraction and Ion Exchange* **2013,** *31* (2), 107-121.

54.Nash, K. L., The Chemistry of TALSPEAK: A Review of the Science. *Solvent Extraction and Ion Exchange* **2014,** *33* (1), 1-55.

55.Weaver, B.; Kappelmann, F. A. *TALSPEAK: A New Method Of Separating Americium and Curium From The Lanthanides By Extraction From An Aqueous Solution Of An Aminopolyacetic Acid Complex With A Monoacidic Organophosphate Or Phosphate*; ORNL-3559; Oak Ridge National Laboratory: Oak Ridge, TN, 1964, 1964; pp 1-60.

56.Hancock, R. D.; Martell, A. E., Ligand Design for Selective Complexation of Metal-Ions in Aqueous-Solution. *Chem. Rev.* **1989,** *89* (8), 1875-1914.

57.Martell, A. E.; Hancock, R. D., *Metal Complexes in Aqueous Solutions*. Plenum Press: New York, 1996; p 253.

58.Shannon, R. D.; Prewitt, C. T., Effective Ionic Radii in Oxides and Fluorides. *Acta Cryst. Sec. B* **1969,** *B25*, 925-946.

59.Shannon, R. D., Revised Effective Ionic-Radii and Systematic Studies of Interatomic Distances in Halides and Chalcogenides. *Acta Crystallogr A* **1976,** *32* (Sep1), 751-767.

60.Pearson, R. G.; Edwards, J. O., The Factors Determining Nucleophilic Reactivities. *JACS* **1962,** *84*, 16-24.

61.Pearson, R. G., Hard and Soft Acids and Bases. *JACS* **1963,** *85* (22), 3533-3539.

62.Pearson, R. G., Recent Advances in the Concept of Hard and Soft Acids and Bases. *J. Chem. Ed.* **1987,** *64* (7), 561-567.

63.Pearson, R. G., Absolute Electronegativity and Hardness: Application to Inorganic Chemistry. *Inorg. Chem.* **1988,** *27*, 734-740.

64.Pearson, R. G., The Principle of Maximum Hardness. *Acc. Chem. Res.* **1993,** *26*, 250-255.

65.Wilson, A. M.; Bailey, P. J.; Tasker, P. A.; Turkington, J. R.; Grant, R. A.; Love, J. B., Solvent extraction: the coordination chemistry behind extractive metallurgy. *Chem Soc Rev* **2014,** *43* (1), 123-34.

66.Carolan, A. N.; Cockrell, G. M.; Williams, N. J.; Zhang, G.; VanDerveer, D. G.; Lee, H. S.; Thummel, R. P.; Hancock, R. D., Selectivity of the Highly Preorganized Tetradentate Ligand 2,9-Di(pyrid-2-yl)-1,10-phenanthroline for Metal Ions in Aqueous Solution, Including Lanthanide(III) Ions and the Uranyl(VI) Cation. *Inorganic Chemistry* **2013,** *52* (1), 15-27.

67.Hancock, R. D., The pyridyl group in ligand design for selective metal ion complexation and sensing. *Chem Soc Rev* **2013,** *42* (4), 1500-24.

68.Hay, B. P.; Hancock, R. D., The role of donor group orientation as a factor in metal ion recognition by ligands. *Coordination Chemistry Reviews* **2001,** *212*, 61-78.

69.Hancock, R. D.; Melton, D. L.; Harrington, J. M.; McDonald, F. C.; Gephart, R. T.; Boone, L. L.; Jones, S. B.; Dean, N. E.; Whitehead, J. R.; Cockrell, G. M., Metal ion recognition in aqueous solution by highly preorganized non-macrocyclic ligands. *Coordination Chemistry Reviews* **2007,** *251* (13-14), 1678-1689.

70.Hudson, M. J.; Harwood, L. M.; Laventine, D. M.; Lewis, F. W., Use of soft heterocyclic N-donor ligands to separate actinides and lanthanides. *Inorg Chem* **2013,** *52* (7), 3414-28.

71.Whittaker, D. M.; Griffiths, T. L.; Helliwell, M.; Swinburne, A. N.; Natrajan, L. S.; Lewis, F. W.; Harwood, L. M.; Parry, S. A.; Sharrad, C. A., Lanthanide speciation in potential SANEX and GANEX actinide/lanthanide separations using tetra-N-donor extractants. *Inorg Chem* **2013,** *52* (7), 3429-44.

72.Lewis, F. W.; Harwood, L. M.; Hudson, M. J.; Drew, M. G.; Desreux, J. F.; Vidick, G.; Bouslimani, N.; Modolo, G.; Wilden, A.; Sypula, M.; Vu, T. H.; Simonin, J. P., Highly efficient separation of actinides from lanthanides by a phenanthroline-derived bis-triazine ligand. *J Am Chem Soc* **2011,** *133* (33), 13093-102.

1.5 Appendix 1A Figures and Tables for Chapter 1

Table 1.1. Anion radii, valence charge, and hydration energies.

Anion	Charge	Radii (Å)	Energy of Hydration[11] (kJ/mol)
Nitrate	−1	1.79	–306
Sulfate	−2	2.30	–1090
Chromate	–2	2.40	–958
Phosphate	−3	2.38	–2773

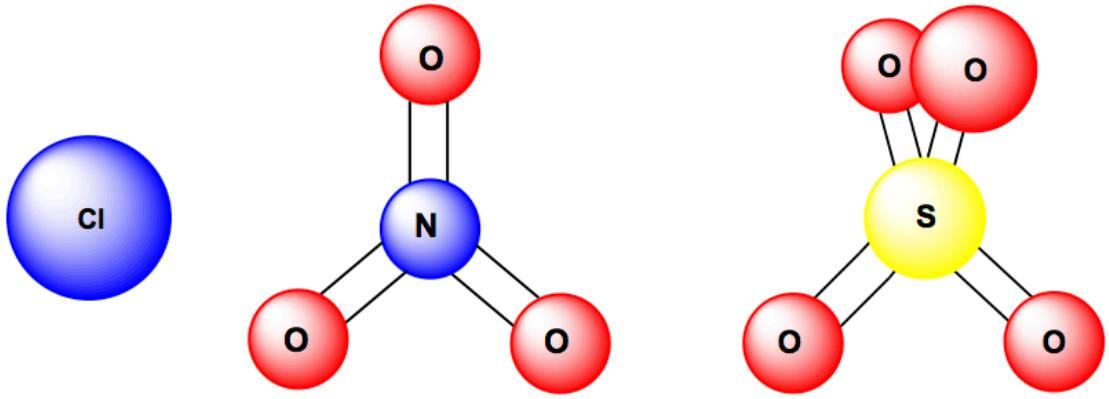

Figure 1.1. Typical geometries of Anions. (1) Spherical (Halide), (2) Trigonal Planar (Carbonate, Nitrate, etc.), (3) Tetrahedral (Sulfate, Phosphate, etc.).

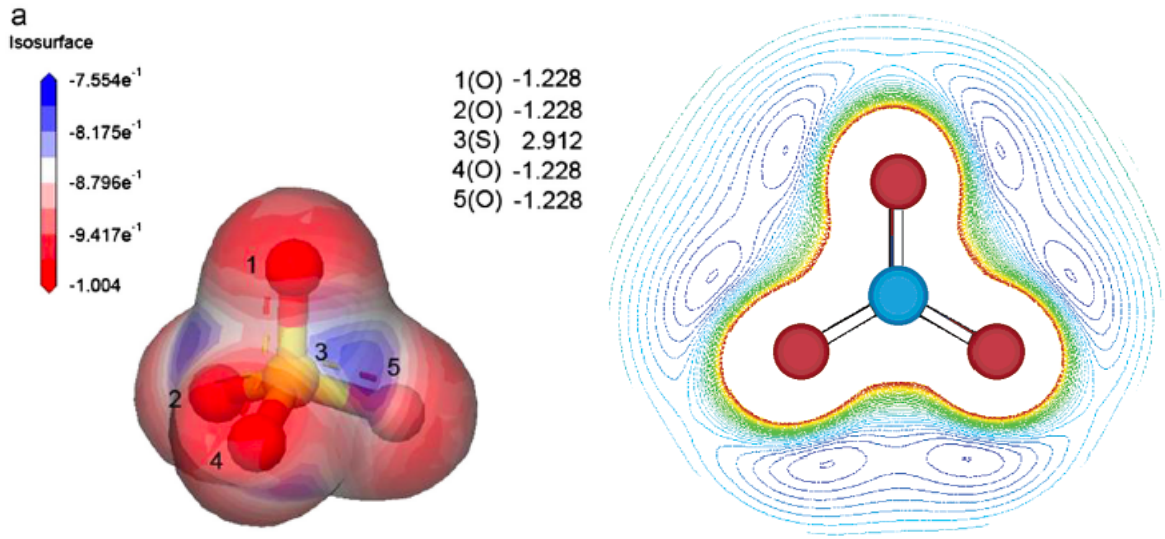

Figure 1.2. Delocalization of charge across oxoanions. Electrostatic potential and Mulliken partial charge for sulfate (Reproduced with permission from Journal) [12] is shown on the left and a contour map of the electrostatic potential for a nitrate (Reprinted with permission from {Hay, B. P.; Gutowski, M.; Dixon, D. A.; Garcza, J.; Vargas, R.; Moyer, B. A.. *JACS* 2004, *126*, 7925-7934.}. Copyright {2004} American Chemical Society.) [13] is shown on the right.

Table 1.2. Dielectric constants and Hildebrand Constants for various solvents arranged in order of decreasing ε.

Solvent	ε[b]	δ/MPa$^{1/2}$ [e]
Water	80.1	47.9
Nitrobenzene	34.82	20.5
1,2-Dichloroethane	10.36	18.2
1-Octanol	10.34[d]	21.1
Tri-*n*-butylphosphate	7.959[c]	21.3[f]
Toluene	2.379	18.2
n-Dodecane	2.02[c]	16.2
Isopar L	~2.00	14.9[g]

[a]As determined by NMR spectroscopy with internal standard. [b]Taken from a published tabulation.[14] [c]Reported for 30 °C. [d]Reported for 20 °C. [e]Taken from a published tabulation unless otherwise noted.[15] [f]From Bermudez[16] [g]From Durkee.[17]

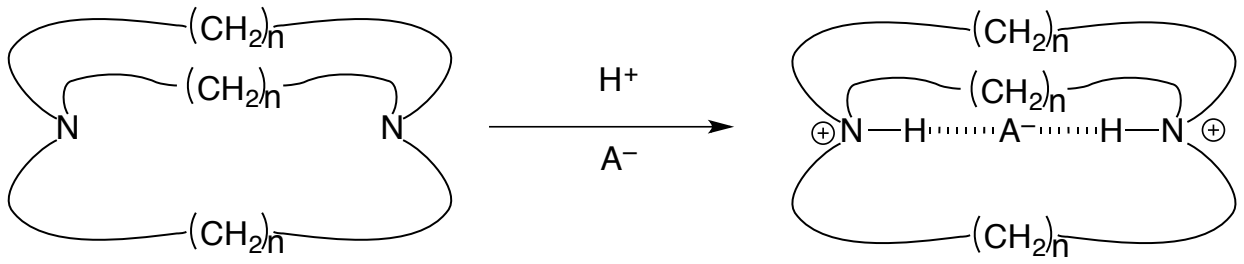

Figure 1.3. Structure of one of the first anion receptors reported by Simmons and Park in the 1960s. On the left is the receptor deprotonated and therefore will not interact favorable with anions, while the structure of the right can interact with anions because it has become protonated in acidity media.

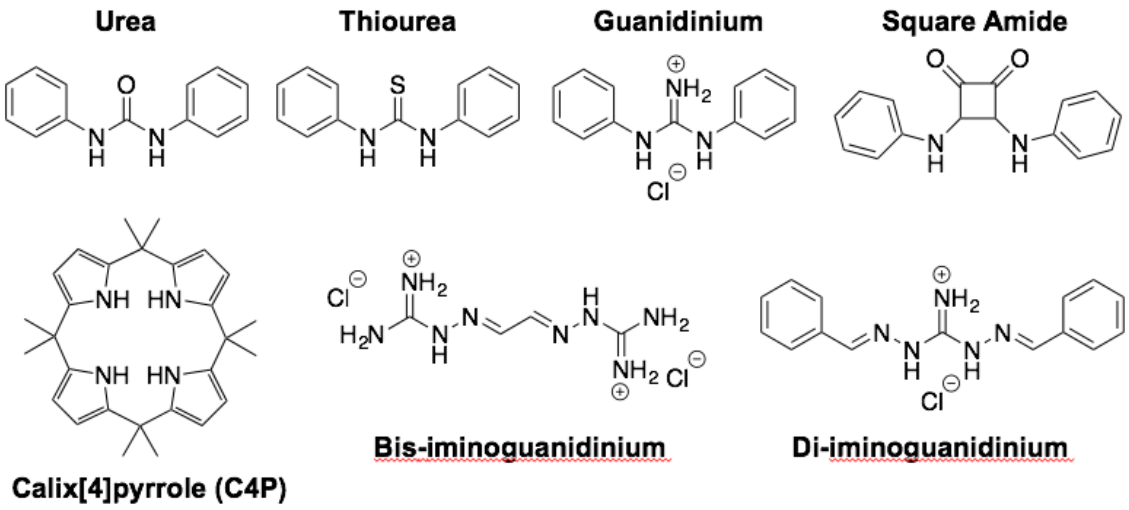

Figure 1.4. Series of anion receptors with hydrogen bonding donors**.**

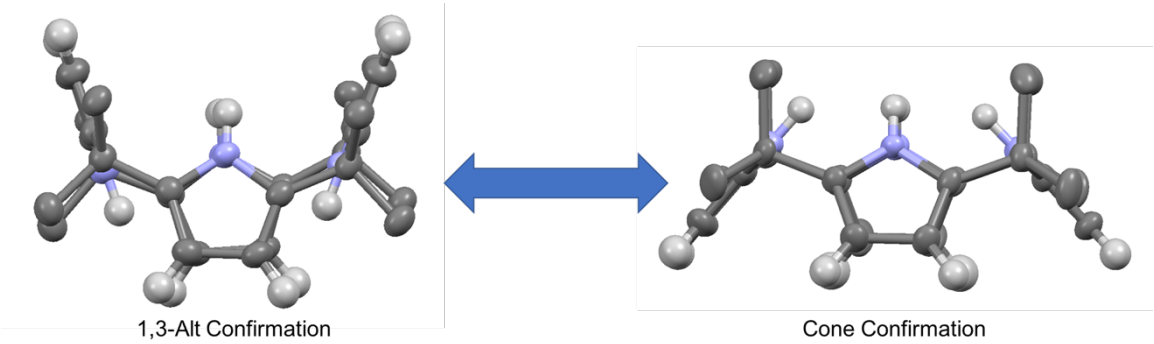

Figure 1.5. Conformations of C4P the unbound 1,3-alt conformation (left) and bound cone conformation (right). The hydrogens have been removed from the eight methyl groups in the C4P to make it easier to see the core of the structure.

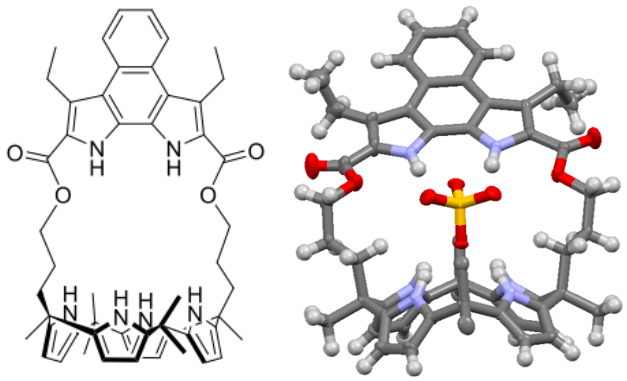

Figure 1.6. Structure of a unbound strapped C4P and crystal structure of a strapped C4P bound to sulfate.[29]

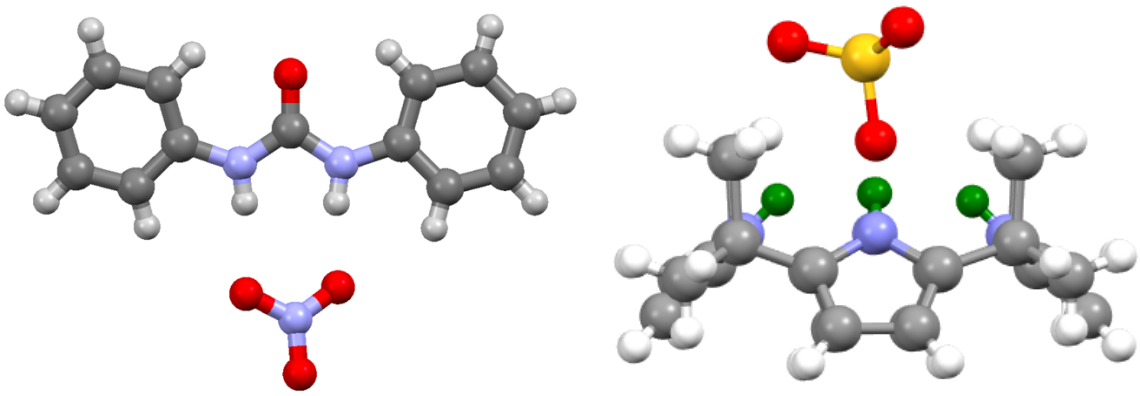

Figure 1.7. On the right: Crystal structure of urea bound along the edge of a nitrate by coordinating to two of the oxygens of nitrate. On the left: Crystal Structure of C4P bound to a single oxygen of a sulfate is an example of axial binding.

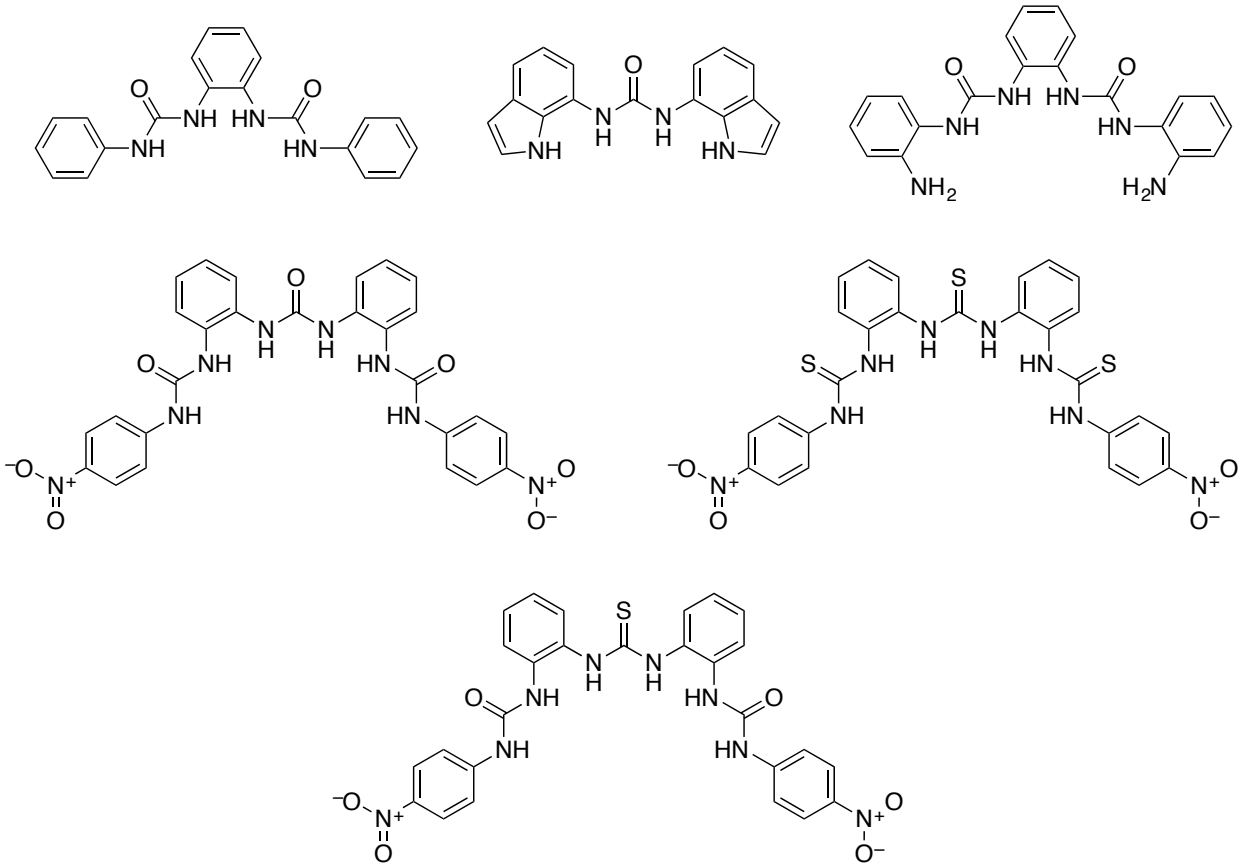

Figure 1.8. Multi-urea/thiourea receptors.

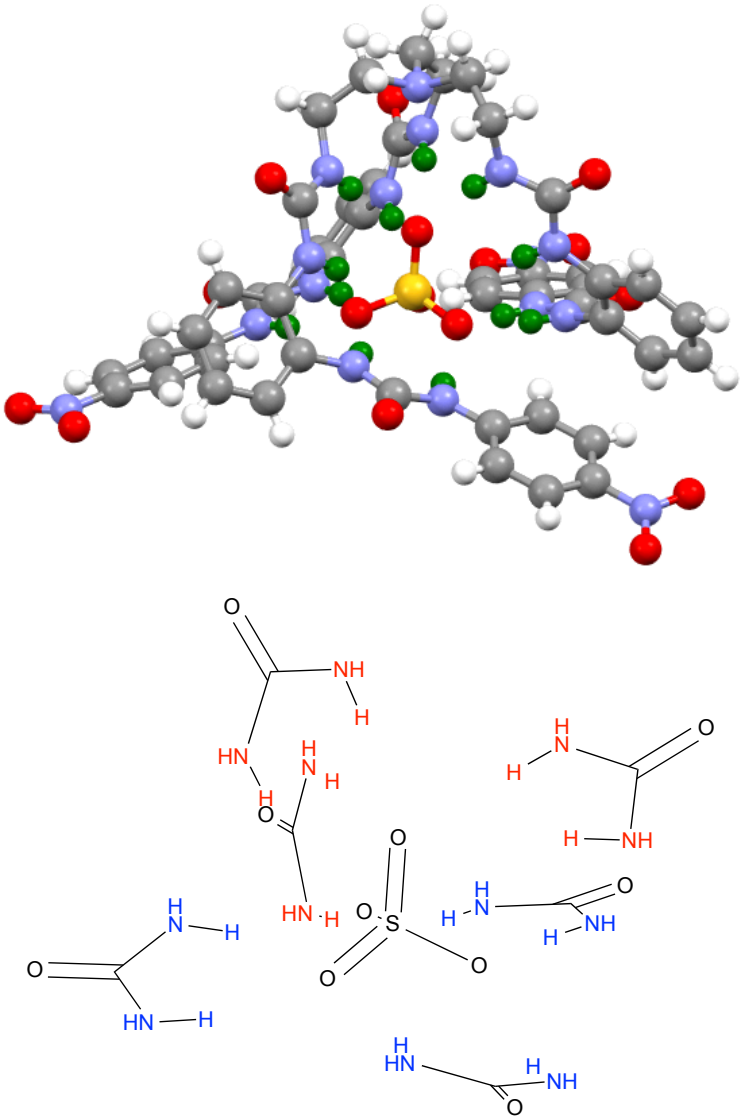

Figure 1.9. Top: Crystal structure of a hexaurea tripodal based anion receptor bound to sulfate, not shown are two quaternary ammoniums present in the crystal structure to offset the -2 charge of the sulfate. Bottom: A Chemdraw representation showing how the six ureas are bound to the sulfate and their arrangement around the sulfate (red NH's of urea are bound along the axial region, while blue NHs are bound equatorial region of the sulfate).[31]

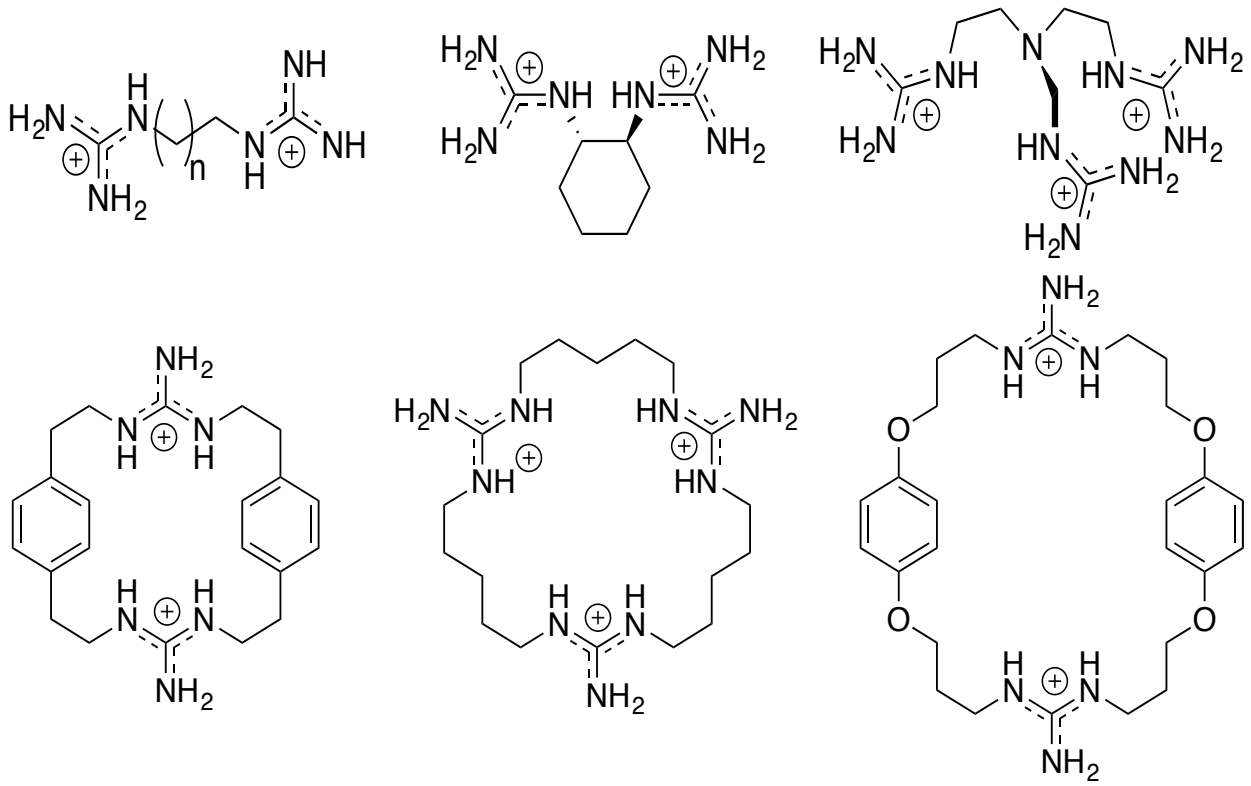

Figure 1.10. Examples of polyguanidiniums synthesized by Lehn and co-workers[38] in the late 1970s. The anion counter balancing the guanidiniums have not been shown in the figure above.

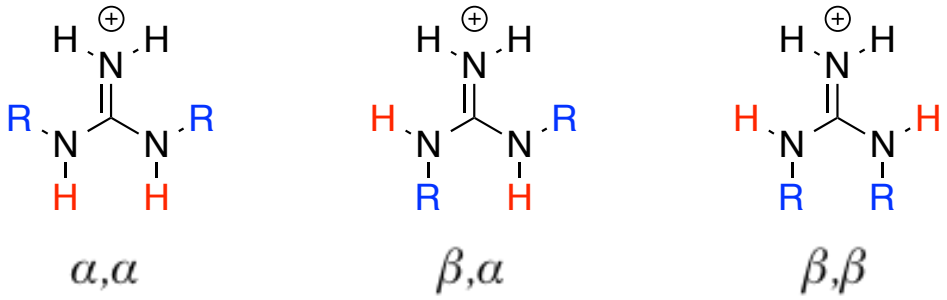

Figure 1.11. Conformations of a substituted –NH guaindiums.

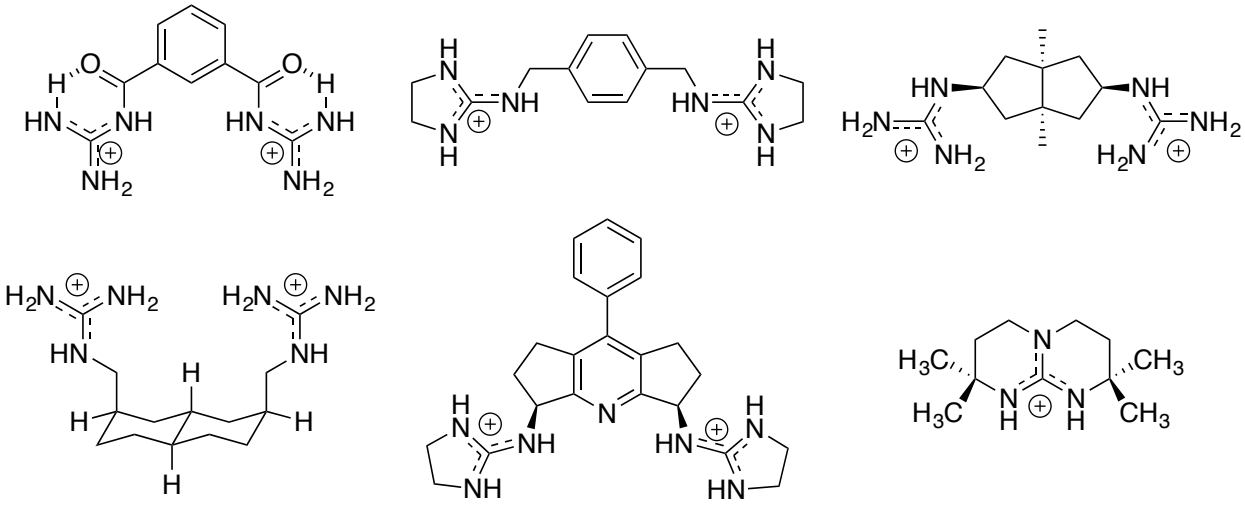

Figure 1.12. Structures of Preorganized guanidinium receptors.

$$
\begin{tikzcd}
{}^{238}_{92}U \arrow[r, "(n,\gamma)"] & {}^{239}_{92}U \arrow[r, "\beta^-"] & {}^{239}_{93}Np \arrow[r, "\beta^-"] & {}^{239}_{94}Pu \arrow[r, "2(n,\gamma)"] & {}^{241}_{94}Pu \arrow[r, "\beta^-"] & {}^{241}_{95}Am \arrow[r, "(n,\gamma)"] & {}^{242}_{95}Am \arrow[r, "(n,\gamma)"] \arrow[d] & {}^{243}_{95}Am \\
 & & & & & & {}^{242}_{96}Cm &
\end{tikzcd}
$$

Figure 1.13. Pathways for the production of ^{241}Am, ^{243}Am, and ^{242}Cm. Not listed in the figure are the half-life of the isotopes for the beta decays ($\boldsymbol{\beta^-}$), the neutron and gamma absorption ($\boldsymbol{n,\gamma}$) by the isotopes occur instantaneously.

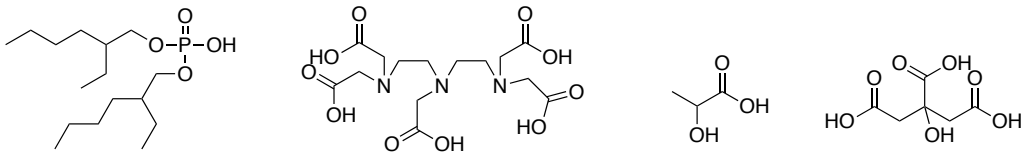

DEHPA **DTPA** **Lactic Acid** **Citric Acid**

Figure 1.14. TALSPEAK chemical components.

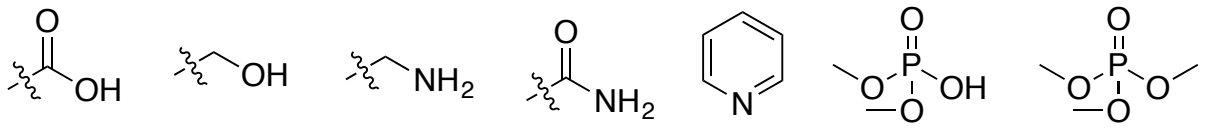

Figure 1.15. Donor Groups for minor actinides.

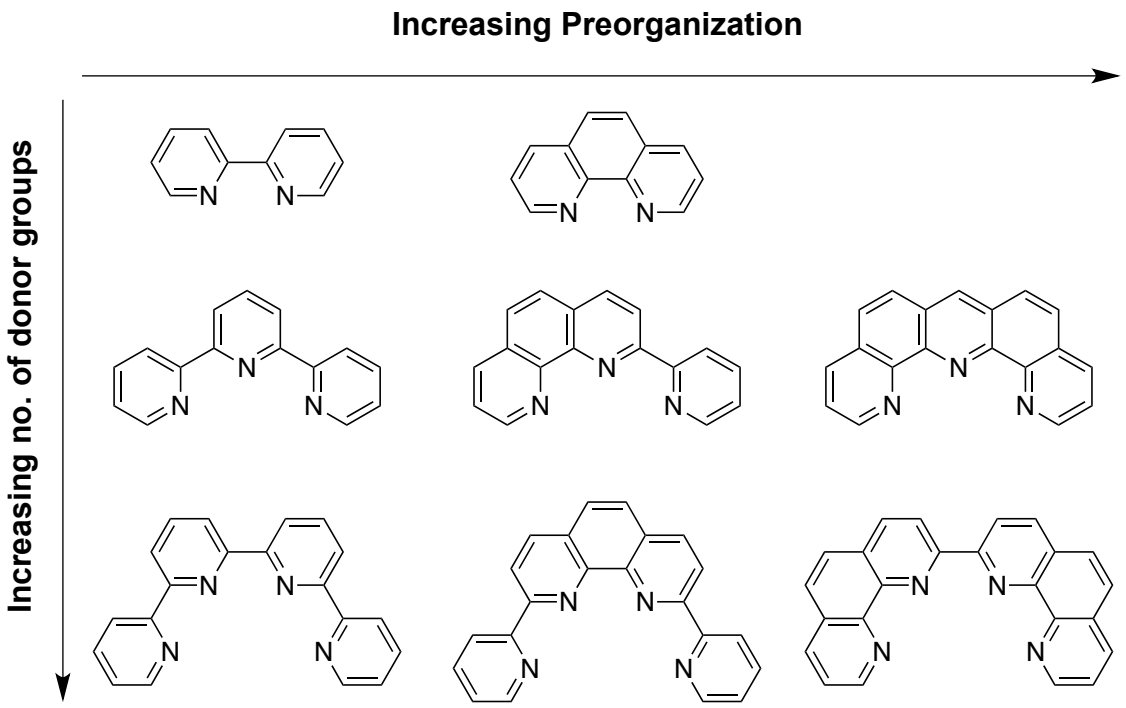

Figure 1.16. Series of ligands used to demonstrate the how increasing levels of both preorganization and number of donor groups can be obtains using pyridine based ligands as an example.

Chapter 2 : $\alpha, \alpha', \alpha'', \alpha'''$-*Meso*-Tetrahexyltetramethyl-Calix[4]Pyrrole: An Easy-to-Prepare, Isomerically Pure Anion Extractant With Enhanced Solubility in Organic Solvents

Publication Statement for Chapter 2

Reference for Original Article:

Williams N.J.; Bryanstev, V.S.; Custelcean R.; Seipp, C.A.; Moyer B.A.; "$\alpha, \alpha', \alpha'', \alpha'''$-*meso*-Tetrahexyltetramethyl-calix[4]pyrrole: An easy-to-prepare, isomerically pure anion extractant with enhanced solubility in organic solvents." *Supramol. Chem.* **2016**, 28, 176–187.

Individual Author Contribution(s):

Williams, N. J. – Synthesis (including isolation and identification), extraction studies, growing crystals of X-ray structural analysis, determined binding constants, writing

Bryanstev, V. S. – Theoretical calculations, writing

Custelcean, R. – Ran and determined X-ray structures of free ligand and bound complexes.

Seipp, C. A. – Determined binding constants and writing

Moyer, B. A. – Writing and edited manuscript, Advisor of N. J. Williams and PI of overall project.

Journals Policy/Permission/Agreement for Reproduction of Article

Copyright Clearance Center RightsLink®

Home | Account Info | Help

Taylor & Francis
Taylor & Francis Group

Title: α,α′,α″,α‴-meso-tetrahexyltetramethyl-calix[4]pyrrole: an easy-to-prepare, isomerically pure anion extractant with enhanced solubility in organic solvents

Author: Neil J. Williams, Vyacheslav S. Bryanstev, Radu Custelcean, et al

Publication: Supramolecular Chemistry

Publisher: Taylor & Francis

Date: Feb 1, 2016

Copyright © 2016 Taylor & Francis

Logged in as:
Neil Williams
Account #:
3001100017
LOGOUT

Thesis/Dissertation Reuse Request

Taylor & Francis is pleased to offer reuses of its content for a thesis or dissertation free of charge contingent on resubmission of permission request if work is published.

BACK | CLOSE WINDOW

Copyright © 2017 Copyright Clearance Center, Inc. All Rights Reserved. Privacy statement. Terms and Conditions.
Comments? We would like to hear from you. E-mail us at customercare@copyright.com

A version of this chapter was originally published by Neil J. Williams, Vyacheslav S. Bryanstev, Radu Custelcean, Charles A. Seipp, and Bruce A. Moyer in *Supramolar Chemistry*

Williams N.J.; Bryanstev, V.S.; Custelcean R.; Seipp, C.A.; Moyer B.A.; "$\alpha, \alpha', \alpha'', \alpha'''$-*meso*-Tetrahexyltetramethyl-calix[4]pyrrole: An easy-to-prepare, isomerically pure anion extractant with enhanced solubility in organic solvents." *Supramol. Chem.* **2016**, 28, 176–187.

The article used as Chapter 2 was modified in the following manner; the formatting was adapted to fit the formatting required by the University of Tennessee Knoxville, the figures and tables were renumbered to make all figures in the ensuing document contiguous. The work/research of the done by the student in the articles is as follows conception, synthesis, radiochemistry, and contributed to the writing for the published work.

Abstract

$\boldsymbol{\alpha, \alpha', \alpha'', \alpha'''}$–*meso*-Tetrahexyltetramethyl-calix[4]pyrrole is easily obtained as a single diastereomer in a one-pot reaction. It exhibits enhanced solubility in organic solvents, including aliphatic solvents, relative to its parent *meso*-octamethylcalix[4]pyrrole (**1**). Somewhat surprisingly, the tetrahexyl derivative (**2**) complexes with tributylmethylammonium chloride in chloroform more strongly than does **1** as shown by NMR titrations. However, **1** and **2** exhibit comparable complexation strength in extraction

experiments, the difference between the NMR and extraction results being attributed to the effect of organic-phase water in the extraction systems. Mass-action analysis indicates the formation of the predominant complex $TBMA^+$(1 or 2)Cl^- in both NMR and extraction systems, and equilibrium constants are reported. X-ray crystal structures were obtained for the free ligand **2** and its complex with tetramethylammonium chloride. The free ligand crystallizes in the 1,3-alt conformation with equatorial hexyl arms. In the chloride complex with **2** in its cone conformation, the hexyl arms adopt an axial orientation, enveloping the anion. DFT calculations show this binding conformation to be the most stable, mostly owing to destabilizing steric interactions involving the pyrrole C–H and alkyl C–H groups positioned equatorially.

2.1 Introduction

Most if not all lines of inquiry in the field of solvent extraction chemistry distil down to two fundamental questions. First, dating back to Nernst, how can we predict and control the partitioning of a species between immiscible liquid phases?[1–3] Second, when bulky hydrophobic groups are substituted on Lewis acids or bases, what is the resulting effect on the interaction of the modified molecule with other species, including self-interactions, binding, and especially selective extraction?[4,5] Introduced by analytical chemists in the 1930s and even earlier, solvent extraction developed as an outgrowth of the field of coordination chemistry.[6] Its distinguishing feature relative to classical coordination chemistry was and still is the use of hydrophobic ligands to effect liquid-liquid distribution of aqueous ions to water-immiscible liquid phases.[5] The effects of the hydrophobic groups

on selectivity, affinity, aggregation, phase stability, interfacial properties, kinetics—that is, virtually all properties of an extraction system—have proven to be profound. Further, the means to confer hydrophobicity are virtually limitless. Even if the chemist confines attention to the use of alkyl groups as the sole type of hydrophobic substituent, the choices regarding point of attachment, number of attachments, size, and branching present a bewildering array of choices.

As molecular sophistication and corresponding means to control selectivity have leaped forward in recent years by the introduction of principles of molecular recognition and supramolecular chemistry to the field of solvent extraction, the familiar question regarding the effect of hydrophobic groups remains paramount. In fact, the number of possible means to confer hydrophobicity has grown exponentially, increasing the potential complexity of the problem. Moreover, given that binding complementarity and preorganization of today's multi-donor designer ligands depend critically on conformation,[7,8] substituent effects become even more important through their effect on conformation, as can be seen in many catalogued examples.[9] The exploration of crown ethers for the selective extraction of metal cations[10] nicely illustrates these realities. Unsubstituted crown ethers are impractically water-soluble to be useful in solvent extraction, and thus workers devoted considerable early efforts to finding suitably hydrophobic derivatives.[11–13] The result was a rich chapter of chemistry involving a large number of crown ether variants whose properties are directed by the nature of the hydrophobic substituents.[10] Detailed conformational analysis of crown ethers[14] related substituent effects on binding affinity to torsional strain in the crown backbone.

Conformational effects were quantitatively correlated with extraction strength of substituted crown ethers for alkali metals.[15–17]

With more recent growth in the study of anion receptors for selective anion separation by solvent extraction,[18] we are naturally led to this now-classic question of how hydrophobic substituents affect binding and extraction, only applied to anions. The simple macrocycle *meso*-octamethylcalix[4]pyrrole (C4P, **1**, see **Figure 2.1**) has shown great promise as an anion receptor by itself[19] and as a useful platform for countless modifications to introduce functionality on either the pyrrole units or the *meso* carbons.[20–25] While the versatility of calixpyrrole chemistry has proven to be astonishing, the limited solubility of calixpyrroles has at times been frustrating to research and likely to applications in industry. In our laboratory, we have performed a number of investigations using simple C4P in liquid-liquid distribution systems in which its concentrations have been by necessity rather low and confined to polar solvents.[26–29] It would be highly desirable to increase its solubility to much greater than a few millimolar and in particular to effect solubility in the hydrocarbon diluents favored in practical extraction systems (e.g., dodecane). Keeping in mind the economics and "greenness" of preparing an alkyl-substituted C4P, it is advantageous to employ a one-step condensation of an appropriate ketone with pyrrole. Ketone choices should be made in such a way that the properties of C4P are preserved or even enhanced. One of the properties of special interest entails the ability of C4P in its cone conformation to recognize monoatomic anions or groups and to accommodate an appropriately sized cation in the resulting aromatic-lined cup on the opposite side of the

molecule.(*30*) The cation can be a large univalent ion like Cs^+, for example, or the methyl group of an organic cation like tributylmethylammonium or methylimmidazolium.[26–31]

In this study, we present the synthesis and characterization of the lipophilic alkyl-substituted C4P $\alpha, \alpha', \alpha'', \alpha'''$-*meso*-tetrahexyltetramethyl-calix[4]pyrrole (**2**) (**Figure 2.1**). The parent *meso*-octamethylcalix[4]pyrrole (**1**) was used as the control for comparison. The synthesis and isolation of the alkylated calix[4]pyrrole was simple and straightforward with **2** being the major product in a one-step reaction. Solubilities of **1** and **2** in several water-immiscible diluents were determined by ^{1}H-NMR. The binding and stoichiometry of the **1** and **2** were determined by NMR titrations and liquid−liquid extraction experiments. X-ray crystallography and DFT calculations were employed to understand the effect of the alkyl substitution on conformation and binding. For simplicity in the comparison, we examined only Cl^- as the guest anion, and tributylmethylammonium as the cation in keeping with the previous data collected for the interaction of these ions with C4P.[28,29,31]

2.2 Results and Discussion

The solubilities of **1** and **2** are compared here in common water-immiscible organic solvents, ranging from a highly polar ionizing solvent (nitrobenzene) to nonpolar hydrocarbons like Isopar L (isoparafinic kerosene) and *n*-dodecane. Hydrogen-bond donor solvents 1-octanol and, more weakly, chloroform, were included along with the electron-pair donor solvent tributyl phosphate (TBP). In the case of TBP, it was of interest to determine if there might be a special binding interaction with the calixpyrroles

manifested in increased solubility. Results are given in **Table 2.1**, where the solvents are arranged in order of decreasing Hildebrand solubility parameter δ. The dielectric constants for the respective solvents are also shown.

As may be seen in **Table 2.1**, the sought increase in organic-phase solubility upon long-chain alkyl substitution was achieved. Except for water, for which the solubility was below detection (<0.005 mM), an increase in solubility for **2** relative to **1** was seen in every case. Even more encouraging was the increase in solubility in aliphatic solvents, exceeding an order of magnitude for the process solvent Isopar L. The smallest increase was for the two solvents, nitrobenzene and 1,2-dichloroethane, in which the unsubstituted **1** is the most soluble. TBP did not give an appreciable solubility and therefore appears not to engage in a special solvent-solute binding interaction.

The solubility behavior determined for the two calixpyrroles qualitatively follows the expectations of regular solution theory. As may be seen in **Table 2.1**, dielectric constant does not serve well in correlating the solubilities. Discounting water, at best a rough trend of increasing solubility with increasing dielectric constant can be seen, and discounting water admits that the correlation fails. On the other hand, regular solution theory[36] predicts a maximum (δ_{max}), which ideally should occur where the solubility parameter for solvent matches that of the solute. Arranging the solvents in decreasing order of δ in fact reveals a maximum at 18.2 $MPa^{1/2}$ for **1**. The solubility falls off for the most cohesive solvents 1-octanol and TBP and for the least cohesive solvents toluene, *n*-dodecane, and Isopar L.

We estimated the value of δ for **1** to be 22.6 $MPa^{1/2}$ [26] from group parameters[33], significantly greater than δ_{max}. The lower value of δ_{max} than expected could reflect the conformational flexibility of the C4P ring, which could allow some internal "matching" of **1** to the solvent environment. Or the mismatch may just reflect the gross assumptions of regular solution theory and the recognized difficulty in applying it to polar solvents.[33] Calixpyrrole **2** also exhibits a maximum, but it is very broad, tailing off slowly toward lower values of δ, which may also result from the even greater conformational flexibility of this molecule.

2.2.1 NMR Titrations

The affinities of **1** and **2** for chloride in homogeneous solution were determined via NMR titrations (see ESI). Given previous results showing that C4P acts as an ion-pair receptor forming a supramolecular assembly with $TBMA^+Cl^-$,[28–32] the same salt was selected for this experiment, consisting of titrations of $TBMA^+Cl^-$ into solutions of either **1** or **2** in $CDCl_3$. In this medium, millimolar concentrations of $TBMA^+Cl^-$ and its complex with C4P behave as neutral species (completely ion-paired), and thus the observed reaction is

$$TBMA^+Cl^- + C4P \rightleftharpoons [TBMA^+(C4P)Cl^-] \quad (1)$$

It was found that the NMR spectra exhibit slow exchange in the $CDCl_3$ solution, where the free calixpyrrole and the complex exhibit two separate sets of peaks corresponding to each state. Slow exchange in NMR spectra is consistent with tight binding between host and guest. By contrast, most other binding reactions of calixpyrroles reported in the literature exhibit fast exchange.[19,22,31]

Binding constants for **1** and **2** corresponding to Eq. 1, expressed as log$K_{1:1}$, were found to be 4.14 ± 0.22 and 5.05 ± 0.34, respectively. For **1** binding $TBMA^+Cl^-$ in dichloromethane and 1,2-dichloroethane, values of log$K_{1:1}$ were previously determined to be 5.18 and 5.72, respectively, using isothermal calorimetry.[31] The order-of-magnitude smaller value for **1** in chloroform seen here is consistent with its weakly competitive C–H hydrogen-bond donor strength. The noted increase in log$K_{1:1}$ for **2** compared to **1** is of interest and was unexpected, as previous studies of calixpyrroles with a cyclohexyl ring present at the *meso*-carbons have shown a decrease in the binding affinity for chloride.(*19*) This unexpected result prompted more detailed investigation by X-ray crystallography and molecular computations as described farther below.

2.2.2 Extraction Results

While the NMR titration results indicate that **2** complexes $TBMA^+Cl^-$ nearly an order of magnitude more strongly than the control **1** in chloroform, **2** extracts $TBMA^+Cl^-$ into chloroform with nearly the same affinity as **1**. Previously we studied competitive chloride extraction by C4P in a synergistic mixture with an anion-exchange extractant, Aliquat 336, which may be described as methyltri(C_8,C_{10})ammonium chloride.(*29*) Employing $^{36}Cl^-$ radiometric tracer techniques, evidence was presented for the special role of the methyltrialkylammonium cation vs long-chain tetraalkylammonium cations that cannot insert into the cup of the C4P in its cone binding conformation. In the present study, a simpler system was employed that would enable a direct comparison of chloride extraction by **1** and **2** and allow inferences regarding ion-pair complex formation. The

experiment was carried out as a direct extraction of $TBMA^+Cl^-$ over a range of concentrations in aqueous solution traced with $^{36}Cl^-$ using 10 mM of **1** or **2** in chloroform. Results are shown in **Figure 2.2** in the form of a plot of the chloride distribution ratio ($D_{Cl} = [Cl^-]_{org}/[Cl^-]_{aq}$) vs the initial aqueous molarity of $TBMA^+Cl^-$. It may be seen that there is little enhancement in the extraction of chloride using **2** compared to **1**.

Figure 18 also suggests aggregation at high concentrations of $TBMA^+Cl^-$. As may be seen, the extraction of chloride by each calixpyrrole appears to climax at the same point, and the rising parts of the curves are linear with similar slopes (0.778 for **1** and 0.780 for **2**), which are subjected to more rigorous analysis below. The bending-over of the curves is due to loading of the calixpyrroles. However, instead of converging to a decreasing linear plot with slope exactly –1 as expected for a loaded system that refuses further uptake, the plots tend to level off, which we take to suggest further interaction of the calixpyrroles with additional $TBMA^+Cl^-$ ion pairs at high concentration. At 0.1 M initial $TBMA^+Cl^-$, the concentration of chloride in the organic phase is 11.0 mM for **1** and 13.4 mM for **2**. Subtracting the small organic-phase concentration of $TBMA^+Cl^-$ in the blank (0.0562 mM) from these values gives an excess extraction of 27.9% for **1** and 4.43% for **2** over the 10 mM that is expected for 1:1 loading. Such aggregation is not surprising in view of the highly dipolar nature of the charge-separated $TBMA^+(C4P)Cl^-$ putative core complex, which is likely to attract free $TBMA^+Cl^-$ ion pairs in solution.

A rigorous analysis of the slope behavior of the extraction data in **Figure 2.3** confirms a 1:1 extraction stoichiometry. The hypothesized reaction is

$$TBMA^{+}_{(aq)} + Cl^{-}_{(aq)} + C4P_{(org)} \rightleftharpoons [TBMA^{+}(C4P)Cl^{-}]_{(org)} \quad (2)$$

where the subscripts refer to the phase in which the species resides. The equilibrium quotient corresponding to Eq. 2 is written

$$K_{ex} = \frac{[TBMA^{+}(C4P)Cl^{-}]_{org}}{[TBMA^{+}]_{aq}\Upsilon\pm^{2}[Cl^{-}]_{aq}\Upsilon\pm^{2}[C4P]_{org}} \quad (3)$$

where we explicitly show the aqueous ion activity coefficients but assume the ratio of organic-phase activity coefficients is unity. Rearranging and taking the logarithm of both sides give

$$\log D_{Cl} = \log[Cl^{-}]_{aq}\gamma^{2} + \log[C4P]_{org} + \log K_{ex} \quad (4)$$

noting the identity $[TBMA^{+}]_{aq} = [Cl^{-}]_{aq}$. Equation 4 predicts that a plot of $\log D_{Cl}$ vs $\log([Cl^{-}]_{aq}\gamma_{\pm}^{2})$ should give an integral slope of 1, neglecting the small extraction of $TBMA^{+}Cl^{-}$ by chloroform alone. We employed the Debye Hückel relation[37] to estimate values of the aqueous activity coefficients $\gamma_{\pm}$ and the equilibrium aqueous Cl^{-} molarities. From the plots shown in **Figure 2.3**, we obtained slopes of 0.98 ± 0.011 and 0.97 ± 0.011 for **1** and **2** respectively, confirming the validity of the hypothesized extraction reaction in Eq. 2. A small loading correction was applied to the distribution ratio, where $D_{Cl,corr} = D_{Cl}([C4P]_{initial}/[C4P]_{free})$. Note that the extraction of $TBMA^{+}Cl^{-}$ by the blank also conforms to the expected slope, consistent with the simple background process

$$TBMA^{+}_{(aq)} + Cl^{-}_{(aq)} \rightleftharpoons [TBMA^{+}Cl^{-}]_{(org)} \quad (5)$$

and corresponding equilibrium quotient

$$K_{ex,TBMACl} = \frac{[TBMA^{+}Cl^{-}]_{org}}{[TBMA^{+}]_{aq}\Upsilon\pm^{2}[Cl^{-}]_{aq}\Upsilon\pm^{2}} \quad (6)$$

Equilibrium constants for the extraction processes can be calculated from the data, allowing an estimation of the homogeneous binding constants in the wet chloroform phase. From the blank extraction distribution ratios, free concentrations of $TBMA^+Cl^-$ in the aqueous and organic phases were calculated along with the aqueous activity coefficients $\gamma_\pm$ for each point in the range $[TBMA^+Cl^-]_{initial}$ = 0.01–0.1 M. Values of $K_{ex,TBMACl}$ were calculated for each data point and averaged to give the value shown in Table 2. A similar procedure was repeated for the extractions by **1** or **2** for each point in the range $[TBMA^+Cl^-]_{initial}$ = 0.001–0.02 M. Chloride distribution ratios were used to determine the equilibrium values of $[Cl^-]_{aq}$ and $[Cl^-]_{org}$. From the determined value of $K_{ex,TBMACl}$ shown in Table 4 the concentrations of $TBMA^+Cl^-$ in the organic phase were found for each point using **1** or **2**, which then gave the organic-phase concentrations of $TBMA^+$(**1**)Cl^- and $TBMA^+$(**2**)Cl^- from $[Cl^-]_{org} - [TBMA^+Cl^-]_{org}$. Table 4 gives the obtained values of $\log K_{ex,1}$ and $\log K_{ex,2}$. Subtraction of $\log K_{ex,TBMACl}$ from $\log K_{ex,1}$ and $\log K_{ex,2}$ then gives the homogeneous complexation constants $\log K_{cpx,1}$ and $\log K_{cpx,2}$ as shown in **Table 2.2**. For comparison the values of $\log K_{cpx,1}$ and $\log K_{cpx,2}$ determined above using NMR are shown also.

The homogeneous binding constants for **1** and **2** obtained from liquid-liquid extraction are similar in magnitude, which contrasts with the much greater complexation strength for **2** vs **1** observed in the NMR experiments. We attribute this difference to the presence of water in the liquid-liquid extraction experiments. It is known that chloride tends to retain part of its hydration sphere on extraction(*38*) and that this has an effect on anion

partitioning.(*39*). We presume that $TBMA^+Cl^-$ is hydrated by one or more waters in the chloroform phase. The calixpyrroles may also be hydrated. The complexation of the calixpyrroles with the quaternary ammonium salt will therefore result in at least a partial displacement of these waters of hydration. As will be shown below, the alkyl tails of **2** tend to envelop the bound Cl^- anion, contrasting with the complex for **1**, in which the bound Cl^- anion is much more exposed. Thus, it may be expected that a greater degree of hydration is lost in binding of Cl^- by **2** than by **1** in the chloroform phase, accounting for the observed decrease in homogeneous complexation by **2**.

2.2.3 Crystal Structures

The crystal structure of the free ligand shows that **2** adopts the commonly observed 1,3-*alt* conformation, with the alkyl chains oriented in the equatorial plane of the structure. In **Figure 2.4**, the top view of the free ligand shows pair-wise intramolecular interactions of the alkyl chains. When tetramethylammonium chloride (TMA^+Cl^-) is bound by **2** (**Figure 2.5**), the cone conformation is adopted with the alkyl chains reorienting from equatorial positions shown in the free ligand to the axial positions in the complex. Besides the four N–H···Cl^- hydrogen bond interactions, four additional C–H contacts occur from the first methylene units of the alkyl tails.

2.2.4 Computational Studies

Density functional theory calculations were performed to elucidate how the addition of the alkyl chain to the *meso*-carbon of the calix[4]pyrrole affects the structure of the ligand,

both in the unbound free state and in a 1:1 complex with chloride, and how it the modulates the chloride binding affinity. Analysis of the relative stabilities of various isomers allowed us to assess the role of steric hindrance and hydrophobic interaction in stabilizing particular conformations observed in the solid state.

Optimized structures and relative energies of two of the four possible stereoisomeric forms of **2** in the free state are shown in Figure 22. The most stable αααα form attains a conformation that maximizes the interaction of the two pairs of alkyl chains, while no such interaction is possible in the least stable αβαβ form. The difference in stability of the two stereoisomers (2.1 kcal/mol in chloroform and 3.8 kcal/mol in the gas phase) gives a measure of the interaction strength between the hydrophobic chains. In the case of the ααββ and αααβ stereoisomers, only a single pair of the alkyl chains is involved in the hydrophobic interaction and, thus, these isomers are expected to show intermediate stability between those of αααα and αβαβ. The relatively high yield of the αααα form is consistent with its greater stability, although the ratio to the other stereoisomers is somewhat higher than predicted by the Boltzmann distribution, suggesting preferential crystallization.

Before discussing relative stabilities of conformations attained in a 1:1 chloride complex of the tetraalkylated ligand **2**, it is instructive to analyze conformational preferences in a 1:1 chloride complex of ligand **3**, containing a single alkyl chain. Consistent with the results for the unsubstituted calix[4]pyrrole **1**, the monosubstituted ligand **3** maximizes the

interaction with the chloride anion by adopting a cone conformation of the calix[4]pyrrole core. As indicated in **Figure 2.7**, the conformers are only different in the position of the alkyl chain relative to the macrocycle cavity. For example, the most stable isomer is denoted **3**•Cl^-ax, indicating the axial position of the alkyl group. The two conformers with the alkyl group in the equatorial position can be oriented either in plane or out of plane formed by nitrogen atoms in the macrocycle. The former conformer (**3**•$Cl^-eq_{in\text{-}plane}$) is ~1.7 kcal/mol less stable than the global minimum, likely as a result of internal steric hindrance manifested by short intramolecular contacts (the shortest contact is 2.244 Å compared to 2.276 Å in **3**•Cl^-ax). Much higher steric strain is exerted in the complex with the out-of-plane orientation of the alkyl group (**3**•$Cl^-eq_{out\text{-}of\text{-}plane}$), as indicated by very short contacts between the alkyl and pyrrole CH hydrogen atoms (1.963 and 2.163 Å), significant deviation from the ideal *anti* conformation (the C_{meso}CCC dihedral angle is 142° compared to that of 169° in **3**•Cl^-ax), a substantial energy penalty compared to the global minimum (5.8 kcal/mol).

Based on steric arguments alone and in the absence of any interactions between four substituents at the *meso*-carbon atoms in the αααα stereorientation, the formation of the so-called deep cavity calix[4]pyrrole scaffold[22,40] in the presence of an anion is highly favorable. Indeed, in the case of the αααα stereoisomer, ligands with different aryl substituents form exclusively deep cavity structures when hydrogen-bonded to an anion.[22,40] The experimental results of the present work show that this is also the case with the aliphatic substituents, such as in ligand **2**. In fact, the lowest energy conformation

of **2**•Cl^- in the gas phase was obtained when geometry optimization was started using the X-ray structure, which contains only two symmetry-related gauche bonds in the linear hydrocarbon chains (**2**•Cl^-ax-1)(**Figure 2.8**). The conformer with all-anti bonds (**2**•Cl^-ax-2) is only 0.9 kcal/mol higher in energy than the solid-state structure **2**•Cl^-ax-1 in the gas phase and nearly isoenergetic to it in solution (0.03 kcal/mol). In accordance with the results for the monosubstituted ligand **3**, the presence of alkyl chains in the equatorial positions, either in plane or out of plane configuration, is highly unfavorable. Considering the energy penalty for introducing each additional equatorial group in **3**•$Cl^-eq_{in\text{-}plane}$ and comparing the result with the relative energy of **2**•$Cl^-eq_{in\text{-}plane}$, we can conclude that the intramolecular interactions of the hydrophobic chains play a secondary role in stabilizing **2**•Cl^-ax conformers (2.2–3.1 kcal/mol in the gas phase and 0.7 kcal/mol in solution). Finally, we note that in order to avoid severe steric clashes between alkyl and pyrrole C-rim hydrogen atoms, the most stable configuration of **3**•$Cl^-eq_{out\text{-}of\text{-}plane}$ is such that the two opposite pyrrole rings are rotated to adopt the 1,3-alternate conformation, typical for a free ligand in the unbound state.

By introducing “greasy” substituents in the *meso* positions of the calix[4]pyrrole ring, an important question arises as to how this modification modulates anion binding affinity. To address this question computationally, we have considered the following complexation reactions:

$$\text{Ligand} + Cl^- \rightarrow \text{Ligand}\bullet Cl^- \quad (7)$$

$$\text{Ligand} + N(CH_3)_4^+Cl^- \rightarrow N(CH_3)_4^+\bullet\text{Ligand}\bullet Cl^- \quad (8)$$

Reaction (7) represents a 1:1 binding of the Cl^- anion to the ligand, while reaction (8) includes the effect of ion-paring, which is known to play an important role in nonpolar solvents.[41] We expect a computational model using a simple implicit solvent representation does not provide the absolute complexation energies in solution, but rather tracks the changes in the binding energy from one ligand to the other.

Complexation energies computed at the M06-2X/6-31+G(d) and B3LYP-D3/6-31+G(d) level of theory are given in **Table 2.3**. The M06-2X density functional was parameterized to account for nonbonded and dispersion interactions by implicitly accounting for "medium-range" electron correlation,[42] while an empirical dispersion correction of Grimmer[43] was added to the B3LYP energy (B3LYP-D3). Both methods, despite very different treatment of dispersion effects, consistently show that ligand **2** exhibits higher affinity for Cl^- than does the unsubstituted ligand **1**. The calculated difference in the interaction energy is 2.6–3.7 kcal/mol in the gas phase and 1.0 kcal/mol in solution. Decomposition of the gas phase interaction energy into the interaction of frozen fragments and the ligand relaxation energy from the bound to a free state indicates that the former term contributes ~80% to a higher binding strength for the complex **2**•Cl^-a compared to **1**•Cl^-. Solvation effects weaken the ligand-anion interaction. This weakening is more significant for **2** that for **1**, because Cl^- is less exposed to the solvent when it is bound to **2**. This is demonstrated in **Figure 2.8**, indicating that Cl^- can accommodate up to four solvent(chloroform) molecules in the complex with **1**, but only two solvent molecules in the complex with **2**.

According to the analysis of anion binding data and crystallographic evidence,[31] a more realistic model of interaction of calix[4]pyrrole and chloride salts in nonpolar solvents should invoke the formation of an ion-pair complex involving some degree of encapsulation of the counteraction into the anion-induces calix[4]pyrrole cup. The simplest tetramethylammonium cation in reaction (7) was chosen for computational expediency. Structures and relative energies of ion-pair complexes formed with ligand **1** are shown in **Figure 2.8**. Consistent with X-ray crystal structures,[41] calculations show two distinct modes of cation inclusion, either with one or two alkyl groups oriented into the cavity. In the most stable orientation, a single methyl group from the cation is directed into the cavity. This mode of cation inclusion is in agreement with solid state structures of **1** with chloride salts containing at least one methyl group in a tetraalkylammonium cation.[31] The solution-phase complexation energies for reaction (2) given in **Table 2.2** indicates that the difference in the ion-pair complexation ability of ligands **1** and **2** is very similar to that for a single chloride anion. The difference in binding for the two ligands in the presence of a counter cation is changed by only 0.1 kcal/mol. Thus, irrespective of a theoretical model to account for dispersion interactions, and the presence of counterions, DFT calculations support a picture in which the chloride binding affinity of **2** with four *meso*-hexyl groups is comparable to or, actually, slightly higher than that of the unsubstituted ligand **1**. The theoretical predictions are generally consistent with the results of titration and extraction experiments. Not surprisingly, for ligands with a significant hydrophobic interaction component, the conventional B3LYP method with no

Grimme's empirical dispersion correction is unable to predict nearly the same binding affinities of **1** and **2** for chloride in chloroform.

2.2 Conclusions

The new highly alkylated calixpyrrole $\boldsymbol{\alpha,\alpha',\alpha'',\alpha'''}$**-***meso*-tetrahexyltetramethyl-calix[4]pyrrole **2** is easily obtained as a single diastereomer in a one-pot reaction. It exhibits enhanced organic-phase solubility, which will promote its use in solvent extraction. Moderate solubility in aliphatic diluents is especially useful toward practical applications. Regarding the ubiquitous question of the effect of the alkylation on binding and extraction, it is also encouraging to find that the long-chain alkyl groups in **2** have a mild enhancing effect compared with **1**. The stoichiometry of complexation of **2** with $TBMA^+Cl^-$ was found to be 1:1, the same as already known for its parent *meso*-octamethylcalix[4]pyrrole (**1**). NMR and extraction data yield similar binding constants for **1**, though the presence of water in the extraction system appears to reduce binding for **2**. X-ray crystal structures proved informative, showing that the hexyl arms in the complex $TBMA^+$(**2**)Cl^- assume an axial configuration, enveloping the anion. The expected cone conformation of the calixpyrrole ring and the insertion of the methyl group of the $TBMA^+$ cation in the calixpyrrole cup, both well-known features of calix[4]pyrrole complex structures, were also observed. DFT calculations helped elucidate the structural features and the relative stability of the complexes of **2** vs **1**. Although some C–H interactions are observed to the bound Cl^- anion from the first methylene unit of each hexyl arm, the

stabilization of the axial configuration appears to result from the higher steric strain that occurs in equatorial forms.

2.4 Experimental

2.4.1 General methods

Liquid scintillation counting was conducted using a Packard Tri-Carb 2500TR Model B2500P3 Liquid Scintillation Analyzer. Liquid–liquid contacting was performed using a Glas-Col laboratory rotator, and samples were phase-separated using a Beckman Coulter refrigerated centrifuge maintained at 25 ± 1.0 °C. The ^{1}H−NMR titration was conducted using a 400 mHz Bruker Advanced III NMR spectrometer; the temperature of the samples in the NMR spectrometer was maintain at 25 ± 0.1 °C.

2.4.2 Materials

Chemical Reagents

The calix[4]pyrrole receptors studied and discussed in this paper were prepared using procedures previously or slightly modified from preparations reported in the literature (see below). The tributylmethylammonium chloride ($TBMA^{+}Cl^{-}$) used in both extraction and titration experiments was purchased from Sigma-Aldrich (≥98%) and used as received. The aqueous solutions were prepared using MilliQ purified water (18 $m\Omega cm^{-1}$). Chloroform (Aldrich Chemical Co.) of ≥99% purity containing amylenes as stabilizer was used as received. 1,2-Dichloroethane (Sigma−Aldrich Chromsolv) of ≥99.8% was used

as received. The chloroform-*d* utilized in ^{1}H−NMR titrations was purchased from Cambridge Isotopes; it had an isotopic purity of 99.9%.

Tracer

The ^{36}Cl radiotracer utilized in the extraction experiments was purchased from Isotope Product Laboratory (Burbank, CA, USA) as the NaCl form in water. ^{36}Cl was spiked into 600 μL aqueous phase containing various concentrations of $TBMA^{+}Cl^{-}$ prior to liquid-liquid contacting on the rotating wheel.

2.4.3 Preparation of Calix[4]pyrroles

Materials used in the synthesis of the calix[4]pyrroles were used as received from the supplier, with the exceptions of the pyrrole which was purified via distillation prior to use. Calix[4]pyrrole **1** was prepared using a modification of a previously reported synthesis.[22] Calix[4]pyrrole **2** was prepared in the following manner: 2-octanone (1.643 mL, 10.50 mmol), pyrrole (0.694 mL, 10.00 mmol), and trifluoroacetic acid (0.383 mL, 5.00 mmol) were combined in 50 mL of dry dichloromethane (DCM) and stirred at room temperature overnight under an inert atmosphere. The resulting brown solution mixture was then neutralized with a 0.1 M NaOH solution, followed by an additional wash with brine solution. The dichloromethane (DCM) layer was then dried over Na_2SO_4. Upon removal of the DCM under reduced pressure, a dark brown semi-solid remained. This semi-solid was triturated with methanol then acetone, leaving behind a white/light tan microcrystalline powder that proved to be the all-α isomer of calix[4]pyrrole 2 (300 mg, yield 17.0%). ^{1}H and ^{13}C-NMR Chemical shifts are reported as δ in ppm using the residual

solvent signal as an internal standard. **^{1}H-NMR** ($CDCl_3$, in ppm) δ –0.84 (t, *J* = 6.92 Hz, 12H, CH_3), 1.02 (s, 8H, CH_2), 1.19 (m, 24H, CH_2), 1.40 (s, 12H, CH_3), 1.79 (t, *J* = 8.23 Hz, 8H, CH_2), 5.87 (d, *J* = 2.62 Hz ,8H, *β*-H), 6.94 (s, 4H, NH). **^{13}C-NMR** ($CDCl_3$, in ppm): δ 14.1, 22.8, 24.3, 26.9, 30.0, 31.9, 38.8, 40.6, 103.6, 137.5. These spectra and the DEPT-135 spectrum with labels are provided below. Analysis: Calc. for $C_{48}H_{76}N_4$ (709.24) C, 81.2; H, 10.7; N, 7.89. Found: C, 80.3; H, 10.8; N, 7.78.

2.4.4 Distribution Experiments

Liquid−liquid extraction experiments were carried out in a manner previously described.[27] All equilibrations were run in duplicate. The extraction experiment used aqueous phases containing various concentrations of $TBMA^+Cl^-$ in the range 0.1–100 mmol. Each individual simple was spiked with 10 *μL* of $Na^{36}Cl$ with an activity of 0.01 mCi/mL. The organic phase consisted of 10 mmol of either **1** or **2** as noted with chloroform ($CHCl_3$) as the diluent. Prior to the addition of the aqueous solutions, the organic solutions were pipetted into centrifuge tubes followed by the careful addition of the aqueous phases. After the samples were spiked, the tubes were closed and placed in 50 mL propylene centrifuge tubes (each 50 mL tube contained 4 samples), these tubes were then secured to the rotating wheel. The wheel was set at 60 rpm and placed in a temperature−regulated air-box (25 ± 0.4 °C). All the samples were contacted by tumbling them end-over-end for a minimum of 45–60 min. Complete phase separation was then accomplished by placing the samples in a Beckman Coulter refrigerated centrifuge maintained at 25 ± 1.0 °C set at 3000 rpm for 5 min. Then the samples were subsampled by removing 300 μL of the

aqueous phase via pipette, which was subsequently pipetted into 20 mL of UltimaGold scintillation cocktail. The remaining aqueous layer was removed using a plastic pipette, prior to subsampling the lower organic phase. The organic phase was subsampled and mixed with the scintillation cocktail in a manner similar to the one described above for the aqueous phase. The organic samples in the scintillation cocktail were counted for 60 min because of the low abundance of counts certain sample solutions. The scintillation cocktail samples containing the aqueous phases were only counted for 5 min due to the greatly increased counts in solution. Additional scintillation cocktail samples containing un-contacted organic and aqueous solutions used in the experiment were spiked with ^{36}Cl to determine if there was a possibility of quenching (artificial reduction of light output) occurring in the samples containing those respective components. No quenching was observed, obviating the need to use a correction factor for quenching. One noticeable affects observed while testing for quenching was the opposite behavior that resulted in an artificial increase in observed recorded counts (boosting) in the solution containing **2**.

2.4.5 ^{1}H-NMR titrations

Titrations were preformed using $CDCl_3$ (D, 99.96%) with 0.03% TMS obtained from Cambridge Isotopes. All solutions used in the titration, contained mesitylene as an internal standard to determine the concentration of the free and bound forms of the receptors as the titration progressed. The initial starting solution placed in the NMR tubes was 1 mL of a 10 mmol solution of either **1** or **2**. To these solutions were added in 10 μL of a 100 mmol solution of $TBMA^{+}Cl^{-}$, each 10 μL addition represented a 0.1 eq addition. The temperature

of the samples was tightly regulated at 25±0.1 °C to ensure additional errors could be excluded. Integration of peaks representing the NH and CH at the beta-positions of the pyrroles was used to determine how much of each was present. All peak were integrated using mesitylene as an internal standard ensuring that the ratios of free to bound C4P were always proportional.

2.4.6 Solubility of 1 and 2 in organic solvents

The solubilities of **1** and **2** were determined in multiple solvents covering a range of polarities and donor types, including protic, nonprotic, and electron-pair donor solvents. The solvents were used as received from commercial sources. To test the solubility of each respective compound, an excess of solid **1** or **2** was placed into a 15 mL polypropylene centrifuge tube, and 10 mL of the respective solvent was added to each individual tube. The tubes were placed on a rotating wheel for a period of 72 h. Samples were taken at 24 h intervals, and the respective concentrations were measured by ^{1}H-NMR in 50% $CDCl_3$ containing 10.0 mmol of tetrakis(trimethylsilyl)silane serving as an internal standard. Using this methodology, the lower limit of solubility measurement was < 5μmol. The results of these studies are shown in **Table 2.1** in the Results and Discussion section.

2.4.7 Crystal Structures of 2, Free ligand, and $TMA^{+}Cl^{-}$ Complex

The crystals of the free ligand **2** and of the **2**−tetramethylammonium chloride ($TMA^{+}Cl^{-}$**)** complex were obtained by slow evaporation. Crystals of the free ligand were obtained by

dissolving 0.014 g of **2** in 2 mL of 1,2-dichloroethane; this solution was allowed to evaporate for 24 h after which colorless crystals appeared. The **2**−TMA^+Cl^- crystals were obtained by dissolving 100 mmol of TMA^+Cl^- with 10 mmol of **2** in 1,2-DCE in a 4 mL vial; after 48 h of slow evaporation, colorless crystals appeared at the bottom of the vial. Elemental analysis of both the free ligand and **2**−TMA^+Cl^- complex conformed the bulk of the crystals were the same as those obtained by X−ray diffraction. The analyses were C−80.34%, H−10.76%, and N−7.78% and C−76.34%, H−10.83%, and N−8.56% for **2** and the complex, respectively. Single-crystal X-ray data were collected on a Bruker SMART APEX CCD diffractometer with fine-focus Mo Kα radiation (λ = 0.71073 Å), operated at 50 kV and 30 mA. The structure was solved by direct methods and refined on F^2 using the SHELXTL software package. Absorption corrections were applied using SADABS, part of the SHELXTL package. All non-hydrogen atoms were refined anisotropically. Hydrogen atoms were placed in idealized positions and refined with a riding model.

2.4.8 Computational Details

Electronic structure calculations were carried out using the Gaussian 09 Revision D.01 software packages.[44] The M06-2X flavor of density functional theory[42] in conjunction with the 6-31+G(d) basis set was employed to compare relative stabilities of various conformers and complexation energies of the parent **1** and alkyl-substituted **2** calix[4]pyrroles with the chloride anion and the tetramethylammonium chloride ion pair. The M06-2X density functional was chosen because it provides a relatively accurate prediction of interaction energies in noncovalent complexes.[42,45] The pure B3LYP density

functional[46,47] is known to strongly underestimate the interaction energies of the dispersion-bonded complexes. To provide a better account of noncovalent interactions, Grimme's D3 dispersion correction[43] was applied to the B3LYP/6-31+G(d) method, which was used as the second method to calculate complexation energies of ligands **1** and **2** with Cl^-. Using the gas phase geometries obtained at each level of theory, implicit solvent corrections for chloroform as a solvent were obtained with the SMD model[48] in Gaussian 09.

2.4 References

(1) Irving, H.; Williams, R. J. P. Liquid-Liquid Extraction. In *Treatise on Analytical Chemistry*: Kolthoff, I. M.; Elving, P. J., Eds.; Interscience Publishers: New York, 1961; Vol. 3, pp 1309–1365.

(2) Leo, J.; Hansch, C.; Elkins, D. *Chem. Rev.* **1971,** *71*, 525–616.

(3) Nernst, W. *Ztschr. Phys. Chem.* **1891,** *8*, 110–139.

(4) Marcus, Y.; Kertes, A. S. *Ion Exchange and Solvent Extraction of Metal Complexes*. Wiley Interscience: New York, 1969.

(5) Rydberg, J.; Cox, M.; Musikas, C.; Choppin, G. R. *Principles and Practices of Solvent Extraction*. Marcel Dekker: New York, 2004.

(6) Morrison, G. H.; Freiser, H. *Solvent Extraction in Analytical Chemistry*. John Wiley & Sons: New York, 1957.

(7) Dietrich, B.; Lehn, J.-M. *Tetrahedron Lett.* **1969**, *34*, 2889–2892.

(8) Cram, D. J.; Cram, J.-M. *Accounts Chem. Res.* **1978**, *11*, 8–14.

(9) Izatt, R. M.; Bradshaw, J. S.; Nielsen, S. A.; Lamb, J. D.; Christensen, J. *J. Chem. Rev.* **1991**, *91*, 1721–2085.

(10) Moyer, B. A. Complexation and Transport. In *Molecular Recognition: Receptors for Cationic Guests*: Gokel, G. W., Ed.; Comprehensive Supramolecular Chemistry; Vol. 1; Atwood, J. L., Davies, J. E. D., MacNicol, D. D., Vögtle, F., Lehn, J.-M., Eds.; Pergamon, Elsevier: Oxford, 1996; pp. 377–416.

(11) McDowell, W. J.; Shoun, R. R. In *An Evaluation of Crown Compounds in Solvent Extraction of Metals*: Proc. International Solvent Extraction Conference (ISEC 77),

Toronto, Ontario, Canada, Sept. 9–16, 1977; Lucas, B. H.; Ritcey, G. M.; Smith, H. W., Eds. The Canadian Institute of Mining and Metallurgy, Montreal, Quebec, Canada: Toronto, Ontario, Canada, 1977; pp 95–100.

(12) Takeda, Y. The Solvent Extraction of Metal Ions by Crown Compounds. In *Host Guest Complex Chemistry III*: Vogtle, F.; Weber, E., Eds.; Springer-Verlag: Berlin, 1984; Vol. 121, pp 1–38.

(13) McDowell, W. J., Crown Ethers as Solvent Extraction Reagents: Where Do We Stand? *Sep. Sci. Technol.* **1988,** *23*, 1251–1268.

(14) Hay, B. P; Rustad, J. R.; Hostetler, C. J. *J. Am. Chem. Soc.* **1993**, *115*, 11158–11164.

(15) Hay, B. P. A Molecular Mechanics Method for Predicting the Influence of Ligand Strucutre on Metal Ion Binding Affinity. In *Macrocyclic Chemistry*, Dietz, M. ACS Symposium Series 716, American Chemical Society: Washington, D.C., 1999; pp. 102–113.

(16) Dietz, M. L.; Bond, A. H.; Clapper, M.; Finch, J. W. *Radiochim. Acta* **1999,** *85* (3-4), 119-129.

(17) Sachleben, R. A.; Moyer, B. A. Ligand Design for Small Cations: The Li^+/14-Crown-4 System. In *Metal Ion Separation and Preconcentration. Progress and Opportunities*: A. H. Bond, M. L. Dietz, and R. D. Rogers, Eds.; ACS Symposium Series 716, American Chemical Society: Washington, D.C., 1999; pp. 114–144.

(18) Gloe, K.; Stephan, H.; Grotjahn, M., Where is the anion extraction going? *Chem. Eng. Technol.* **2003,** *26* (11), 1107–1117.

(19) Gale, P. A.; Sessler, J. L.; Král, V.; Lynch, V. *J. Am. Chem. Soc.* **1996**, *118*, 5140–5141.

(20) Adriaenssens, L; Gil-Ramírez, G.; Frontera, A.; Quiñonero, D.; Escudero-Adán, E. C.; Ballester, P. *J. Am. Chem. Soc.* **2014**, *136*, 3208–3218.

(21) Kim, S.; Lee, J.; Williams, N. J., Lynch, V. M.; Hay, B. P.; Moyer, B. A.; Sessler, J. L. *J. Am. Chem. Soc.* **2014**, *136*, 15079–15085.

(22) Anzenbacher, P., Jr.; Jursokova, K.; Lynch, V. M.; Gale, P. A.; Sessler, J. L. *J. Am. Chem. Soc.* **1999**, *121*, 11020–11021.

(23) Saha, I.; Lee, J. T.; Lee. C. *Eur. J. Org. Chem.* **2015**, *18*, 3859–3885.

(24) Busschaert, N.; Caltagirone, C.; Van Rossom, W.; Gale, P. A. *Chem. Rev.* **2015**, *115*, 8038–8155.

(25) Wenzel, M.; Hiscock, J. R.; Gale, P. A. *Chem. Soc. Rev*. **2012**, *41*, 480–520.

(26) Wintergerst, M. P.; Levitskaia, T. G.; Moyer, B. A.; Sessler, J. L.; Delmau, L. H. *J. Am. Chem. Soc.* **2008**, *130*, 4129–4139.

(27) Moyer, B. A.; Sloop, F. V. Jr.; Fowler, C. J.; Haverlock, T. J.; Kang, H.; Delmau, L. H.; Bau, D. M.; Hossain, M. D.; Bowman-James, K.; Shriver, J. A.; Bill, N. L.; Gross, D. E.; Marquez, M.; Lynch V. M.; Sessler, J. L. *Supramol. Chem.* **2010**, *22*, 653–671.

(28) Borman, C. J.; Custelcean, R.; Hay, B. P.; Bill, N. L.; Sessler, J. L.; Moyer, B. A. *Chem. Commun.* **2011**, *47*, 7611–7613.

(29) Borman, C. J.; Bonnesen, P. V.; Moyer, B. A. *Anal. Chem.* **2012**, *84*, 8214–8221.

(30) Custelcean, R.; Delmau, L. H.; Moyer, B. A.; Sessler, J. L.; Cho, W. S.; Gross, D.; Bates, G. W.; Brooks, S. J.; Light, M. L.; Gale, P. A. *Angew. Chem., Int. Ed. Engl.* **2005**, *44*, 2537–2542.

(31) Sessler, J. L.; Gross, D. E.; Cho, W.-S.; Lynch, V. M.; Schmidtchen, F. P.; Bates, G. W.; Light, M. E.; Gale, P. A. *J. Am. Chem. Soc.* **2006**, *128*, 12281–12288.

(32) Riddick, J. A.; Bunger, W. B. *Techniques of Chemistry: Organic Solvents*; Wiley & Sons: New York, 1970; Vol. 2.

(33) Barton, A. F. M. *Handbook of Solubility Parameters and Other Cohesion Parameters, 2nd Ed.;* CRC Press: Boca Raton, 1991.

(34) Bermudez, A.; Foco, G.; Bottini, S. B. *J. Chem. Eng. Data.* **2000**, *45*, 1105–1107.

(35) Durkee, J. B. *Cleaning with Solvents*, Elsevier: New York, 2014.

(36) Hildebrand, J. H.; Scott, R. L., *The Solubility of Nonelectrolytes*. 3rd ed.; Reinhold Publishing Corp.: New York, 1950.

(37) Robinson, R. A.; Stokes, R. H. *Electrolyte Solutions*, *Revised Ed.*; Butterworths: Washington D.C., 1965.

(38) Kenjo, T.; Diamond, R. M. *J. Inorg. Nucl. Chem.* **1974,** *36*, 183–188.

(39) Moyer B. A.; Bonnesen, P. V. Physical Factors in Anion Separations. In *Supramolecular Chemistry of Anions*; Bianchi, A.; Bowman-James, K.; Garcia-Espana, E., Eds.; Wiley-VCH: New York, 1997; Chap. 1, pp. 1–44

(40) Woods, C. J.; Camiolo, S.; Light, M. E.; Coles, S. J.; Hursthouse, M. B.; King, M. A.; Gale, P. A.; Essex, J. W. *J. Am. Chem. Soc.* **2002**, *124*, 8644–8652.

(41) Kim, S. K.; Sessler, J. L.; Gross, D. E.; Lee, C. H.; Kim, J. S.; Lynch, V. M.; Delmau, L. H.; Hay, B. P. *J. Am. Chem. Soc*. **2010**, *132*, 5827–5836.

(42) Zhao, Y.; Truhlar, D. G. *Theor. Chem. Acc.* **2008**, *120*, 215–241.

(43) Grimme, S.; Antony, J.; Ehrlich, S.; Krieg, H. *J. Chem. Phys.* **2010,** *132*, 154104.

(44) Gaussian 09, Revision D.01, Frisch, M. J.; Trucks, G. W.; Schlegel, H. B.; Scuseria, G. E.; Robb, M. A.; Cheeseman, J. R.; Scalmani, G.; Barone, V.; Mennucci, B.; Petersson, G. A.; Nakatsuji, H.; Caricato, M.; Li, X.; Hratchian, H. P.; Izmaylov, A. F.; Bloino, J.; Zheng, G.; Sonnenberg, J. L.; Hada, M.; Ehara, M.; Toyota, K.; Fukuda, R.; Hasegawa, J.; Ishida, M.; Nakajima, T.; Honda, Y.; Kitao, O.; Nakai, H.; Vreven, T.; Montgomery, J. A., Jr.; Peralta, J. E.; Ogliaro, F.; Bearpark, M.; Heyd, J. J.; Brothers, E.; Kudin, K. N.; Staroverov, V. N.; Kobayashi, R.; Normand, J.; Raghavachari, K.; Rendell, A.; Burant, J. C.; Iyengar, S. S.; Tomasi, J.; Cossi, M.; Rega, N.; Millam, J. M.; Klene, M.; Knox, J. E.; Cross, J. B.; Bakken, V.; Adamo, C.; Jaramillo, J.; Gomperts, R.; Stratmann, R. E.; Yazyev, O.; Austin, A. J.; Cammi, R.; Pomelli, C.; Ochterski, J. W.; Martin, R. L.; Morokuma, K.; Zakrzewski, V. G.; Voth, G. A.; Salvador, P.; Dannenberg, J. J.; Dapprich, S.; Daniels, A. D.; Farkas, Ö.; Foresman, J. B.; Ortiz, J. V.; Cioslowski, J.; Fox, D. J. Gaussian, Inc., Wallingford CT, 2009.

(45) Riley, K. E.; Pitonak, M.; Jurecka, P.; Hobza, P. *Chem. Rev.* **2010**, *110*, 5023–5063.

(46) Becke, A. D. *Chem. Phys.* **1993**, *98*, 5648–5652.

(47) Lee, C.; Yang, W.; Parr, R. G. *Phys. Rev. B* **1988**, *37*, 785–789.

(48) Marenich, A. V.; Cramer, C. J.; Truhlar, D. G. *J. Phys. Chem. B*, **2009**, *113*, 6378–6396.

2.6 Appendix 2A Supplemental Information for Chapter 2

2.6.1. Determination of Binding Constants via Solvent Extraction.

To determine the strength of binding between tributylmethylammonium chloride ($TBMA^+Cl^-$) and either **1** or **2**, solvent extraction experiments were performed. Prior to determining the binding between $TBMA^+Cl^-$ with **1** or **2**, the partitioning behavior of the quaternary ammonium chloride between the aqueous and the organic phases in the absence of **1** or **2** was investigated. From the experimentally determined distribution ratios (*D*) obtained using a ^{35}Cl radiotracer, it was possible to calculate the $TBMA^+Cl^-$ concentrations in both phases. For the calculations it was assumed that the $TBMA^+$ and Cl^- were partitioning as an ion pair. The equilibrium concentration of chloride in the aqueous phase was determined using Eq. **(S1).**

$$[Cl^-]_{aq} = \frac{([\boldsymbol{Cl^-}]_{\boldsymbol{aq,init.}} + [\boldsymbol{Cl^-}]_{\boldsymbol{org,init}}) \times \frac{\boldsymbol{V_o}}{\boldsymbol{V_a}}}{\boldsymbol{1} + \boldsymbol{D} \times \frac{\boldsymbol{V_o}}{\boldsymbol{V_a}}} \quad \textbf{(S1)}$$

In this work, $V_o = V_a$, and $[Cl^-]_{org,\ init} = 0$. Using the calculated $[Cl^-]_{aq}$, it was possible to determine the organic-phase chloride concentration using Eq. **(S2).**

$$[Cl^-]_{org} = D[Cl^-]_{aq} \quad (\textbf{S2})$$

The calculated $[Cl^-]_{aq}$ and $[Cl^-]_{org}$ are integral in determining the association constant of extraction (K_{ex}) of chloride with **1** or **2**. Before calculating the K_{ex}, the activity coefficients ($\gamma_\pm$) for the chloride were determined from the equilibrium $[Cl^-]_{aq}$ using Eq. (S**3**). In Eq. (S**3**), *I* represents the ionic strength in the aqueous phase, which corresponds here to the aqueous equilibrium chloride concentration.

$$\gamma\pm = 10^{\left(-0.509\times1\times\left(\sqrt{I}\right)\right)} \quad \textbf{(S3)}$$

After the activity coefficients were determined it was possible to calculate the equilibrium constant for extraction (K_{ex}) using Eq. (S**4)**

$$K_{ex} = \frac{[TBMA^{+}Cl^{-}]_{org}}{\left([TBMA^{+}]_{aq}\,\gamma\pm^{2}\,\gamma\pm^{2}\,[Cl^{-}]_{aq}\gamma\pm^{2}\right)} \quad \textbf{(S4)}$$

The log K_{ex} for $TBMA^{+}Cl^{-}$ is calculated by taking the log of the K_{ex} calculated in Eq. (**S4**). These same approach used and discussed above can be used to determine the log K_{ex} for $TBMA^{+}Cl^{-}$ with either **1** and **2**.

The slope analysis of $TBMA^{+}Cl^{-}$ with either **1** and **2** was done by first correcting for the partitioning of $TBMA^{+}Cl^{-}$ between the two phases in the absence of the anion receptor. To determine the corrected log*D*, a correction factor (C_F) for loading was calculated using Eq. (S**5**). Once the correction factor is known, it is applied to the experimentally obtained D_{Cl} as shown in Eq. (S**6**); then the log of the corrected *D* is taken to give the log $D_{corrected}$.

$$C_F = \frac{[L]_{init}}{[L]_{init}-[Cl^{-}]_{org}} \quad \textbf{(S5)}$$

$$D_{(Corrected)} = D_{Cl} \times C_F \quad \textbf{(S6)}$$

The X–axis was determined by taking the log of the $[Cl^{-}]_{aq}$ multiplied by the ionic strength (*I*) squared.

2.6.2. Determination of Binding Constants by ^{1}H–NMR.

Binding constants were determined by titration of host with guest in deuterated chloroform, and the ratio of the two N-H protons (slow exchange) were used to determine

the ratio of host to guest. One-to-one binding constants were calculated in Excel® based off of the equilibrium [H] + [G] $\rightleftharpoons$ [HG]. The concentration of the complex was calculated via the equation:

$$[HG] = \frac{1 + G_0K + H_0K - \sqrt{-4G_0H_0K^2 + (-1 - G_0K - H_0K)^2}}{2K}$$

where G_0, H_0, and K are the initial guest concentration, the initial host concentration, and equilibrium constant, respectively. For each complex, only the eight to ten points nearest the maximum were utilized in the minimization of squares in order to get the most accurate value possible. To account for errors present in purity of the host and the hygroscopic nature of the guest, the starting host and guest calculations were also refined simultaneously with the refinement of K_a. All starting reagent concentrations refined within 5% (X) of their predicted amounts.

Host:	**log K_a:**	**$X * H_0$**	**$X * G_0$**
Greasy C[4]P	5.04 ± 0.34	0.95	1.00
C[4]P	4.15 ± 0.22	0.98	1.02

G_0, H_0, and K_a are the as-weighed initial guest concentration, initial host concentration, and equilibrium constant respectively. X represents the refined constant for initial concentrations to take into account errors due to weighing/measuring errors, purity issues, and hygroscopic hosts/guests.

2.6.3. Data for Greasy C[4]P.

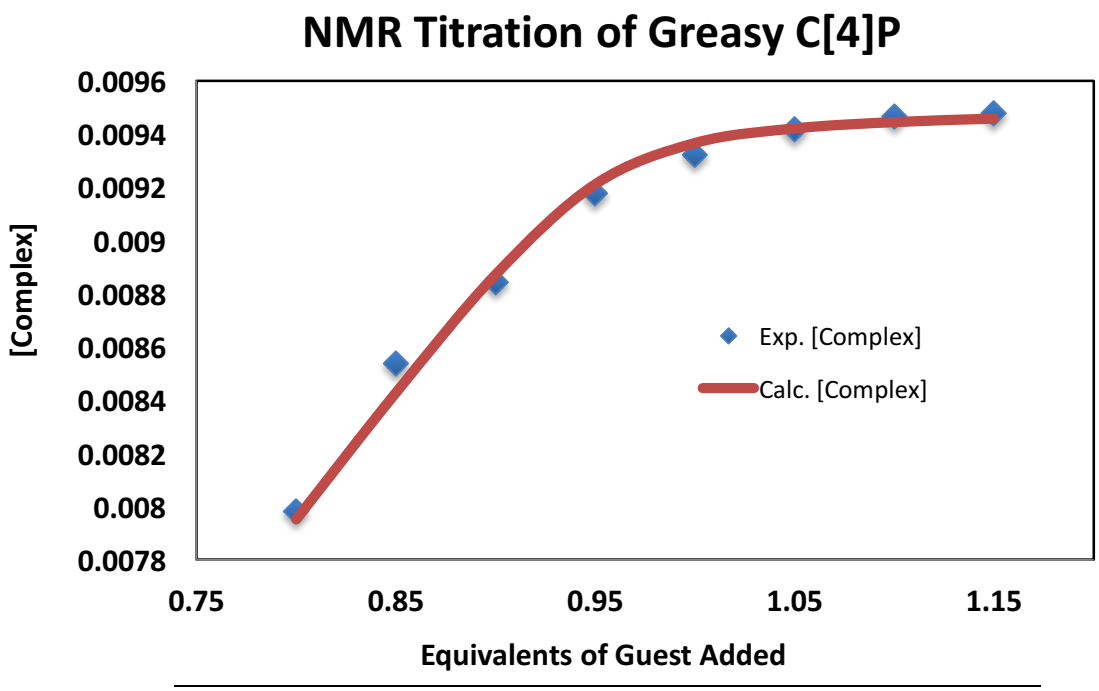

[Host] mM	Guest eq. Added	Integration of Free Host	Integration of Complex
10	0.8	0.35	1.84
10	0.85	0.22	1.95
10	0.9	0.15	2.02
10	0.95	0.07	1.99
10	1	0.04	2.1
10	1.05	0.02	2.26
10	1.1	0.008	2.14
10	1.15	0.005	2.18

2.6.4. Representative NMRs for greasy C[4]P showing effect of increasing amounts of chloride.

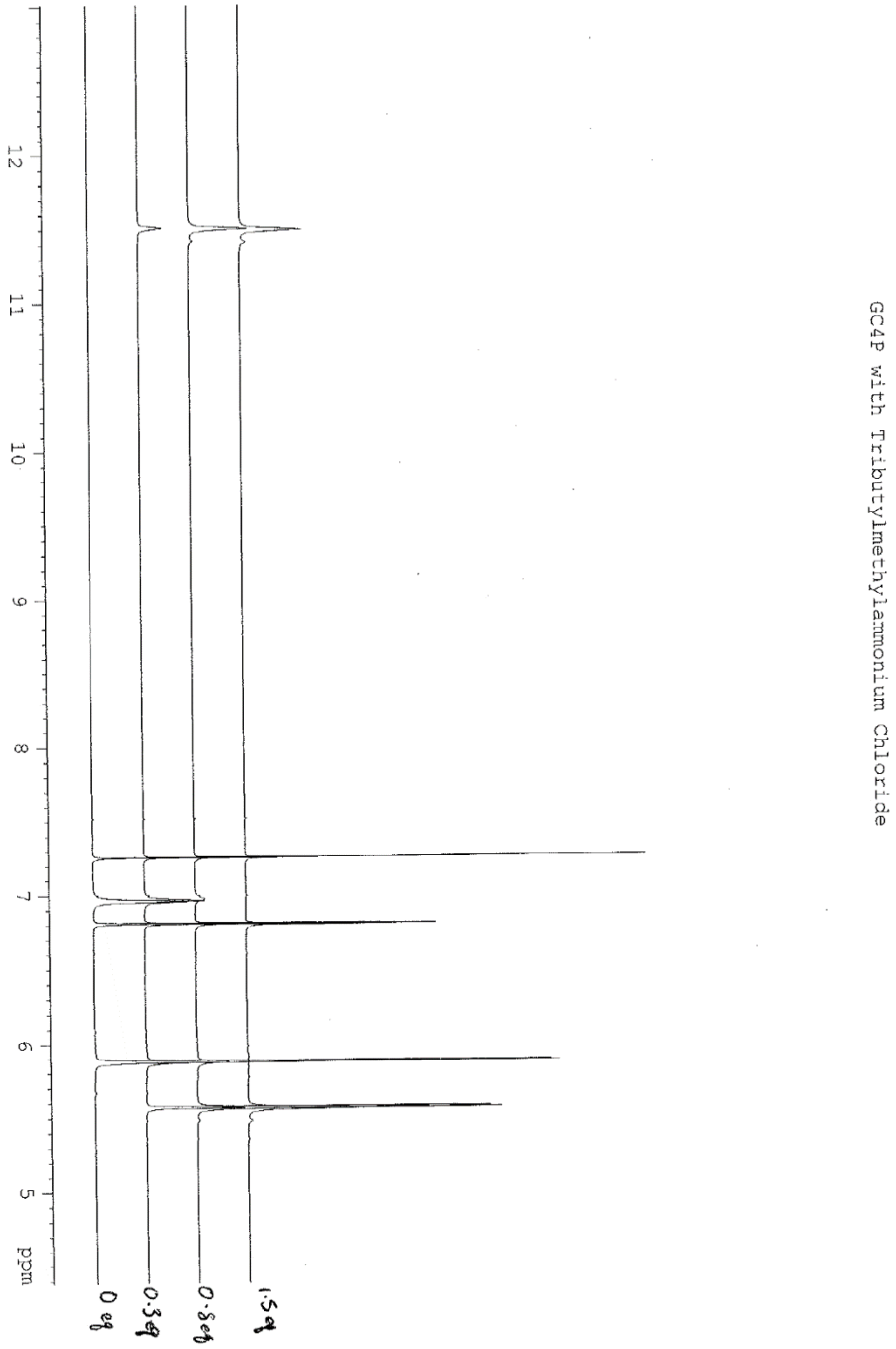

2.6.5. Data for C[4]P.

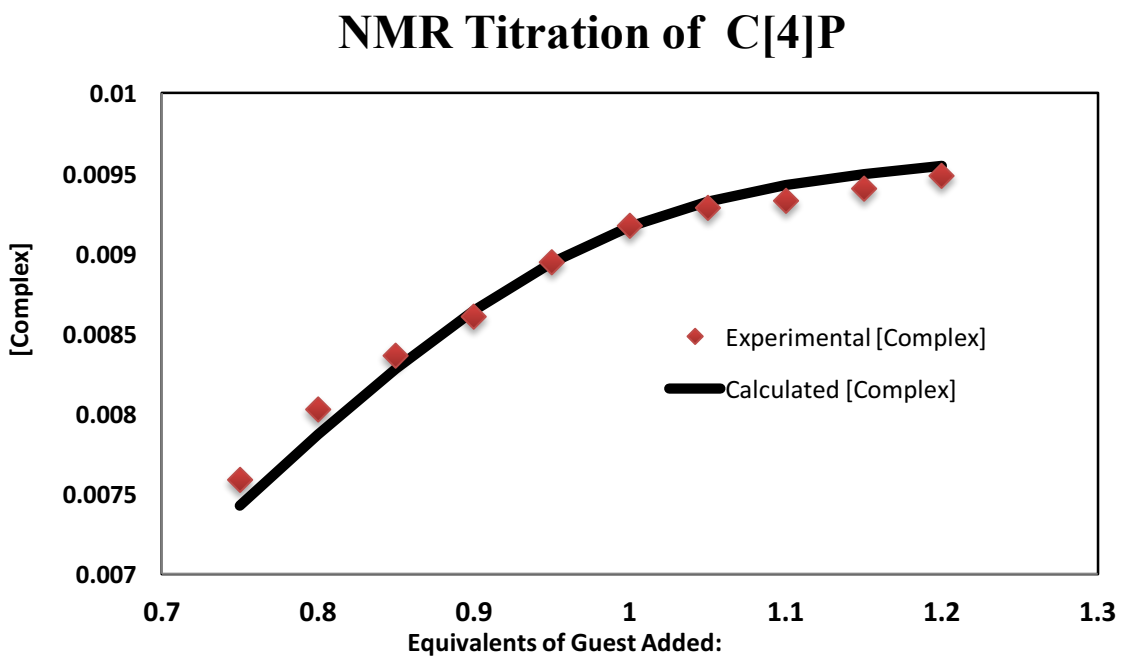

[Host] mM	Guest eq. Added	Integration of Free Host	Integration of Complex
10	0.75	1.015	3.4825
10	0.8	0.828	3.744
10	0.85	0.6845	3.9775
10	0.9	0.589	4.237
10	0.95	0.429	4.485
10	1	0.32	4.68
10	1.05	0.2665	4.8175
10	1.1	0.252	4.977
10	1.15	0.215	5.117
10	1.2	0.176	5.258

2.6.6. Representative NMRs for C[4]P showing effect of increasing amounts of chloride.

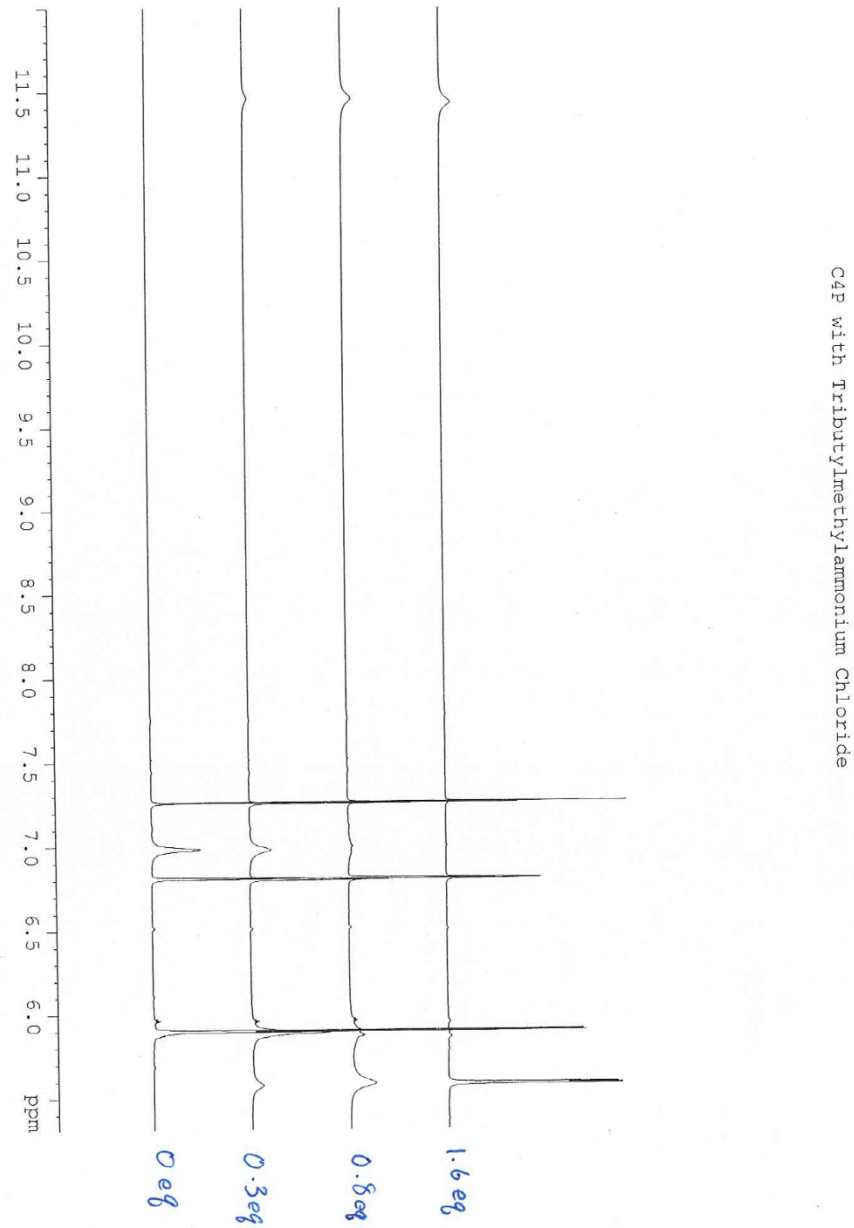

2.7 Appendix 2B Figures and Tables for Chapter 2

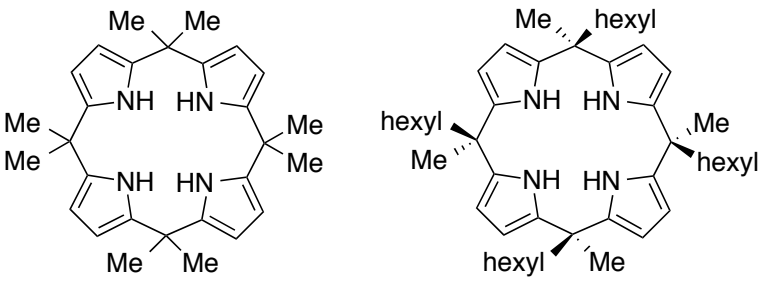

1 **2**

Figure 2.1. Structure of the *meso*-octamethylcalix[4]pyrrole (**1**) and the $\boldsymbol{\alpha}, \boldsymbol{\alpha}', \boldsymbol{\alpha}'', \boldsymbol{\alpha}'''$-*meso*-tetrahexyltetramethyl-calix[4]pyrroles (**2**).

Table 2.1. Solubilities of **1** and **2** in various neat solvents.[a]

Solvent	ε[b]	δ/MPa$^{1/2}$ [e]	**1** (mM)	**2** (mM)
Water	80.1	47.9	0.00[h]	0.00 [h]
Tri-*n*-butylphosphate	7.959[c]	21.3[f]	6.61	12.9
1-Octanol	10.34[d]	21.1	5.18	21.4
Nitrobenzene	34.82	20.5	26.5	33.3
1,2-Dichloroethane	10.36	18.2	30.0	31.5
Toluene	2.379	18.2	6.67	20.3
n-Dodecane	2.02[c]	16.2	2.28	15.1
Isopar L	~2.00	14.9[g]	2.02	21.3

[a]As determined by NMR spectroscopy with internal standard. [b]Taken from a published tabulation.[32] [c]Reported for 30 °C. [d]Reported for 20 °C. [e]Taken from a published tabulation unless otherwise noted.[33] [f]From Bermudez.[34] [g]From Durkee.[35] [h]Concentration of **1** and **2** were below the detection limit of the instrument (<5μmol) used to measure the concentrations in solution.

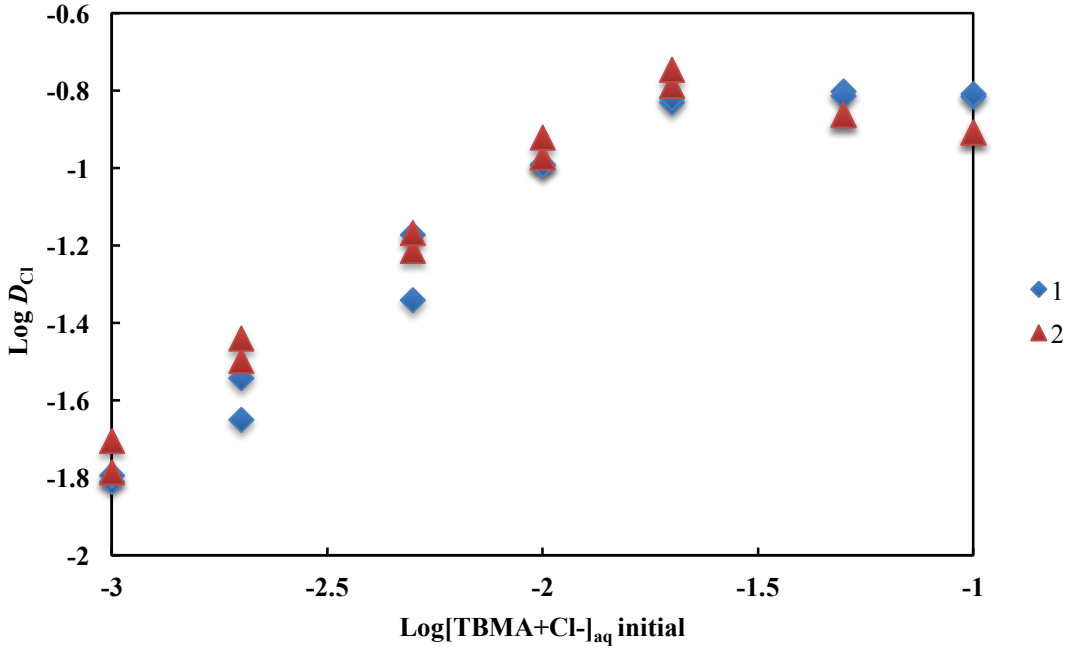

Figure 2.2. Results of the liquid−liquid extraction experiment in which 10 mM solutions of 1 or 2 in chloroform were equilibrated at 25 °C with equal volumes of aqueous solutions of 0.001–0.1 M $TBMA^{+}Cl^{-}$ traced with $^{36}Cl^{-}$. Data for a blank without calixpyrrole show weak, though noticeable extraction of $TBMA^{+}Cl^{-}$ by chloroform alone.

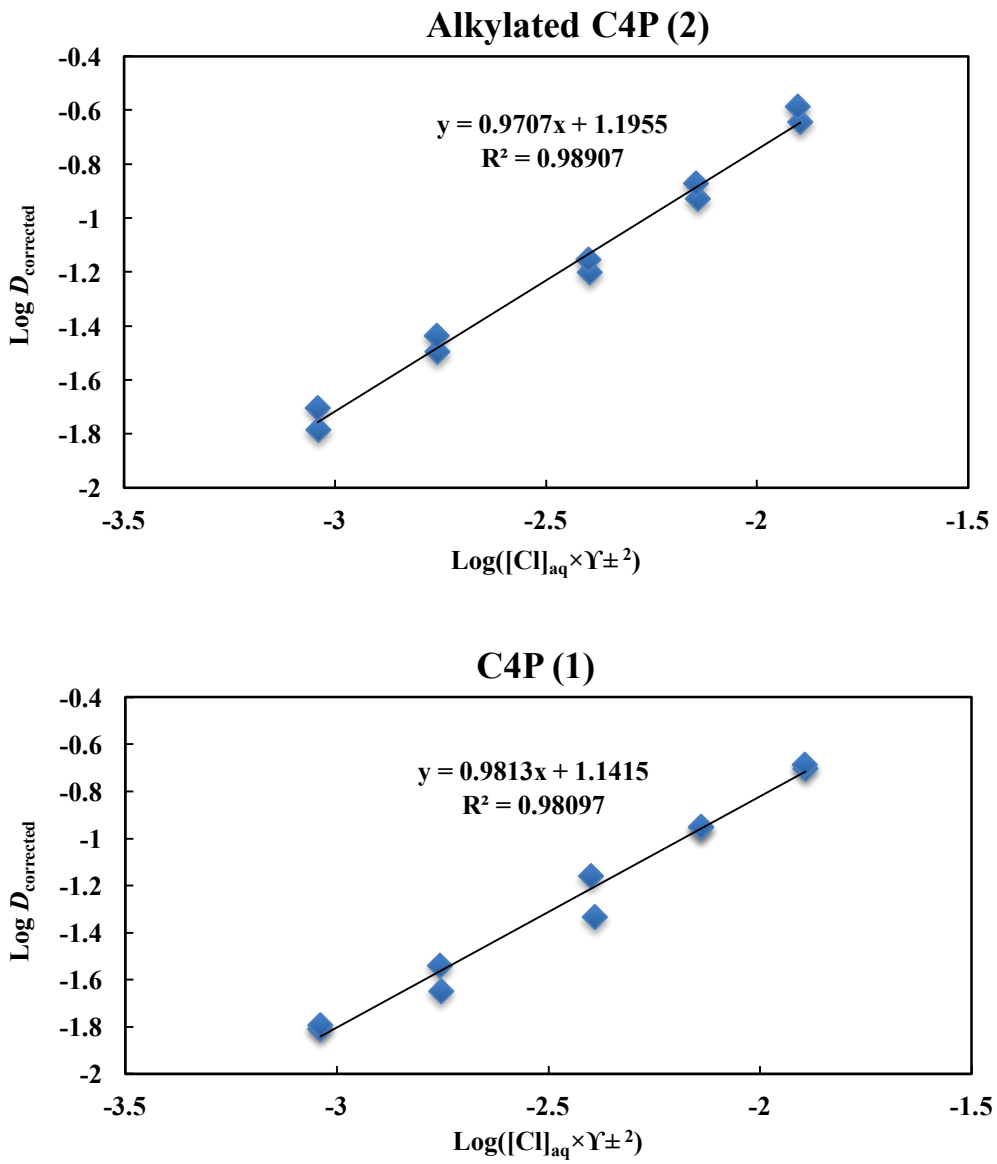

Figure 2.3. Slope analysis of the extraction of $TBMA^{+}Cl^{-}$ from aqueous solution into chloroform using calixpyrroles **1** and **2** at 10 mM. Also shown is the blank extraction of $TBMA^{+}Cl^{-}$ into chloroform alone. Data were taken from **Figure 2.2** and treated as discussed in the text.

Table 2.2. Determined equilibrium constants.

Equilibrium	Quotient	log*K*	Exper.
$TBMA^+_{(aq)} + Cl^-_{(aq)} \rightleftharpoons [TBMA^+Cl^-]_{(org)}$	$K_{ex,TBMACl}$	–0.884 ± 0.13	SX blank
$TBMA^+_{(aq)} + Cl^-_{(aq)} + \mathbf{1}_{(org)} \rightleftharpoons [TBMA^+(\mathbf{1})Cl^-]_{(org)}$	$K_{ex,1}$	3.18 ± 0.06	SX
$TBMA^+_{(aq)} + Cl^-_{(aq)} + \mathbf{2}_{(org)} \rightleftharpoons [TBMA^+(\mathbf{2})Cl^-]_{(org)}$	$K_{ex,2}$	3.26 ± 0.05	SX
$TBMA^+Cl^-_{(org)} + \mathbf{1}_{(org)} \rightleftharpoons [TBMA^+(\mathbf{1})Cl^-]_{(org)}$	$K_{cpx,1}$	4.06 ± 0.14	SX
$TBMA^+Cl^-_{(org)} + \mathbf{2}_{(org)} \rightleftharpoons [TBMA^+(\mathbf{2})Cl^-]_{(org)}$	$K_{cpx,2}$	4.14 ± 0.14	SX
$TBMA^+Cl^-_{(org)} + \mathbf{1}_{(org)} \rightleftharpoons [TBMA^+(\mathbf{1})Cl^-]_{(org)}$	$K_{cpx,1}$	4.14 ± 0.22	NMR
$TBMA^+Cl^-_{(org)} + \mathbf{2}_{(org)} \rightleftharpoons [TBMA^+(\mathbf{2})Cl^-]_{(org)}$	$K_{cpx,2}$	5.05 ± 0.34	NMR

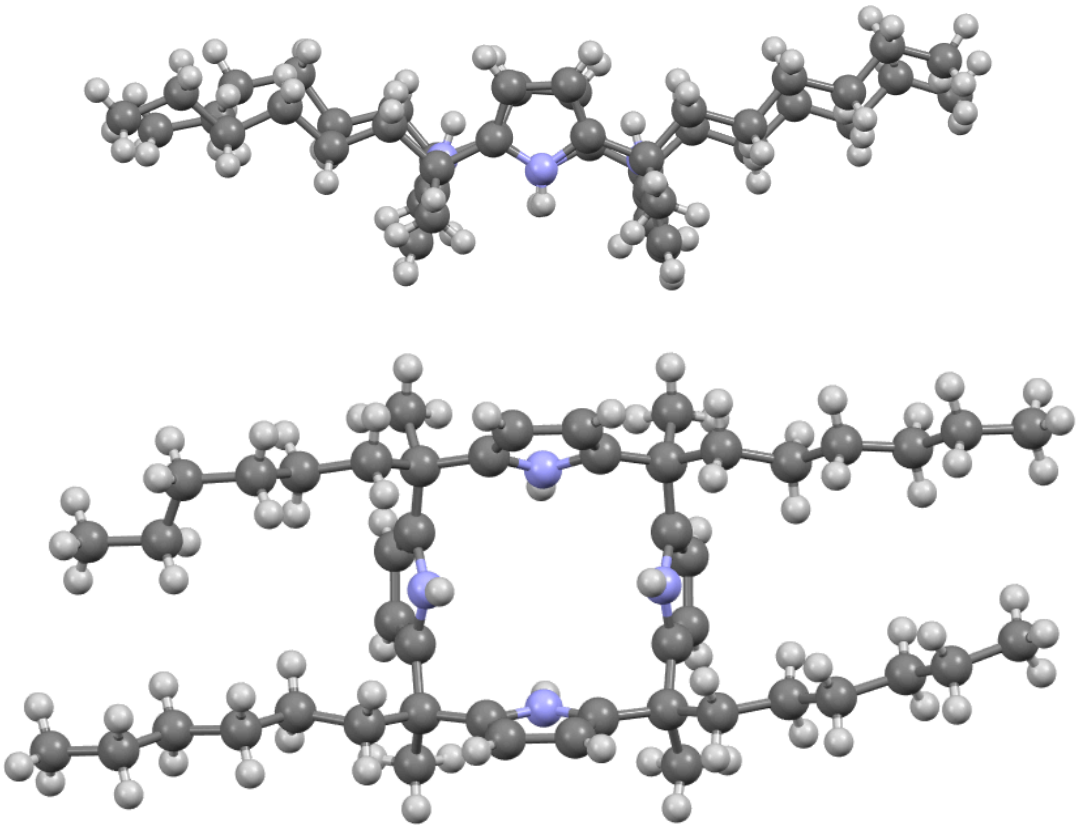

Figure 2.4. Crystal Structure of unbound **2**, side view (left) and top view (right).

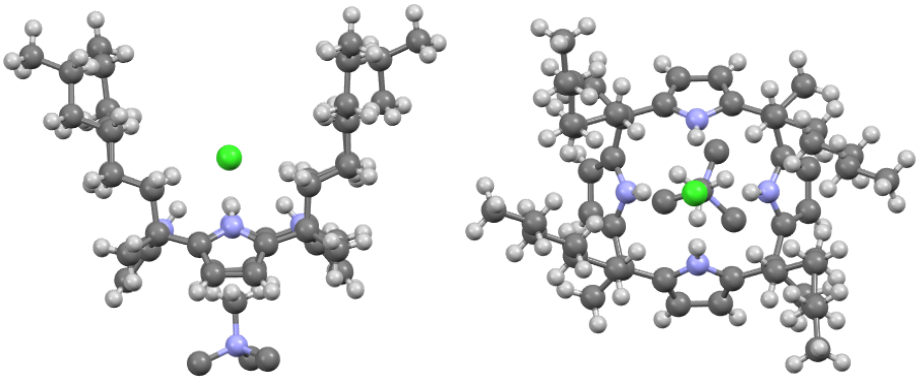

Figure 2.5. Crystal Structure of **2** bound to $TMA^{+}Cl^{-}$, side view (left) and top view (right).

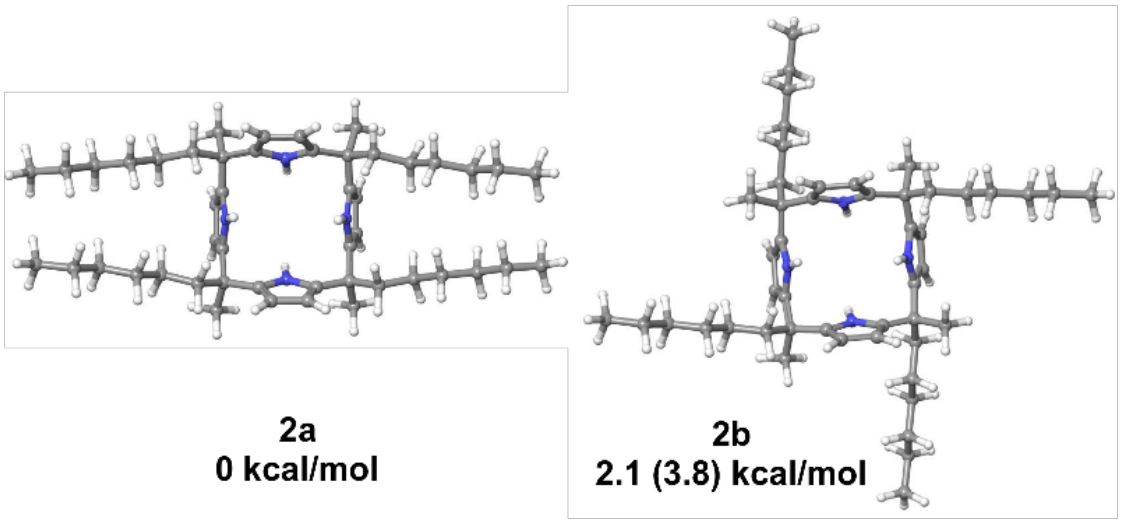

Figure 2.6. Structures and relative energies of 2a ($\boldsymbol{\alpha}, \boldsymbol{\alpha}, \boldsymbol{\alpha}, \boldsymbol{\alpha}$) and 2b ($\boldsymbol{\alpha}, \boldsymbol{\beta}, \boldsymbol{\alpha}, \boldsymbol{\beta}$) in the unbound free state obtained after geometry optimization at the M06-2X/6-31+G(d) level of theory. Solvent corrections are included using the SMD model for chloroform). Relative energies in the gas phase are shown in parentheses.

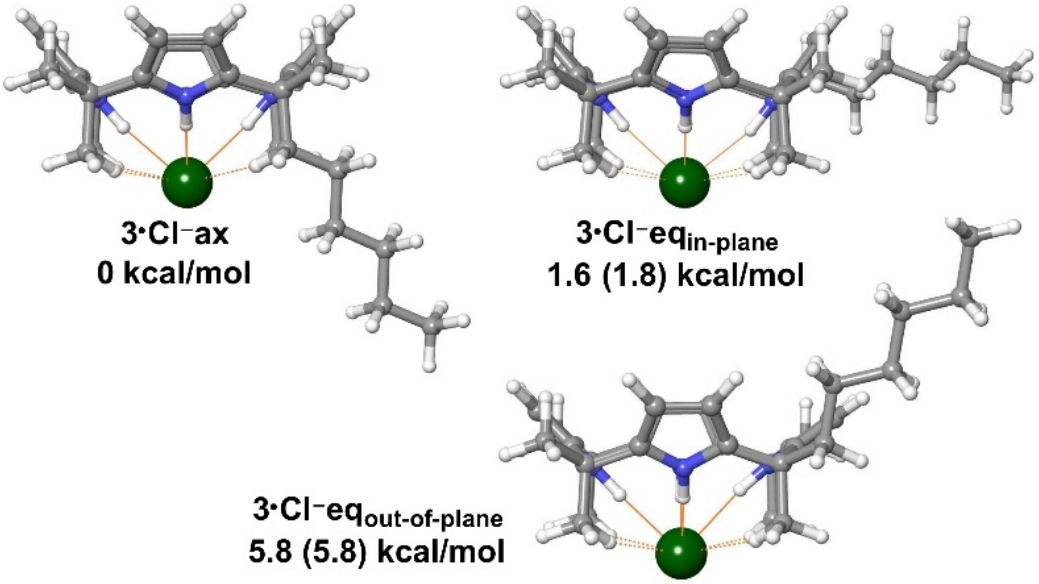

Figure 2.7. Structures and relative energies of 1:1 chloride – ligand 3 complexes obtained after geometry optimization at the M06-2X/6-31+G(d) level of theory. Solvent corrections are included using the SMD model for chloroform. Relative energies in the gas phase are shown in parentheses. Thin lines indicate hydrogen bonds and dashed lines indicate close contacts between the C–H groups of alkyl chains and the chloride anion.

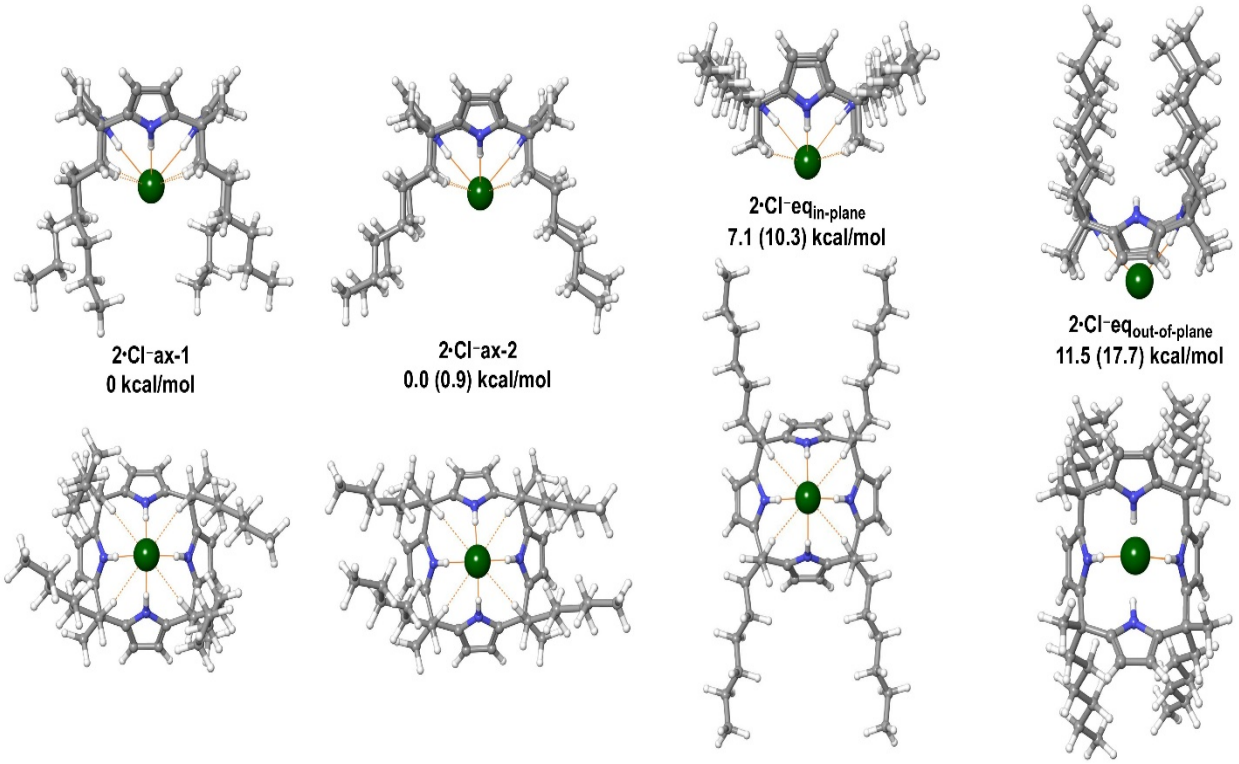

Figure 2.8. Structures (side and bottom views) and relative energies of 1:1 chloride – ligand **2** complexes obtained after geometry optimization at the M06-2X/6-31+G(d) level of theory. Solvent corrections are included using the SMD model for chloroform. Relative energies in the gas phase are shown in parentheses. Thin lines indicate hydrogen bonds and dashed lines indicate close contacts between the C–H groups of alkyl chains and the chloride anion.

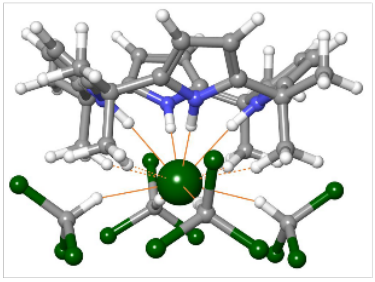

1·Cl⁻(CHCl$_3$)$_4$

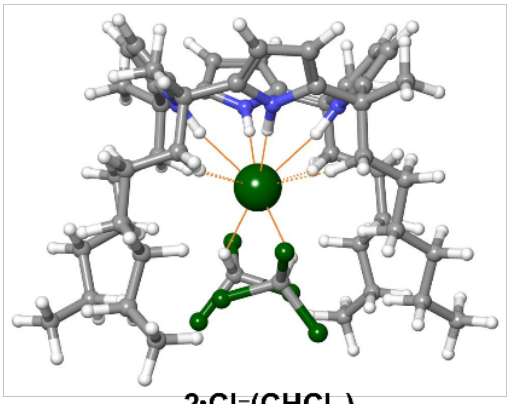

2·Cl⁻(CHCl$_3$)$_2$

Figure 2.9. M06-2X/6-31+G(d) optimized structures of 1:1 chloride – ligand complexes indicating that chloride can accommodate up to four chloroform molecules in the first solvation shell when bound to ligand 1 and two chloroform molecules when bound to ligand 2. Thin lines indicate hydrogen bonds and dashed lines indicate close contacts between the alkyl C-H groups and the chloride anion.

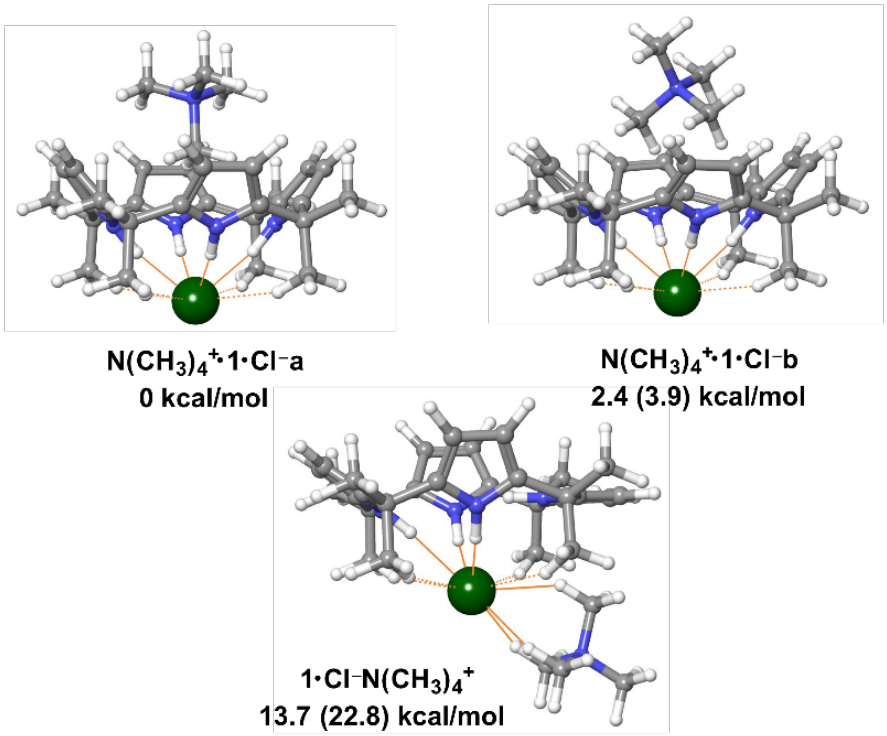

Figure 2.10. Structures and relative energies of ion-pairs formed with ligand 1 obtained after geometry optimization at the M06-2X/6-31+G(d) level of theory. Solvent corrections are included using the SMD model for chloroform. Relative energies in the gas phase are shown in parentheses. Thin lines indicate hydrogen bonds and dashed lines indicate close contacts between the alkyl C–H groups and the chloride anion.

Table 2.3. Complexation energies for reactions (7) and (8) obtained at the M06-2X/6-31+G(d) and B3LYP-D3/6-31+G(d) levels of theory (kcal/mol). Solvent corrections (ΔG_{solv}) are included using the SMD model for chloroform.

Ligand	Reaction[1]	ΔE_{gas}		$\Delta E_{gas} + \Delta G_{solv}$	
		M06-2X	B3LYP-D3	M06-2X	B3LYP-D3
1	(7)	–41.2		–11.7	–8.9
2	(7)	–44.9[2]	-38.8	–12.7[2]	–9.9[3]
1	(8)	–44.6	-41.4[3]	–24.2	
2	(8)	–45.7[3]		–25.3[3]	

[1]Tetramethylammonium employed as the countercation in reaction (8). [2]Conformation 2•Cl^-a (**Figure 2.9**) is the most stable in solution at this level of theory. [3]Conformation 2•Cl^-b (**Figure 2.9**) is the most stable in solution at this level of theory.

Chapter 3 : Selective Separation of Sulfate Via Implementation of a New Highly Soluble Di-iminoguanidinium in a Solvent Extraction System

Abstract

The development and testing of a new simple guanidinium oxoanion receptor soluble in most organic solvent will be discussed in this chapter. The selective separation of oxoanions by solvents extraction methods has been a difficult challenge. By designing new simple receptor based of iminoguanidiniums it was possible to develop and easily synthesize highly selective extractant for sulfate. Using radiotracers studies, slope analysis, Karl Fischer titrations and small angle X-ray scattering it was possible to gain insight into why these new receptors achieved the unprecedented success for sulfate extraction even being functioning in hydrocarbon based solvents.

3.1 Introduction

The selective separation of sulfate has been a difficult challenge to address because of the highly enthalpies of hydration, the vastly different geometry compared to the spherical halides, and the highly-charged species with the charge being spread throughout the anion. In chapter I, the issues that make oxoanion separations difficult are discussed in great detail, for this reason I shall refrain for going into greater detail on them. A subject that has not been greatly discussed in detail is the technique of liquid-liquid extraction also referred to as solvent extraction, which has become one of the preferred methods utilized in industries for the selective separation of ions.[1]

Solvent extraction processes are comprised of two phased systems, these two phases are comprised of an organic phase and an aqueous phase. The extractants are dissolved

in the organic phases in some cases additional compounds known as modifiers are added to the organic solvent to help solubilize the extractants and an some cases can participate in the extraction of the target ions. An industrial solvent extraction process can consist of multiple stages which are subdivided into one of three main categories; an extraction stage, scrubbing stage (removes possible impurities prior to stripping), and stripping stage (back-extraction, recover target ion from organic phase into a fresh aqueous phase).[1] There can be additional follow on stage such as the wash stage and regeneration stage is necessary.[1] In this chapters, I will focus on the extraction stage and will not cover the other stages mentioned above.

To determine the effectiveness of the extractants and the process extraction process a series of metrics are used. The metrics used to determine the effectiveness of each stage is the distribution value (*D*) which uses the concentrations of the analyte in the organic and aqueous phases. The measure of success for an extraction step is a high *D* value indicating that much of the target analyte as has been extracted into the organic phase from the aqueous phase. During the strip stage the lower the *D* value the more effective the stripping solution was at recovering the analyte from the organic phase. The equation used to determine the *D* value for sulfate is shown in equation 3.1.

$$D_{SO_4^{2-}} = \frac{[SO_4^{2-}]_{org}}{[SO_4^{2-}]_{aq}} \tag{3.1}$$

The work covered and discussed in this chapter will focus on a new class of highly organic soluble diiminoguanidinium anion receptors. This new anion receptor was appealing because the ease of synthetic accessibility and the past examples of guanidinium

receptors in the literature that have been shown to be selective for oxoanions particularly sulfate.[2] While the effective use of iminoguanidinium receptors for separation of sulfate via crystallization has recently been reported,[3-5] no examples have been reported in the literature of an organic soluble from of these receptors in solvent extraction. Since receptors based on iminoguanidinium were highly successful separating sulfate via crystallization, it can be logically assumed that the selectivity for sulfate will remain constant. The main challenge that must be overcome to make an organic soluble form of a iminoguanidinium receptor is the low solubility which made their use in crystallization separation systems advantageous. One method for increasing the solubility of a receptor in solvents are the addition of long aliphatic hydrocarbon chained such as octyl, decyl, etc. groups. To add this chains to the iminoguanidinium receptor it was necessary to find a precursor that contains synthetic handles which allow for the addition of these long alkyl chains. One additional consideration that factored into the selection of the selection of the initial precursor was the synthetic method that would be used to attach the chains to the precursor. Many metal based carbon-carbon coupling reactions and techniques have been developed, however the used of these reactions for the addition of long chained alkyl groups has not been greatly investigated. The cases from the literature where these techniques have been used to attach the long chains to various functionalities such as phenyl rings generally had fairly low synthetic yield ≤10-15%. For these reason, I looked for other synthetic reaction for attaching long alkyl chains to a phenyl ring, eventually settling on the Williamson ether synthesis for the attachment of the alkyl groups to the phenyl ring. The Williamson ether synthesis has a long and successful track record in the

literature of being synthetically adaptable for various reaction, easily available and low costing reagents, and generally high yields for products. Based on the use of the Williamson ether synthesis for addition of the alkyl chains the cheap commercially available precursor 3,4-dihyroxybenzaldehyde was selected. The reaction of this precursor with the bromoalkane derivatives of both the octyl and decyl chains have high synthetic yields greater than 90%. The 3,4-dialkyloxobenzaldehydes were reacted with aminoguanidinium chloride in ethanol resulting in the formation of highly insoluble emulsions. Additional reactions were attempted with the two reagents in other organic solvents (e.g. THF, dioxane, DMF, etc.) with the same results as the ethanol an insoluble emission formation. This led to the decision to use branched alkyl chains which have been shown to increase the solubility of compounds in organic solvents. One chain was of interest, 3,7-dimethyloctyl has been shown to dramatically improve solubility. The Williamson ether synthesis was done using this alkyl chain in place of the n-alkyl chains, the resulting yield was still good at 82%. However, the final synthetic step of using the benzaldehyde with the branched resulted in the same emulsion formation as observed with the n-alkyl benzaldehydes. In the end, the amphiphilic nature of the resulting receptors was too much to overcome making it necessary to look for other available options.

While the formation of emulsions when trying to make an aliphatic iminoguanidinium receptors was frustrating there still were additional options available. Another viable option was available in the form of the symmetric bis-N,N'-aminoguanidinium chloride

which was also commercially available. Use of the symmetric bis-N,N'-aminoguanidinium chloride made it was possible to attach two dialkylated phenyl rings to the receptor, which greatly reduces the amphiphilic nature of the charged guanidinium. The resulting receptor based on bis-N,N'-aminoguanidinium were found to be very soluble most organic solvents including hydrocarbon based solvent typically used in solvent extraction processes. The likely structure of the initial iminoguanidinium receptor and the structure of the successfully made diiminoguanidinium receptor is shown in **Figure 3.1**. The diiminoguanidinium receptor shown in **Figure 3.1** is known as TABEDIG (tetra-alkyl-bis-phenyl-diether-diiminoguanidinium) to make it simple to refer to.

3.2 Experimental

3.2.1 Synthesis of Diiminoguanidinium Receptor

The synthetic route for making the TABEDIG chloride salt is shown in **Figure 3.2**, below. The in-depth synthetic procedures for each step and the purification methods after each step is described following the synthetic route in **Figure 3.2**.

All reagents and solvents used in the synthesis of TABEDIG were obtained and purchased commercially from Fisher Scientific or Sigma Aldrich and were ACS reagent grade or better.

3.2.2 Synthesis of 3,7-dimethyl-1-iodooctane

32.34 g of 3,7-dimethyl-1-octanol (1 eq., 0.204 *M*), 64.30 g triphenylphosphine (1.2 eq., 0.245 *M*) and 20.86 g imidazole (1.5 eq., 0.306 *M*) were combined in a two-necked one liter round flask. To this mixture was added around 500 mL of dichloromethane. The reaction mixture was then placed in an ice bath to cool the reaction mixture to 0° C, which cooling the mixture was stirred using mechanical stirring. Once all the solids in the round bottom flask had dissolved, the reaction mixture was allowed to stir for 30 minutes, prior to the slow addition of 67.42 g iodine (1.3 eq., 0.265 *M*) via a solid addition funnel. The complete amount of iodine was added over the course of three hours, ice was periodically added to the ice bath to keep the temperature of the reaction around 0° C. As the batches of iodine were added the color of the reaction solution would turn initially yellow, as the iodine was consumed during the reaction the color disappears and the mixture would become colorless. Over the course of the reaction as the triphenylphosphine oxide by-product built up the dicholomethane solvent would hit a saturation point and it would crash-out as a white solid. Once a large majority of the starting alcohol was converted to the desired iodoalkane product the unreacted iodine caused the color of the reaction to turn brown. Once this point was reached the remaining iodine was added in one batch and the reaction was allowed to stir and come to room temperature for six hours or overnight. Then an aqueous solution of 10% sodium thiosulfate was added to this mixture to neutralize the iodine present in the solution. Within 10 minutes of the addition of thiosulfate while stirring the reaction color will change from dark brown to colorless. Once the solution became colorless the organic and aqueous phases were separated and the

organic phase was placed on the rotovap to remove a majority of the dichloromethane. Once much of the dichloromethane was remove, around 400-500 mL of hexanes were added to the round bottom flask to causing the triphenylphosphine oxide to precipitate out of solution. The suspension was then filtered using a funnel with a medium pore sintered glass frit removing the majority of the triphenylphosphine oxide from the solution containing the product. (Note: This step and the prior one adding in hexanes are not necessary. However, these two simple steps make the purification by column chromatography (CC) much easier and cheap by reducing the amount of solvent need for CC.) Once the solution is filtered the resulting hexanes containing the product with a small amount of by-products can be simply purified by passing this solution through a large plug of silica gel. The by-products from the reaction was very polar and will stick to the top of the silica gel plug which the iodoalkane is completely nonpolar and will run down the column in pure hexanes. (Note: For larger scale production of the iodoalkane it is necessary to use a large plug of silica gel.). The plug was washed with an additional one liter of hexanes, the filtrate will contain the pure iodoalkane. Once the hexanes were removed via rotovap the pure iodoalkane product will remain as a slightly viscous oil. The yield from the was quantitative, 54.70 g of 3,7-dimethyl-iodooctane.

3.2.3 Synthesis of 3,4-bis(3,7-dimethyloctyl)oxy)benzaldehyde

In a one liter round bottom flask were combined 16.69 g (2.2 eq, 62.23 mmol) 3,7-dimethyl-1-iodooctane, 3.91 g (1 eq., 28.29 mmol) 3,4-dihydroxybenzaldehyde, and 15.63 g (4 eq., 113.2 mmol) of potassium carbonate.(Note: It was later found that adding

the potassium carbonate after addition of the acetone, while the mixture was stirring with a magnetic stir bar resulted in a better stirring of the solution) To this mixture was added around 500 mL of acetone (Note: acetone was used because both of the iodoalkane and dihydroxybenzaldehyde were soluble in it), then the reaction mixture was heated to reflux (65-70° C) for 36 hours. After 36 hours, the reaction mixture was allowed to cool to room temperature and then filtered through a Buchner funnel to remove the unreacted potassium carbonate and the potassium salts formed during the progression of the reaction. The filtrate was then rotovaped to remove the acetone which resulted in a yellow/light brown oil and solid suspension. To this suspension was first added DI water to dissolve the solid most likely a potassium salt, then hexanes was added to dissolve the oil. This aqueous and organic mixture were poured into a 500 mL separatory funnel where the initially aqueous layer was removed prior to washing the organic layer with brine and then drying the organic layer with sodium sulfate. Then the organic layer was rotovaped to remove the hexanes, resulting in a yellow oil, which was purified by column chromatography. The product was purified using an automatic combiflash autocolumn system. The oil was placed on a 65 g silica gel precolumn and purified used a 120 g silica gel column. The autocolumn used a solvent system consisting of hexanes and ethyl acetate, a solvent gradient was used to separate the product from unreacted starting materials and by-products. The solvent gradient is as follows: pure hexanes for five minutes, increasing the ethyl acetate by 10% over the course of 5 minutes, then holding steady at 10% for 20 minutes, then further increasing the ethyl acetate percentage to 20% over two minutes, and holding steady at 20% for the remain four minutes of run time. The

use of this solvent gradient using the combiflash resulted in four different fractions. The first fraction was the unreacted iodoalkane starting material, the second fraction was the desired product, and the third and fourth fractions were the mono-substituted benzaldehydes. 9.72 g of the 3,4-bis(3,7-dimethyloctyl)oxy)benzaldehyde were synthesized from this reaction, the resulting yield for the reaction was 82%.

3.2.4 Synthesis of TABEDIG Cl

5.00 grams of 3,4-bis(3,7-dimethyloctyl)oxy)benzaldehyde and 0.750 grams of diaminoguanidine hydrochloride were combined 50 mL of neat ethanol in a 100 mL round bottom flask and heated to 65° C overnight. After heating overnight the reaction mixture was removed from the oil heating bath and placed in the refrigator overnight causing the desired product to separate from the ethanol as a dense oil at the bottom of the round bottom flask. The ethanol was then decanted from the round bottom and a drop of water was added prior to vigorously stirring the think oil which after 10 minutes turned from a viscous oil into a yellow solid with a waxy/taffy like consistency. The yield from this step of the synthesis was 70% (3.60 grams), the overall yield for the three steps used to make the TABEDIG Cl was 57.4%.

3.2.5 Liquid-Liquid Extraction Studies of Sulfate Removal Using TABEDIG

For the liquid-liquid extraction studies using TABEDIG used four different organic solvents, three commonly available solvents (toluene, 1,2-dichloroethane (1,2-DCE), and

1-octanol) were from Acros Organics reagent grade (99+ % pure) purchased from Fisher Scientific. The less common Isopar L which is a branched hydrocarbon averaging C12 was obtained from Exxon Mobil as a generous donation. The aqueous phase in the liquid-liquid extraction studies consisted of 10 mmol sodium chloride and 0.1 mmol sodium sulfate both of which were ≥ 99% pure and were obtained from Fisher Scientific. The salts were dissolved in MilliQ water (resistivity 18.2 $M\Omega cm^{-1}$). The radiolabeled sulfur-35 sodium sulfate solution was obtained from PerkinElmer as a one milliliter solution with an activity of 5 mCi/mL.

To determine the effectiveness of TABEDIG for extracting sulfate from aqueous solutions radiotracer experiments were conducted. The TABEDIG Cl salt was dissolved in various individual solvents. (Note: Prior to use the 1-octanol was pre-wetted by mixing the 1-octanol three time with fresh batches of MilliQ water with an organic to aqueous ratio (O:A) of 1:1). The TABEDIG Cl was dissolved as a 100 mmol stock solution in each solvent and then a serial dilution was done from these stocks to make additional samples with concentration of 30, 10, 3, and 1 mmol for the liquid-liquid extraction tests. For these experiments a large bulk aqueous solution was made containing 10 mmol sodium chloride and 0.1 mmol sodium sulfate dissolved in MilliQ water. The mixing (contacting) of the organic and aqueous phases were done in 2 mL Eppendorf tubes, all points were done in duplicate to reduce the chance of an error being incorrectly reported. For all experiments an O:A of 1:1 was used with 600 μL of each phase being used, respectively. Prior to contacting a 5 μL spike of a 50 $\mu Ci/mL$ solution of $Na_2{}^{35}SO_4$ radiotracer was

added to each solution. All contacting was done in a temperature controlled air-box set at 25 $\pm$ 0.2 °C for a period of one hour. After one hour, the samples were then centrifuged for 5 minutes at 3000 rpm at 25 $\pm$ 0.2 °C in a temperature controlled Beckmann-Coulter centrifuge. After centrifuging the samples were then subsampled by removing 300 μL from each phase. The 300 μL from each phase of each sample were pipetted into individual HDPE scintillation vials which contained 10 mL of UltimaGold scintillation cocktail. Once the samples were added to the vials containing the scintillation cocktail, the vials were sealed and vigorously shaken to ensure complete dissolution and homogenization of the sample in the cocktail. In addition to the samples resulting from contacting, samples were prepared to ensure that the organic and aqueous solutions did not quench (absorption of emitted light) the fluorescence that would be otherwise detected in the liquid scintillation counter. All samples were counted in a beta liquid scintillation counter for 30 minutes and the counts per a minute were corrected for background and possible quenching if it occurred (if there was a difference of more than 3% a correction factor was applied).

3.2.6 Karl Fischer Titrations of Pre- and Post Contacting Isopar L Solutions

Karl Fischer Titrations were performed on solutions of Isopar L containing TABEDIG to determine the amount of water taken up after contacting. The water analysis was done using a Metrohm 831 KF Coulometer. Water determination was done by injecting a known

weight of the solution into the cell of the 831 KF Coulometer which contained Fluka Hydranal solution which was a premixed containing the Karl Fischer reagent.

3.3 Results and Discussion

3.3.1 Removal of Sulfate Using Guanidiniums

The initial testing of the TABEDIGs performance for the extraction of sulfate from aqueous solutions was done in 1,2-DCE. By testing TABEDIGs effectiveness for sulfate extraction into 1,2-DCE allowed for a direct comparison with simple guanidinium which had been synthesized and tested by ORNL's Chemical Separations Group but has not yet been published. Similar test conditions were used to allow for a direct head-to-head comparison of TABEDIG and the series of simple guanidiniums. The structures of the series of simple guanidinium and TABEDIG are shown in **Figure 3.3**.

The results of the extraction tests in 1,2-DCE shown in **Figure 3.4**, indicated that TABEDIGs performance surpassed the series of simple guanidiniums. In **Figure 3.4**, the log of the $D_{SO_4^{2-}}$ values are graphed against the log of the concentration of the extractants. By using log of both concentration and $D_{SO_4^{2-}}$ make it possible to do a slope analysis to determine what the possible stoichiometry of the extracted complex could be. For Di-henyl, Tri-pheny, and TABEDIG the slopes were close to two, which is indicative of a 2:1 receptor to sulfate ratio in the 1,2-DCE.

After analyzing the data for the 1,2-DCE extraction experiments the question of how effective would TABEDIG be in other organic solvents. One case of great interest was what effect would the use hydrocarbon based solvents, particularity Isopar L have on TABEDIG's ability to extract sulfate from aqueous solutions. From this reason three solvents were selected to be tested, toluene which has been used in the past to test extractants, 1-octanol since it can provide additional H-bonding donors during extraction, and Isopar L which is used commercially in solvent extraction processes. The results from the extraction tests in various solvents are shown in **Figure 3.5** and the $D_{SO_4^{2-}}$ in each solvent at each concentration are listed in **Table 3.1**.

The high performance of the TABEDIG in all the solvent was completely unexpected, as many of the other anion receptors had been unable to extraction meaningful amounts of sulfate into any solvent. Most other receptors were only able to achieve a high $D_{SO_4^{2-}}$ value when used in large concentrations in solvent like 1-octanol which aids in the extraction by H-bonding to the sulfate. In prior experiments where a few of the simple guanidiniums (shown in **Figure 3.3**), were dissolved in 1-octanol, it was found that the extraction was dominated by the solvent with the guanidinium merely acting to balance the charge of the sulfate. From **Table 3.1** it becomes apparent that in the hydrocarbon based solvents (e.g. toluene and Isopar L) the TABEDIG easily achieves a $D_{SO_4^{2-}}$ value greater than one at 3 and 1 mmol, respectively. The solubilizing TABEDIG in Isopar L was a major step forward. Its' extremely high $D_{SO_4^{2-}}$ value was the most unexpected outcome of this experiments.

Slope analysis of data similar to what was done with the simple guanidinium in 1,2-DCE gave interesting results. In 1-octanol the slope was two, indicating that similar to 1,2-DCE the complex formed was 2:1 receptor-to-sulfate. However, in toluene and more so in Isopar are the concentration of the receptor was increased the slope decrease from 2 to 1 eventually in the case of Isopar L the slope went to 0.3. This marked decrease in the slope from 2 to 1 or less is indicative of the formation aggregates in the organic phase.

To further investigate what could possibly be occurring during the extraction of sulfate Karl Fischer titration were performed. Karl Fischer (KF) titrations allows for the determination of the water concentration in an organic solvent. For the KF titrations samples containing 100 mmol of TABEDIG in Isopar L and 1,2-DCE were contacted/mixed with aqueous solutions containing various concentrations of sulfate (1.0, 0.1, 0.01, 0.001) and just MilliQ water. In addition to the contacted samples of the TABEDIG, KF titrations were also done on the neat organic solutions and the solutions of TABEDIG that had not been contacted were also used and tested to determine the concentrations of water. The concentration of water in each of the neat organic solvents was subtracted for the concentrations of the uncontacted TABEDIG solutions in each respective solvent. From this initial data it was determined that for each TABEDIG Cl that was a corresponding 0.5 water molecules. The results of the KF titrations on the TABEDIG solutions contacted with just MilliQ water revealed that the concentration of water in the samples increased by a factor of two, making it one water molecule per one TABEDIG in solution for both the Isopar L and 1,2-DCE, respectively. The concentrations

of water in the solvents when contacted with the aqueous solutions that contained various sulfate concentrations increased. However, the variation of the concentration of the sulfate did not have an apparent effect on the amount of water taken up. In the case of 1,2-DCE is the amount of water increased from 1 to 1.5 waters per a TABEDIG while in Isopar L the amount increased from 1 to 2 waters after contacting with the sulfate solutions. Although there was no noticeable increase in the amount of water as the sulfate concentration increased the fact that there was an increase when sulfate was present is of interest. This uptake of water could be a reason for the increased $D_{SO_4^{2-}}$ values during extraction. When the water is taken up in addition to the sulfate the energetic penalty for desolvation of the sulfate during extraction is greatly reduced.

While the formation of aggregates and increased concentrations of water during the extraction of sulfates does help to explain why the $D_{SO_4^{2-}}$ value in Isopar L it does not give a complete picture of what is occurring during extraction. In an efforted to more accurately determine what occurred during the extraction process additional experiments were done by Dr. Ross Ellis at ORNL using small angle x-ray scattering (SAXS) to look at the sizes of the aggregates. In this chapter, I will not discuss the SAXS data in detail, although this information will be published at a later date. A quick summary of what was learned from the SAXS is as follows; TABEDIG does form reversed micelles in Isopar L even at low concentrations. The fact that reversed micelles were present in the Isopar L is of great interest as it raises the question of whether the inclusion of the water in the micelles

formed during extraction indicates the formation of sulfate-water clusters which are formed and encapsulated in a TABEDIG reversed micelle.

Currently we are not able to definitively determine what the complete composition of the micelles are because there are no current techniques which could elucidate complete structure inside of the reversed micelles. Additionally, the question of which possible conformational arrangement of TABEDIG is predominate in the reversed micelles cannot not be answered either due to the complexity of the extracted species. Some insight could be obtained using computational modelling once force-field parameters for the core diiminoguanidiniums are developed to predict the structures in the micelles and further SAXS are done on additional solutions. Three possible conformers for the TABEDIGs in the micelles are proposed in **Figure 3.6**, below. Of the three conformers, the most likely one is the one on the far right. This conformer allows for the greatest number of hydrogen bonding interaction's between TABEDIG and the waters and anions inside of the micelles.

3.4 Conclusion

This new class of receptors based on diiminoguandiniums represents a leap forward for oxoanion extractants. The synthetic accessibility and high synthetic yields with only a moderate number of synthetic steps make TABEDIG an attractive anion receptor. Additionally, the ease with which the alkyl substituents can be changed on the core of the receptor make it possible to tailor the receptor for specific tasks for oxoanion extraction. The four alkyl groups on TABEDIG greatly enhance the solubility that has

been a limiting factor in their use in solvent extraction. Once in solution, TABEDIG has out preformed all known sulfate anion receptors, with an improvement of 420× over the next best known sulfate receptor which is also a guanidinium. TABEDIG's high solubility in hydrocarbon diluents like Isopar L make it an attractive target for further development into an actual solvent extraction process to selectively remove sulfate.

3.5 References

1.Rydberg, J.; Cox, M.; Musikas, C.; Choppin, G. R., *Solvent Extraction Principles and Practice*. 2nd ed.; Marcel Dekker, Inc.: New York, 2004.

2.Seipp, C. A.; Williams, N. J.; Bryantsev, V. S.; Custelcean, R.; Moyer, B. A., A conformationally persistent pseudo-bicyclic guanidinium for anion coordination as stabilized by dual intramolecular hydrogen bonds. *RSC Adv.* **2015,** *5* (130), 107266-107269.

3.Custelcean, R.; Williams, N. J.; Seipp, C. A., Aqueous Sulfate Separation by Crystallization of Sulfate-Water Clusters. *Angew Chem Int Ed Engl* **2015,** *54* (36), 10525-9.

4.Custelcean, R.; Williams, N. J.; Seipp, C. A.; Ivanov, A. S.; Bryantsev, V. S., Aqueous Sulfate Separation by Sequestration of [(SO4)2 (H2 O)4]4- Clusters within Highly Insoluble Imine-Linked Bis-Guanidinium Crystals. *Chemistry* **2016,** *22* (6), 1997-2003.

5.Seipp, C. A.; Williams, N. J.; Kidder, M. K.; Custelcean, R., CO2 Capture from Ambient Air by Crystallization with a Guanidine Sorbent. *Angew Chem Int Ed Engl* **2017,** *56* (4), 1042-1045.

3.6 Appendix 3A Supplemental Information for Chapter 3

3.6.1 Attempts at Guanylation Reactions in Mixed Urea-Guanidinium Anion Receptors

An initial approach taken in my research for achieving shape recognition and charge complementary in oxoanion receptors involved the synthesis of mixed donor receptors. These mixed-donor receptors incorporated hydrogen bond donors such as ureas and guanidiniums arranged in a manner that would be ideal for achieving the correct shape and charge complementary for sulfate and phosphate anions. The structures of these receptors are shown in **Figure 3.7**; the three receptors shown were designed to be selective for phosphate or sulfate. The mono-urea-guanidiniums (MUGs) and tri-urea-guanidiniums (TUGs) were designed to be ideal for binding to tribasic phosphate, providing the twelve hydrogen bonds and off-setting the negative-three charge of the phosphate with positively charged guanidiniums. The bis-urea-guanidiniums (BUGs) were designed to be selective for sulfate, forming a 2-to-1 complex with a net charge of zero. The general synthetic route attempted for these compounds used methods and procedures that have been previously employed in the literature.[1,2] The urea-thiourea precursors generated using the previously reported literature methods are shown in **Figure 3.8**.[1,2]

The conversion of the thioureas to guanidinium was attempted using procedures previously reported in the literature.[3] This literature procedure employed a two-step

synthesis, where the thioureas is converted to a *S*-methylthiouronoium iodide salt and subsequently reacted with ammonia or an amine depending on the desired substitution of the guanidinium. The two-step procedure is shown in **Figure 3.9** below. To methylate the thioureas, the reactant (thiourea) is dissolved in absolute ethanol, and the methylating reagent (iodomethane) is added in 5- to 10-mol. fold excess to the thiourea. The methylating reagent is added after the reaction mixture has been cooled to 0 °C. After addition of the iodomethane, the reaction mixture is allowed to stir and come to room temperature overnight.

The methyl-thiouronium is not isolated prior to use in the next step; this is due to the high reactivity of the methyl-thiouronium intermediate and the likelihood that the compound would decompose during the purification process. In the next step, the methyl-thiouronium is suspended/dissolved in absolute ethanol; then the desired amine or ammonia is added to the reaction mixture and heated to reflux for 24-72 hours. (Note: this reaction should have a bubbler containing 10% bleach hooked up to it, due to the production and subsequent off-gassing of the highly toxic methylsulfide generated as the guanylation progresses.)

After multiple unsuccessful attempts to guanylate the mixed urea-thiourea precursors receptors, it was found that the methyl-thiouronium intermediate or intended guanidiniums were highly unstable due to the presence of the –NH of the adjacent urea(s). The proposed method for guanylation is shown in **Figure 3.10**.

When the reaction products were isolated after the guanylation step, it was found that the –NH of the urea had reacted with the methyl-thiouronium or guanidinium to form the compounds in **Figure 3.11**. The initial starting amine used when making the initial urea-thiourea precursors was isolated after guanylation; this was one the indicators for the formation of the cyclic guanidinium shown in **Figure 3.11**. The other breakdown product from the urea was not isolated most likely because it decomposed either during the reaction or from the subsequent work-up of the reaction.

Other guanylation methods were used in attempt to make the mixed urea-guanidinium donors. The other methods from the literature[3,4] that were used in an attempt to generate the urea-guanidinium receptor, went through carbodiimide intermediates to get to the guanidiniums. These methods used harsher reagents like lead carbonate, triethylbenzylammonium permanganate, etc. to generate the carbodimide intermediate. However, all these other methods also result in the formation of the undesirable cyclic guanidinium and amine. In conclusion, the nature of the urea-guanidiniums receptors are such that the systems themselves are highly unstable and easily prone to cyclization to form the cyclic guanidinium and amine. Before more attempts were done on synthetic experiments where the electronic and structure of the urea-guanidinium receptors, the new diiminoguanidinium receptors like TABEDIG discovered, drawing our attention to its characterization.

3.7 Appendix References

1. Jia, C.; Wu, B.; Li, S.; Huang, X.; Zhao, Q.; Lu, Q.-S.; Yang, X.-J., Highly Efficient Extraction of Sulfate Ions with a Tripodal Hexaurea Receptor. *Angew. Chem. Int. Ed. Engl.* **2011**, 486-490.
2. Zhang, Y.; Zhang, R.; Zhao, Y.; Ji, L.; Jia, C.; Wu. B. Anion binding of tris-(thio)urea ligands. *New J. Chem*. **2013**, 2266-2270.
3. Seipp, C. A.; Williams, N. J.; Bryantsev, V. S.; Custelcean, R.; Moyer, B. A., A conformationally persistent pseudo-bicyclic guanidinium for anion coordination as stabilized by dual intramolecular hydrogen bonds. *RSC Adv.* **2015,** *5* (130), 107266-107269.
4. Li, J.-H.; Snyder, J.H.. Selective oxidation of canthines to canthin-6-ones with triethylbenzylammonium permanganate. *Tet. Lett.* **1994**. 1485-1488.

3.8 Appendix 3B Figures and Tables for Chapter 3

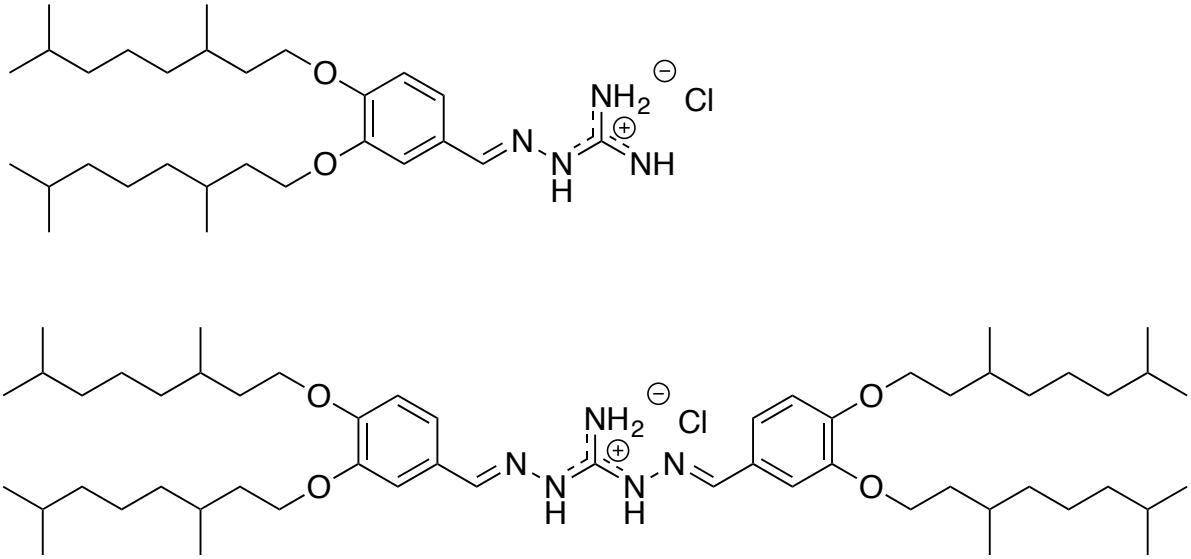

Figure 3.1. Structures of iminoguaniginium chloride and diiminoguanidinium chloride**.**

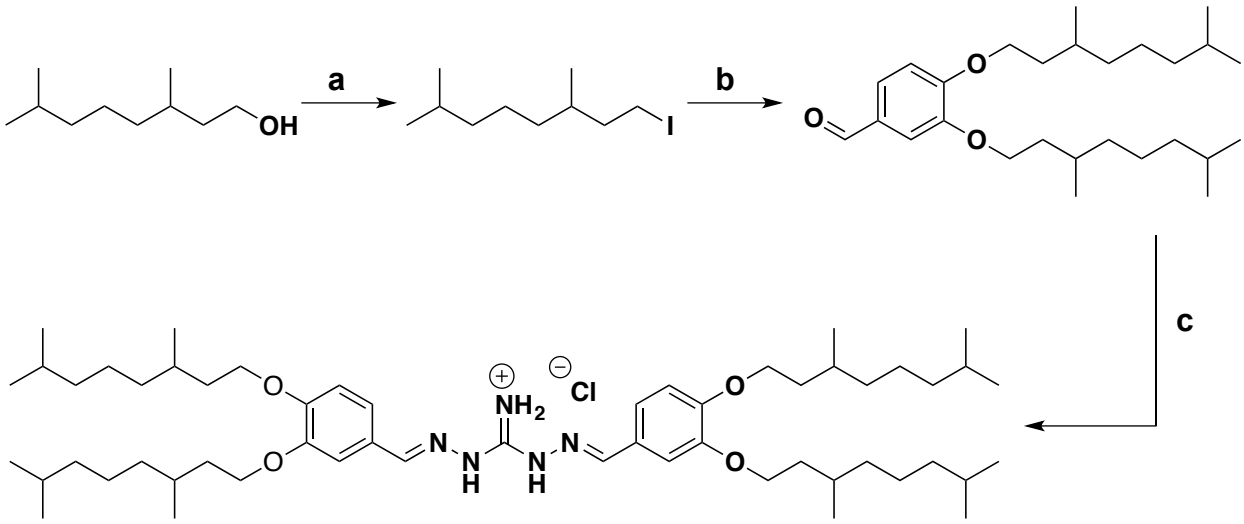

Figure 3.2. Synthetic route for TABEDIG Cl. a.) I_2, imidazole, PPh_3, DCM, $\mathbf{0^oC}$→ RT b.) 3,4-dihydroxybenzaldehyde, K_2CO_3, Acetone, 65 °C c.) diaminoguanidinium chloride, EtOH, 65 °C, overnight.

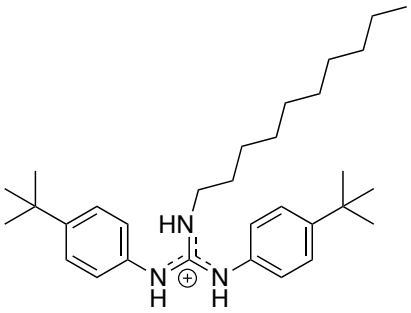

N,N'-bis-(4-*tert*-butylphenyl)-N'-decylguanidinium (DIphenyl)

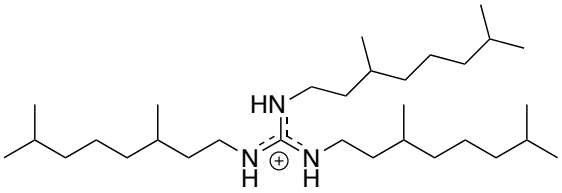

N,N',N"-Tris-(3,7-dimethyloctyl)guanidinium (Trialkyl)

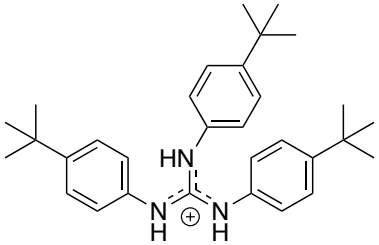

N,N',N"-Tris-(4-*tert*-butylphenyl)guanidinium (Triphenyl)

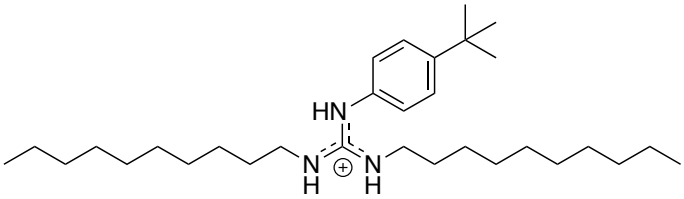

N,N'-bis-decyl-N"-(4-*tert*-butylphenyl)lguanidinium (Monophenyl)

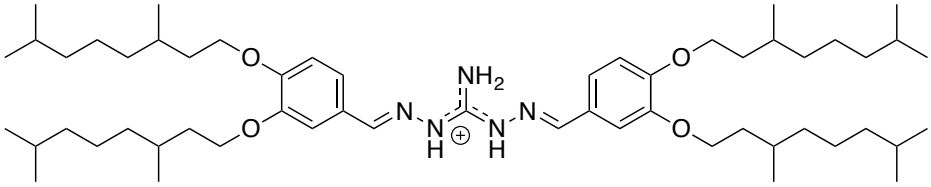

TABEDIG

Figure 3.3. Structures of the simple guanidiniums and TABEDIG.

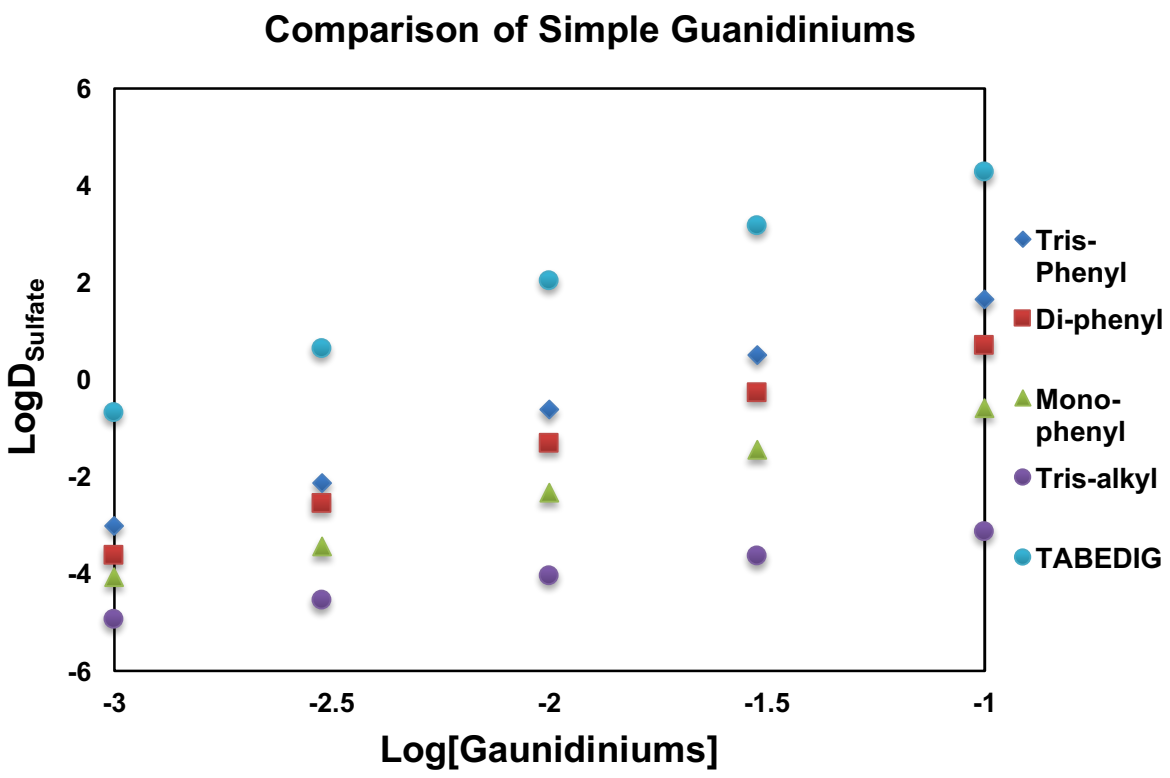

Figure 3.4. Comparison of simple guanidinium sulfate extraction versus TABEDIG's sulfate extraction.

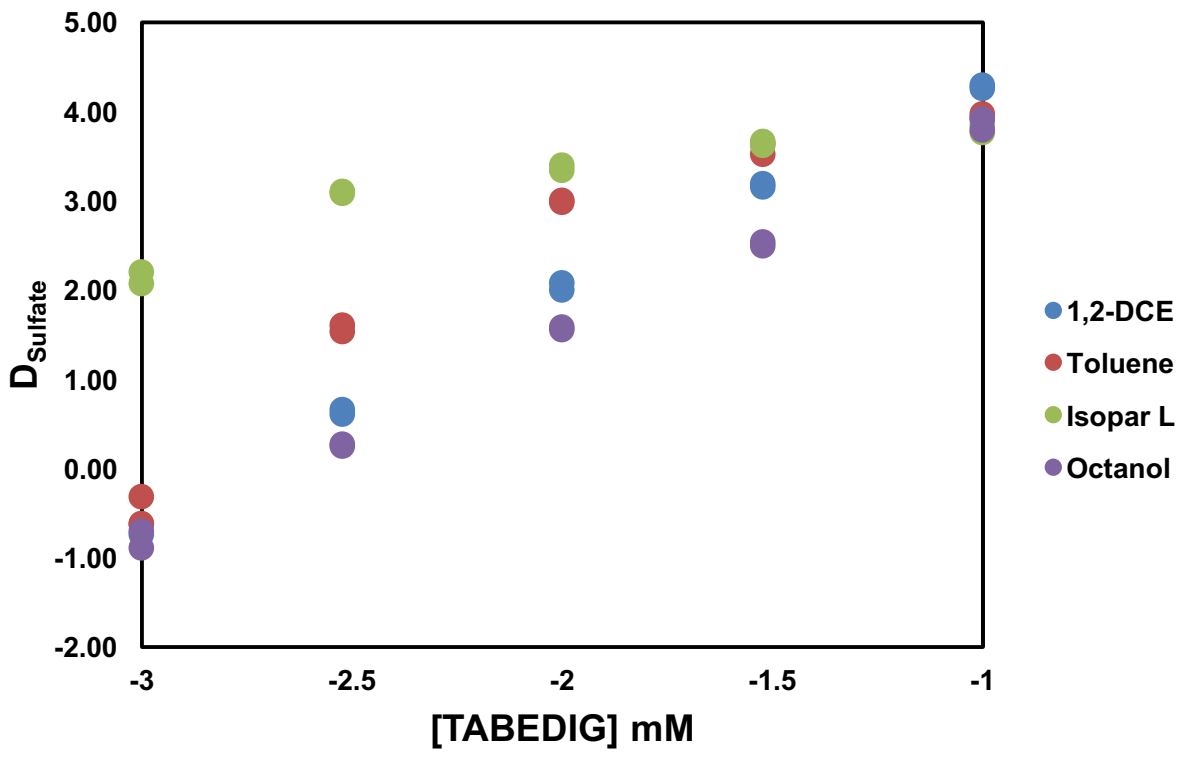

Figure 3.5. TABEDIG performance for sulfate extraction in various solvents. The axis and values are shown as in log form.

Table 3.1. List of distribution values (Dvalues) obtained with TABEDIG in various solvents during the sulfate extraction experiments.

[TABEDIG] mmol	1-Octanol	1,2-DCE	Toluene	Isopar
1	0.164	0.210	0.360	137.05
3	1.81	4.32	37.17	1238.9
10	37.1	109.1	984.2	4328.3
30	329.1	1478.3	3828.9	4388.2
100	1839.7	18837.4	8904.8	6370.1

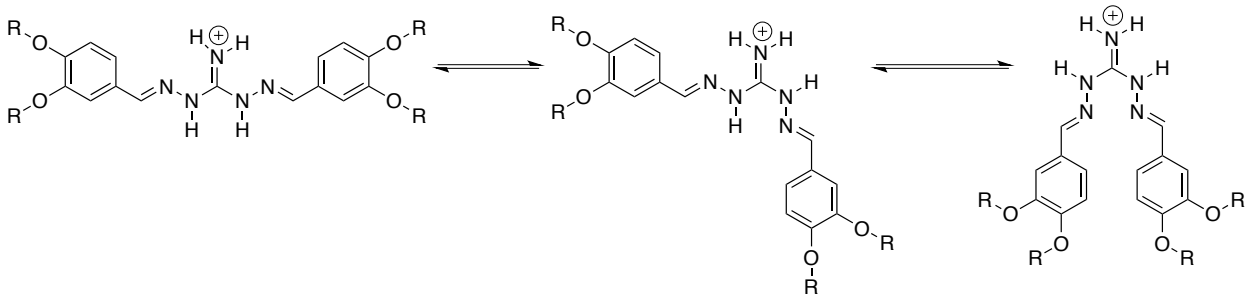

Figure 3.6. Possible conformations of TABEDIG in the reversed micelles.

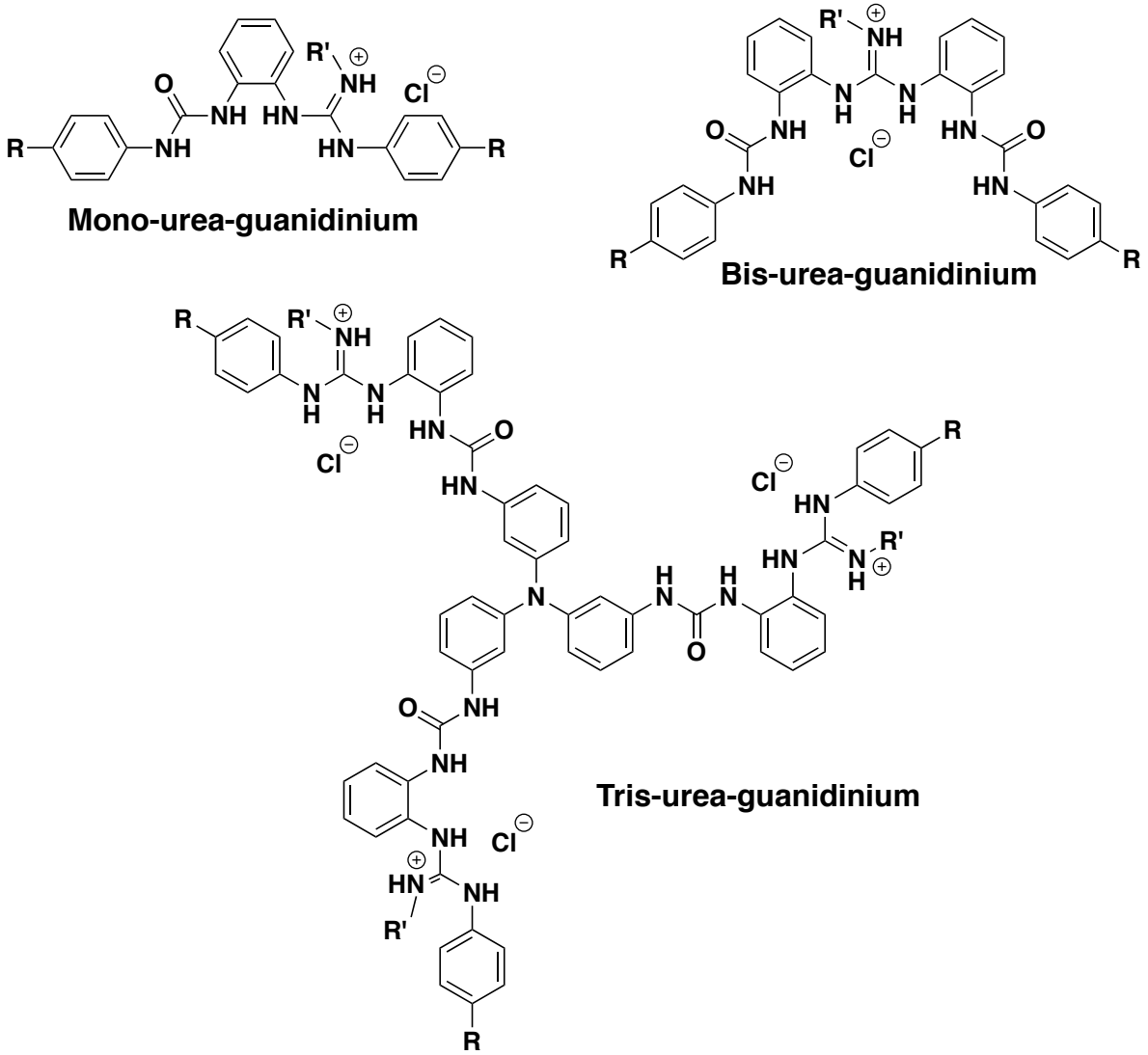

Figure 3.7. Initial target oxoanion receptors of the selective recognition sulfate and phosphate via shape and charge complementarity.

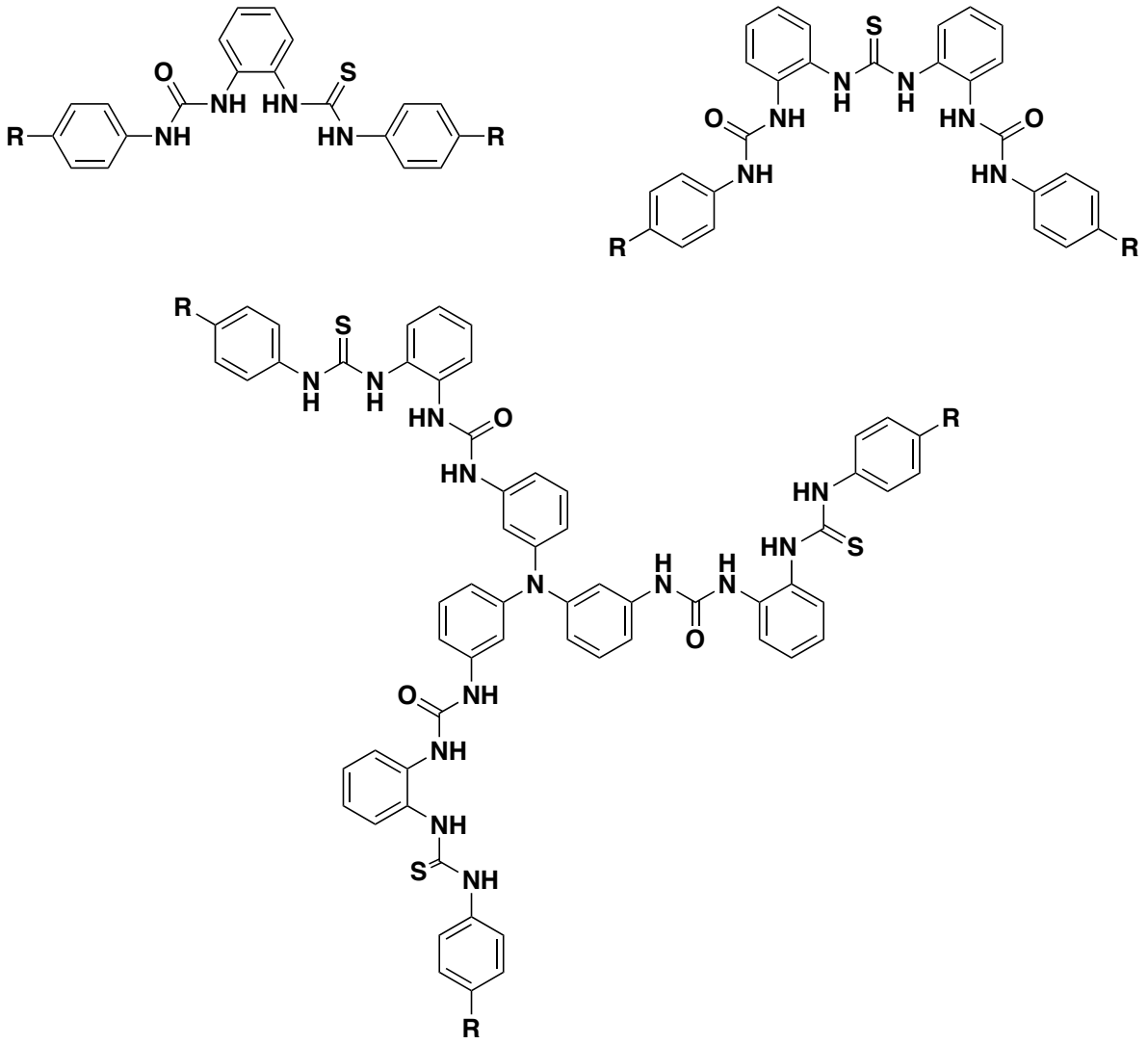

Figure 3.8. Urea-thiourea precursors for the mixed urea-guanidinium oxoanion receptors.

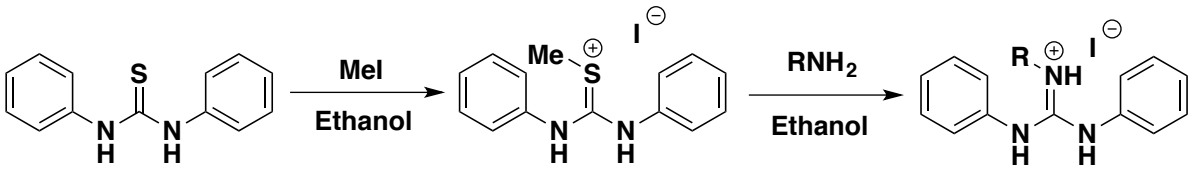

Figure 3.9. General two-step procedure used to convert thioureas to guanidiniums.

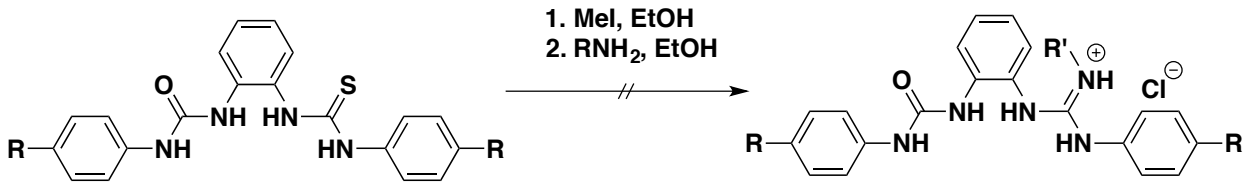

Figure 3.10. Proposed synthetic route for the mixed urea-guanidinium receptors.

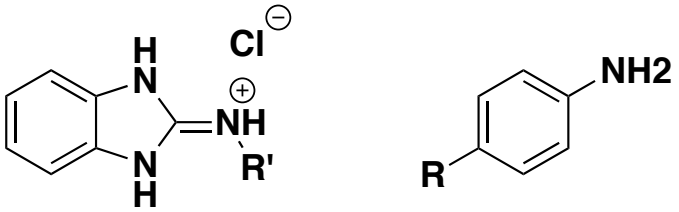

Figure 3.11. Isolated products for the guanylation reaction, cyclic guanidinium and corresponding amine.

Chapter 4 : Aqueous Sulfate Separation by Crystallization of Sulfate–Water Clusters

Publication Statement for Chapter 4

Reference for Original Article:

Custelcean R.; Williams N.J.; Seipp, C.A. “Aqueous Sulfate Separation by Crystallization of Sulfate–Water Clusters.” *Angew. Chem. Int. Ed.* **2015**, 54, 10525–10529.

Individual Author Contribution(s):

Custelcean, R. – Made initial discovery of ligands interactions with oxoanions, grew crystals of ligand with oxoanions, competitive crystallizations, XRD and powder XRD of solid complexes, wrote and edited final manuscript

Williams, N. J. – Synthesis of ligands, determined solubility of ligands salts via UV-Spectroscopy, writing

Seipp, C. A. – Took IR spectra of ligand complexes with various salts and writing

Journals Policy/Permission/Agreement for Reproduction of Article

JOHN WILEY AND SONS LICENSE
TERMS AND CONDITIONS

Mar 16, 2017

This Agreement between Neil J Williams ("You") and John Wiley and Sons ("John Wiley and Sons") consists of your license details and the terms and conditions provided by John Wiley and Sons and Copyright Clearance Center.

License Number	4070851215290
License date	Mar 16, 2017
Licensed Content Publisher	John Wiley and Sons
Licensed Content Publication	Angewandte Chemie International Edition
Licensed Content Title	Aqueous Sulfate Separation by Crystallization of Sulfate-Water Clusters
Licensed Content Author	Radu Custelcean,Neil J. Williams,Charles A. Seipp
Licensed Content Date	Aug 7, 2015
Licensed Content Pages	5
Type of use	Dissertation/Thesis
Requestor type	Author of this Wiley article
Format	Print and electronic
Portion	Full article
Will you be translating?	No
Title of your thesis / dissertation	Ion Separations: Achieving Selectivity Through Rational Design in Solvent Extraction and Crystallization Systems
Expected completion date	May 2017
Expected size (number of pages)	400
Requestor Location	Neil J Williams Oak Ridge National Laboratory PO Box 2008 MS6119 OAK RIDGE, TN 37831 United States Attn: Neil J Williams
Publisher Tax ID	EU826007151
Billing Type	Invoice
Billing Address	Neil J Williams Oak Ridge National Laboratory PO Box 2008 MS6119 OAK RIDGE, TN 37831 United States Attn: Neil J Williams
Total	0.00 USD
Terms and Conditions	

TERMS AND CONDITIONS

This copyrighted material is owned by or exclusively licensed to John Wiley & Sons, Inc. or one of its group companies (each a"Wiley Company") or handled on behalf of a society with which a Wiley Company has exclusive publishing rights in relation to a particular work (collectively "WILEY"). By clicking "accept" in connection with completing this licensing transaction, you agree that the following terms and conditions apply to this transaction (along with the billing and payment terms and conditions established by the Copyright Clearance Center Inc., ("CCC's Billing and Payment terms and conditions"), at the time that you opened your RightsLink account (these are available at any time at http://myaccount.copyright.com).

Terms and Conditions

- The materials you have requested permission to reproduce or reuse (the "Wiley Materials") are protected by copyright.

- You are hereby granted a personal, non-exclusive, non-sub licensable (on a stand-alone basis), non-transferable, worldwide, limited license to reproduce the Wiley Materials for the purpose specified in the licensing process. This license, **and any CONTENT (PDF or image file) purchased as part of your order,** is for a one-time use only and limited to any maximum distribution number specified in the license. The first instance of republication or reuse granted by this license must be completed within two years of the date of the grant of this license (although copies prepared before the end date may be distributed thereafter). The Wiley Materials shall not be used in any other manner or for any other purpose, beyond what is granted in the license. Permission is granted subject to an appropriate acknowledgement given to the author, title of the material/book/journal and the publisher. You shall also duplicate the copyright notice that appears in the Wiley publication in your use of the Wiley Material. Permission is also granted on the understanding that nowhere in the text is a previously published source acknowledged for all or part of this Wiley Material. Any third party content is expressly excluded from this permission.

- With respect to the Wiley Materials, all rights are reserved. Except as expressly granted by the terms of the license, no part of the Wiley Materials may be copied, modified, adapted (except for minor reformatting required by the new Publication), translated, reproduced, transferred or distributed, in any form or by any means, and no derivative works may be made based on the Wiley Materials without the prior permission of the respective copyright owner.**For STM Signatory Publishers clearing permission under the terms of the STM Permissions Guidelines only, the terms of the license are extended to include subsequent editions and for editions in other languages, provided such editions are for the work as a whole in situ and does not involve the separate exploitation of the permitted figures or extracts,** You may not alter, remove or suppress in any manner any copyright, trademark or other notices displayed by the Wiley Materials. You may not license, rent, sell, loan, lease, pledge, offer as security, transfer or assign the Wiley Materials on a stand-alone basis, or any of the rights granted to you hereunder to any other person.

- The Wiley Materials and all of the intellectual property rights therein shall at all times remain the exclusive property of John Wiley & Sons Inc, the Wiley Companies, or their respective licensors, and your interest therein is only that of having possession of and the right to reproduce the Wiley Materials pursuant to Section 2 herein during the continuance of this Agreement. You agree that you own no right, title or interest in or to the Wiley Materials or any of the intellectual property rights therein. You shall have no rights hereunder other than the license as provided for above in Section 2. No right, license or interest to any trademark, trade name, service mark or other branding

- Any fee required for this permission shall be non-refundable after thirty (30) days from receipt by the CCC.

- These terms and conditions together with CCC's Billing and Payment terms and conditions (which are incorporated herein) form the entire agreement between you and WILEY concerning this licensing transaction and (in the absence of fraud) supersedes all prior agreements and representations of the parties, oral or written. This Agreement may not be amended except in writing signed by both parties. This Agreement shall be binding upon and inure to the benefit of the parties' successors, legal representatives, and authorized assigns.

- In the event of any conflict between your obligations established by these terms and conditions and those established by CCC's Billing and Payment terms and conditions, these terms and conditions shall prevail.

- WILEY expressly reserves all rights not specifically granted in the combination of (i) the license details provided by you and accepted in the course of this licensing transaction, (ii) these terms and conditions and (iii) CCC's Billing and Payment terms and conditions.

- This Agreement will be void if the Type of Use, Format, Circulation, or Requestor Type was misrepresented during the licensing process.

- This Agreement shall be governed by and construed in accordance with the laws of the State of New York, USA, without regards to such state's conflict of law rules. Any legal action, suit or proceeding arising out of or relating to these Terms and Conditions or the breach thereof shall be instituted in a court of competent jurisdiction in New York County in the State of New York in the United States of America and each party hereby consents and submits to the personal jurisdiction of such court, waives any objection to venue in such court and consents to service of process by registered or certified mail, return receipt requested, at the last known address of such party.

WILEY OPEN ACCESS TERMS AND CONDITIONS

Wiley Publishes Open Access Articles in fully Open Access Journals and in Subscription journals offering Online Open. Although most of the fully Open Access journals publish open access articles under the terms of the Creative Commons Attribution (CC BY) License only, the subscription journals and a few of the Open Access Journals offer a choice of Creative Commons Licenses. The license type is clearly identified on the article.

The Creative Commons Attribution License

The Creative Commons Attribution License (CC-BY) allows users to copy, distribute and transmit an article, adapt the article and make commercial use of the article. The CC-BY license permits commercial and non-

Creative Commons Attribution Non-Commercial License

The Creative Commons Attribution Non-Commercial (CC-BY-NC)License permits use, distribution and reproduction in any medium, provided the original work is properly cited and is not used for commercial purposes.(see below)

Creative Commons Attribution-Non-Commercial-NoDerivs License

The Creative Commons Attribution Non-Commercial-NoDerivs License (CC-BY-NC-ND) permits use, distribution and reproduction in any medium, provided the original work is properly cited, is not used for commercial purposes and no modifications or adaptations are made. (see below)

Use by commercial "for-profit" organizations

Use of Wiley Open Access articles for commercial, promotional, or marketing purposes requires further explicit permission from Wiley and will be subject to a fee.
Further details can be found on Wiley Online Library
http://olabout.wiley.com/WileyCDA/Section/id-410895.html

Other Terms and Conditions:

v1.10 Last updated September 2015

Questions? customercare@copyright.com or +1-855-239-3415 (toll free in the US) or +1-978-646-2777.

("Marks") of WILEY or its licensors is granted hereunder, and you agree that you shall not assert any such right, license or interest with respect thereto

- NEITHER WILEY NOR ITS LICENSORS MAKES ANY WARRANTY OR REPRESENTATION OF ANY KIND TO YOU OR ANY THIRD PARTY, EXPRESS, IMPLIED OR STATUTORY, WITH RESPECT TO THE MATERIALS OR THE ACCURACY OF ANY INFORMATION CONTAINED IN THE MATERIALS, INCLUDING, WITHOUT LIMITATION, ANY IMPLIED WARRANTY OF MERCHANTABILITY, ACCURACY, SATISFACTORY QUALITY, FITNESS FOR A PARTICULAR PURPOSE, USABILITY, INTEGRATION OR NON-INFRINGEMENT AND ALL SUCH WARRANTIES ARE HEREBY EXCLUDED BY WILEY AND ITS LICENSORS AND WAIVED BY YOU.

- WILEY shall have the right to terminate this Agreement immediately upon breach of this Agreement by you.

- You shall indemnify, defend and hold harmless WILEY, its Licensors and their respective directors, officers, agents and employees, from and against any actual or threatened claims, demands, causes of action or proceedings arising from any breach of this Agreement by you.

- IN NO EVENT SHALL WILEY OR ITS LICENSORS BE LIABLE TO YOU OR ANY OTHER PARTY OR ANY OTHER PERSON OR ENTITY FOR ANY SPECIAL, CONSEQUENTIAL, INCIDENTAL, INDIRECT, EXEMPLARY OR PUNITIVE DAMAGES, HOWEVER CAUSED, ARISING OUT OF OR IN CONNECTION WITH THE DOWNLOADING, PROVISIONING, VIEWING OR USE OF THE MATERIALS REGARDLESS OF THE FORM OF ACTION, WHETHER FOR BREACH OF CONTRACT, BREACH OF WARRANTY, TORT, NEGLIGENCE, INFRINGEMENT OR OTHERWISE (INCLUDING, WITHOUT LIMITATION, DAMAGES BASED ON LOSS OF PROFITS, DATA, FILES, USE, BUSINESS OPPORTUNITY OR CLAIMS OF THIRD PARTIES), AND WHETHER OR NOT THE PARTY HAS BEEN ADVISED OF THE POSSIBILITY OF SUCH DAMAGES. THIS LIMITATION SHALL APPLY NOTWITHSTANDING ANY FAILURE OF ESSENTIAL PURPOSE OF ANY LIMITED REMEDY PROVIDED HEREIN.

- Should any provision of this Agreement be held by a court of competent jurisdiction to be illegal, invalid, or unenforceable, that provision shall be deemed amended to achieve as nearly as possible the same economic effect as the original provision, and the legality, validity and enforceability of the remaining provisions of this Agreement shall not be affected or impaired thereby.

- The failure of either party to enforce any term or condition of this Agreement shall not constitute a waiver of either party's right to enforce each and every term and condition of this Agreement. No breach under this agreement shall be deemed waived or excused by either party unless such waiver or consent is in writing signed by the party granting such waiver or consent. The waiver by or consent of a party to a breach of any provision of this Agreement shall not operate or be construed as a waiver of or consent to any other or subsequent breach by such other party.

- This Agreement may not be assigned (including by operation of law or otherwise) by you without WILEY's prior written consent.

A version of this chapter was originally published by Radu Custelcean, Neil J. Williams and Charles A. Seipp in *Angewandte Chemie International Edition*

Custelcean R.; Williams N.J.; Seipp, C.A. "Aqueous Sulfate Separation by Crystallization of Sulfate–Water Clusters." *Angew. Chem. Int. Ed.* **2015**, 54, 10525–10529.

The article used as Chapter 4 was modified in the following manner; the formatting was adapted to fit the formatting required by the University of Tennessee Knoxville, the figures and tables were renumbered to make all figures in the ensuing document contiguous. The work/research of the done by the student in the articles is as follows synthesis, measured solubility of salts of the compounds, and contributed to the writing for the electronic supplementary information.

Abstract

An effective approach to sulfate separation from aqueous solutions is based on the crystallization of extended $[SO_4(H_2O)_5^{2-}]_n$ sulfate–water clusters with a bis(guanidinium) ligand. The ligand was generated in situ by hydrazine condensation in water, thereby bypassing the need for elaborate syntheses, tedious purifications, and organic solvents. Crystallization of sulfate–water clusters represents an alternative approach to the now established sulfate separation strategies that involve encapsulation of the "naked" anion

4.1 Introduction

With a free energy of hydration of –1080 kJmol^{-1},[1] sulfate is one of the most hydrophilic anions found in nature. The extreme water affinity of sulfate originates from its high charge density and its ability to accept multiple hydrogen bonds from water. Theoretical and experimental studies have demonstrated the existence of a variety of $SO_4(H_2O)_n^{2-}$ sulfate–water clusters in the gas, liquid, or crystalline state, and indicated that it takes twelve water molecules to complete the first hydration sphere of sulfate.[2a-g] As a result of its strongly hydrated structure, sulfate is difficult to separate effectively and selectively from aqueous solutions, especially from mixtures containing less hydrophilic anions, such as nitrate or perchlorate.[3] Although a number of sulfate-binding receptors have been reported,[4] to date, only a small fraction of them have been demonstrated to separate sulfate efficiently from water by either solvent extraction[5a,b] or crystallization.[6a-d] By analogy with natural anion receptors, such as the sulfate-binding protein, it had generally been assumed that for strongly hydrophilic anions (e.g., sulfate, phosphate, selenate, chromate), effective aqueous binding and separation from water requires tight encapsulation of the anion within rigid, complementary host structures that completely sequester the anion from the water solvent.[7a-d] Whereas these principles remain valid and will continue to guide the design of anion receptors, we herein report an alternative approach to sulfate separation from water, where extended $[SO_4(H_2O)_5^{2-}]_n$ sulfate–water clusters are selectively crystallized with a bis(amidiniumhydrazone) cation self-assembled in situ from water-soluble subcomponents. This study demonstrates that at least in the case of crystallization, separation of the anion as a water cluster offers a viable

alternative to the now established approach involving encapsulation of the “naked” anion. Condensation of different aminoguanidinium salts with glyoxal in water yielded glyoxal bis(amidiniumhydrazone) (GBAH) as the sulfate (A), chloride (B), nitrate (C), or perchlorate (D) salt (**Figure 4.1**).

GBAH salts were first reported by Dralle and Thiele in 1898,[8] and more recently, they were studied as antileukemic agents.[9] These compounds caught our attention as potential anion separation agents because of the guanidinium groups contained in their structures. Guanidines are well-known oxoanion-binding groups,[10a-g] which prompted us to explore their potential for oxoanion separation by selective crystallization, an approach that proved so productive with the structurally related urea groups.[6a-d] We expected that the positive charge on the guanidinium groups would provide enhanced anion-binding strength through charge-assisted hydrogen bonding and improved water solubility compared to urea analogues. In the case of GBAH, we found the prospect of aqueous in situ self-assembly by hydrazine condensation particularly appealing, which could completely eliminate the need for extensive ligand synthesis and the utilization of organic solvents, which render so many traditional anion receptors impractical for real-world applications. Mixing aqueous solutions of aminoguanidinium sulfate and glyoxal led to in situ formation of the GBAH cation and its crystallization as the sulfate salt A. Single-crystal X-ray diffraction analysis[11] revealed that A crystallized with five water molecules (**Figure 4.2a**). Hydrogen bonding between the water molecules and the sulfate anion led to the formation of one-dimensional $[SO_4(H_2O)_5^{2-}]_n$ clusters running along the crystallographic

b axis (**Figure 4.2b**). Each sulfate in the cluster accepts eight hydrogen bonds from neighboring water molecules, with O–H⋯O contact distances ranging from 1.89 to 2.14 Å and O-H-O angles between 133.8 and 176.28º. Thus, sulfate retained two thirds of its hydrogen bonding upon crystallization, considering that on average, this anion accepts twelve hydrogen bonds from the first hydration sphere in the aqueous state.[2] Additional hydrogen bonding between water molecules completes the cluster network, which comprises three types of sulfate–water ring topologies, with $R_5^3(10)$, $R_4^4(12)$, and $R_6^5(14)$ graph set notations. The clusters have an ellipsoid-shaped cross-section measuring approximately 10.5 Å between the two outmost points.

The GBAH cations adopt a virtually planar conformation in the crystal and stack along the crystallographic b axis with mean interplanar distances alternating between 3.10 and 3.20 Å (**Figure 4.2c**). Adjacent cations within each stack are slightly offset relative to each other, thereby creating arrays of four N–H hydrogen-bond donors spaced approximately 3.5–3.7 Å apart, each donating a hydrogen bond to a different water molecule in the

cluster (**Figure 4.2d**). The fifth water molecule is isolated from the rest of the cluster and accepts an N–H hydrogen bond from the other end of the cationic stack. The peripheral water molecules in the cluster also accept an additional hydrogen bond from neighboring stacks, and each sulfate anion accepts three N–H⋯O hydrogen bonds from two guanidinium groups in adjacent stacks. Therefore, it appears that the observed structure of the sulfate–water cluster is determined to a large extent by the geometry of the GBAH

cation and its stacking in the crystal. The overall crystal packing, consisting of alternating cationic stacks and anionic sulfate–water clusters, is illustrated in **Figure 4.2e**.

Reaction of aminoguanidinium nitrate or perchlorate with glyoxal in water led to crystallization of the corresponding GBAH salts C and D. Singlecrystal X-ray diffraction analysis[11] showed that both salts crystallized in layered structures held together by anion–guanidinium hydrogen bonding (**Figure 4.3**). In the nitrate structure, the layers are almost perfectly flat and stacked on top of each other, whereas in the perchlorate structure, the layers are corrugated and interlinked by additional N–H⋯O hydrogen bonds between the guanidinium and the perchlorate ions.

The chloride salt B could also be synthesized in situ from aqueous aminoguanidinium chloride and glyoxal. However, no crystallization was observed under these conditions owing to the much higher aqueous solubility of this salt.[12] During the initial crystallization experiments, it became apparent that all of the oxoanions studied formed relatively insoluble salts with the GBAH cation, which prompted us to investigate the possibility for selective oxoanion separation by crystallization of these simple bis(guanidinium) salts. Table 1 lists the measured aqueous solubilities of A to D at 258 ºC, which follow the order B≫D>C>A. Thus sulfate salt A has the lowest aqueous solubility in the series, in spite of the much higher free energy of hydration of SO_4^{2-} compared to the other anions.[1] The corresponding solubility product constant (K_{sp}) for A is 3.2(5) x 10^{-7}, which is comparable to that of $SrSO_4$ (K_{sp} = 3.4 x 10^{-7}), one of the least soluble inorganic sulfate salts. For

comparison, the aqueous solubilities of plain guanidinium salts are much higher, and follow the order sulfate>chloride≫nitrate>perchlorate,[13] which essentially reflects the order of the free energies of hydration of the anions (Hofmeister bias).

The observed solubility trend in the A to D series suggested that this simple bis(guanidine) system might prove effective in aqueous sulfate separation by selective crystallization of A. To test this hypothesis, we performed a series of competitive crystallization experiments consisting of the in situ synthesis of the GBAH cation (according to **Figure 4.1**) in aqueous solution in the presence of various anion mixtures (**Table 4.1**). The identity of the resulting crystalline product was conformed by powder X-ray diffraction (PXRD) and Fourier-transformed infrared spectroscopy (FTIR) for each experiment. None of the starting aminoguanidinium salts can crystallize under these conditions owing to their much higher solubilities (3.0 to 3.7 M)[14] compared to the GBAH salts. An equimolar aqueous mixture of sulfate (0.25 M) and perchlorate (0.25 M), which are the most and the

The observed solubility trend in the A to D series suggested that this simple bis(guanidine) system might prove effective in aqueous sulfate separation by selective crystallization of A. To test this hypothesis, we performed a series of competitive crystallization experiments consisting of the in situ synthesis of the GBAH cation (according to **Figure 4.1**) in aqueous solution in the presence of various anion mixtures (**Table 4.1**). The identity of the resulting crystalline product was confirmed by powder X-ray diffraction (PXRD) and Fourier-transformed infrared spectroscopy (FTIR) for each experiment. None

of the starting aminoguanidinium salts can crystallize under these conditions owing to their much higher solubilities (3.0 to 3.7 M)[14] compared to the GBAH salts. An equimolar aqueous mixture of sulfate (0.25 M) and perchlorate (0.25 M), which are the most and the least hydrophilic anions in the series, led to exclusive crystallization of A in 89% yield (**Table 4.2**, entry 1), resulting in a reduction of the sulfate concentration in solution to 0.0275 M. Similarly, A crystallized exclusively from a mixture of sulfate (0.25 M) and chloride (0.25 M), with a maximum observed yield of 93%, corresponding to a final sulfate concentration of 0.02 M (entry 2). On the other hand, a crystalline mixture of A and C was isolated from the competition experiment between sulfate and nitrate (entry 3), whereas C crystallized exclusively from a mixture of nitrate and perchlorate (entry 4). Thus the anion selectivities from these pairwise competitive crystallizations are generally consistent with the measured solubilities of A to D. Finally, a competitive crystallization experiment with an aqueous mixture containing all four anions (entry 5) led once more to co-precipitation of A and C, the two least soluble compounds of the series.

The demonstrated anion selectivity in the crystallization of the GBAH salts is remarkable for such a simple bis(guanidinium) ligand. The observed selectivity for sulfate and nitrate stands in direct contrast with the anion selectivity in competitive crystallization of plain guanidinium salts, which favored the least hydrophilic perchlorate anion, in agreement with the Hofmeister bias.[13] Unlike previously reported ligands used for sulfate crystallizations,[6a-d,15] which require cumbersome syntheses and purifications involving toxic reagents and solvents, the GBAH ligand can be generated in situ in pure water from

simple subcomponents, which makes for a more practical, cheaper, and greener anion separation method. Furthermore, as the GBAH ligand was generated by hydrazone condensation, a reversible bond forming reaction commonly employed in dynamic combinatorial chemistry (DCC),[16] it may be expected that even less soluble and more selective sulfate crystallization systems could be identified by DCC. Meanwhile, the current system may already find practical applications related to sulfate or/and nitrate separation. For example, both sulfate and nitrate can pose environmental problems as they are the main constituents of acid rain and can contaminate the groundwater.[17a-c] The presence of sulfate in seawater presents challenges for oil field injection operations because of scale formation.[18a,b] Sulfate is also a problematic constituent of legacy nuclear wastes,[3] which could be targeted for sulfate separation alongside the more abundant nitrate. We envision that this crystallization approach could be applied to either the individual separation of sulfate or nitrate or a mixture of the two anions, depending on the practical need and the solution composition.

From a fundamental perspective, the present system demonstrates a new paradigm in sulfate separation, wherein the anion is crystallized as a sulfate–water cluster. This strategy presents some potential advantages over the traditional approach based on sequestration of the “naked” anion, such as a lower thermodynamic penalty associated with anion dehydration and enhanced selectivity based on exclusive recognition patterns associated with the unique structure of the cluster. In the case in point, sulfate crystallization as $[SO_4(H_2O)_5^{2-}]_n$ clusters proved far more effective and selective than

crystallization of plain guanidinium sulfate, even though in the latter case, the sulfate is completely dehydrated and coordinatively saturated by twelve NH hydrogen bonds.[19] We attribute the much lower solubility of A compared to plain guanidinium sulfate to mainly two factors: an energetically favorable stacking of the GBAH cations and a lower dehydration penalty for sulfate, as the anion retains two thirds of the water hydrogen bonds from its first hydration sphere in crystalline A. On the other hand, the sulfate selectivity could be rationalized based on the specific recognition of the $[SO_4(H_2O)_5^{2-}]_n$ clusters by hydrogen bonding from the GBAH stacks. Whereas this structure was discovered serendipitously, it could inspire the rational design of future sulfate crystallization systems based on the recognition of other sulfate–water clusters.

4.2 References

1. Marcus, Y., Thermodynamics of Solvation of Ions, Part 5. —Gibbs Free Energy of Hydration at 298.15 K. *J. Chem. Soc. Faraday Trans.* **1991**, *87*, 2995-2999.

2. a) B. Gao, Z. Liu, A first principles study on the solvation and structure of SO_4^{2-} $(H_2O)_n$, n = 6 – 12. *J. Chem. Phys.* **2004**, *121*, 8299-8306; b) J. Zhou, G. Santambrogio, M. Brummer, D. T. Moore, L. Woste, G. Meijer, D. N. Neumark, K. R. Asmis, Infrared spectroscopy of hydrated sulfate dianions. *J. Chem. Phys.* **2006**, *125*, 111102; c) M. F. Bush, R. J. Saykally, E. R. Williams, Evidence for Water Rings in the Hexahydrated Sulfate Dianion from IR Spectroscopy. *J. Am. Chem. Soc.* 2007, *129*, 2220-2221; d) V. Vchirawongkwin, B. M. Rode, I. Persson, J. Phys. Chem. B 2007, 111, 4150; e) D. S. Lambrecht, G. N. I. Clark, T. Head-Gordon, M. Head-Gordon, J. Phys. Chem. A 2011, 115, 11438; f) K. R. Asmis, D. M. Neumark, Acc. Chem. Res. 2012, 45, 43; g) Q. Wan, L. Spanu, G. Galli, J. Phys. Chem. B 2012, 116, 9460; h) M. N. Hoque, A. Basu, G. Das, Cryst. Growth Des. 2014, 14, 6; i) M. N. Hoque, G. Das, Cryst. Growth Des. 2014, 14, 2962.

[3] B. A. Moyer, R. Custelcean, B. P. Hay, J. L. Sessler, K. Bowman- James, V. W. Day, S.-O. Kang, Inorg. Chem. 2013, 52, 3473.

[4] I. Ravikumar, P. Ghosh, Chem. Soc. Rev. 2012, 41, 3077.

[5] a) H. Stephan, K. Gloe, P. Schiessl, F. P. Schmidtchen, Supramol. Chem. 1995, 5, 273; b) C. Jia, B. Wu, S. Li, X. Huang, Q. Zhao, Q. Li, X. Yang, Angew. Chem. Int. Ed. 2011, 50, 486; Angew. Chem. 2011, 123, 506.

[6] a) R. Custelcean, A. Bock, B. A. Moyer, J. Am. Chem. Soc. 2010, 132, 7177; b) A. Rajbanshi, B. A. Moyer, R. Custelcean, Cryst. Growth Des. 2011, 11, 2702; c) R. Custelcean, Chem. Commun. 2013, 49, 2173; d) R. Custelcean, F. V. Sloop, Jr., A. Rajbanshi, S. Wan, B. A. Moyer, Cryst. Growth Des. 2015, 15, 517.

[7] a) S. O. Kang, J. M. Llinares, V. W. Day, K. Bowman-James, Chem. Soc. Rev. 2010, 39, 3980; b) P. Ballester, Chem. Soc. Rev. 2010, 39, 3810; c) S. Kubik, Chem. Soc. Rev. 2010, 39, 3648; d) R. Custelcean, Chem. Soc. Rev. 2014, 43, 1813.

[8] J. Thiele, E. Dralle, Justus Liebigs Ann. Chem. 1898, 302, 275.

[9] P. Seppanen, R. Fagerstrom, L. Alhonen-Hongisto, H. Elo, P. Lumme, J. Janne, Biochem. J. 1984, 221, 483.

[10] a) G. Mîller, J. Riede, F. P. Schmidtchen, Angew. Chem. Int. Ed. Engl. 1988, 27, 1516; Angew. Chem. 1988, 100, 1574; b) P. Schiessl, F. P. Schmidtchen, J. Org. Chem. 1994, 59, 509; c) M. Berger, F. P. Schmidtchen, Angew. Chem. Int. Ed. 1998, 37, 2694; Angew. Chem. 1998, 110, 2840; d) M. D. Best, S. L. Tobey, E. V. Anslyn, Coord. Chem. Rev. 2003, 240, 3; e) P. Blondeau, M. Segura, R. Perez-Fernandez, J. de Mendoza, Chem. Soc. Rev. 2007, 36, 198; f) C. Schmuck, Coord. Chem. Rev. 2006, 250, 3053; g) M. Li, S. Schlesiger, S. K. Knauer, C. Schmuck, Angew. Chem. Int. Ed. 2015, 54, 2941; Angew. Chem. 2015, 127, 2984. [11] CCDC 1404313, 1404314, and 1404315 contain the supplementary crystallographic data for this paper. These data can be obtained free of charge from The Cambridge Crystallographic Data Centre.

[12] Slow evaporation of most of the water over two weeks led to single crystals whose unit cell corresponded to the previously reported crystal structure of B; see: I. Mutikainen, H. Elo, P. Lumme, J. Chem. Soc. Perkin Trans. 2 1986, 291.

[13] The gravimetrically measured solubilities of guanidinium sulfate, chloride, and nitrate are 9.64(5), 8.71(3), and 1.10(4)m, respectively. The solubility of guanidinium perchlorate could not be measured owing to its explosive nature. However, slow evaporation of an equimolar aqueous mixture of guanidinium sulfate, chloride, nitrate, and perchlorate led to competitive crystallization of guanidinium perchlorate, as confirmed by determination of the unit cell using single-crystal X-ray diffraction

[14] The gravimetrically measured solubilities of aminoguanidinium chloride, sulfate, and nitrate are 3.67(8), 3.66(5), and 3.01(9)m, respectively. Slow evaporation of an equimolar aqueous mixture of these salts resulted in the formation of a viscous syrup upon water removal, with no crystallization occurring over the course of one month.

[15] W. I. Stephen, Anal. Chim. Acta 1970, 50, 413.

[16] Dynamic Combinatorial Chemistry (Eds.: J. N. H. Reek, S. Otto), Wiley-VCH, Weinheim, 2010.

[17] a) R. Dutta, P. Ghosh, Chem. Commun. 2015, 51, 9070; b) E. V. S. Prakasa Rao, K. Puttanna, Curr. Sci. 2006, 91, 1335; c) R. Haghsheno, A. Mohebbi, H. Hashemipour, A. Sarrafi, J. Hazard. Mater. 2009, 166, 961.

[18] a) M. S. H. Bader, Desalination 2006, 201, 100; b) M. S. H. Bader, J. Pet. Sci. Eng. 2007, 55, 93.

[19] P. Dera, A. Katrusiak, M. Szafranski, Pol. J. Chem. 2000, 74, 1637.

4.3 Appendix 4A Supplemental Information for Chapter 4

4.3.1 Supporting Information

Stock solutions of aminoguanidinium chloride, sulfate, nitrate, and perchlorate were prepared from aminoguanidine hydrogen carbonate (Alpha Aesar) and the corresponding aqueous acids (Caution: aminoguanidinium perchlorate is potentially explosive and should be handled with care). The glyoxal bis(amidinohydrazone) chloride (B) used for solubility studies was prepared according to a literature procedure.[S1] FT-IR spectra were collected on a Digilab FTS 7000 Series Infrared Spectrometer using a diamond ATR setup. UV spectra were measured in 10 mm path length quartz glass cuvettes using a Cary Varian 5000 spectrometer and analyzed with Cary WinUV software. Powder X-ray diffraction (PXRD) measurements were done with a Panalytical Empyrean diffractometer using a flat sample stage in reflection mode.

4.3.2 Synthesis and Crystallization of Glyoxal bis(amidinohydrazone) Sulfate (A), Nitrate (C), and Perchlorate (D).

A: Aqueous aminoguanidinium sulfate (1 mL, 0.5 M) and glyoxal (1 mL, 0.5 M) were mixed together resulting in a clear solution. A white precipitate started to form after about 1 min. The resulting crystalline solid was filtered after one week and washed with water. Yield 0.163 g (91%). M.p. 278-279 °C (lit. 280-281 °C).[S2] X-ray quality single crystals of **A** · $5H_2O$ were obtained by using a 10-fold more dilute aqueous glyoxal solution (10 mL, 0.05 M) to slow down the crystallization process. Needle-shaped single crystals started

to appear after about 1 h and were collected from the solution after 1-2 2 days. The simulated powder pattern from the single-crystal X-ray structural analysis matched the experimental PXRD pattern of bulk A·5H2O (**Figure 4.4**).

C: Aqueous aminoguanidinium nitrate (1 mL, 0.5 M) and glyoxal (0.5 mL, 0.5 M) were mixed together resulting in a clear solution. A white precipitate started to form after less than 1 min. The resulting crystalline solid was filtered after one week and washed with water. Yield 0.073 g (99%). M.p. 294 °C with decomposition (lit. 292 °C).[S2] X-ray quality single crystals of **C** were obtained by using a 10-fold more dilute aqueous glyoxal solution (5 mL, 0.05 M) to slow down the crystallization process. Needle-shaped single crystals started to appear after about 30 min and were collected from the solution after 1-2 days. The simulated powder pattern from the single-crystal X-ray structural analysis matched the experimental PXRD pattern of bulk **C** (**Figure 4.5**).

D: Aqueous aminoguanidinium perchlorate (1 mL, 0.5 M) and glyoxal (0.5 mL, 0.5 M) were mixed together resulting in a clear solution. A white precipitate started to form after about 15 min. The resulting crystalline solid was filtered after one week and washed with water. Yield 0.071 g (77%). M.p. 245-250 °C with decomposition. X-ray quality single crystals of **D** were obtained by using a 10-fold more dilute aqueous glyoxal solution (5 mL, 0.05 M) to slow down the crystallization process. Prism-shaped single crystals formed after a few days. The simulated powder pattern from the single-crystal X-ray structural analysis matched the experimental PXRD pattern of bulk **D** (**Figure 4.6**).

4.3.3 Single-Crystal X-Ray Structural Determination

Single-crystal X-ray data for **A**·$5H_2O$, **C**, and **D** were collected on a Bruker SMART APEX CCD diffractometer with fine-focus Mo Kα radiation (λ = 0.71073 Å), operated at 50 kV and 30 mA. The structures were solved by direct methods and refined on F2 using the SHELXTL software package (Bruker AXS, Inc., Madison, WI, 1997). Absorption corrections were applied using SADABS, part of the SHELXTL package. All nonhydrogen atoms were refined anisotropically. Hydrogen atoms were placed in idealized positions and refined with a riding model, except for the water hydrogen atoms in A·$5H_2O$, which were located from difference Fourier maps and refined isotropically. CCDC 1404313-1404315 contain the supplementary crystallographic data for this paper. These data can be obtained free of charge from The Cambridge Crystallographic Data Centre via www.ccdc.cam.ac.uk/data_request/cif.

Crystal data for **A**·$5H_2O$: $C_4H_{22}N_8O_9S$, M = 358.36, colorless needle, 0.37 × 0.11 × 0.06 mm^3, monoclinic, space group *P*2(1)/c, a = 11.1795(8), b = 6.6468(5), c = 21.3170(16)Å, β = 100.152(2)°, *V* = 1559.2(2) $Å^3$, *Z* = 4, D_c = 1.527 g/cm^3, MoKα radiation, λ = 0.71073 Å, T = 173(2)K, 2ϑmax = 56.7º, 11367 reflections collected, 3873 unique (R_{int} = 0.0250). Final *GooF* = 1.042, R_1 = 0.0438, wR_2 = 0.1125, R indices based on 3082 reflections with I >2σ(I) (refinement on F^2), 239 parameters, 0 restraints. Lp and absorption corrections applied, μ = 0.267 mm^{-1}.

Crystal data for **C**: $C_4H_{22}N_{10}O_6$, M = 296.24, colorless prism, 0.23 × 0.22 × 0.18 mm3, monoclinic, space group *C*2/c, a = 6.5696(9), b = 13.2985(18), c = 14.053(2) Å, β =92.558(3)°, *V* = 1226.5(3) Å3, Z = 4, D*c* = 1.604 g/cm^3, MoKα radiation, λ = 0.71073 Å, T = 173(2)K, 2ϑmax = 56.7º, 4978 reflections collected, 1525 unique (R_{int} = 0.0183). Final *GooF* = 1.071, R_1 = 0.0488, wR_2 = 0.1278, *R* indices based on 1246 reflections with I >2σ(I) (refinement on F^2), 91 parameters, 0 restraints. Lp and absorption corrections applied, μ = 0.145 mm^{-1}.

Crystal data for **D**: $C_4H_{12}N_8O_8Cl_2$, M = 371.12, colorless prism, 0.30 × 0.15 × 0.15 mm^3, monoclinic, space group *P*2(1)/n, a = 5.4067(7), b = 13.3394(16), c = 9.4476(12) Å, β = 99.438(2)°, *V* = 672.16(15) Å3, Z = 2, D_c = 1.834 g/cm^3, MoKα radiation, λ = 0.71073 Å, T = 173(2)K, 2ϑmax = 56.6º, 4454 reflections collected, 1656 unique (R_{int} = 0.0186). Final *GooF* = 1.045, R_1 = 0.0391, wR_2 = 0.1054, *R* indices based on 1502 reflections with I>2σ(I) (refinement on F^2), 104 parameters, 0 restraints. Lp and absorption correctionsapplied, μ = 0.543 mm^{-1}.

4.3.4 Solubility Measurements of the GBAH Salts A-D

The solubilities of the sulfate (**A**), nitrate (**B**) and perchlorate (**D**) salts were determined by UV spectroscopy. Prior to determining the solubility of these salts, a calibration curve was made utilizing the more soluble chloride salt (**B**). The UV calibration spectra and curve for the GBAH cation are shown in **Figures 4.7** and **4.8**, respectively. Saturated solutions of the salts were prepared as follows. A large excess of the corresponding salt

was placed in a 15 mL polypropylene centrifuge tube and 2 mL of deionized water (milli-Q) was added the tube. The suspension was mixed for 4 days using a rugged rotator set at 60 rpm. To maintain a constant temperature the rotator was place inside an incubator set at 25 °C, and the temperature was monitored using a NIST standardized thermometer, which showed a temperature variation of less than ±0.5 °C. The suspension was subsequently centrifuged for 10 mins at 3000 rpm to separate the aqueous and solid phases. The aqueous layer was then carefully removed using a 0.22 μm syringe filter. The concentrations of the GBAH cation were too high for UV determination, making it necessary to dilute the samples. The dilution factor for each salt, the absorbance at 286 nm, and the resulting GBAH solubilities are given in Table 9.

The solubility of the chloride salt (**B**) was determined gravimetrically. A saturated solution of **B** was obtained in the same manner as for the other salts (see above), except the aqueous suspension of the salt was stirred for 24 h. One mL of the saturated solution was then pipetted into a pre-weighted glass vial containing a stir bar. The water was then removed under reduced pressure and gentle heating (~50 °C) while stirring. The resulting solid was left under vacuum overnight to ensure complete removal of the water, prior to weighting the vial. The weight of the recovered solid was 0.196 g, corresponding to an aqueous solubility of 0.88(8) M (average of three different measurements).

4.3.5 Solubility Measurements of the Guanidinium and Aminoguanidinium Salts

The solubility of the chloride, nitrate, and sulfate salts of guanidine and aminoguanidine were measured gravimetrically in the same manner as for **B** (see above). The guanidinium and aminoguanidinium perchlorates could not be measured due to their explosive nature. Tables 10 and 11 list the measured solubilities for the guanidinium and aminoguanidinium salts, respectively.

4.3.6 Competitive Crystallizations

SO_4^{2-}/ClO_4^-: Aqueous aminoguanidine perchlorate (1 mmol, 2 mL, 0.5 M), Na_2SO_4 (1 mmol, 1 mL, 1 M) and glyoxal (0.5 mmol, 1 mL, 0.5 M) were mixed in a 20 mL vial. Needle-shaped crystals started to form in 1-2 min. The solution was stirred at room temperature for 16 h. The resulting crystalline solid was filtered and washed with water. PXRD (**Figure 4.9**) and FT-IR (**Figure 4.10**) analyses confirmed the crystallized solid was pure **A**$\cdot 5H_2O$. Yield 0.160 g (89%).

SO_4^{2-}/Cl^-: a) Aqueous aminoguanidinium chloride (1 mmol, 2 mL, 0.5 M), Na_2SO_4 (1 mmol, 1 mL, 1 M) and glyoxal (0.5 mmol, 1 mL, 0.5 M) were mixed in a 20 mL vial. Needle-shaped crystals started to form in 5-10 min. The solution was stirred at room temperature for 18 h. The resulting crystalline solid was filtered and washed with water. PXRD (**Figure 4.11**) and FT-IR (**Figure 4.12**) analyses confirmed the crystallized solid was pure **A**$\cdot 5H_2O$. Yield 0.096 g (54%).

b) Aqueous preformed **B** (1.5 mmol, 3 mL, 0.5 M) and Na_2SO_4 (1 mmol, 1 mL, 1 M) were mixed in a 20 mL vial. A white instant precipitate of **A**$\cdot 5H_2O$ formed instantly, which was filtered and dried under vacuum. Yield 0.333 g (93%).

SO_4^{2-}/NO_3^-: Aqueous aminoguanidinium nitrate (1 mmol, 2 mL, 0.5 M), Na2SO4 (1 mmol, 1 mL, 1 M) and glyoxal (0.5 mmol, 1 mL, 0.5 M) were mixed in a 20 mL vial. Crystals started to form in about 1 min. The mixture was stirred at room temperature for 4 days. The resulting crystalline solid was filtered and washed with water. PXRD (**Figure 4.13**) and FT-IR (**Figure 4.14**) analyses showed the crystallized solid was a mixture of **A** $5H_2O$ and **C**. Yield 0.157 g.

The anionic composition of the mixture was determined by gravimetric precipitation of $BaSO_4$, as follows. 29.2 milligrams of the crystalline product was dissolved in 7 mL of 1N HCl and sonicated until the solution was clear. Excess barium chloride in 1.5 mL of 1N HCl was then added. Precipitation of barium sulfate occurred immediately, but the mixture was allowed to stir for three days. The suspension was filtered through a dry and pre-weighed syringe filter, and the syringe filter (with barium sulfate precipitate) was dried in a vacuum oven at 70 °C over night, leaving 5.6 mg of barium sulfate. Thus, the molar composition of the crystalline mixture consists of 25.6% **A**$\cdot 5H_2O$ (sulfate) and 74.3% **C** (nitrate).

NO_3^-/ClO_4^-: Aqueous aminoguanidinium perchlorate (1 mmol, 2 mL, 0.5 M), $NaNO_3$ (1 mmol, 1 mL, 1 M) and glyoxal (0.5 mmol, 1 mL, 0.5 M) were mixed in a 20 mL vial. Crystals started to form in 1 min. The solution was stirred at room temperature for 18 h. The resulting crystalline solid was filtered and washed with water. PXRD (**Figure 4.15**) and FT-IR (**Figure 4.16**) analyses confirmed the crystallized solid was pure **C**. Yield 0.132 g (89%).

$SO_4^{2-}/Cl^-/NO_3^-/ClO_4^-$: Aqueous aminoguanidinium perchlorate (1.5 mmol, 3 mL, 0.5 M), Na_2SO_4 (1 mmol, 1 mL, 1 M), $NaNO_3$ (1 mmol, 1 mL, 1 M), NaCl (1 mmol, 1 mL, 1 M) glyoxal (0.5 mmol, 1 mL, 0.5 M), and water (7 mL) were mixed in a 20 mL vial. Prism-shaped crystals formed after a few hours. One of the crystals was retrieved from solution and analyzed by single-crystal X-ray diffraction, which confirmed its identity as C. The vial was left undisturbed for 24 h resulting in the formation of needle-shaped crystals whose identity was confirmed by single-crystal X-ray diffraction to be **A**$\cdot 5H_2O$. The crystalline mixture was left undisturbed at room temperature for 1 week, then it was filtered and washed with water. PXRD (**Figure 4.17**) and FT-IR (**Figure 4.18**) analyses showed the crystallized solid was a mixture of **A**$\cdot 5H_2O$ and **C**. Yield 0.127 g.

The anionic composition of the mixture was determined by gravimetric precipitation of $BaSO_4$, as follows. 48.2 milligrams of the crystalline product was dissolved in 8 mL of 1N HCl and sonicated until the solution was clear. Excess barium chloride in water (4 mL) was then added to the solution. Precipitation of barium sulfate occurred immediately, but

the mixture was sonicated for 4 hours to ensure quantitative precipitation. The compound was filtered through a dry pre-weighed piece of quantitative filter paper, and subsequently dried in a vacuum oven at 70 °C for three hours leaving behind 8.8 mg of barium sulfate. Thus, the molar composition of the crystalline mixture consists of 24.3% **A** · $5H_2O$ (sulfate) and 75.7% **C** (nitrate).

4.4 Appendix References

[S1] I. Mutikainen, H. Elo, P. Lumme, J. Chem. Soc. Perkin Trans. 2 1986, 291.

[S2] J. Thiele, E. Dralle, Justus Liebigs Annalen der Chemie 1898, 275.

4.5 Appendix 4B Figures and Tables for Chapter 4

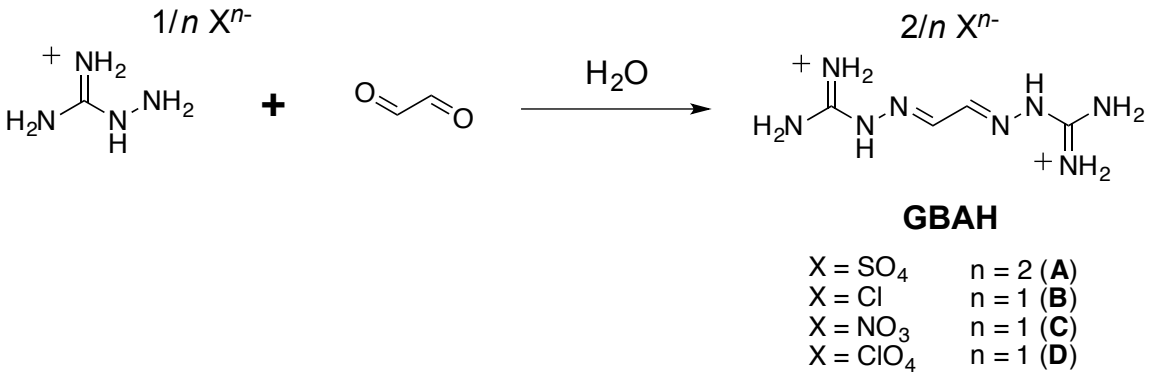

Figure 4.1. Preparation of the GBAH salts A to D by hydrazine condensation in water.

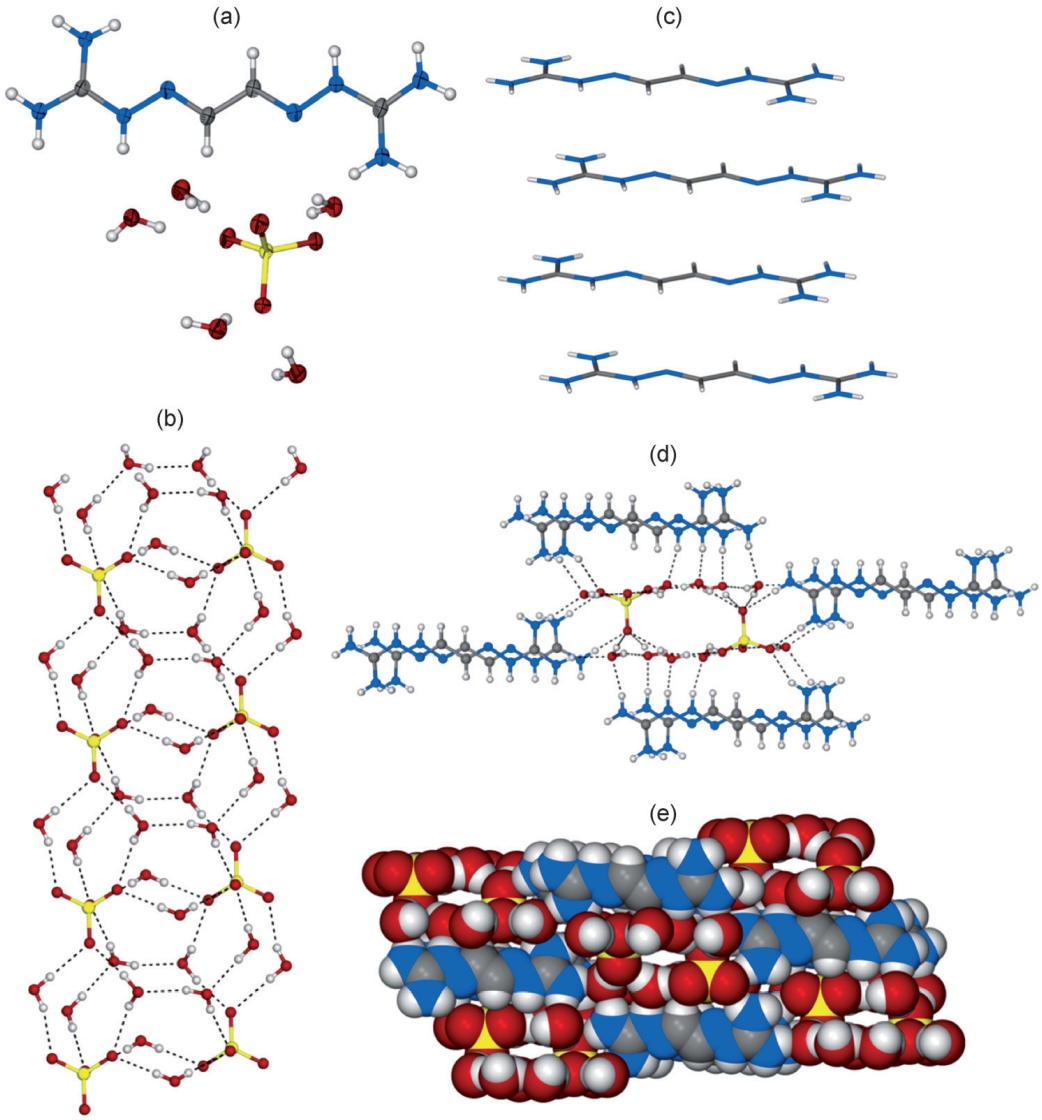

Figure 4.2. X-ray crystal structure of A. a) ORTEP representation showing the GBAH cation and the anionic $SO_4(H_2O)_5^{2-}$ cluster. b) Hydrogen-bonded $[SO_4(H_2O)_5^{2-}]_n$ clusters. c) Stacking of the GBAH cations. d) Hydrogen bonding of the sulfate–water clusters by the cationic GBAH stacks, viewed down the crystallographic b axis. e) Space-filling representation of the crystal packing viewed down the crystallographic b axis.

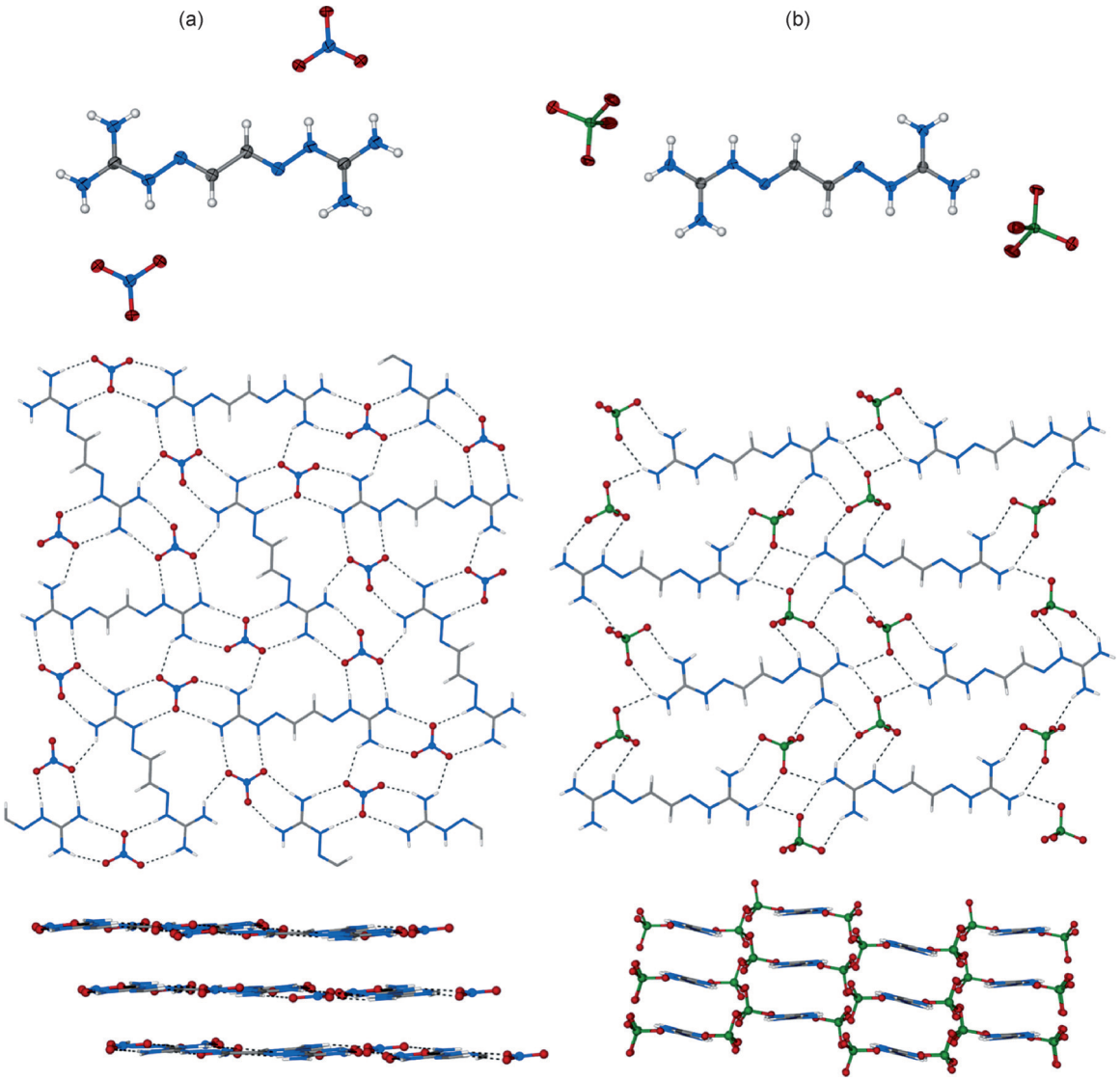

Figure 4.3. X-ray crystal structures of C (a) and D (b). Top: ORTEP representations; middle: hydrogen-bonded layers; bottom: packing of the layers.

Table 4.1. Aqueous solubilities of A to D at 25 °C. [a] Measured by UV spectroscopy. [b] Determined gravimetrically.

Compound (anion)	Solubility [M]
A (SO_4^{2-})[a]	7.2(6) x 10^{-4}
B (Cl^-)[b]	0.88(8)
C (NO_3^-)[a]	1.2(2) x 10^{-3}
D (ClO_4^-)[a]	1.36(1) x 10^{-2}

Table 4.2. Competitive crystallization experiments.[a]

Entry	Anion mixture (M)	Crystalline product
1	SO_4^{2-} (0.25), ClO_4^- (0.25)	**A**
2	SO_4^{2-} (0.25), Cl^- (0.25)	**A**
3	SO_4^{2-} (0.25), NO_3^- (0.25)	**A** (26%) **C** (74%)[b]
4	NO_3^- (0.25), ClO_4^- (0.25)	**C**
5	SO_4^{2-} (0.07), Cl^- (0.07) NO_3^- (0.07), ClO_4^- (0.07)	**A** (24%) **C** (76%)[b]

[a] All crystallizations were done in deionized water at room temperature. [b] Molar composition determined gravimetrically by dissolution of the crystals with 1 M HCl and sulfate precipitation with $BaCl_2$.

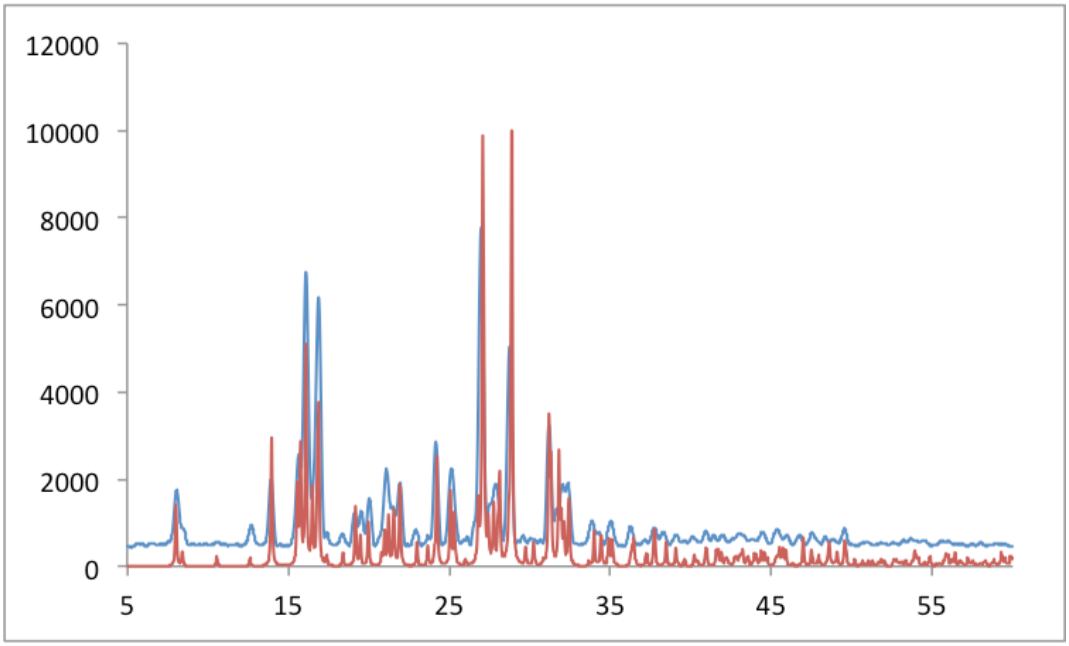

Figure 4.4. PXRD patterns for A·5H2O. Red: simulated pattern from the single-crystal;Blue: experimental pattern from the bulk crystalline powder.

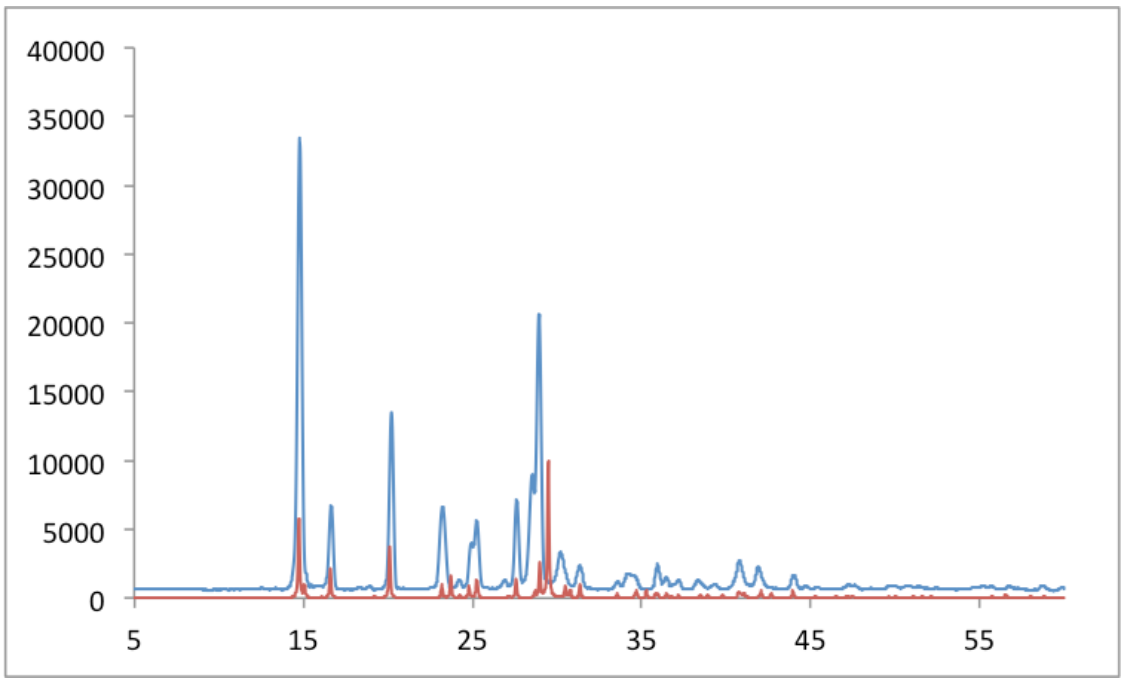

Figure 4.5. PXRD patterns for C. Red: simulated pattern from the single-crystal; Blue:experimental pattern from the bulk crystalline powder.

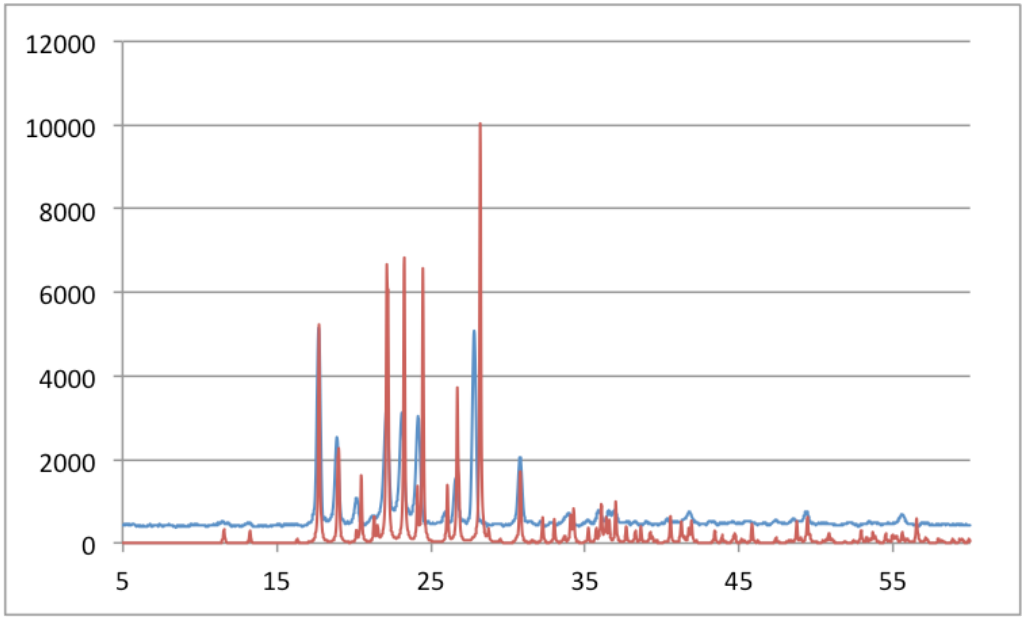

Figure 4.6. PXRD patterns for D. Red: simulated pattern from the single-crystal; Blue: experimental pattern from the bulk crystalline powder.

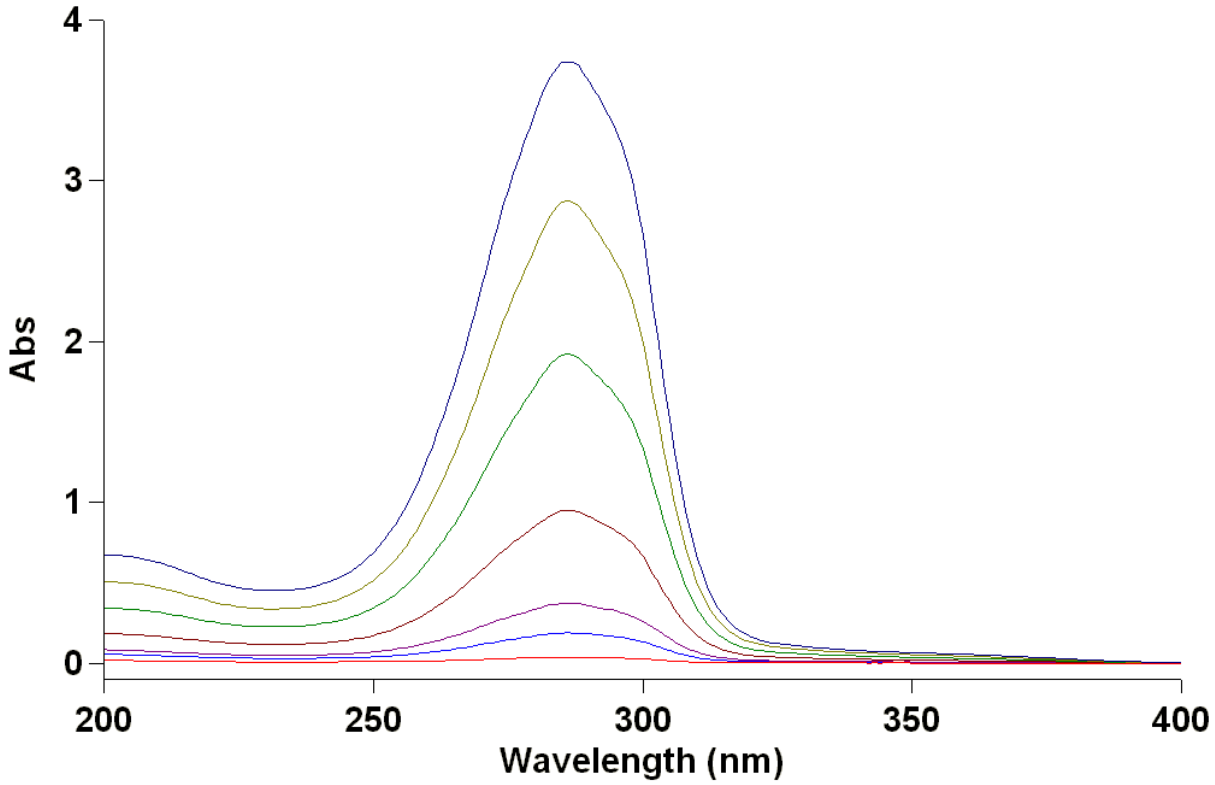

Figure 4.7. UV calibration spectra obtained using the chloride salt B. The concentrations of the GBAH cation ranged from a minimum of 1 Å~ 10−6 to a maximum of 1 Å~ 10-4 M.

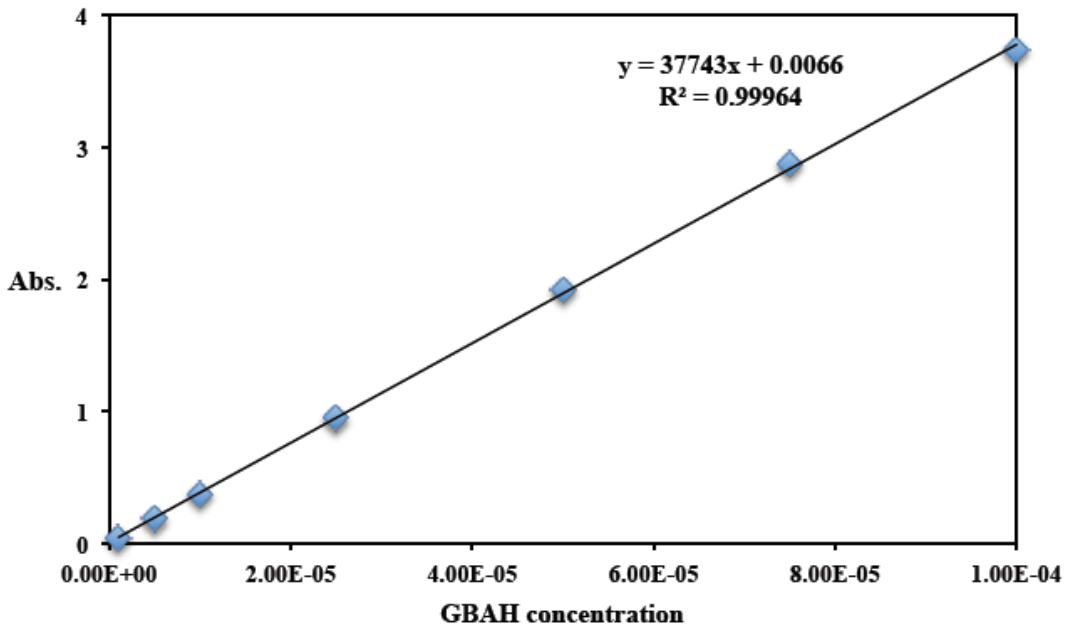

Figure 4.8. UV calibration curve obtained using the absorbance of GBAH at 286 nm.

Table 4.3. Solubilities of GBAH salts at 25 °C, determined via UV spectroscopy. Absorbance and dilution factors are also given for each compound. The reported solubility for each salt is the average of three different measurements, with the standard deviation representing the uncertainty.

Compound	Dilution Factor	Abs. at 286 nm	Solubility (mM)
A	10	2.987	0.72(6)
C	20	1.940	1.2(2)
D	240	2.160	13.6(1)

Table 4.4. Aqueous solubilities of the guanidinium salts determined gravimetrically.

Guanidinium salt[a]	Solubility (M)[b]
SO_4^{2-}	9.64(5)[c]
Cl^-	8.71(3)
NO_3^-	1.10(4)

[a] All measurements were done at 25 °C. [b] The reported solubility for each salt is the average of two different measurements, with the standard deviation representing the uncertainty. [c] Sulfate salt as $[CH_6N_3][SO_4]_{0.5}$.

Table 4.5. Aqueous solubilities of the aminoguanidinium salts determined gravimetrically.

Aminoguanidinium salt[a]	Solubility (M)[b]
SO_4^{2-}	3.66(5)[c]
Cl^-	3.67(8)
NO_3^-	3.01(9

[a] All measurements were done at 25 °C. [b] The reported solubility for each salt is the average of three different measurements, with the standard deviation representing the uncertainty. [c] Sulfate salt as $[CH_7N_4][SO_4]_{0.5}$.

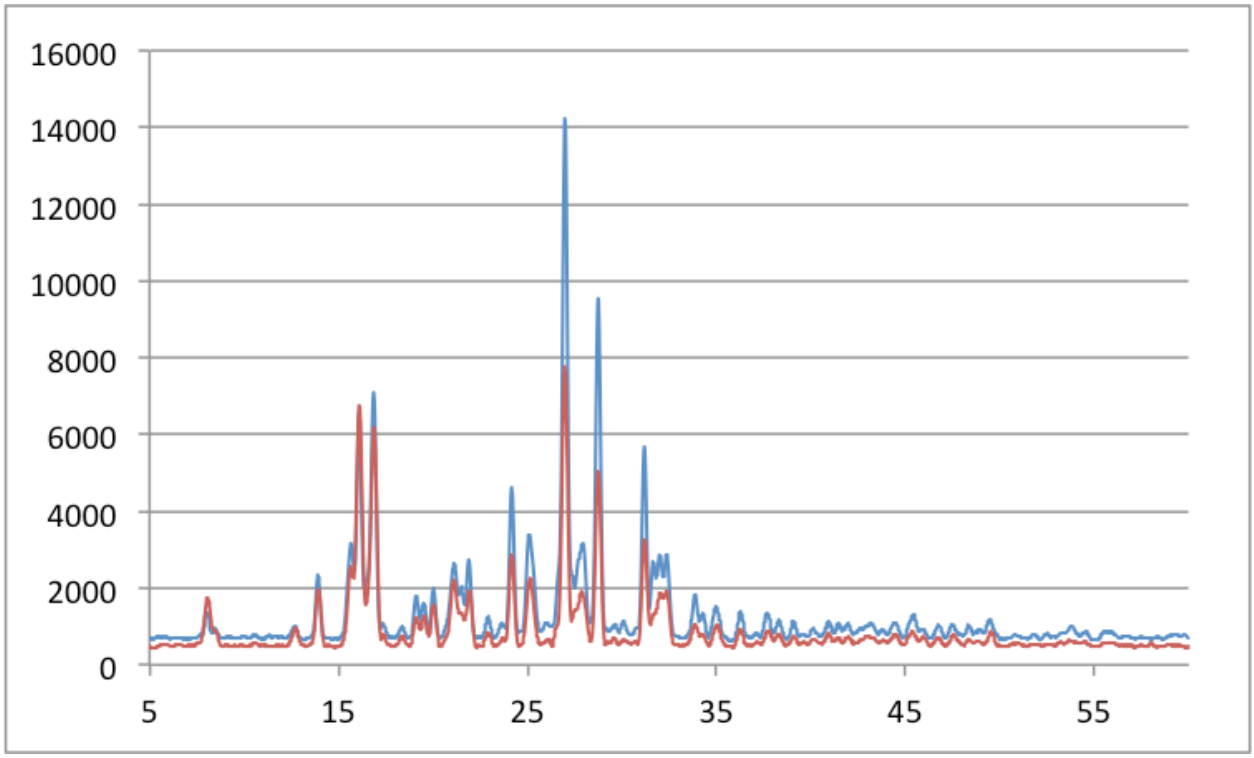

Figure 4.9. PXRD patterns for $A \cdot 5H_2O$ (red) and the product of the SO_4^{2-}/ClO_4^- competitive crystallization (blue).

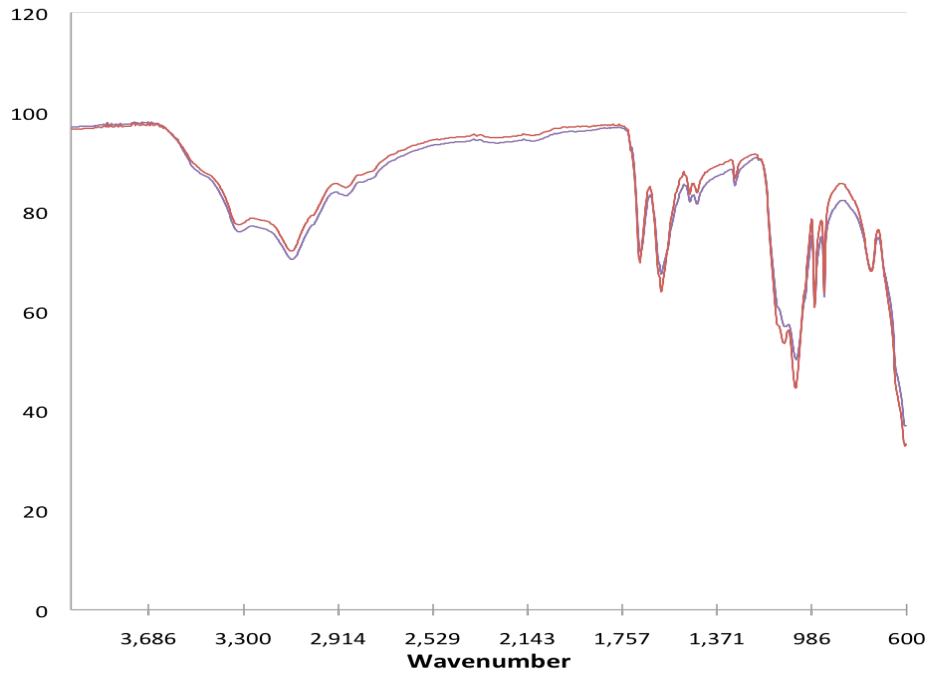

Figure 4.10. FTIR spectra of $A \cdot 5H_2O$ (blue) and the product of the SO_4^{2-}/ClO_4^- competitive crystallization (red).

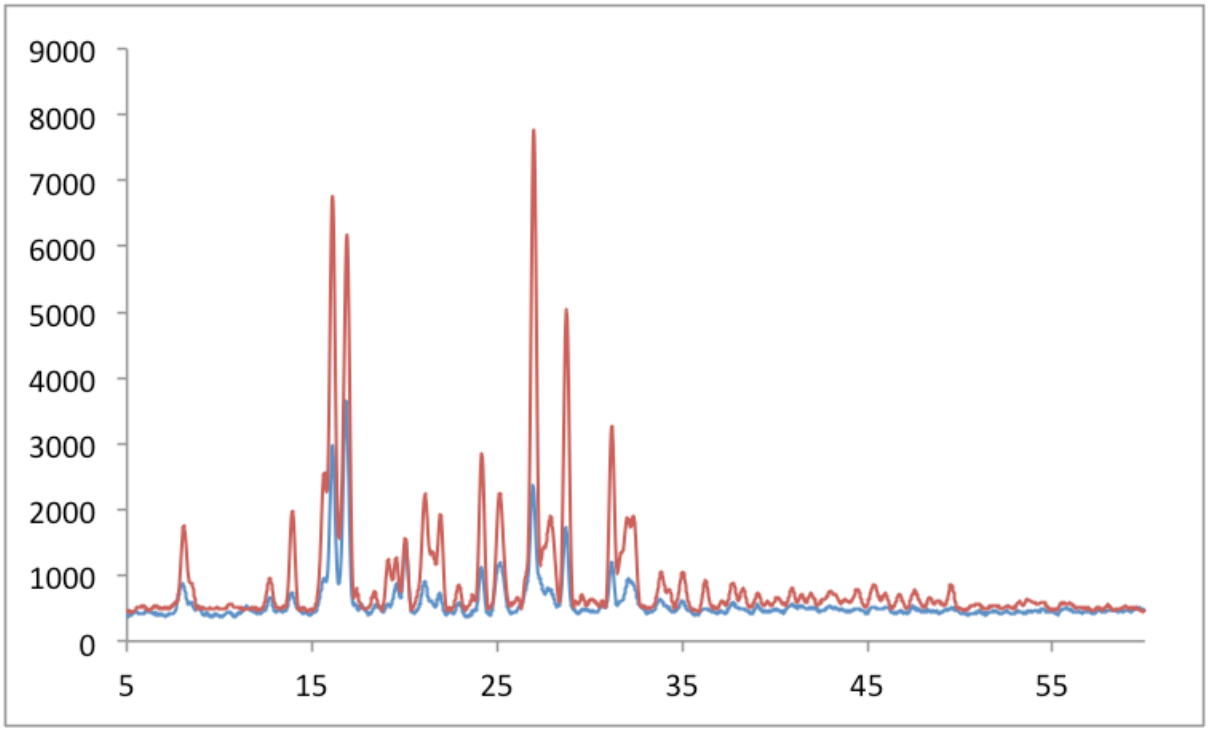

Figure 4.11. PXRD patterns for $A \cdot 5H_2O$ (red) and the product of the SO_4^{2-}/Cl^- competitive crystallization (blue).

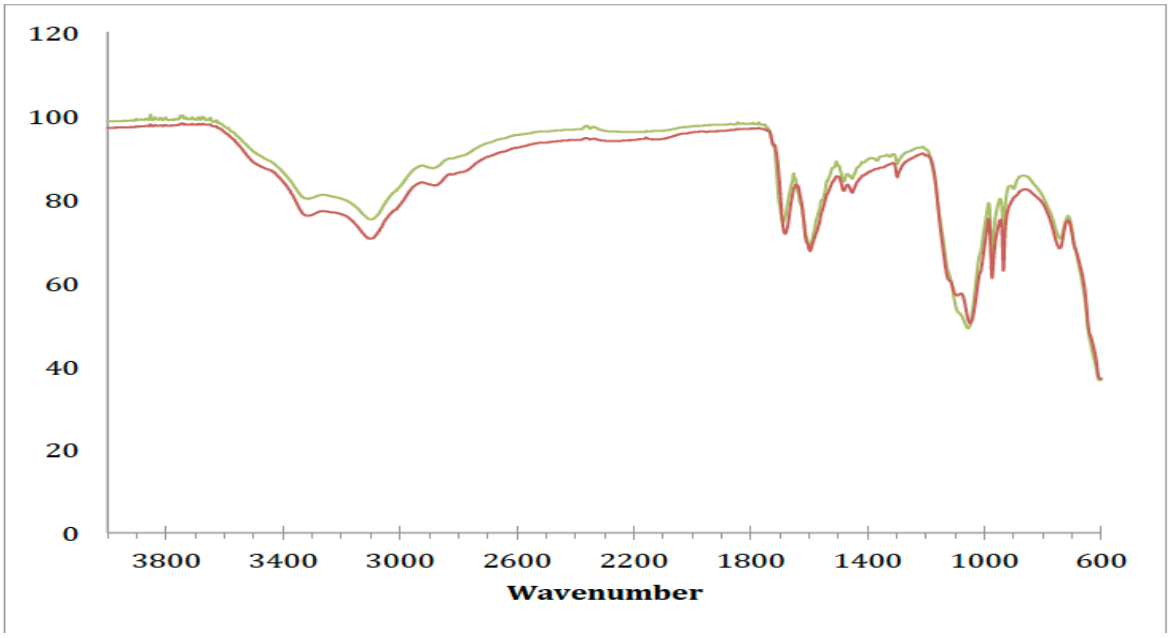

Figure 4.12. FTIR spectra of A · 5H2O (red) and the product of the SO_4^{2-}/Cl^- competitive crystallization (green).

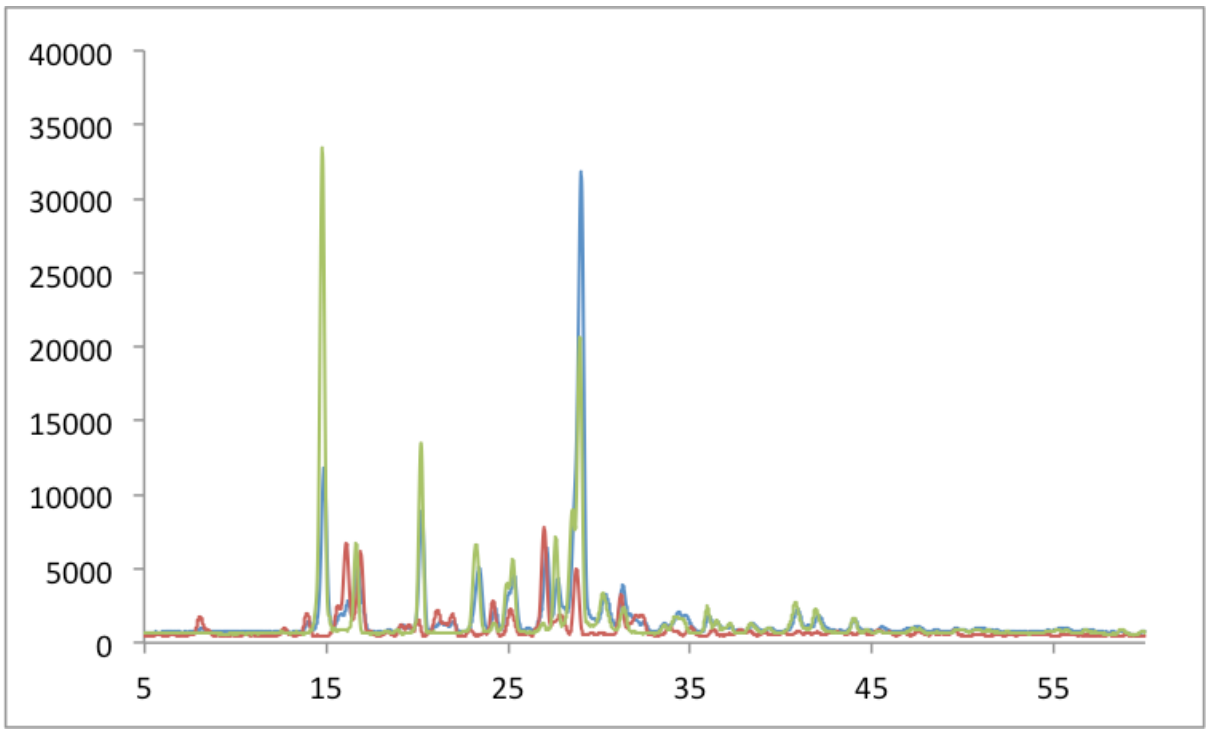

Figure 4.13. PXRD patterns for A·5H_2O (red), C (green) and the product of the SO_4^{2-} /NO_3^- competitive crystallization (blue).

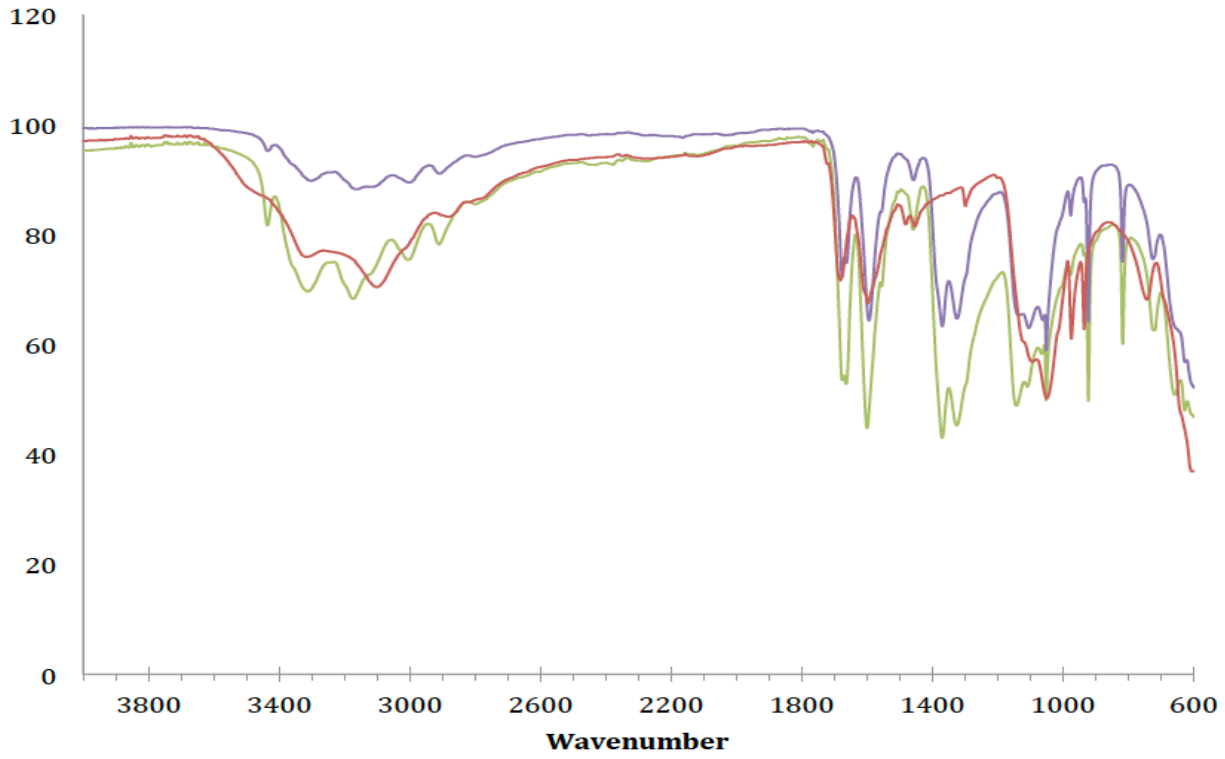

Figure 4.14. FTIR spectra of A · $5H_2O$ (red), C (green) and the product of the SO_4^{2-}/NO_3^- competitive crystallization (blue).

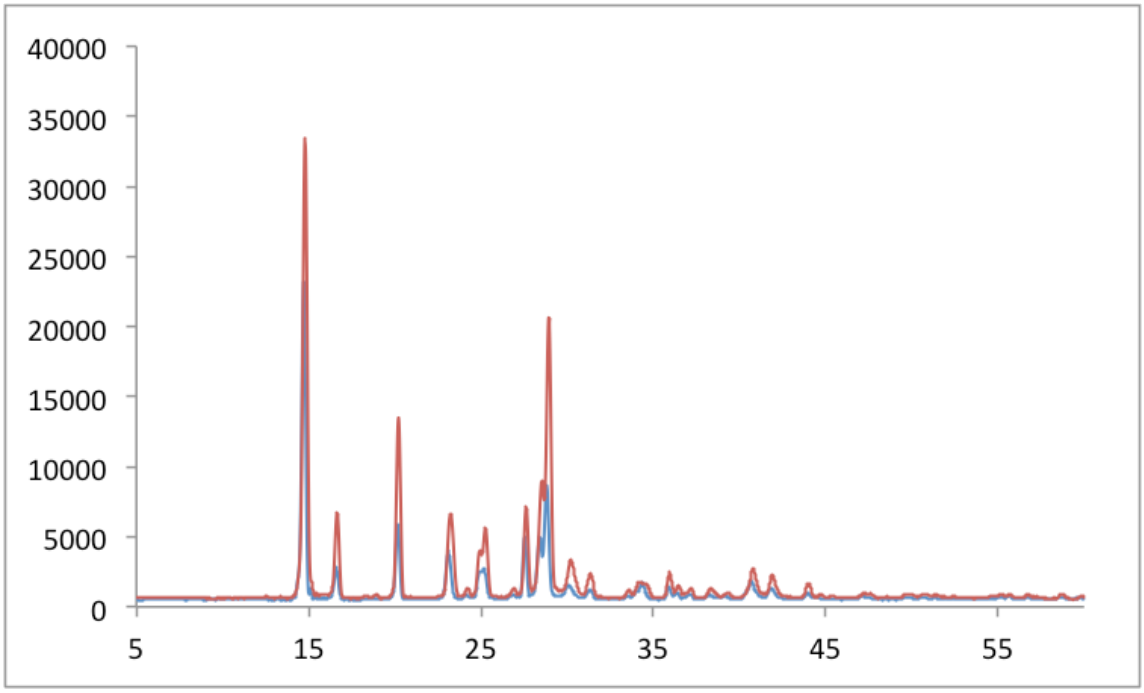

Figure 4.15. PXRD patterns for C (red) and the product of the NO_3^-/ClO_4^- competitive crystallization (blue).

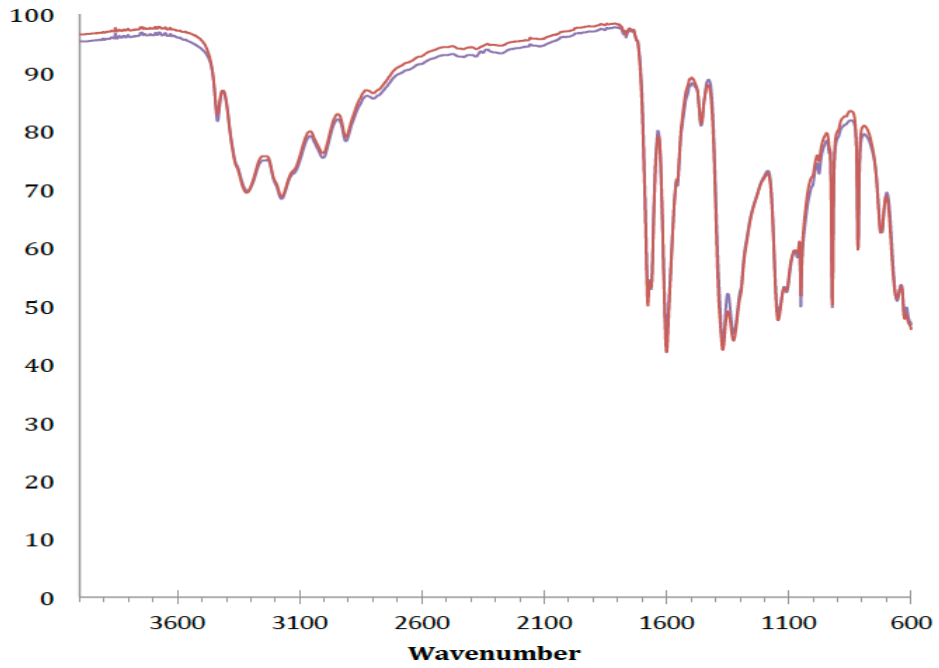

Figure 4.16. FTIR spectra of C (blue) and the product of the NO_3^-/ClO_4^- competitive crystallization (red).

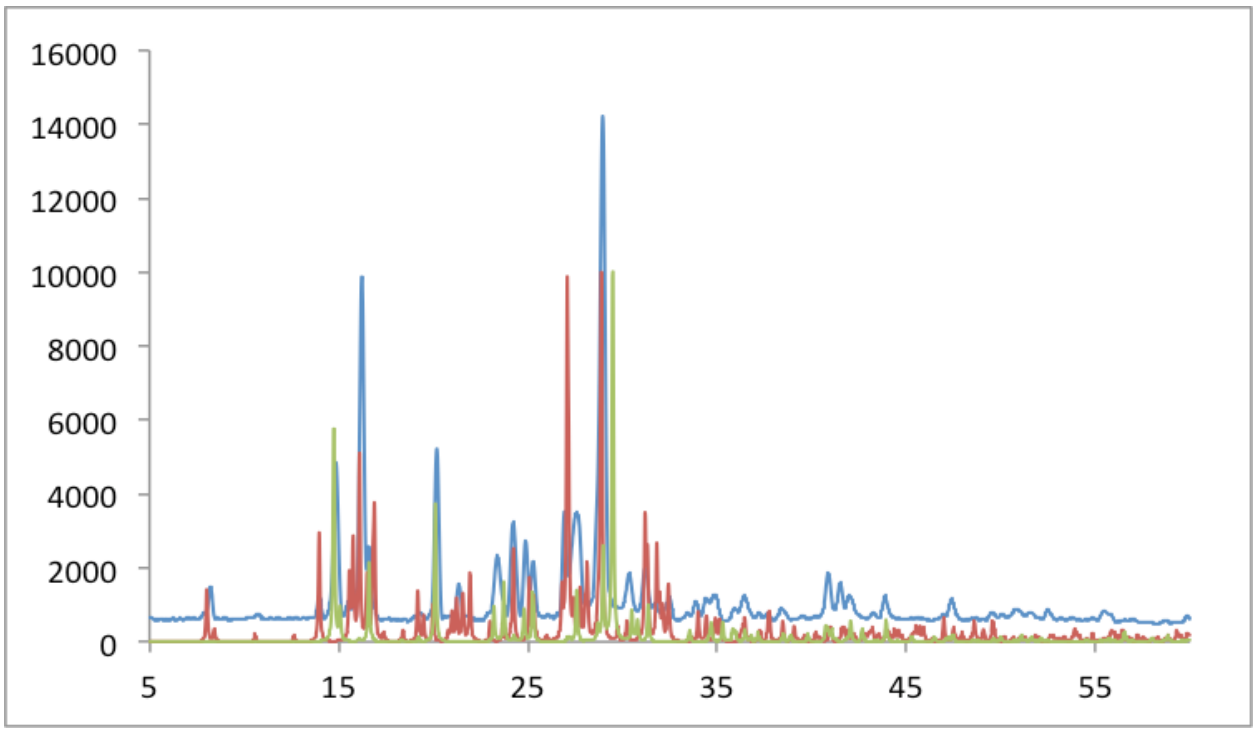

Figure 4.17. PXRD patterns for A·5H_2O (red), C (green) and the product of the SO_4^{2-}/NO_3^-/Cl^-/ClO_4^- competitive crystallization (blue).

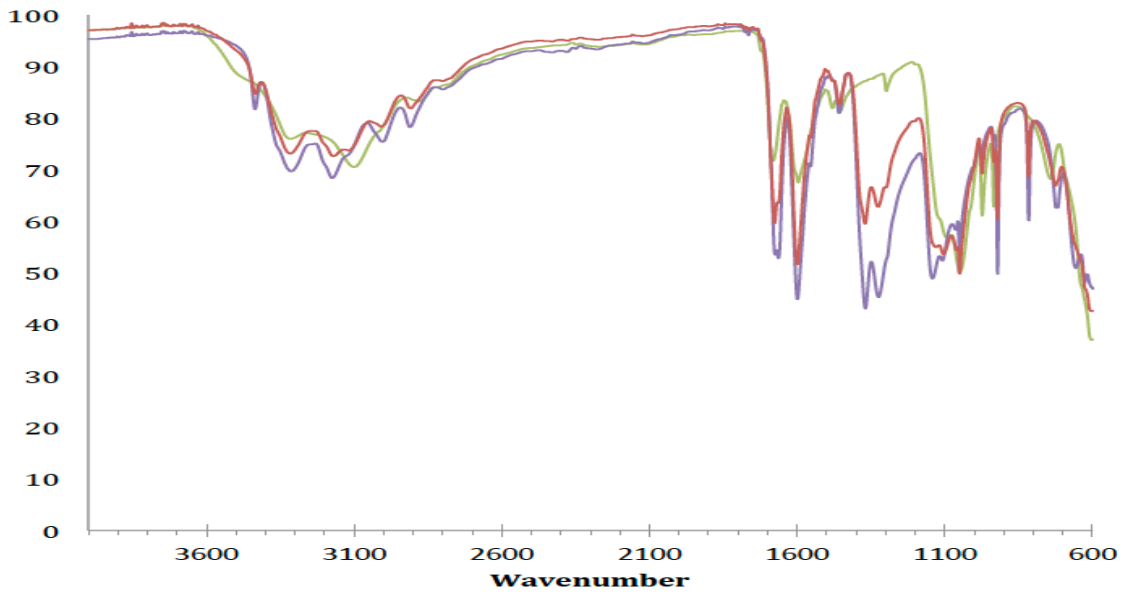

Figure 4.18. FTIR spectra of A · $5H_2O$ (green), C (blue) and the product of the $SO_4^{2-}/NO_3^-/Cl^-/ClO_4^-$ competitive crystallization (red).

Chapter 5 : Aqueous Sulfate Separation by Sequestration of $[(SO_4)_2(H_2O)_4]^{4-}$ Clusters within Highly Insoluble Imine-Linked Bis-Guanidinium Crystals

Publication Statement for Chapter 5

Reference for Original Article:

Custelcean R.; Williams N. J.; Seipp, C. A.; Ivanov, A. S.; Bryantsev, V. S. "Aqueous Sulfate Separation by Sequestration of $[(SO_4)_2(H_2O)_4]^{4-}$ Clusters within Highly Insoluble Imine-Linked Bis-Guanidinium Crystals." *Chem. Eur. J.* **2016**, 22, 1997–2003.

Individual Author Contribution(s):

Custelcean, R. – Co-discover of ligands interactions with oxoanions, grew crystals of ligand with oxoanions, competitive crystallizations, XRD and powder XRD of solid complexes, wrote and edited final manuscript

Williams, N. J. – Co-discover of ligands interactions with oxoanions, synthesis of ligands, determined solubility of ligands salts via UV-Spectroscopy, radiochemistry experiments writing

Seipp, C. A. – Took IR spectra of ligand complexes with various salts, worked on the recycle of the ligand for sulfate capture and release and writing

Ivanov, A. S. – Computational modeling and calculations and writing

Bryantsev, V. S. – Computational modeling and calculations and writing

Journals Policy/Permission/Agreement for Reproduction of Article

TERMS AND CONDITIONS

This copyrighted material is owned by or exclusively licensed to John Wiley & Sons, Inc. or one of its group companies (each a"Wiley Company") or handled on behalf of a society with which a Wiley Company has exclusive publishing rights in relation to a particular work (collectively "WILEY"). By clicking "accept" in connection with completing this licensing transaction, you agree that the following terms and conditions apply to this transaction (along with the billing and payment terms and conditions established by the Copyright Clearance Center Inc., ("CCC's Billing and Payment terms and conditions"), at the time that you opened your RightsLink account (these are available at any time at http://myaccount.copyright.com).

Terms and Conditions

- The materials you have requested permission to reproduce or reuse (the "Wiley Materials") are protected by copyright.

- You are hereby granted a personal, non-exclusive, non-sub licensable (on a stand-alone basis), non-transferable, worldwide, limited license to reproduce the Wiley Materials for the purpose specified in the licensing process. This license, **and any CONTENT (PDF or image file) purchased as part of your order,** is for a one-time use only and limited to any maximum distribution number specified in the license. The first instance of republication or reuse granted by this license must be completed within two years of the date of the grant of this license (although copies prepared before the end date may be distributed thereafter). The Wiley Materials shall not be used in any other manner or for any other purpose, beyond what is granted in the license. Permission is granted subject to an appropriate acknowledgement given to the author, title of the material/book/journal and the publisher. You shall also duplicate the copyright notice that appears in the Wiley publication in your use of the Wiley Material. Permission is also granted on the understanding that nowhere in the text is a previously published source acknowledged for all or part of this Wiley Material. Any third party content is expressly excluded from this permission.

- With respect to the Wiley Materials, all rights are reserved. Except as expressly granted by the terms of the license, no part of the Wiley Materials may be copied, modified, adapted (except for minor reformatting required by the new Publication), translated, reproduced, transferred or distributed, in any form or by any means, and no derivative works may be made based on the Wiley Materials without the prior permission of the respective copyright owner.**For STM Signatory Publishers clearing permission under the terms of the STM Permissions Guidelines only, the terms of the license are extended to include subsequent editions and for editions in other languages, provided such editions are for the work as a whole in situ and does not involve the separate exploitation of the permitted figures or extracts,** You may not alter, remove or suppress in any manner any copyright, trademark or other notices displayed by the Wiley Materials. You may not license, rent, sell, loan, lease, pledge, offer as security, transfer or assign the Wiley Materials on a stand-alone basis, or any of the rights granted to you hereunder to any other person.

- The Wiley Materials and all of the intellectual property rights therein shall at all times remain the exclusive property of John Wiley & Sons Inc, the Wiley Companies, or their respective licensors, and your interest therein is only that of having possession of and the right to reproduce the Wiley Materials pursuant to Section 2 herein during the continuance of this Agreement. You agree that you own no right, title or interest in or to the Wiley Materials or any of the intellectual property rights therein. You shall have no rights hereunder other than the license as provided for above in Section 2. No right,

JOHN WILEY AND SONS LICENSE
TERMS AND CONDITIONS

Mar 16, 2017

This Agreement between Neil J Williams ("You") and John Wiley and Sons ("John Wiley and Sons") consists of your license details and the terms and conditions provided by John Wiley and Sons and Copyright Clearance Center.

License Number	4070851344069
License date	Mar 16, 2017
Licensed Content Publisher	John Wiley and Sons
Licensed Content Publication	Chemistry - A European Journal
Licensed Content Title	Aqueous Sulfate Separation by Sequestration of [(SO4)2(H2O)4]4– Clusters within Highly Insoluble Imine-Linked Bis-Guanidinium Crystals
Licensed Content Author	Radu Custelcean,Neil J. Williams,Charles A. Seipp,Alexander S. Ivanov,Vyacheslav S. Bryantsev
Licensed Content Date	Dec 8, 2015
Licensed Content Pages	7
Type of use	Dissertation/Thesis
Requestor type	Author of this Wiley article
Format	Print and electronic
Portion	Full article
Will you be translating?	No
Title of your thesis / dissertation	Ion Separations: Achieving Selectivity Through Rational Design in Solvent Extraction and Crystallization Systems
Expected completion date	May 2017
Expected size (number of pages)	400
Requestor Location	Neil J Williams Oak Ridge National Laboratory PO Box 2008 MS6119 OAK RIDGE, TN 37831 United States Attn: Neil J Williams
Publisher Tax ID	EU826007151
Billing Type	Invoice
Billing Address	Neil J Williams Oak Ridge National Laboratory PO Box 2008 MS6119 OAK RIDGE, TN 37831 United States Attn: Neil J Williams
Total	0.00 USD
Terms and Conditions	

license or interest to any trademark, trade name, service mark or other branding ("Marks") of WILEY or its licensors is granted hereunder, and you agree that you shall not assert any such right, license or interest with respect thereto

- NEITHER WILEY NOR ITS LICENSORS MAKES ANY WARRANTY OR REPRESENTATION OF ANY KIND TO YOU OR ANY THIRD PARTY, EXPRESS, IMPLIED OR STATUTORY, WITH RESPECT TO THE MATERIALS OR THE ACCURACY OF ANY INFORMATION CONTAINED IN THE MATERIALS, INCLUDING, WITHOUT LIMITATION, ANY IMPLIED WARRANTY OF MERCHANTABILITY, ACCURACY, SATISFACTORY QUALITY, FITNESS FOR A PARTICULAR PURPOSE, USABILITY, INTEGRATION OR NON-INFRINGEMENT AND ALL SUCH WARRANTIES ARE HEREBY EXCLUDED BY WILEY AND ITS LICENSORS AND WAIVED BY YOU.

- WILEY shall have the right to terminate this Agreement immediately upon breach of this Agreement by you.

- You shall indemnify, defend and hold harmless WILEY, its Licensors and their respective directors, officers, agents and employees, from and against any actual or threatened claims, demands, causes of action or proceedings arising from any breach of this Agreement by you.

- IN NO EVENT SHALL WILEY OR ITS LICENSORS BE LIABLE TO YOU OR ANY OTHER PARTY OR ANY OTHER PERSON OR ENTITY FOR ANY SPECIAL, CONSEQUENTIAL, INCIDENTAL, INDIRECT, EXEMPLARY OR PUNITIVE DAMAGES, HOWEVER CAUSED, ARISING OUT OF OR IN CONNECTION WITH THE DOWNLOADING, PROVISIONING, VIEWING OR USE OF THE MATERIALS REGARDLESS OF THE FORM OF ACTION, WHETHER FOR BREACH OF CONTRACT, BREACH OF WARRANTY, TORT, NEGLIGENCE, INFRINGEMENT OR OTHERWISE (INCLUDING, WITHOUT LIMITATION, DAMAGES BASED ON LOSS OF PROFITS, DATA, FILES, USE, BUSINESS OPPORTUNITY OR CLAIMS OF THIRD PARTIES), AND WHETHER OR NOT THE PARTY HAS BEEN ADVISED OF THE POSSIBILITY OF SUCH DAMAGES. THIS LIMITATION SHALL APPLY NOTWITHSTANDING ANY FAILURE OF ESSENTIAL PURPOSE OF ANY LIMITED REMEDY PROVIDED HEREIN.

- Should any provision of this Agreement be held by a court of competent jurisdiction to be illegal, invalid, or unenforceable, that provision shall be deemed amended to achieve as nearly as possible the same economic effect as the original provision, and the legality, validity and enforceability of the remaining provisions of this Agreement shall not be affected or impaired thereby.

- The failure of either party to enforce any term or condition of this Agreement shall not constitute a waiver of either party's right to enforce each and every term and condition of this Agreement. No breach under this agreement shall be deemed waived or excused by either party unless such waiver or consent is in writing signed by the party granting such waiver or consent. The waiver by or consent of a party to a breach of any provision of this Agreement shall not operate or be construed as a waiver of or consent to any other or subsequent breach by such other party.

- This Agreement may not be assigned (including by operation of law or otherwise) by you without WILEY's prior written consent.

- Any fee required for this permission shall be non-refundable after thirty (30) days from receipt by the CCC.

- These terms and conditions together with CCC's Billing and Payment terms and conditions (which are incorporated herein) form the entire agreement between you and WILEY concerning this licensing transaction and (in the absence of fraud) supersedes all prior agreements and representations of the parties, oral or written. This Agreement may not be amended except in writing signed by both parties. This Agreement shall be binding upon and inure to the benefit of the parties' successors, legal representatives, and authorized assigns.

- In the event of any conflict between your obligations established by these terms and conditions and those established by CCC's Billing and Payment terms and conditions, these terms and conditions shall prevail.

- WILEY expressly reserves all rights not specifically granted in the combination of (i) the license details provided by you and accepted in the course of this licensing transaction, (ii) these terms and conditions and (iii) CCC's Billing and Payment terms and conditions.

- This Agreement will be void if the Type of Use, Format, Circulation, or Requestor Type was misrepresented during the licensing process.

- This Agreement shall be governed by and construed in accordance with the laws of the State of New York, USA, without regards to such state's conflict of law rules. Any legal action, suit or proceeding arising out of or relating to these Terms and Conditions or the breach thereof shall be instituted in a court of competent jurisdiction in New York County in the State of New York in the United States of America and each party hereby consents and submits to the personal jurisdiction of such court, waives any objection to venue in such court and consents to service of process by registered or certified mail, return receipt requested, at the last known address of such party.

WILEY OPEN ACCESS TERMS AND CONDITIONS
Wiley Publishes Open Access Articles in fully Open Access Journals and in Subscription journals offering Online Open. Although most of the fully Open Access journals publish open access articles under the terms of the Creative Commons Attribution (CC BY) License only, the subscription journals and a few of the Open Access Journals offer a choice of Creative Commons Licenses. The license type is clearly identified on the article.
The Creative Commons Attribution License
The Creative Commons Attribution License (CC-BY) allows users to copy, distribute and transmit an article, adapt the article and make commercial use of the article. The CC-BY license permits commercial and non-
Creative Commons Attribution Non-Commercial License
The Creative Commons Attribution Non-Commercial (CC-BY-NC)License permits use, distribution and reproduction in any medium, provided the original work is properly cited and is not used for commercial purposes.(see below)

Creative Commons Attribution-Non-Commercial-NoDerivs License
The Creative Commons Attribution Non-Commercial-NoDerivs License (CC-BY-NC-ND) permits use, distribution and reproduction in any medium, provided the original work is properly cited, is not used for commercial purposes and no modifications or adaptations are made. (see below)

Use by commercial "for-profit" organizations
Use of Wiley Open Access articles for commercial, promotional, or marketing purposes requires further explicit permission from Wiley and will be subject to a fee.
Further details can be found on Wiley Online Library
http://olabout.wiley.com/WileyCDA/Section/id-410895.html

Other Terms and Conditions:

v1.10 Last updated September 2015

Questions? customercare@copyright.com or +1-855-239-3415 (toll free in the US) or +1-978-646-2777.

A version of this chapter was originally published by Radu Custelcean, Neil J. Williams, Charles A. Seipp, Alexander S. Ivanov and Vyacheslav S. Bryanstev. in *Chemistry A European Journal*

Custelcean R.; Williams N.J.; Seipp, C.A.; Ivanov, A.S.; Bryantsev, V.S. "Aqueous Sulfate Separation by Sequestration of $[(SO_4)_2(H_2O)_4]^{4-}$ Clusters within Highly Insoluble Imine-Linked Bis-Guanidinium Crystals." *Chem. Eur. J.* **2016**, 22, 1997–2003.

The article used as Chapter 5 was modified in the following manner; the formatting was adapted to fit the formatting required by the University of Tennessee Knoxville, the figures and tables were renumbered to make all figures in the ensuing document contiguous. The work/research of the done by the student in the articles is as follows synthesis, measured solubility of salts of the compounds, radiochemical experiments for sulfate removal from sea water and contributed to the writing for the experimental section and electronic supplementary information.

Abstract

Selective crystallization of sulfate with a simple bis-guanidinium ligand, self-assembled in situ from terephthalaldehyde and aminoguanidinium chloride, was employed as an effective way to separate the highly hydrophilic sulfate anion from aqueous solutions. The resulting bis-iminoguanidinium sulfate salt has exceptionally low aqueous solubility ($K_{sp} = 2.4 \times 10^{-10}$), comparable to that of $BaSO_4$. Single-crystal X-ray diffraction analysis

showed the sulfate anions are sequestered as $[(SO_4)_2(H_2O)_4]^{4-}$ clusters within the crystals. Variable-temperature solubility measurements indicated the sulfate crystallization is slightly endothermic ($\Delta H_{cryst} = 3.7$ kJmol^{-1}), thus entropy driven. The real-world utility of this crystallization-based approach for sulfate separation was demonstrated by removing up to 99% of sulfate from seawater in a single step.

5.1 Introduction

Effective separation of highly hydrophilic anions (e.g., sulfate, selenate, chromate, phosphate) from competitive aqueous solutions remains a major challenge, despite the tremendous progress in anion receptor chemistry over the past decade.[1a,b] In the particular case of sulfate, although a significant number of sulfate-binding receptors have been reported,[2] only a handful of them have proven effective in the separation of this anion from water.[3a-g] The bottleneck in the development of anion receptors is often the multistep syntheses required for their assembly, which generally involve tedious purifications and toxic reagents and solvents. If the receptors could self-assemble in water from simple subcomponents, thereby combining the synthesis and the anion separation into one step, it would lead to greener, cheaper, and more practical anion separation methods.

One approach that has proven particularly effective for aqueous anion separation is selective anion crystallization with organic ligands functionalized with hydrogen bonding groups.[4a-c] This approach combines elements of anion receptor chemistry and crystal

engineering, as it entails recognition of the targeted anion through complementary hydrogen bonding, and formation of stable crystals through favorable packing. The challenge with anion crystallization from water is to identify anion-binding ligands that can effectively compete against the strong anion hydration, and that are also able to self-assemble with the anions of interest into crystals with low aqueous solubility. Along this line, we recently discovered that crystallization of sulfate, in the form of extended $[SO_4(H_2O)_5^{2-}]n$ clusters, with rigid and planar bis-guanidinium ligands, can strike a favorable energetic balance that allows for the efficient separation of the highly hydrophilic sulfate anion from water.[5] In this demonstrated prototype, the bis-guanidinium ligand was synthesized in situ by condensation of glyoxal with aminoguanidinium sulfate, resulting in a sulfate salt with low aqueous solubility ($K_{sp} = 3.2 \times 10^{-7}$), comparable with that of $SrSO_4$. The very low solubility of this bis-guanidinium sulfate salt is in stark contrast with the typically high solubility of organic sulfate salts. We rationalized these results based on the favorable stacking of the planar bis-guanidinium cation in the crystalline state and the reduced dehydration penalty of the sulfate–water cluster compared to the naked anion.

Encouraged by the unexpected effectiveness of the glyoxal based bis-guanidinium prototype system in sulfate crystallization, we decided to explore the generality of this simple approach to aqueous sulfate separation, seeking to achieve even higher sulfate crystallization efficiency through crystal engineering. We hypothesized that replacing the glyoxal linker with a more extended p system would lead to more favorable stacking of the bis-guanidinium cations, which in turn would result in lower aqueous solubility for the sulfate salt. Herein we demonstrate the effective separation of aqueous sulfate based on

crystallization of $[(SO_4)_2(H_2O)_4]^{4-}$ clusters with an imine linked bis-guanidinium ligand self-assembled in situ from terephthalaldehyde and aminoguanidinium chloride. The resulting sulfate salt is exceptionally insoluble in water, on a par with $BaSO_4$, and the bis-guanidine ligand can be easily recycled. The real-world utility of this method was demonstrated by effective separation of sulfate from seawater.

5.2 Results and Discussion

Aqueous condensation of aminoguanidinium chloride with terephthalaldehyde
led to the in situ formation of the 1,4-benzene-bis(iminoguanidinium) cation (BBIG), which crystallized as the sulfate (BBIG-SO_4) or nitrate (BBIG-NO_3) salt in the presence of Na_2SO_4 or $NaNO_3$, respectively (**Figure 5.1**).

The single-crystal X-ray structural analysis[6] of BBIG-SO_4 revealed a virtually planar conformation for the bis(iminoguanidinium) cation, and the inclusion of two water molecules of hydration in the crystal (**Figure 5.2a**). Pairs of sulfate anions are linked together by four water molecules into centrosymmetric $[(SO_4)_2(H_2O)_4]^{4-}$ clusters (**Figure 5.2b**).[7a-d] Each sulfate anion in the cluster accepts four water hydrogen bonds, with observed OH···O contact distances of 1.82, 1.84, 1.88, and 2.20 Å, and OH-O angles of 169.8, 174.2, 156.6, and 167.38, respectively. There are two crystallographically distinct BBIG cations in the crystal; one is perfectly planar, whereas the other is slightly bent, with its terminal NH_2 groups deviating by 0.2 Å out of the mean plane of the cation. The two cations are stacked in an antiparallel fashion in an ABAB pattern in the crystal, with a

mean interplanar distance of 3.39 Å (**Figure 5.2c**). The shortest intermolecular contacts between adjacent cations in the stacks are shown in black and red dashed lines in **Figure 5.2c**, corresponding to contacts between the imine N atoms and the centroids of the benzene rings (3.35, 3.48 Å), and between terminal NH_2 groups and the centers of the C=N imine bonds (3.19, 3.33 Å), respectively. The anionic $[(SO_4)_2(H_2O)_4]^{4-}$ clusters in the crystal are flanked by four cationic BBIG stacks, accepting a total of 20 NH···O hydrogen bonds from the guanidinium groups, of which 14 are to the sulfate anions, and 6 to the water molecules in the cluster (**Figure 5.2d**). Thus, the total coordination number of each sulfate anion is 11, consisting of 7 NH···O hydrogen bonds from guanidinium groups, and 4 OH···O hydrogen bonds from water.

The X-ray crystal structure of BBIG-NO_3 is shown in **Figure 5.3**.[6] Like in the analogous sulfate structure, the BBIG cations are stacked within the crystal, though in this case they are oriented parallel to each other, with a mean interplanar distance of 3.27 Å between adjacent cations in the stack. The nitrate anions link the stacks into a three-dimensional hydrogen-bonded network, with each anion accepting five hydrogen bonds from three neighboring guanidinium groups (**Figure 5.3c**).

Effective aqueous anion separation by crystallization of guanidines requires in the first place that the guanidinium salt of the targeted anion is relatively insoluble in water. For the crystallization to be selective, the guanidinium salt of the targeted anion also needs to be significantly less soluble than the corresponding salts of the competing anions.

Table 12 lists the measured aqueous solubilities of the sulfate, nitrate, and chloride salts of BBIG. The aqueous solubility of the sulfate salt was found to be lower than the corresponding solubilities of the nitrate and chloride analogues, by a factor of about 40 and 4000, respectively. Notably, the solubility of BBIG-SO_4 is also lower by a factor of 45 than the solubility of the glyoxal-bis-(iminoguanidinium) sulfate salt, previously reported by us.[5a,b] The corresponding solubility product (K_{sp}) of BBIG-SO_4 is 2.4($\pm$0.6) $\times$ 10^{-10}, which is only marginally higher than the K_{sp} of $BaSO_4$ (1.1 $\times$ 10^{-10}). Variable-temperature dissolution measurements indicated the solubility of BBIG-SO_4 slightly decreases with increasing temperatures. The enthalpy of dissolution obtained from the slope of the van't Hoff plot (**Figure 5.4**) is –3.7($\pm$0.8) $\times$ 10^{-10} kJmol^{-1}. Thus, crystallization of BBIG-SO_4 is slightly endothermic and entropy driven.

The exceptionally low aqueous solubility of BBIG-SO_4 is quite unusual for a guanidinium sulfate salt.[5a,b] This low solubility implies high stability for the BBIG-SO_4 crystals. We have proposed that one of the structural factors contributing to the stability of these crystals is the favorable stacking of the planar bis-iminoguanidinium cations.[5a,b] This proposal is consistent with previous observations that guanidinium cations have a propensity to stack to each other or to aromatic rings.[8] Electronic-structure calculations (see Supporting Information for details) usingdensity functional theory (DFT) indicated the stacking interactions between the bis-iminoguanidinium cations in the BBIGSO_4 crystals are mainly electrostatic in nature (**Figure 5.5**). The electrostatic potential maps of the BBIG cation, either in the BBIG-SO_4 crystal (**Figure 5.5**), or isolated in the gas phase (**Figure**

5.5b), showed that the C atoms, including those of the phenyl ring, tend to be electropositive, whereas the N atoms of the guanidinium and imine groups are all electronegative. The atomic charges of the BBIG cation, calculated using the Bader scheme, are shown in **Figure 5.5c**. These charges are generally consistent with the relative offset of the BBIG cations observed in the BBIG-SO_4 crystals (**Figure 5.2c**), so that the closest intercationic contacts are between the terminal N atoms of the guanidinium groups (–1.31 charge) and the C atoms of the imine groups (+0.77 charge), and between the imine N atoms (–0.75 charge) and the C atoms of the Ph ring (+0.21, +0.13 charges). It thus appears that the stacking of the BBIG cations in these crystals is determined to a large extent by complementary electrostatic attractions between positive and negative regions of the planar cations.[9]

Consistent with the measured aqueous solubilities that showed the sulfate salt was the least soluble in the series, crystallization of BBIG-SO_4 from an aqueous mixture containing chloride (0.1 M), nitrate (0.07 M), and sulfate (0.034 M) proved highly selective, resulting in exclusive separation of the sulfate anion in quantitative yield. The BBIG ligand was easily recovered by deprotonation of the guanidinium groups with 10% aqueous NaOH, which resulted in crystallization of the neutral BBIG ligand[6a-d] in 93% yield. The ligand can be recycled by converting it back into the cationic form with aqueous HCl. The overall sulfate separation cycle is depicted in **Figure 5.6**.

To demonstrate the real-world utility of this sulfate separation method, the removal of sulfate from seawater by selective crystallization of BBIG-SO_4 was attempted. The presence of relatively high concentrations of sulfate in seawater (0.30 mM) poses scale deposits (as $CaSO_4$, $SrSO_4$, and $BaSO_4$) are difficult to remove and cause major operational problems with high remedial costs, and in some cases result in irreversible damage and well shutdown. It is therefore highly desirable to prevent the scale problems by removing sulfate from seawater.[10a,b]

Table 5.2 shows the results from the sulfate separation from seawater by crystallization of BBIG-SO_4. The sulfate concentration in solution was monitored by using radiolabeled $Na_2{}^{35}SO_4$ and b liquid scintillation counting, an analytical method typically used in liquid–liquid extractions, and recently demonstrated to also be effective in crystallization-based sulfate separations.[11] Crystallization of BBIG-SO_4 from seawater proved very efficient, with 99% of sulfate being removed by using only 1.5 molar equivalents of the BBIG cation.

5.3 Conclusion

We have demonstrated here an effective approach to aqueous sulfate separation by selective crystallization with an imine linked bis-guanidinium ligand self-assembled in situ from simple building blocks. The high sulfate crystallization efficiency stems from the exceptionally low aqueous solubility of the BBIG-SO_4 salt, which is significantly lower than the aqueoussolubility of most, if not all known organic sulfate salts,[12a,b] and comparable to that of $BaSO_4$. Furthermore, compared to precipitation with $BaCl_2$, the crystallization-

based approach described here offers a greener alternative to aqueous sulfate separation that circumvents the use of toxic barium. An important factor in the stability of the BBIG-SO_4 crystals appears to be the favorable stacking of the rigid and planar bis-iminoguanidinium cations, which are arranged to optimize the electrostatic attraction between the positive and negative areas of the cationic ligands. Another structural factor likely to play a key role in the low solubility of the BBIG-SO_4 crystals and the high sulfate crystallization selectivity is the sequestration of the sulfate anions as $[(SO_4)_2(H_2O)_4]^{4-}$ clusters and their complementary hydrogen bonding by the guanidinium groups. However, in the end the BBIG-SO_4 crystallization is entropy driven, presumably reflecting the entropically favorable release of water molecules from the strongly hydrated sulfate anions and the planar BBIG cations.[13a,b] Thus, this example of selective sulfate crystallization as sulfate–water clusters represents a complex recognition phenomenon that extends far beyond the simple lock-and-key principle commonly invoked in supramolecular chemistry.[14] It involves a multitude of factors, including the mutual recognition of molecular and ionic components, a fine interplay of enthalpy and entropy,[15] and a series of binding, self-assembly, and solvent exchange events that lead in the end to the nucleation and growth of highly insoluble crystals. Understanding and ultimately controlling all these factors through systematic crystal engineering and structure–solubility relationship studies offer prospects for predictive design of advanced separation systems for sulfate and other environmentally and energy relevant anions.

5.4 Experimental Section

Aminoguanidinium chloride and terephthalaldehyde were purchased from Sigma Aldrich and used as received. $Na_2{}^{35}SO_4$ was purchased from PerkinElmer. 1,4-Benzene-bis(iminoguanidinium) chloride (BBIG-Cl) used for solubility and crystallization studies was prepared according to a literature procedure.[16] FT-IR spectra were collected on a Digilab FTS 7000 Series Infrared Spectrometer using a diamond ATR setup. UV spectra were measured in 10 mm path length quartz glass cuvettes using a Cary Varian 5000 spectrometer and analyzed with Cary WinUV software. Powder X-ray diffraction (PXRD) measurements were done with a Panalytical Empyrean diffractometer using a flat sample stage in reflection mode.

5.4.1 Synthesis and crystallization of 1,4-benzene-bis(iminoguanidinium) sulfate (BBIG-SO_4) and nitrate (BBIG-NO_3)

BBIG-SO_4: A mixture of solid terephthalaldehyde (0.5 mmol, 0.067 g), aqueous aminoguanidinium chloride (1.1 mmol, 2.2 mL, 0.5 M), and water (10 mL) was stirred magnetically for 4 h resulting in a slightly yellow solution. Addition of sodium sulfate (0.5 mmol, 0.5 mL, 1 M) to this solution resulted in instant precipitation of a crystalline white solid. The crystalline solid was filtered after two weeks and washed with water. Yield 0.164 g (86 %). HRMS (ESI-MS): m/z calcd for $C_{10}H_{15}N_8^+$: 247.14140; found: 247.14100.; elemental analysis calcd (%) for $C_{10}H_{20}N_8O_6S$: C 31.58, H 5.30, N 29.46; found: C 31.61, H 5.53, N 29.04. X-ray quality single crystals were obtained by slow evaporation of a solution containing aminoguanidinium chloride, terephthalaldehyde, and

tetrabutylammonium sulfate in water/DMF. The simulated powder pattern from the single-crystal X-ray structural analysis matched the experimental PXRD pattern of bulk BBIG-SO4 precipitated from water (Supporting Information, **Figure 5.7**).

BBIG-NO_3: A mixture of solid terephthalaldehyde (0.5 mmol, 0.067 g), aqueous aminoguanidinium chloride (1.5 mmol, 3 mL, 0.5 M), and water (10 mL) was stirred magnetically for 5 h resulting in a slightly yellow solution. Addition of sodium nitrate (1 mmol, 1 mL, 1 M) to this solution resulted in precipitation of a crystalline white solid after about 10 min. The mixture was stirred for 12 h then the crystalline solid was filtered and washed with water and ethanol. Yield 0.150g (81%). HRMS (ESI-MS): m/z calcd for $C_{10}H_{15}N_8^+$: 247.14140; found: 247.14130; elemental analysis calcd(%) for $C_{10}H_{16}N_{10}O_6$: C 32.26, H 4.33, N 37.62; found: C 32.57, H 4.50, N 36.64. X-ray quality single crystals were obtained by leaving the mixture containing the initially precipitated solid undisturbed for 2 weeks. The simulated powder pattern from the single-crystal X-ray structural analysis matched the experimental PXRD pattern of bulk BBIG-NO3 precipitated from water (in Chapter 5 Appendix, **Figure 5.8**).

5.4.2 Solubility measurements of BBIG-Cl, BBIG-SO_4, and BBIG-NO_3.

The solubility of BBIG-Cl was determined gravimetrically. A saturated solution of BBIG-Cl was obtained by placing an excess of the salt in a 15 mL polypropylene centrifuge tube and adding 2 mL of deionized water (milli-Q). The resulting suspension was mixed for 48 h using a rugged rotator set at 60 rpm, inside an incubator set at 258 °C. After 48 h the

suspension was centrifuged for 10 min at 3000 rpm to separate the aqueous and solid phases. The aqueous layer was then carefully removed using a 0.22 μm syringe filter to remove any remaining suspended solid from the solution. One mL of the saturated salt solution was then pipetted into a pre-weighed glass vial containing a magnetic stir bar. The water was then removed under reduced pressure and gentle heating (–50 °C) while stirring. The resulting solid was left under vacuum overnight to ensure complete removal of the water, prior to weighing the vial. The solubility measurements were run in triplicate, and the average weight of the recovered chloride salt was 0.0202 g, corresponding to an aqueous solubility of $6.3(\pm 0.2) \times 10^{-2}$ M.

The solubilities of BBIG-SO_4 and BBIG-NO_3 were determined by UV spectroscopy. Prior to determining the solubility of these salts, a calibration curve was obtained using the more soluble BBIG-Cl salt (the UV calibration spectra and curve for the BBIG-Cl solutions are shown in **Figures 5.9** and **5.10** in Chapter 5 Appendix). Saturated solutions of the BBIG-SO_4 and BBIG-NO_3 salts were prepared the same way as for BBIG-Cl. These solutions were then diluted to ensure the concentrations of the BBIG dication were in the concentration range of the calibration curve. The BBIG-NO_3 solutions were diluted 100-fold, whereas the BBIG-SO4 solutions were diluted tenfold. The solubilities were then determined from the UV spectra of these diluted solutions by measurement of the absorbance maxima at 322 nm and comparison with the calibration curve. The solubility measurements were run in triplicate, and the obtained averages and standard deviations for BBIG-SO_4 and BBIG-NO_3 were $1.6(2) \times 10^{-5}$ and $6.5(5) \times 10^{-4}$ M, respectively.

5.4.3 Variable-temperature solubility measurements of BBIG-SO4

All measurements were done in triplicate and the reported solubilities are the average values. Excess amounts of BBIG-SO_4 were mixed with 10 mL of MilliQ water in 15 mL polypropylene centrifuge tubes. The resulting suspensions were mixed for 72 h using a rugged rotator set at 60 rpm, inside an incubator set at 15, 20, 25, 30, or 35 °C. Subsequently, the samples were removed and centrifuged for 10 min at 3000 rpm to separate the aqueous and solid phases. A 3 mL aliquot was then removed from each sample for UV analysis. Then 3 mL of fresh MilliQ water was added to the samples to replace the aliquot of solution removed, and the samples were mixed for an additional 72 h at the next desired temperature before further subsampling. The temperatures were maintained by using temperature controlled incubators containing NIST certified thermometers. The 3 mL aliquots of subsampled solutions were filtered through a 0.22 mm syringe filter to ensure any suspended solid was removed from the solutions prior to diluting the samples using the same dilution factors used in determining the solubilities at 258 °C, as described above. The solubilities were determined by UV spectrometry, as described in the previous section. The obtained solubilities are listed in **Table 5.3** of the Supporting Information, and the van't Hoff plot is shown in **Figure 5.4**.

5.4.4 Competitive crystallization of BBIG-SO_4 from an aqueous mixture of sulfate, nitrate, and chloride

First, BBIG-Cl was generated in situ from terephtalaldehyde and aminoguanidinium chloride, as follows. Terephthalaldehyde (0.5 mmol, 0.067 g), aminoguanidinium chloride

(1.5 mmol, 3 mL, 0.5 M) and water (10 mL) were added to a 20 mL vial. The mixture was stirred at room temperature for 5 h, which resulted in dissolution of most of the suspended solid. A few drops of 1 M HCl were then added to adjust the pH to around 5, which resulted in a clear, slightly yellow solution. Aqueous sodium sulfate (0.5 mmol, 0.5 mL, 1 M) and sodium nitrate (1 mmol, 1 mL, 1 M) were then added, which resulted in the formation of a white precipitate after about 2 min. The mixture was stirred at room temperature for 12 h, then the crystalline solid was filtered and washed with water. Yield 0.190 g (100%). PXRD (**Figure 5.11**, in Chapter 5 Appendix) and FT-IR (**Figure 5.12**, in Chapter 5 Appendix) analyses confirmed the crystallized solid was pure BBIG-SO_4.

5.4.5 Recovery of the BBIG ligand

BBIG-SO_4 (53.1 mg,0.14 mmol) was added to a 2 mL solution of NaOH (10%) and the mixture was stirred for 2 h at room temperature, resulting in the formation of a yellow precipitate. The solid was filtered using a pre-weighed filter paper, rinsed with 200 mL of water, then dried under vacuum. Yield 31.8 mg (93%) as yellow powder. 1H NMR (400 MHz, CD_3OD): d=7.660 (s, 4H; CH), 8.015 ppm (s, 2H; N=CH). Dissolution of the yellow powder in 1 M HCl resulted in a clear solution of BBIG-Cl, which could be reused for sulfate separation, as demonstrated by precipitation of BBIGSO_4 upon addition of aqueous sodium sulfate. X-ray quality single crystals of BBIG·$2H_2O$ were obtained by slow evaporation of a solution containing a small amount of the recovered yellow powder dissolved into aqueous ethanol. The crystal structure of the BBIG·$2H_2O$ is shown in **Figure 5.13** in Chapter 5 Appendix.

5.4.6 Sulfate separation from seawater

The seawater used in the experiment was collected from the gulf stream in the Atlantic Ocean. Prior to use, the water was pre-filtered to remove suspended particulates and small organisms. After filtration, 10 mL of the ocean water was spiked with 96 mL of the ^{35}S radiotracer (as $Na_2{}^{35}SO_4$) for β liquid scintillation counting (see below). The sulfate concentration in seawater was estimated around 30 mM by titration with $BaCl_2$. Stock solutions of BBIG-Cl in MiliQ water were prepared, with concentrations of 15, 30, 33, 45, and 60 mM. A volume of 0.75 mL of each of these solutions was pipetted into a 2 mL Eppendorf microcentrifuge tube, and 0.75 mL of seawater pre-spiked with the ^{35}S radiotracer was added. The resulting solution mixtures were mixed for 24h using a rotating wheel set at 60 rpm in a temperature-controlled air-box set at 25$\pm$0.2 °C. The tubes were then centrifuged for 10 min at 3000 rpm to separate the aqueous and solid phases, and 1 mL aliquot solutions were removed using 0.22 μm syringe filters for β liquid scintillation counting (see below).

5.4.7 Analysis of sulfate concentration by β liquid scintillation counting

The radiolabeled ^{35}S radiotracer is a β emitter, thereby allowing determination of the sulfate concentration of a solution spiked with a known amount of $Na_2{}^{35}SO_4$ by β liquid scintillation counting. The seawater solutions were pre-spiked with 96 mL of the ^{35}S radiotracer (see above). The amount of radiotracer used was based on the need to ensure approximately 4.5 to 5 million initial counts per minute (CMP)/mL of solution (Ci/mL^{-1}). The volume of the spike solution was determined by factoring in the original activity of the

solution and correcting for the short half-life of the ^{35}S radiotracer. The $Na_2{}^{35}SO_4$ solution had completed 3.8 half-lives before use in this experiment. The liquid scintillation counting was done with a Packard Tri-Carb 2500TR Liquid Scintillation Analyzer. The 1 mL aliquot solutions removed from seawater (see above) were pipetted into 20 mL of Ultima Gold scintillation cocktail (PerkinElmer). It was necessary to use 20 mL of the cocktail to ensure complete solubility of the seawater solutions in the cocktail. The resulting mixtures were vigorously shaken to allow for complete dissolution and dispersion of the salt solutions. The samples were then placed on the analyzer and counted for 30 min after allowing 60 min for dark-adaption.

5.4.8 Single-crystal X-ray structural determination

Single-crystal X-ray data were collected on a Bruker SMART APEX CCD diffractometer with fine-focus $Mo_{K\propto}$ radiation ($\lambda = 0.71073$ Å), operated at 50 kV and 30 mA. The structures were solved by direct methods and refined on F^2 using the SHELXTL software package (Bruker AXS, Inc., Madison, WI, 1997). Absorption corrections were applied using SADABS, part of the SHELXTL package. All non-hydrogen atoms were refined anisotropically. Hydrogen atoms were placed in idealized positions and refined with a riding model, except for the water hydrogen atoms, which were located from difference Fourier maps and refined isotropically.

Crystal data for BBIG-SO4 (CCDC 1430158): $C_{10}H_{20}N_8O_6S$, M = 380.40, colorless needle, 0.39 × 0.05 × 0.04 mm^3, monoclinic, space group $P2_1/n$, a = 9.6336(13), b =

12.8588(18), c = 13.8643(18) Å , b = 108.552(3)8, V = 1628.2(4) $Å^3$, Z = 4, ρ_{cald} = 1.552 gcm^{-3}, $Mo_{K\propto}$ radiation, λ = 0.71073 Å, T = 173(2) K, $2\theta_{max}$ = 56.78, 16493 reflections collected, 4058 unique (R_{int} = 0.0436). Final *GooF* = 1.030, R_1 = 0.0533, wR_2 = 0.1363, *R* indices based on 2902 reflections with $I>2\sigma(I)$ (refinement on F^2), 242 parameters, 0 restraints. Lp and absorption corrections applied, μ = 0.248 mm^{-1}.

Crystal data for BBIG-NO3 (CCDC 1430159): $C_5H_8N_5O_3$, *M* = 186.16, colorless needle, 0.27 × 0.05 × 0.04 mm^3, monoclinic, space group $P2_1/c$, a = 4.2677(19), b = 16.048(7), c = 12.682(5) Å, β = 108.167(14)º, *V* = 825.3(6) $Å^3$, Z = 4, ρ_{cald} = 1.498 gcm^{-3}, $Mo_{K\propto}$ radiation, λ = 0.71073 Å, T = 173(2 K, $2\theta_{max}$ = 50.0º, 5551 reflections collected, 1435 unique (R_{int} = 0.0545). Final *GooF* = 1.030, R_1 = 0.1037, wR_2 = 0.2583, R indices based on 898 reflections with $I > 2\sigma(I)$ (refinement on F^2), 118 parameters, 0 restraints. Lp and absorption corrections applied, μ = 0.125 mm^{-1}.

Crystal data for BBIG·2H2O (CCDC 1430160)**:** $C_{10}H_{18}N_8O_2$, *M* = 282.32, yellow plate, 0.32 × 0.24 × 0.01 mm^3, monoclinic, space group $P2_1/c$, a = 14.818(3), b = 3.9508(7), c=12.263(2) Å, b = 104.322(4)8, V = 695.6(2) $Å^3$, Z = 2, ρ_{cald} = 1.348 gcm^{-3}, $Mo_{K\propto}$ radiation, l = 0.71073 Å, T=173(2 K, $2\theta_{max}$ = 56.68, 4427 reflections collected, 1738 unique (R_{int} = 0.0252). Final *GooF* = 1.040, R_1 = 0.0527, wR_2 = 0.1348, *R* indices based on 1188 reflections with $I > 2\sigma(I)$ (refinement on F^2), 106 parameters, 0 restraints. Lp and absorption corrections applied, μ = 0.100 mm^{-1}.

5.5 References

[1] N. Busschaert, C. Caltagirone, W. Van Rossom, P. A. Gale, Chem. Rev. 2015, 115, 8038; b) N. H. Evans, P. D. Beer, Angew. Chem. Int. Ed. 2014, 53, 11716; Angew. Chem. 2014, 126, 11908.

[2] I. Ravikumar, P. Ghosh, Chem. Soc. Rev. 2012, 41, 3077.

[3] a) H. Stephan, K. Gloe, P. Schiessl, F. P. Schmidtchen, Supramol. Chem. 1995, 5, 273; b) L. R. Eller, M. Stepien, C. J. Fowler, J. T. Lee, J. L. Sessler, B. A. Moyer, J. Am. Chem. Soc. 2007, 129, 11020; c) C. J. Borman, R. Custelcean, B. P. Hay, N. L. Bill, J. L. Sessler, B. A. Moyer, Chem. Commun. 2011, 47, 7611; d) C. Jia, B. Wu, S. Li, X. Huang, Q. Zhao, Q. Li, X. Yang, Angew. Chem. Int. Ed. 2011, 50, 486; Angew. Chem. 2011, 123, 506; e) M. Wenzel, Q. W. Knapp, P. G. Plieger, Chem. Commun. 2011, 47, 499; f) I. R. Fernando, S. A. Surmann, A. E. Urech, A. M. Poulsen, G. Mezei, Chem. Commun. 2012, 48, 6860; g) S. K. Kim, J. Lee, N. J. Williams, V. M. Lynch, B. P. Hay, B. A. Moyer, J. L. Sessler, J. Am. Chem. Soc. 2014, 136, 15079.

[4] a) R. Custelcean, Curr. Opin. Solid State Mater. Sci. 2009, 13, 68; b) R. Custelcean, Chem. Soc. Rev. 2010, 39, 3675; c) R. Custelcean, Chem. Commun. 2013, 49, 2173.

[5] R. Custelcean, N. J. Williams, C. A. Seipp, Angew. Chem. Int. Ed. 2015, 54, 10525; Angew. Chem. 2015, 127, 10671.

[6] CCDC 1430158, 1430159, and 1430160 contain the supplementary crystallographic data for this paper. These data are provided free of charge by The Cambridge Crystallographic Data Centre.

[7] Recent examples of sulfate-water clusters in organic or metal-organic crystals: a) D. A. Jose, D. K. Kumar, B. Ganguly, A. Das, Inorg. Chem. 2007, 46, 5817; b) M. N. Hoque, A. Basu, G. Das, Cryst. Growth Des. 2014, 14, 6; c) M. N. Hoque, G. Das, Cryst. Growth Des. 2014, 14, 2962; d) R. Dutta, B. Akhuli, P. Ghosh, Dalton Trans. 2015, 44, 15075.

[8] a) P. E. Mason, G. W. Neilson, J. E. Enderby, M.-L. Saboungi, C. E. Dempsey, A. D. MacKerell, J. W. Brady, J. Am. Chem. Soc. 2004, 126, 11462; b) P. E. Mason, C. E. Dempsey, G. W. Neilson, S. R. Kline, J. W. Brady, J. Am. Chem. Soc. 2009, 131, 16689.

[9] Similar complementary electrostatic interactions were demonstrated to be important in the stacking of anionic quinoid rings: K. Molcˇanov, J. Stare, B. Kojic-Prodic, C. Lecomte, S. Dahaoui, C. Jelsch, E. Wenger, A. Santic, B. Zarychta, CrystEngComm 2015, 17, 8645.

[10] a) M. S. H. Bader, Desalination 2006, 201, 100; b) M. S. H. Bader, J. Pet. Sci. Eng. 2007, 55, 93.

[11] R. Custelcean, F. V. Sloop Jr., A. Rajbanshi, S. Wan, B. A. Moyer, Cryst. Growth Des. 2015, 15, 517.

[12] Examples of organic sulfate salts with low aqueous solubility (S): a) 2-aminoperimidine sulfate, S=4.3 × 10^{-5} M: W. I. Stephen, Anal. Chim. Acta 1970, 50, 413; b) $[Mg(H_2O)_6][SO_4(L)_2]$ (L=tris[2-(3-pyridylurea)ethyl]-amine) S=4.7 × 10^{-5} M: R. Custelcean, A. Bock, B. A. Moyer, J. Am. Chem. Soc. 2010, 132, 7177.

[13] The binding of sulfate by guanidinium receptors in polar solvents has also been shown to be entropy driven: a) M. Berger, F. P. Schmidtchen, Angew. Chem. Int. Ed.

1998, 37, 2694; Angew. Chem. 1998, 110, 2840; b) M. Berger, F. P. Schmidtchen, J. Am. Chem. Soc. 1999, 121, 9986.

[14] H.-J. Schneider, Int. J. Mol. Sci. 2015, 16, 6694.

[15] For an example of entropy maximization as a design element in ion complexation, see: A. Ursu, F. P. Schmidtchen, Angew. Chem. Int. Ed. 2012, 51, 242; Angew. Chem. 2012, 124, 246.

[16] K. Khownium, S. J. Wood, K. A. Miller, R. Balakrishna, T. B. Nguyen, M. R. Kimbrell, G. I. Georg, S. A. David, Bioorg. Med. Chem. Lett. 2006, 16,1305.

5.6 APPENDIX 5A Supplemental Information for Chapter 5

5.6.1 Electronic-Structure Calculations

Density functional theory (DFT) with the Perdew–Burke–Ernzerhof (PBE) exchangecorrelation functional[S1,S2] was employed to obtain electron density and electrostatic potentials. All periodic DFT calculations were carried out on the reported crystal structures using VASP - the Vienna ab initio simulation package.[S3-S5] The Kohn–Sham equations were solved using the projector-augmented wave (PAW) method.[S6,S7] The energy cutoff for plane waves was set to 600 eV. Standard PAW potentials were used for the elemental constituents, with valence configurations of $1s^1$ for H, $2s^22p^2$ for C, $2s^22p^3$ for N, $2s^22p^4$ for O, and $3s^23p^4$ for S. Nonperiodic DFT calculations were performed at the B3LYP/6-31+G(d) level of theory[S8,S9] using Gaussian 09 simulation package.[S10] Bader charges in the studied periodic systems were computed using the Bader scheme.[S11] The Visualization for Electronic and Structural Analysis software (VESTA, series 3)[S12] was used for electron density and structure visualization. Tables S2-S4 and Figures[S8,9] summarize the results of the calculations for BBIG-SO_4, BBIG-NO_3, and BBIG · $2H_2O$ crystals.

5.7 Appendix References

[S1] Perdew, J. P.; Burke, K.; Ernzerhof, M. Generalized Gradient Approximation Made Simple. Phys. Rev. Lett. 1996, 77, 3865–3868.

[S2] Perdew, J. P.; Burke, K.; Ernzerhof, M.Generalized Gradient Approximation Made Simple. Phys. Rev. Lett. 1997, 78, 1396– 1396.

[S3] Kresse, G.; Furthmüller, J. Efficiency of ab-initio total energy calculations for metals and semiconductors using a plane-wave basis set. Comput. Mater. Sci. 1996, 6, 15–50.

[S4] Kresse, G.; Furthmüller, J. Efficient iterative schemes for ab initio total-energy calculations using a plane-wave basis set. Phys. Rev. B 1996, 54, 11169–11186.

[S5] Kresse, G.; Hafner, J. Ab initio molecular dynamics for liquid metals. Phys. Rev. B 1993, 47, 558–561.

[S6] Blöchl, P. E. Projector augmented-wave method. Phys. Rev. B 1994, 50, 17953–17979.

[S7] Kresse, G.; Joubert, D. From ultrasoft pseudopotentials to the projector augmentedwave
method. Phys. Rev. B 1999, 59, 1758–1775.

[S8] Becke, A. D. Density functional thermochemistry. III. The role of exact exchange. J. Chem. Phys. 1993, 98, 5648–5652.

[S9] Lee, C.; Yang, W.; Parr, R. G. Development of the Colle-Salvetti correlation-energy formula into a functional of the electron density. Phys. Rev. B, 1988, 37, 785–789.

[S10] Frisch, M. J.; Trucks, G. W.; Schlegel, H. B.; Scuseria, G. E.; Robb, M. A.;

Cheeseman, J. R.; Scalmani, G.; Barone, V.; Mennucci, B.; Petersson, G. A. Gaussian 09,
revision B.01; Gaussian, Inc.: Wallingford, CT, 2009.
[S11] Tang, W.; Sanville, E.; Henkelman, G. A grid-based Bader analysis algorithm without lattice bias. J. Phys.: Condens. Matter 2009, 21, 084204.
[S12] Momma, K.; Izumi, F. VESTA 3 for Three-Dimensional Visualization of Crystal, Volumetric and Morphology Data. J. Appl. Crystallogr. 2011, 44, 1272–1276.

5.8 Appendix 5B Figures and Tables for Chapter 5

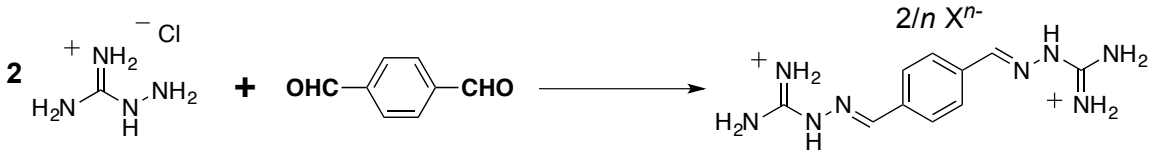

Figure 5.1. Synthesis of BBIG-SO_4 and BBIG-NO_3 by imine condensation in water.

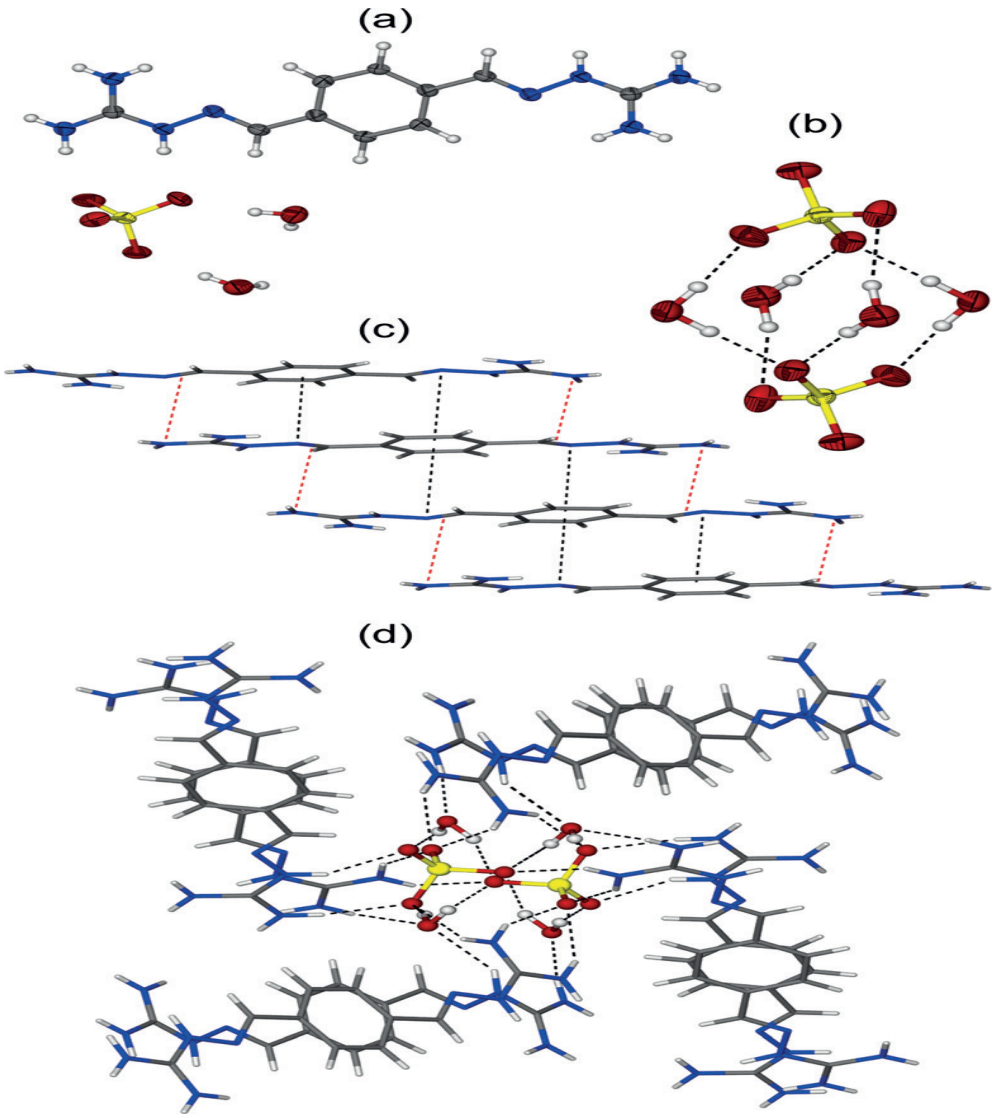

Figure 5.2. X-ray crystal structure of BBIG-SO_4. a) ORTEP representation showing the planar BBIG cation and the sulfate with the two water molecules of hydration. b) $[(SO_4)_2(H_2O)_4]^{4-}$ cluster. c) Stacking of the BBIG cations, with the black and red dashed lines corresponding to the C=N(imine)···Ph and H_2N···C=N(imine) intermolecular contacts. d) Hydrogen bonding of the sulfate–water clusters by the guanidinium groups of the BBIG stacks, viewed down the crystallographic a axis.

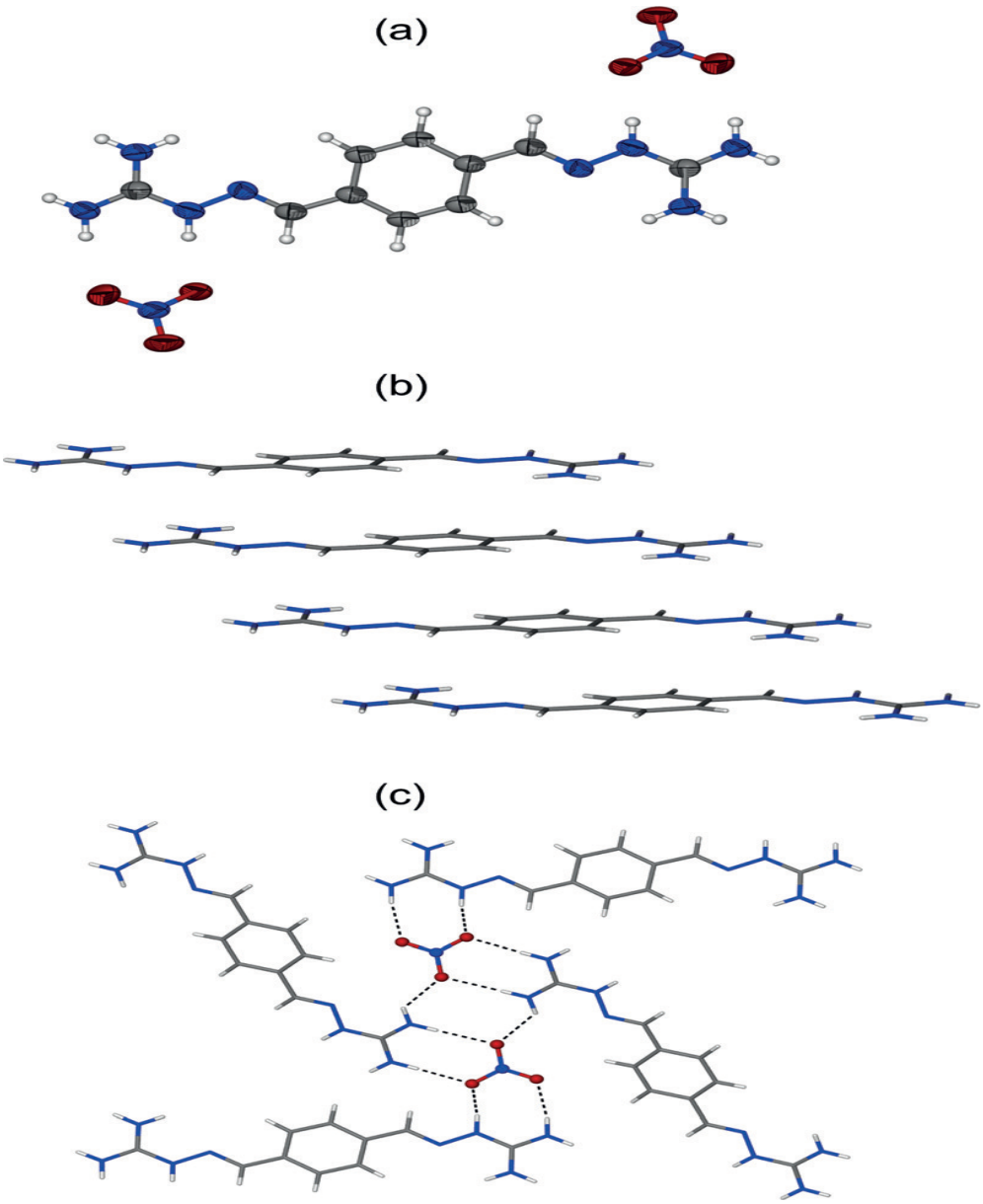

Figure 5.3. X-ray crystal structure of BBIG-NO_3. a) ORTEP representation. b) Stacking of the BBIG cations. c) Hydrogen bonding of the nitrate anions by the guanidinium groups of the BBIG cations.

Table 5.1. Aqueous solubilities of different BBIG salts at 25 ºC.

BBIG salt	Solubility [M]
Sulfate[a]	$1.6(2) \times 10^{-5}$
Nitrate[a]	$6.5(5) \times 10^{-4}$
Chloride[b]	$6.3(2) \times 10^{-2}$

[a] Measured by UV spectroscopy. [b] Measured gravimetrically.

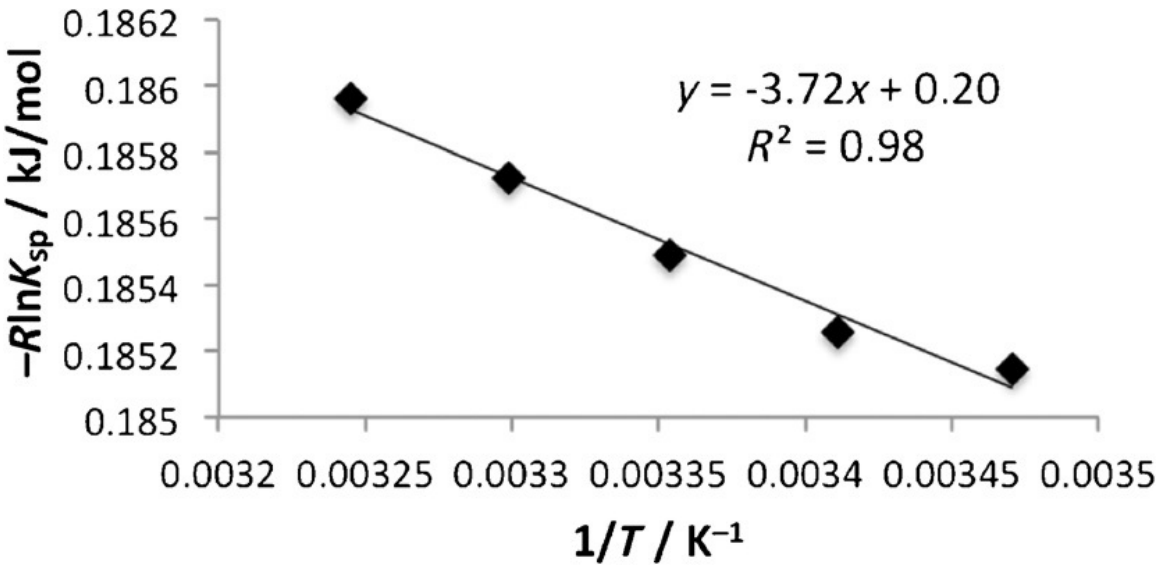

Figure 5.4. Van't Hoff plot for dissolution of BBIG-SO_4 in the 15–35 °C temperature range.

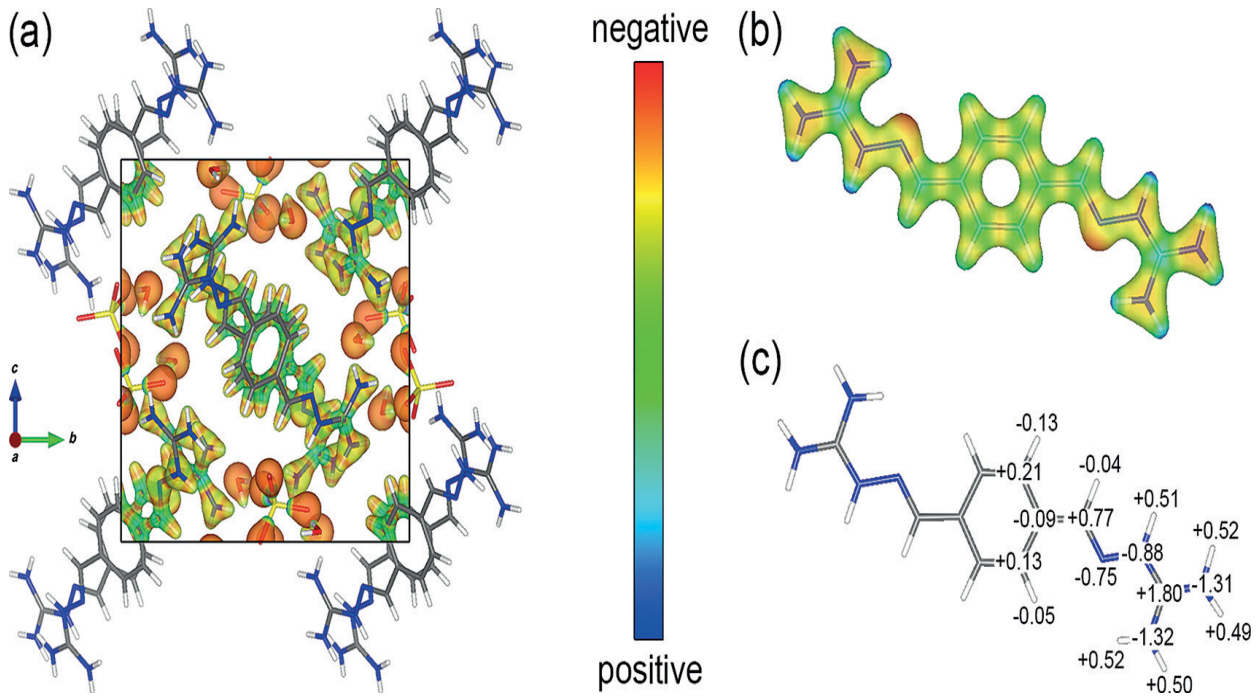

Figure 5.5. Results from DFT calculations. a) Electrostatic potential map (0.24 e/a_0^3 isovalue) for the BBIG-SO_4 crystal, obtained from periodic calculations. b) Electrostatic potential map (0.11 e/a_0^3 isovalue) for the isolated BBIG cation, obtained from non-periodic calculations. c) Atomic charges for the BBIG cation in the BBIG-SO_4 crystal, calculated using the Bader scheme.

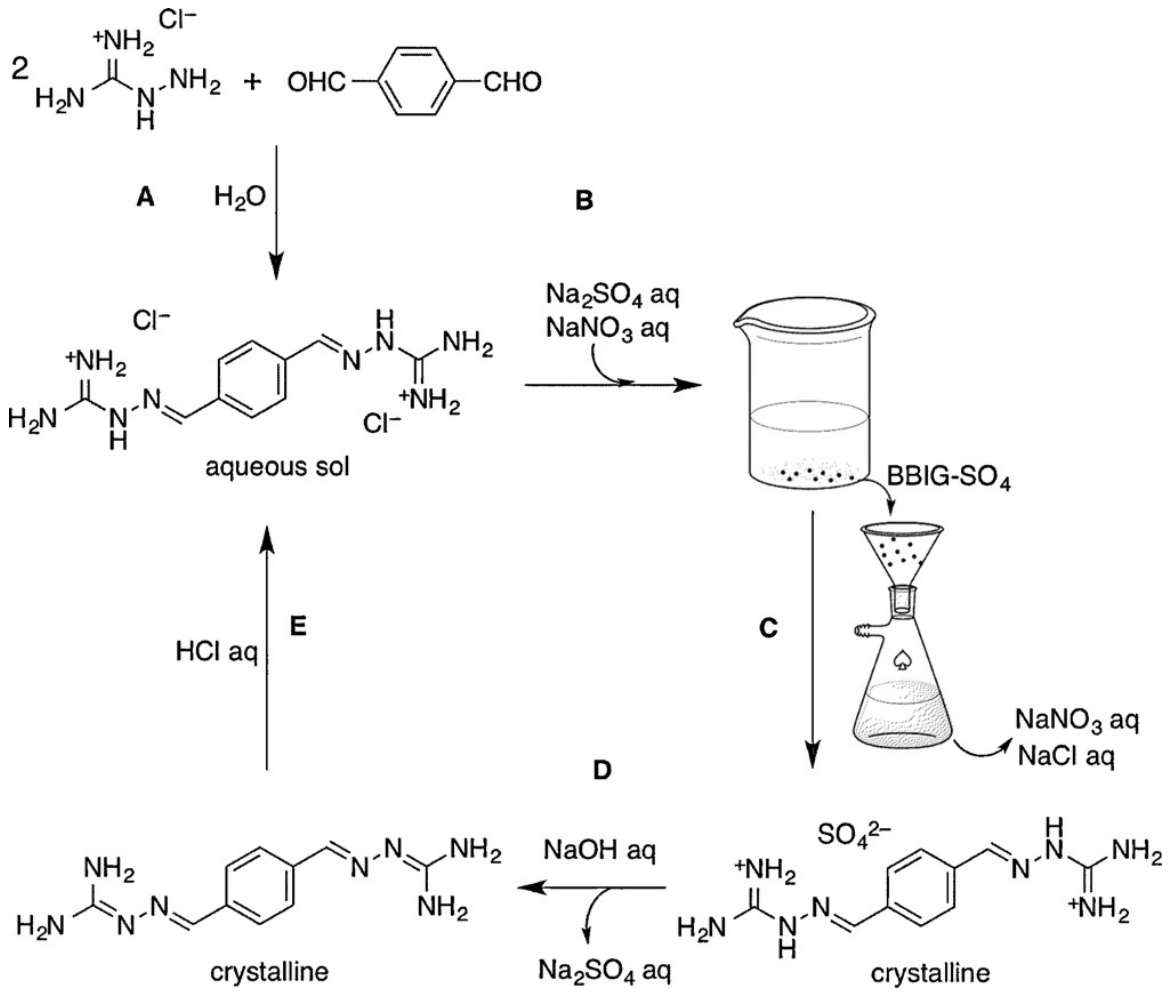

Figure 5.6. Complete separation cycle for sulfate removal by crystallization of BBIG-SO_4. A) In situ synthesis of BBIG dichloride salt from aqueous aminoguanidinium chloride and terephthalaldehyde. B) Selective crystallization of BBIG-SO_4. C) Filtration of BBIG-SO_4. D) Ligand recovery by neutralization of BBIG-SO_4 with NaOH and crystallization of neutral BBIG; sulfate is removed as aqueous Na_2SO_4. E) Regeneration of the BBIG dichloride salt, which can be recycled for another separation cycle.

Table 5.2. Sulfate separation from seawater.[a]

BBIG [equiv][b]	$[SO_4^{2-}]$ left [mM][c]	Amount of SO_4^{2-} removed [%]
1	3.5	88
1.1	1.6	95
1.5	0.3	99
2	0.3	99

[a] Seawater from the Gulf Stream; the initial sulfate concentration was estimated at 30 mm by titration with $BaCl_2$. [b] Molar equivalents of the BBIG dichloride salt added relative to the sulfate in seawater. [c] Corresponding sulfate concentration left in the seawater, measured by using radiolabeled $Na_2{}^{35}SO_4$ and β liquid scintillation counting

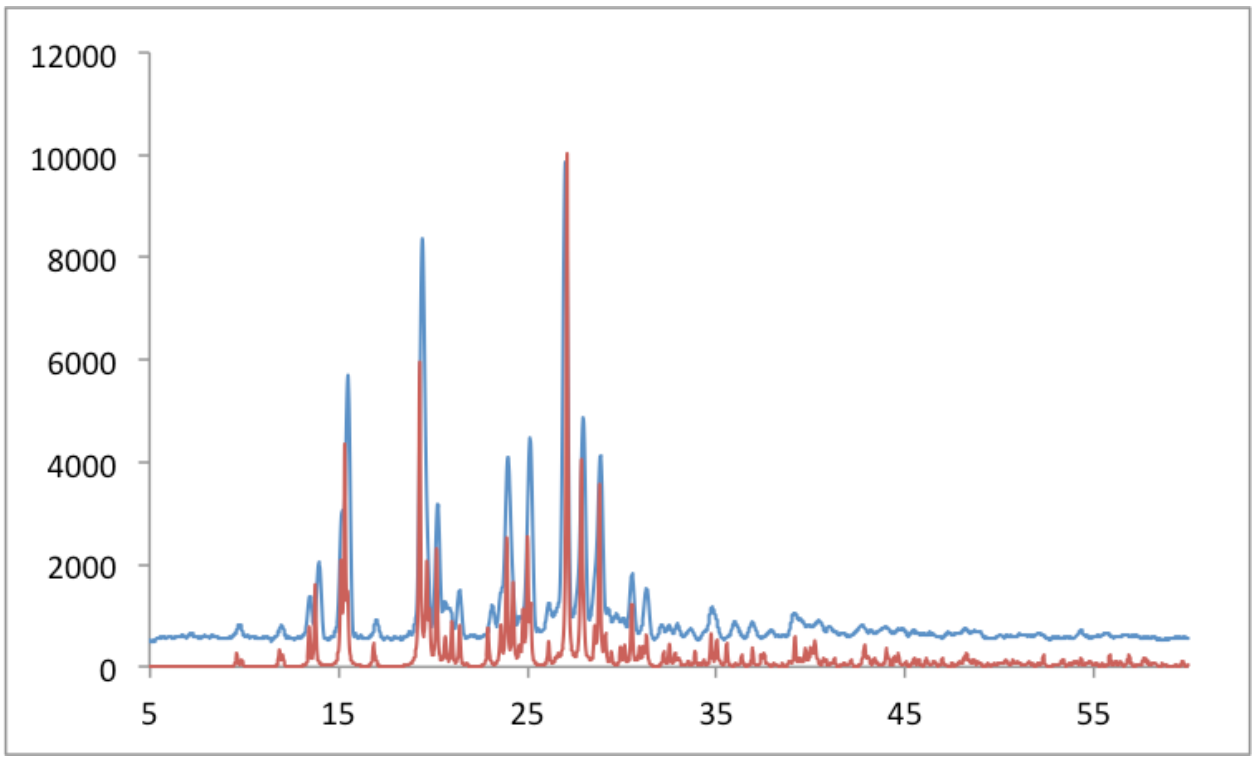

Figure 5.7. PXRD patterns for BBIG-SO_4. Red: simulated pattern from the single-crystal;Blue: experimental pattern from the bulk crystalline powder.

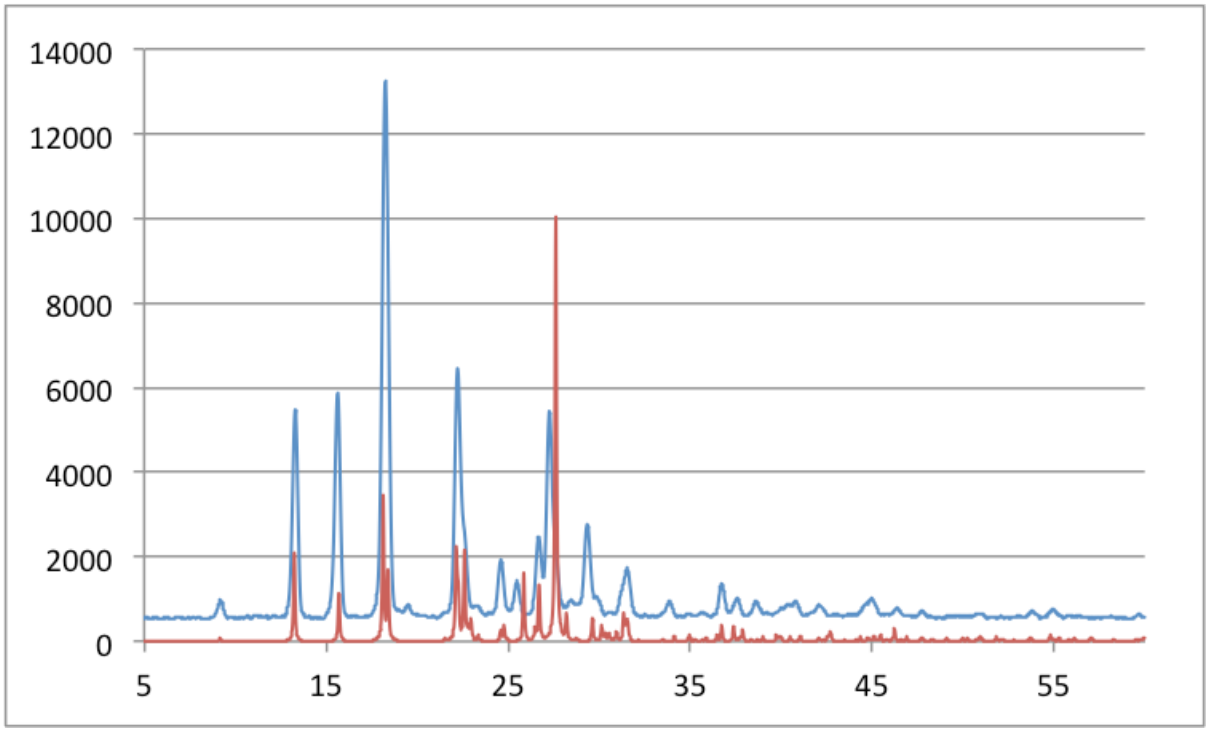

Figure 5.8. PXRD patterns for BBIG-NO_3. Red: simulated pattern from the single crystal; Blue: experimental pattern from the bulk crystalline powder.

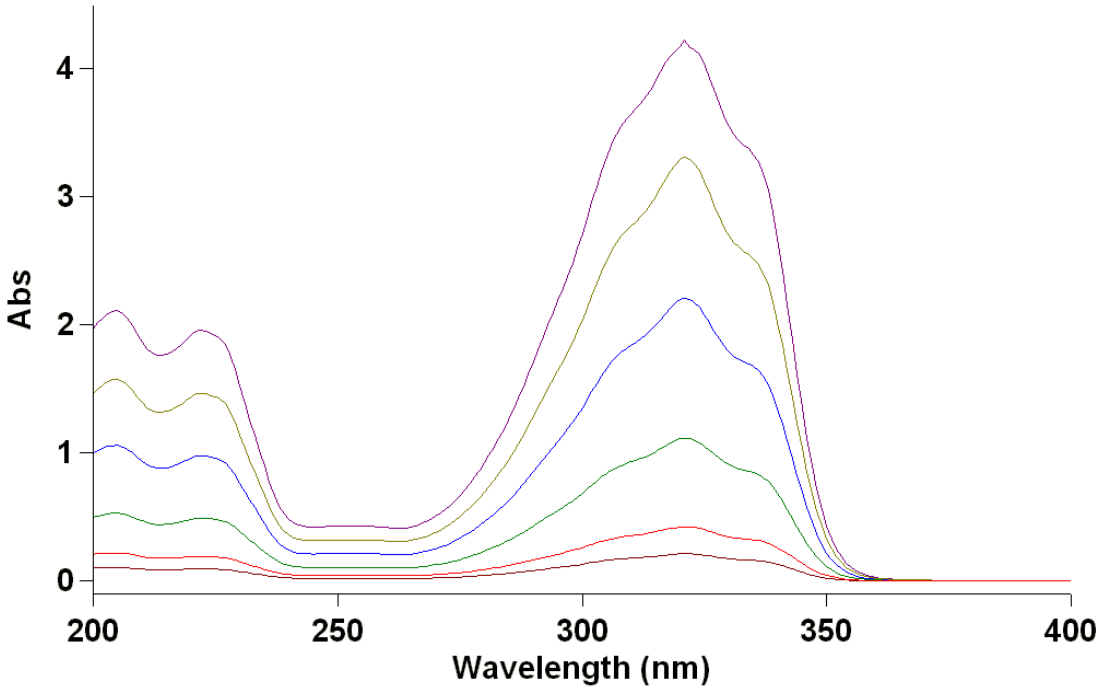

Figure 5.9. UV calibration spectra obtained using the BBIG-Cl salt. The concentrations of the GBAH cation ranged from a minimum of 5×10^{-7} to a maximum of 1×10^{-5} M.

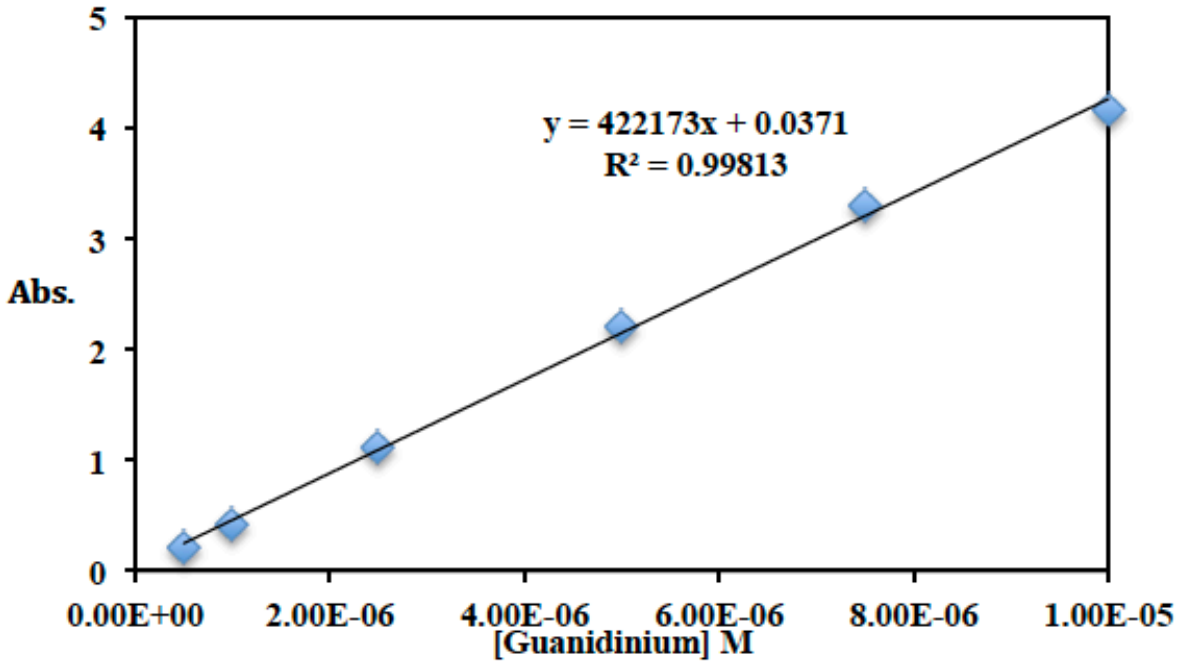

Figure 5.10. UV calibration curve obtained using the absorbance of the BBIG dication at 322 nm.

Table 5.3. Aqueous solubilities of BBIG-SO4 in the 15–35 °C temperature range.

T (°C)	Solubility × 10^5 (M)
15	1.46
20	1.45
25	1.43
30	1.41
35	1.39

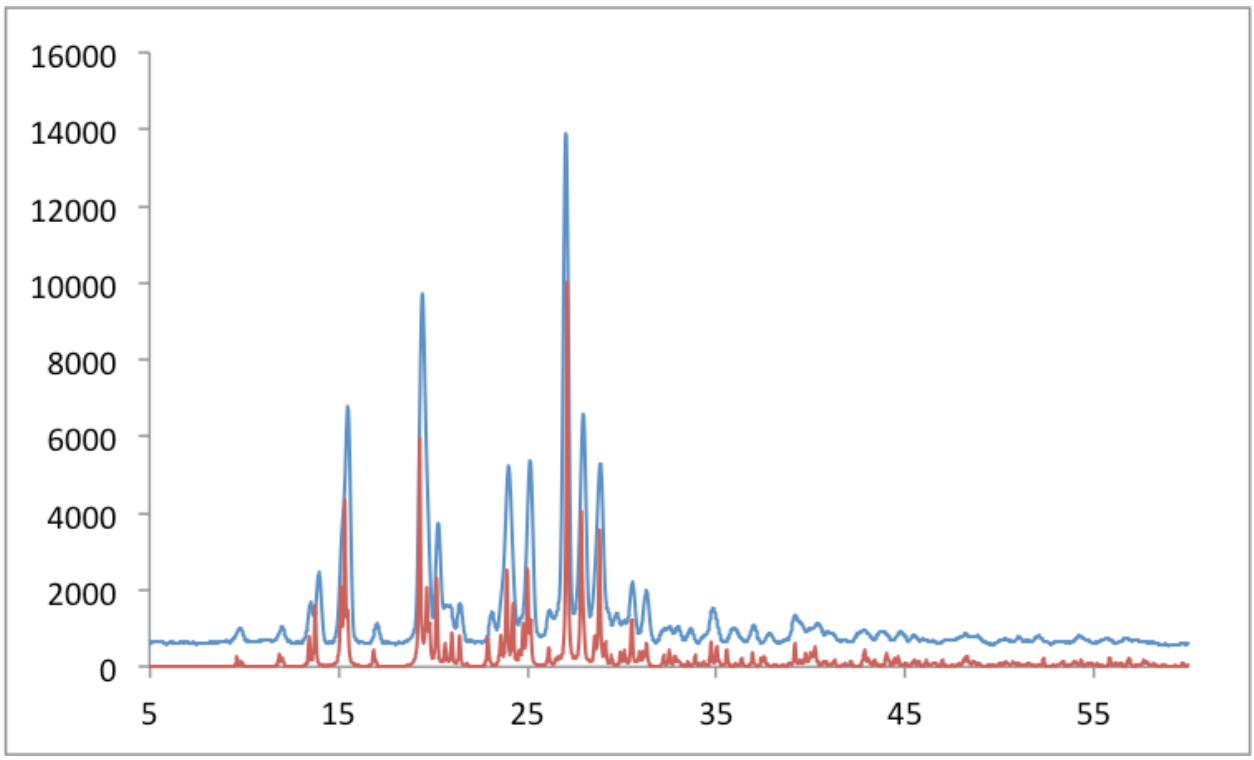

Figure 5.11. Experimental PXRD pattern of the crystalline solid obtained from the competitive crystallization experiment (blue) overlaid over the simulated PXRD pattern from the single-crystal X-ray structure of BBIG-SO_4 (red).

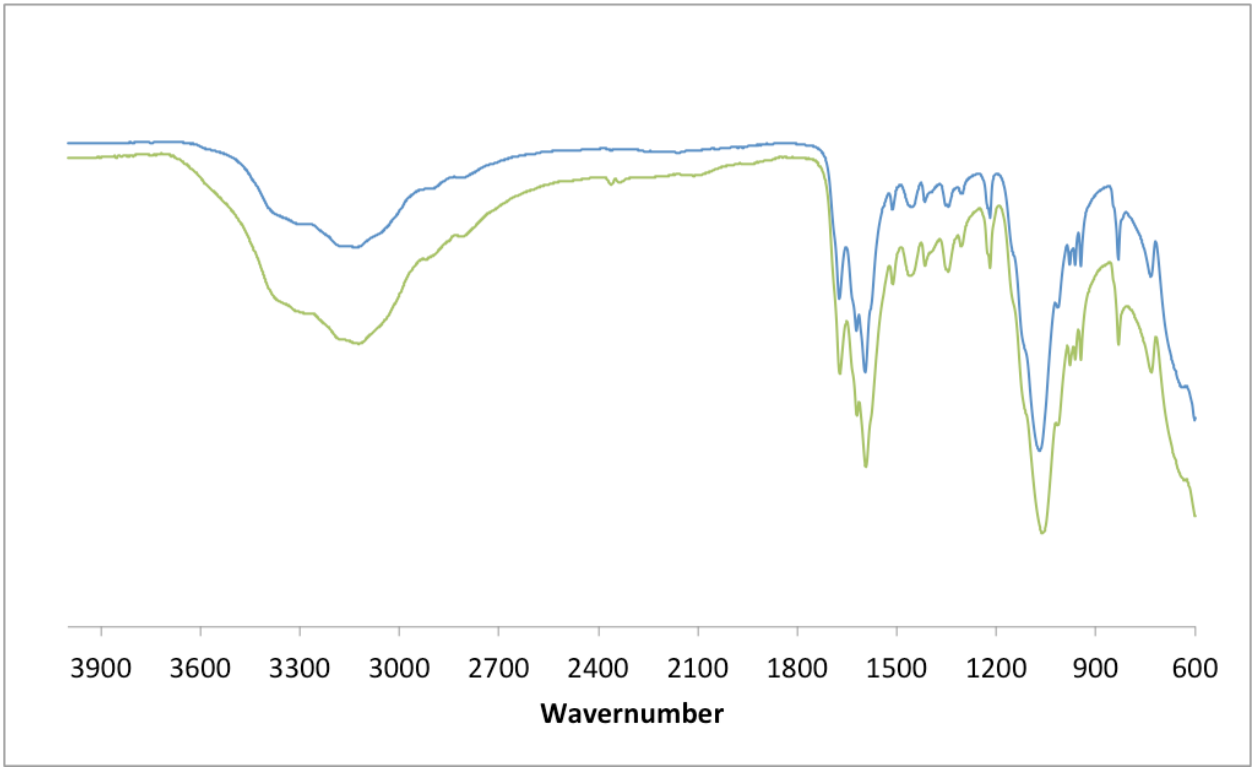

Figure 5.12. Overlay of the FTIR spectra for BBIG-SO_4 (blue) and the product of the competitive crystallization experiment (green)

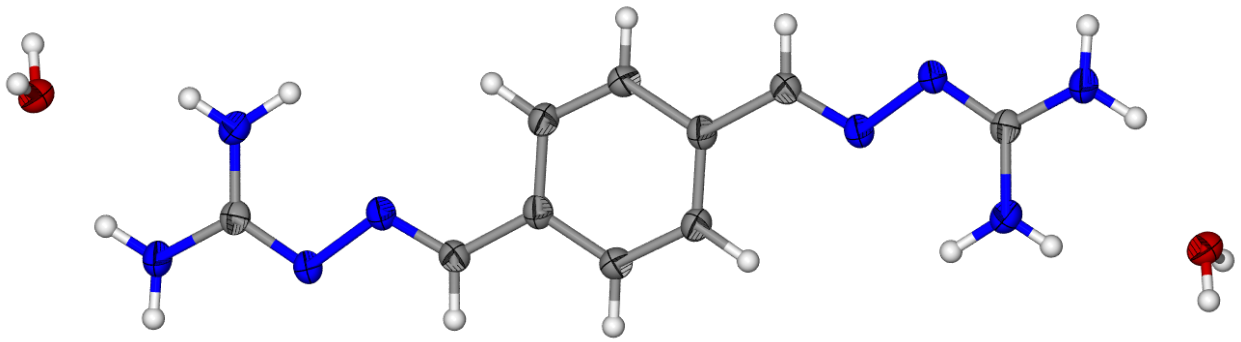

Figure 5.13. X-Ray crystal structure of BBIG · 2H2O.

Table 5.4. Bader charge analysis for the BBIG-SO_4 crystal. Charges on atoms are tabulated and shown for the asymmetric unit.

Complex SO_4^{2-}	*Charge (H)*	*Charge (C)*	*Charge (N)*	*Charge (O)*	*Charge (S)*
-C_6H_4- *fragment*	–0.06 [H_{20}] –0.14 [H_{22}] –0.11 [H_{40}] –0.04 [H_{42}]	+0.15 [C_{19}] +0.25 [C_{21}] –0.12 [C_{17}] +0.17 [C_{39}] +0.10 [C_{41}] +0.05 [C_{38}]	---	---	---
-$C_2H_4H_6$- *fragment*	0.00 [H_{14}] –0.07 [H_{36}] +0.52 [H_{16}] +0.49 [H_{34}] +0.51 [H_{11}] +0.52 [H_{12}] +0.48 [H_{30}] +0.52 [H_{31}] +0.47 [H_7] +0.51 [H_8] +0.50 [H_{27}] +0.53 [H_{28}]	+0.74 [C_{13}] +0.79 [C_{35}] +1.80 [C_9] +1.79 [C_{32}]	–1.28 [N_6] –1.33 [N_{10}] –1.34 [N_{26}] –1.30 [N_{29}] –0.92 [N_{15}] –0.74 [N_{18}] –0.84 [N_{33}] –0.75 [N_{37}]	---	---
H_2O	+0.63 [H_{24}] +0.66 [H_{25}] +0.61 [H_{44}] +0.67 [H_{45}]	---	---	–1.32 [O_{23}] –1.30 [O_{43}]	---
SO_4^{2-}	---	---	---	–1.40 [O_2] –1.43 [O_3] –1.43 [O_4] –1.41 [O_5]	+3.95 [S_1]

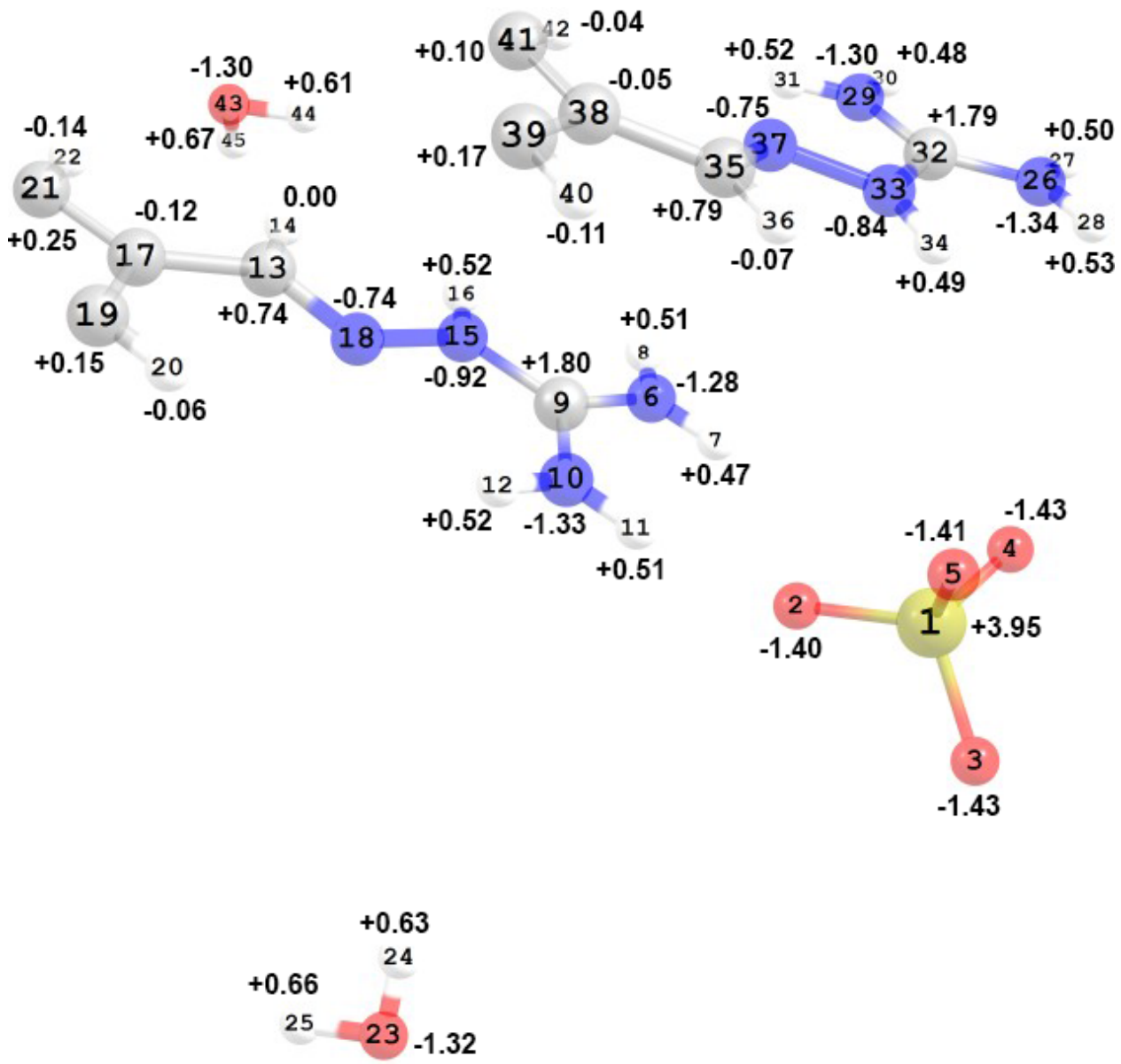
41
42
-0.04
+0.10
38
-0.05
39
+0.17
40
-0.11
35
+0.79
36
-0.07
37
-0.75
+0.52
31
-1.30
29
30
+0.48
32
+1.79
33
-0.84
34
+0.49
26
+0.50
27
-1.34
28
+0.53
-1.30
43
+0.61
44
+0.67
45
21
-0.14
22
+0.25
17
-0.12
13
0.00
14
19
+0.15
20
-0.06
18
-0.74
+0.74
15
+0.52
16
-0.92
9
+1.80
6
+0.51
8
-1.28
7
+0.47
10
12
+0.52
-1.33
11
+0.51
1
+3.95
2
-1.40
5
-1.41
4
-1.43
3
-1.43

+0.63
24
+0.66
25
23
-1.32

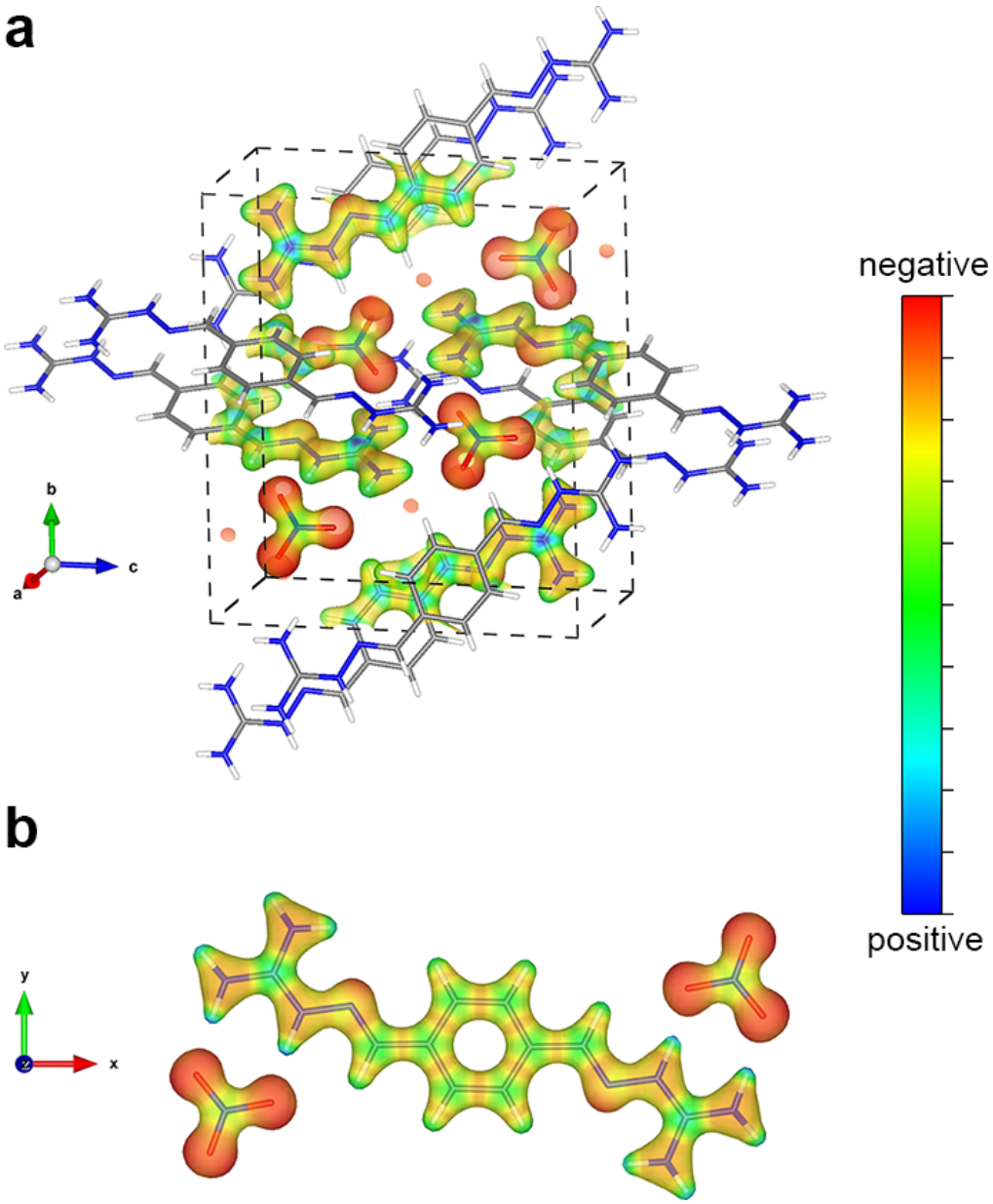

Figure 5.14. Electron density isosurfaces colorized according to the values of the electrostatic potentials for (a) BBIG-NO_3 crystal, (b) isolated BBIG$(NO_3)_2$ complex. Positive and negative regions are shown in blue and red, respectively. The isovalues are 0.24 e/a_0^3 for (a) and 0.14 e/a_0^3 for (b), where a_0 is the Bohr radius.

Table 5.5. Bader charge analysis for the BBIG-NO_3 crystal. Charges on atoms aretabulated and shown for the asymmetric unit.

Complex NO_3^-	*Charge (H)*	*Charge (C)*	*Charge (N)*	*Charge (O)*
-C_6H_4- *fragment*	–0.02 [H_{18}] –0.12 [H_{21}]	+0.02 [C_{14}] +0.02 [C_{17}] +0.18 [C_{20}]	---	---
-$C_2H_4H_6$- *fragment*	–0.03 [H_{10}] +0.49 [H_{16}] +0.49 [H_7, H_8] +0.49 [H_{12}, H_{13}]	+1.80 [C_5] +0.76 [C_9]	–1.28 [N_6] –1.33 [N_{10}] –1.34 [N_{26}] –1.30 [N_{29}]	---
NO_3^-	---	---	+0.94 [N_{23}]	–0.58 [O_1] –0.65 [O_1] –0.60 [O_1]

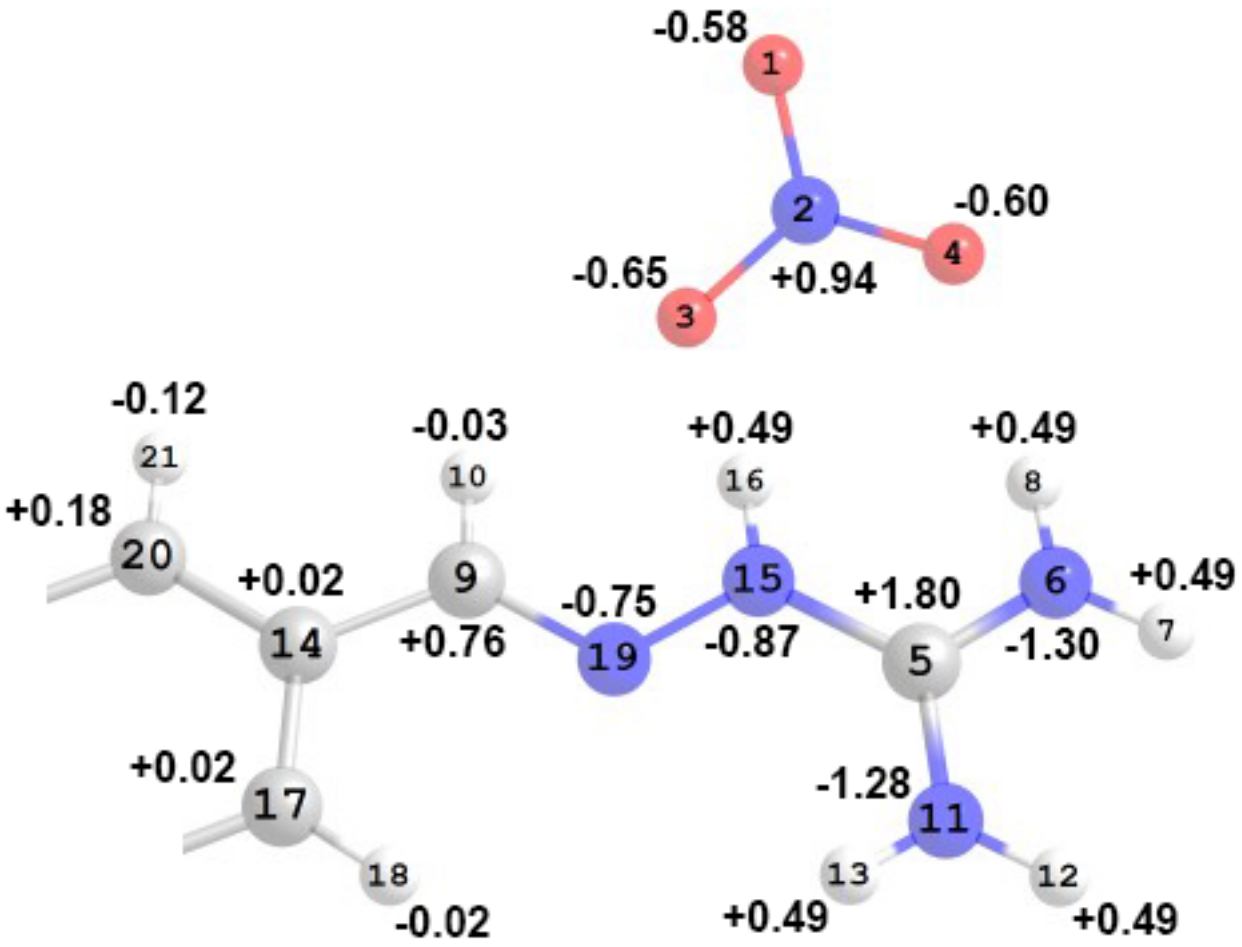
-0.58
1
2
-0.60
4
-0.65
+0.94
3
-0.12
21
-0.03
10
+0.49
16
+0.49
8
+0.18
20
+0.02
9
-0.75
15
+1.80
6
+0.49
14
+0.76
19
-0.87
5
-1.30
7
+0.02
17
-1.28
11
18
13
12
-0.02
+0.49
+0.49

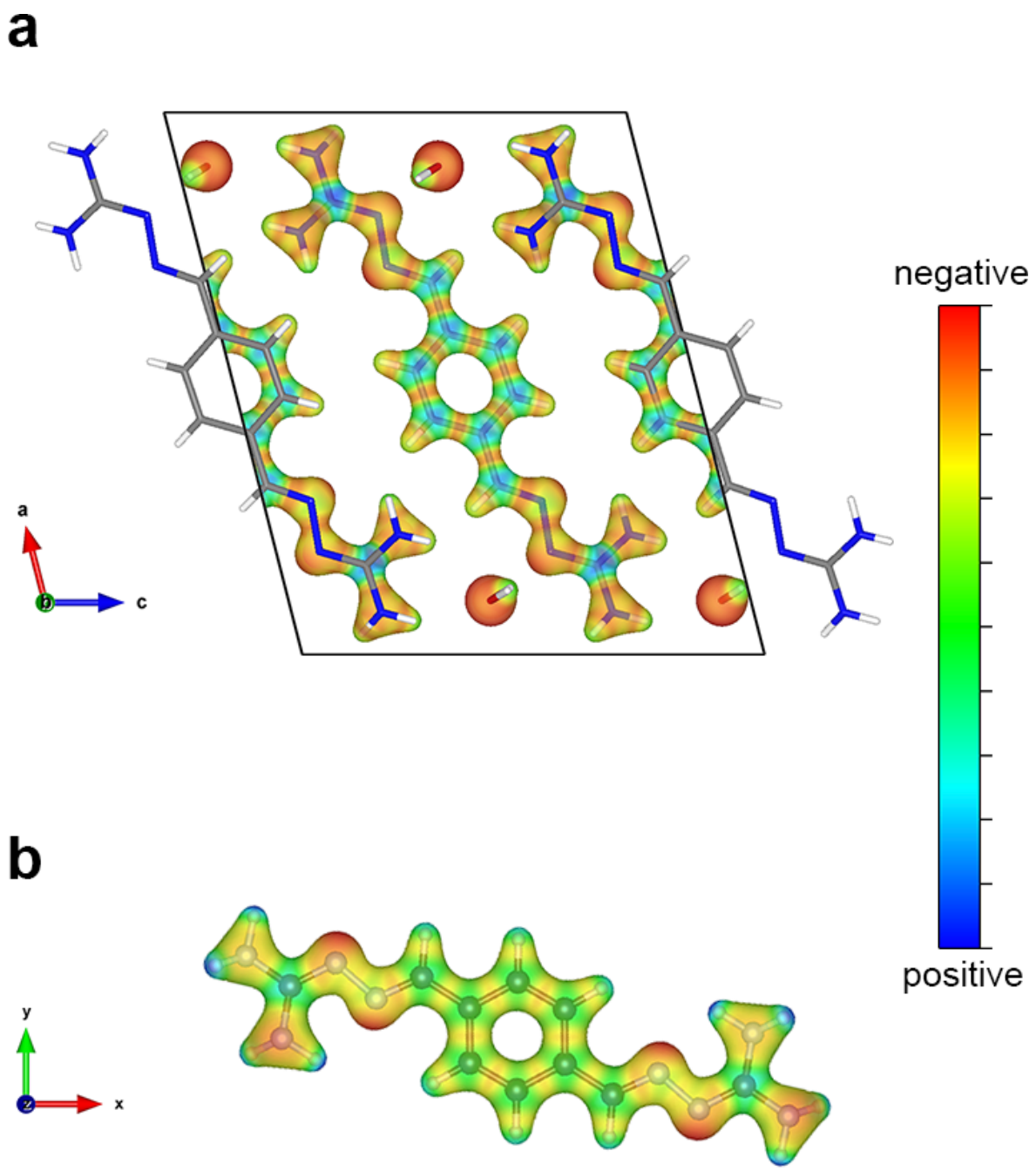

Figure 5.15. Electron density isosurfaces colorized according to the values of the electrostatic potentials for (a) BBIG·$2H_2O$ crystal, (b) isolated BBIG ligand. Positive and negative regions are shown in blue and red, respectively. The isovalues are 0.19 e/a_0^3 for (a) and 0.11 e/a_0^3 for (b), where a_0 is the Bohr radius.

Table 5.6. Bader charge analysis for the BBIG·$2H_2O$ crystal. Charges on atoms are tabulated and shown for the asymmetric unit.

Complex NO_3^-	*Charge (H)*	*Charge (C)*	*Charge (N)*	*Charge (O)*
-C_6H_4- *fragment*	–0.02 [H_{18}] –0.12 [H_{21}]	+0.02 [C_{14}] +0.02 [C_{17}] +0.18 [C_{20}]	---	---
-$C_2H_4H_6$- *fragment*	–0.03 [H_{10}] +0.49 [H_{16}] +0.49 [H_7, H_8] +0.49 [H_{12}, H_{13}]	+1.80 [C_5] +0.76 [C_9]	–1.28 [N_6] –1.33 [N_{10}] –1.34 [N_{26}] –1.30 [N_{29}]	---
NO_3^-	---	---	+0.94 [N_{23}]	–0.58 [O_1] –0.65 [O_1] –0.60 [O_1]

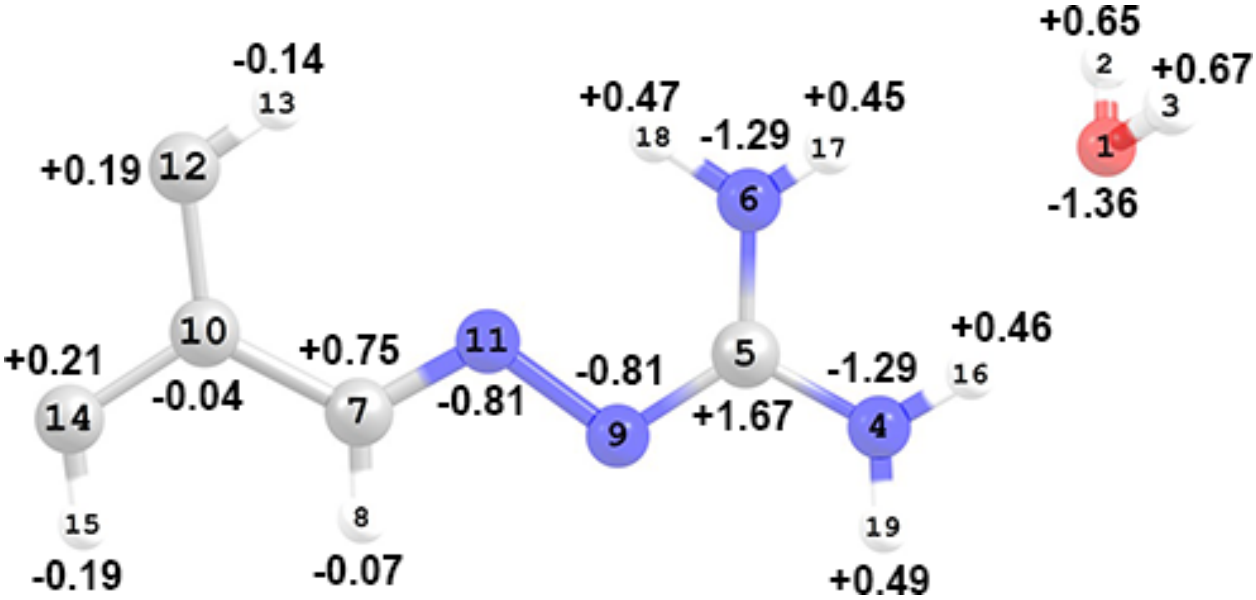

Chapter 6 : CO_2 Capture from Ambient Air by Crystallization with a Guanidine Sorbent

Publication Statement for Chapter 6

Reference for Original Article:

Seipp, C.A.; Williams N.J.; Kidder, M.K.; Custelcean R. "CO_2 Capture from Ambient Air by Crystallization with a Guanidine Sorbent." *Angew. Chem. Int. Ed.* **2017**, 56, 1042–1045.

Individual Author Contribution(s):

Seipp, C. A. – Co-discover of ligand, discovery the direct-air capture of CO_2 took IR spectra of ligand complexes with various salts and writing

Williams, N. J. – Synthesis of ligands, determined solubility of ligands salts via UV-Spectroscopy, and writing

Kidder, M.K. – Thermogravitational analysis and analyzed data

Custelcean, R. – Co-discover of ligands, XRD and powder XRD of solid complexes, wrote and edited final manuscript

Journals Policy/Permission/Agreement for Reproduction of Article

JOHN WILEY AND SONS LICENSE
TERMS AND CONDITIONS

Mar 16, 2017

This Agreement between Neil J Williams ("You") and John Wiley and Sons ("John Wiley and Sons") consists of your license details and the terms and conditions provided by John Wiley and Sons and Copyright Clearance Center.

License Number	4070851018774
License date	Mar 16, 2017
Licensed Content Publisher	John Wiley and Sons
Licensed Content Publication	Angewandte Chemie International Edition
Licensed Content Title	CO2 Capture from Ambient Air by Crystallization with a Guanidine Sorbent
Licensed Content Author	Charles A. Seipp,Neil J. Williams,Michelle K. Kidder,Radu Custelcean
Licensed Content Date	Dec 21, 2016
Licensed Content Pages	4
Type of use	Dissertation/Thesis
Requestor type	Author of this Wiley article
Format	Print and electronic
Portion	Full article
Will you be translating?	No
Title of your thesis / dissertation	Ion Separations: Achieving Selectivity Through Rational Design in Solvent Extraction and Crystallization Systems
Expected completion date	May 2017
Expected size (number of pages)	400
Requestor Location	Neil J Williams Oak Ridge National Laboratory PO Box 2008 MS6119 OAK RIDGE, TN 37831 United States Attn: Neil J Williams
Publisher Tax ID	EU826007151
Billing Type	Invoice
Billing Address	Neil J Williams Oak Ridge National Laboratory PO Box 2008 MS6119 OAK RIDGE, TN 37831 United States Attn: Neil J Williams
Total	0.00 USD
Terms and Conditions	

TERMS AND CONDITIONS

This copyrighted material is owned by or exclusively licensed to John Wiley & Sons, Inc. or one of its group companies (each a"Wiley Company") or handled on behalf of a society with which a Wiley Company has exclusive publishing rights in relation to a particular work (collectively "WILEY"). By clicking "accept" in connection with completing this licensing transaction, you agree that the following terms and conditions apply to this transaction (along with the billing and payment terms and conditions established by the Copyright Clearance Center Inc., ("CCC's Billing and Payment terms and conditions"), at the time that you opened your RightsLink account (these are available at any time at http://myaccount.copyright.com).

Terms and Conditions

- The materials you have requested permission to reproduce or reuse (the "Wiley Materials") are protected by copyright.

- You are hereby granted a personal, non-exclusive, non-sub licensable (on a stand-alone basis), non-transferable, worldwide, limited license to reproduce the Wiley Materials for the purpose specified in the licensing process. This license, **and any CONTENT (PDF or image file) purchased as part of your order,** is for a one-time use only and limited to any maximum distribution number specified in the license. The first instance of republication or reuse granted by this license must be completed within two years of the date of the grant of this license (although copies prepared before the end date may be distributed thereafter). The Wiley Materials shall not be used in any other manner or for any other purpose, beyond what is granted in the license. Permission is granted subject to an appropriate acknowledgement given to the author, title of the material/book/journal and the publisher. You shall also duplicate the copyright notice that appears in the Wiley publication in your use of the Wiley Material. Permission is also granted on the understanding that nowhere in the text is a previously published source acknowledged for all or part of this Wiley Material. Any third party content is expressly excluded from this permission.

- With respect to the Wiley Materials, all rights are reserved. Except as expressly granted by the terms of the license, no part of the Wiley Materials may be copied, modified, adapted (except for minor reformatting required by the new Publication), translated, reproduced, transferred or distributed, in any form or by any means, and no derivative works may be made based on the Wiley Materials without the prior permission of the respective copyright owner.**For STM Signatory Publishers clearing permission under the terms of the STM Permissions Guidelines only, the terms of the license are extended to include subsequent editions and for editions in other languages, provided such editions are for the work as a whole in situ and does not involve the separate exploitation of the permitted figures or extracts,** You may not alter, remove or suppress in any manner any copyright, trademark or other notices displayed by the Wiley Materials. You may not license, rent, sell, loan, lease, pledge, offer as security, transfer or assign the Wiley Materials on a stand-alone basis, or any of the rights granted to you hereunder to any other person.

- The Wiley Materials and all of the intellectual property rights therein shall at all times remain the exclusive property of John Wiley & Sons Inc, the Wiley Companies, or their respective licensors, and your interest therein is only that of having possession of and the right to reproduce the Wiley Materials pursuant to Section 2 herein during the continuance of this Agreement. You agree that you own no right, title or interest in or to the Wiley Materials or any of the intellectual property rights therein. You shall have no rights hereunder other than the license as provided for above in Section 2. No right, license or interest to any trademark, trade name, service mark or other branding

("Marks") of WILEY or its licensors is granted hereunder, and you agree that you shall not assert any such right, license or interest with respect thereto

- NEITHER WILEY NOR ITS LICENSORS MAKES ANY WARRANTY OR REPRESENTATION OF ANY KIND TO YOU OR ANY THIRD PARTY, EXPRESS, IMPLIED OR STATUTORY, WITH RESPECT TO THE MATERIALS OR THE ACCURACY OF ANY INFORMATION CONTAINED IN THE MATERIALS, INCLUDING, WITHOUT LIMITATION, ANY IMPLIED WARRANTY OF MERCHANTABILITY, ACCURACY, SATISFACTORY QUALITY, FITNESS FOR A PARTICULAR PURPOSE, USABILITY, INTEGRATION OR NON-INFRINGEMENT AND ALL SUCH WARRANTIES ARE HEREBY EXCLUDED BY WILEY AND ITS LICENSORS AND WAIVED BY YOU.

- WILEY shall have the right to terminate this Agreement immediately upon breach of this Agreement by you.

- You shall indemnify, defend and hold harmless WILEY, its Licensors and their respective directors, officers, agents and employees, from and against any actual or threatened claims, demands, causes of action or proceedings arising from any breach of this Agreement by you.

- IN NO EVENT SHALL WILEY OR ITS LICENSORS BE LIABLE TO YOU OR ANY OTHER PARTY OR ANY OTHER PERSON OR ENTITY FOR ANY SPECIAL, CONSEQUENTIAL, INCIDENTAL, INDIRECT, EXEMPLARY OR PUNITIVE DAMAGES, HOWEVER CAUSED, ARISING OUT OF OR IN CONNECTION WITH THE DOWNLOADING, PROVISIONING, VIEWING OR USE OF THE MATERIALS REGARDLESS OF THE FORM OF ACTION, WHETHER FOR BREACH OF CONTRACT, BREACH OF WARRANTY, TORT, NEGLIGENCE, INFRINGEMENT OR OTHERWISE (INCLUDING, WITHOUT LIMITATION, DAMAGES BASED ON LOSS OF PROFITS, DATA, FILES, USE, BUSINESS OPPORTUNITY OR CLAIMS OF THIRD PARTIES), AND WHETHER OR NOT THE PARTY HAS BEEN ADVISED OF THE POSSIBILITY OF SUCH DAMAGES. THIS LIMITATION SHALL APPLY NOTWITHSTANDING ANY FAILURE OF ESSENTIAL PURPOSE OF ANY LIMITED REMEDY PROVIDED HEREIN.

- Should any provision of this Agreement be held by a court of competent jurisdiction to be illegal, invalid, or unenforceable, that provision shall be deemed amended to achieve as nearly as possible the same economic effect as the original provision, and the legality, validity and enforceability of the remaining provisions of this Agreement shall not be affected or impaired thereby.

- The failure of either party to enforce any term or condition of this Agreement shall not constitute a waiver of either party's right to enforce each and every term and condition of this Agreement. No breach under this agreement shall be deemed waived or excused by either party unless such waiver or consent is in writing signed by the party granting such waiver or consent. The waiver by or consent of a party to a breach of any provision of this Agreement shall not operate or be construed as a waiver of or consent to any other or subsequent breach by such other party.

- This Agreement may not be assigned (including by operation of law or otherwise) by you without WILEY's prior written consent.

- Any fee required for this permission shall be non-refundable after thirty (30) days from receipt by the CCC.

- These terms and conditions together with CCC's Billing and Payment terms and conditions (which are incorporated herein) form the entire agreement between you and WILEY concerning this licensing transaction and (in the absence of fraud) supersedes all prior agreements and representations of the parties, oral or written. This Agreement may not be amended except in writing signed by both parties. This Agreement shall be binding upon and inure to the benefit of the parties' successors, legal representatives, and authorized assigns.

- In the event of any conflict between your obligations established by these terms and conditions and those established by CCC's Billing and Payment terms and conditions, these terms and conditions shall prevail.

- WILEY expressly reserves all rights not specifically granted in the combination of (i) the license details provided by you and accepted in the course of this licensing transaction, (ii) these terms and conditions and (iii) CCC's Billing and Payment terms and conditions.

- This Agreement will be void if the Type of Use, Format, Circulation, or Requestor Type was misrepresented during the licensing process.

- This Agreement shall be governed by and construed in accordance with the laws of the State of New York, USA, without regards to such state's conflict of law rules. Any legal action, suit or proceeding arising out of or relating to these Terms and Conditions or the breach thereof shall be instituted in a court of competent jurisdiction in New York County in the State of New York in the United States of America and each party hereby consents and submits to the personal jurisdiction of such court, waives any objection to venue in such court and consents to service of process by registered or certified mail, return receipt requested, at the last known address of such party.

WILEY OPEN ACCESS TERMS AND CONDITIONS

Wiley Publishes Open Access Articles in fully Open Access Journals and in Subscription journals offering Online Open. Although most of the fully Open Access journals publish open access articles under the terms of the Creative Commons Attribution (CC BY) License only, the subscription journals and a few of the Open Access Journals offer a choice of Creative Commons Licenses. The license type is clearly identified on the article.

The Creative Commons Attribution License

The Creative Commons Attribution License (CC-BY) allows users to copy, distribute and transmit an article, adapt the article and make commercial use of the article. The CC-BY license permits commercial and non-

Creative Commons Attribution Non-Commercial License

The Creative Commons Attribution Non-Commercial (CC-BY-NC)License permits use, distribution and reproduction in any medium, provided the original work is properly cited and is not used for commercial purposes.(see below)

Creative Commons Attribution-Non-Commercial-NoDerivs License

The Creative Commons Attribution Non-Commercial-NoDerivs License (CC-BY-NC-ND) permits use, distribution and reproduction in any medium, provided the original work is properly cited, is not used for commercial purposes and no modifications or adaptations are made. (see below)

Use by commercial "for-profit" organizations

Use of Wiley Open Access articles for commercial, promotional, or marketing purposes requires further explicit permission from Wiley and will be subject to a fee.
Further details can be found on Wiley Online Library
http://olabout.wiley.com/WileyCDA/Section/id-410895.html

Other Terms and Conditions:

v1.10 Last updated September 2015

Questions? customercare@copyright.com or +1-855-239-3415 (toll free in the US) or +1-978-646-2777.

A version of this chapter was originally published by Charles A. Seipp, Neil J. Williams, Michelle K. Kidder, Radu Custelcean. in *Angewandte Chemie International Edition*

Seipp, C.A.; Williams N.J.; Kidder, M.K.; Custelcean R. "CO_2 Capture from Ambient Air by Crystallization with a Guanidine Sorbent." *Angew. Chem. Int. Ed.* **2017**, 56, 1042–1045.

The article used as Chapter 6 was modified in the following manner; the formatting was adapted to fit the formatting required by the University of Tennessee Knoxville, the figures and tables were renumbered to make all figures in the ensuing document contiguous. The work/research of the done by the student in the articles is as follows synthesis, measured solubility of salt of the compounds, and contributed to the writing for the electronic supplementary information.

Abstract

Carbon capture and storage (CCS) is an important strategy aimed at stabilizing the atmospheric CO_2 concentration and thereby the global temperature. However, with our current rate of increase in the atmospheric CO_2 concentration, we may soon commit ourselves to significant global temperature increases. A possible approach toward reversing this trend is to pursue a 'negative emissions' strategy, whereby the CO_2 is removed directly from ambient air (direct air capture). Herein we report a simple aqueous guanidine sorbent that captures CO_2 from air and binds it as a crystalline carbonate salt

via guanidinium hydrogen bonding. The resulting solid has very low aqueous solubility (K_{sp} = 1.0(4) × 10^{-8}), which facilitates its separation from solution by filtration. The bound CO_2 can be released by relatively mild heating of the crystals at 80-120 °C, which regenerates the guanidine sorbent quantitatively. Thus, this crystallization-based approach to CO_2 separation from air requires minimal energy and chemical input, and offers the prospect for low-cost direct air capture technologies that could stabilize or even reduce the atmospheric CO_2 concentration.

6.1. Introduction

Removal of greenhouse gases from dilute emissions has recently been identified as one of seven chemical separations to change the world.[1] Along this line, carbon capture and storage (CCS)[2,3] has been proposed as a strategy to stabilize the increasing concentration of CO_2 in the atmosphere, and thereby the global temperature. However, point-source CCS, which captures the CO_2 emitted by power plants, does not address the dispersed CO_2 emissions, such as those originating from automobiles and airplanes, which account for about 50% of total greenhouse emissions. Furthermore, given our society's inertia in dealing with the climate change, we may soon reach a point when merely implementing the point-source CCS will not be sufficient to stabilize the atmospheric CO_2 concentration at the desirable level, and will require us to achieve 'negative emissions', that is to reduce the amount of CO_2 in the atmosphere by extracting it directly from air (direct air capture).[4-7]

Due to the very low concentration of CO_2 in the atmosphere (~400 ppm), effective and economical direct air capture (DAC) requires a sorbent that optimally combines a number of attributes such as strong CO_2-binding affinity, fast sorption kinetics, high capacity, good selectivity against other components in the air (especially water), easy regeneration with minimal energy input, long-term stability, and low cost. While a material with all these characteristics has yet to be identified, sustained efforts in the last two decades[6] led to the development of different classes of sorbents with promising DAC performance, such as alkali and alkaline earth bases (e.g., NaOH, KOH, $Ca(OH)_2$),[8-11] solid-supported amine-based sorbents,[12-16] and metal-organic frameworks (MOFs).[17-19]

Most systems used to date in DAC involve chemisorbents, taking advantage of their strong and selective binding of CO_2 in the form of carbonate or carbamate anions.[6] Unfortunately, an undesirable consequence associated with strong CO_2 binding is the typically high temperatures required to release the gas and regenerate the sorbent. Furthermore, if the sorbent is in the aqueous state, a substantial amount of energy is required to heat the solutions due to the high heat capacity of water. For instance, aqueous NaOH, a benchmark chemisorbent for DAC, has very high capacity and fast kinetics of CO_2 absorption. However, the resulting sodium carbonate is too soluble in water, requiring a substantial amount of energy to concentrate the solution and isolate the solid Na_2CO_3, which then needs to be calcined at temperatures above 800 °C to decompose it into CO_2 and Na_2O. Alternatively, the aqueous Na_2CO_3 solution can be reacted with $Ca(OH)_2$ to precipitate $CaCO_3$ and regenerate the NaOH solution, but the

thermal decomposition of calcium carbonate to release the CO_2 requires very high temperatures of about 900 °C.[6,7] Thus, the sorbent regeneration step is by far the most energetically demanding and expensive component of the overall DAC process, prompting the development of new sorbent materials with lower regeneration temperatures.[7] Here we report a simple aqueous guanidine sorbent that captures CO_2 from air and binds it as a crystalline carbonate salt of low aqueous solubility, which can be effectively removed from solution by filtration. The CO_2 can then be released under relatively mild conditions by heating the carbonate crystals at 80-120 °C, which regenerates the guanidine sorbent quantitatively.

2,6-Pyridine-bis(iminoguanidine) (PyBIG) was readily obtained by imine condensation of 2,6-pyridinedialdehyde with aminoguanidinium chloride, followed by neutralization with aqueous NaOH, which led to precipitation of the pure ligand (See Chapter 6 Appendix **Figures 6.4** and **6.5**) as a crystalline hydrate (PyBIG·2.5H_2O) (See Chapter 6 Appendix **Figure 6.6**). PyBIG belongs to the general class of bis-iminoguanidine ligands (BIGs) that have recently been found to form with oxoanions crystalline hydrogen-bonded salts with very low aqueous solubilities, which facilitates the separation of this class of anions by crystallization.[20,21] We had reasoned that the electron withdrawing pyridine ring in PyBIG would impart enhanced acidity to the guanidinium groups, thereby leading to stronger binding and more effective separation of oxoanions.

An aqueous solution of PyBIG that was left open to ambient air for a few days led to the formation of large prism-shaped single crystals with an elemental composition consistent with the tetrahydrated carbonate salt of PyBIG ($PyBIGH_2(CO_3)(H_2O)_4$). Single crystal X-ray diffraction analysis confirmed this composition (**Figure 6.1a**), and revealed the presence of extended one-dimensional $[CO_3(H_2O)_4^{2-}]_n$ clusters in the crystals (**Figure 6.1b**). Each carbonate anion in the cluster accepts four water hydrogen bonds, with O–H···O contact distances ranging between 1.89 and 2.06 Å. The quasi-planar $PyBIGH_2^{2+}$ cations form extended stacks that flank the anionic $[CO_3(H_2O)_4^{2-}]_n$ clusters and bind them via multiple hydrogen bonds between the guanidinium groups and the carbonate anion and water, as well as between the pyridine N atom and water (**Figure 6.1d**). Each carbonate anion accepts five guanidinium hydrogen bonds with N–H···O contact distances ranging between 1.84 and 2.00 Å (**Figure 6.1c**).

Preliminary measurements indicated that aqueous PyBIG can act as a good sorbent for atmospheric CO_2. To quantify the sorption performance, an aqueous solution of PyBIG (5 mL, 9.6 mM) was placed in a 20 mL scintillation vial and left open to ambient air. Small crystals started to form within two days and were collected by vacuum filtration after one week. FTIR spectroscopic analysis of the crystals showed strong peaks at 1357 and 1327 cm^{-1} characteristic to the carbonate anion. The powder X-ray diffraction (PXRD) pattern of the bulk crystalline product matched well the powder pattern simulated from the single-crystal X-ray data for $PyBIGH_2(CO_3)(H_2O)_4$ (**Figure 6.1e**), thereby confirming the identity and phase purity of the crystallized solid. The crystallization was run in duplicate, and the

observed average yield was 50.3 ± 0.4%. While these preliminary data reveal a moderate reaction yield and relatively slow kinetics of crystallization, we note here that these CO_2 sorption measurements were done under completely passive conditions, with no efforts to maximize the contact between the air and the aqueous solution, or to optimize the reaction parameters (e.g., reaction time, temperature, concentration). We expect the optimization of the reaction conditions, especially increasing the airflow and the air-water interfacial area to enhance the CO_2 transport rate, will significantly improve the efficacy of CO_2 absorption. On the other hand, the recovery of the crystallized $PyBIGH_2(CO_3)(H_2O)_4$ from solution is greatly facilitated by its very low aqueous solubility. The solubility product of $PyBIGH_2(CO_3)(H_2O)_4$, measured by UV-Vis spectroscopy, is estimated around $1.0(4) \times 10^{-8}$, which is comparable to the corresponding value of $CaCO_3$ ($K_{sp} = 3.4 \times 10^{-9}$).

Effective sorbent regeneration is critical for any CO_2 capture system to be of practical utility. We found that heating the $PyBIGH_2(CO_3)(H_2O)_4$ crystals at relatively low temperatures releases the CO_2 and the included water, and regenerates the PyBIG sorbent quantitatively (**Figure 6.2**).

Examination of the $PyBIGH_2(CO_3)(H_2O)_4$ crystals by optical microscopy revealed that upon heating in open air in an oven at 120 °C for one hour, the crystals changed their color from cream to yellow and became opaque (**Figure 6.2a,b**). Thermogravimetric analysis coupled with mass spectrometry (TGA-MS) provided a more quantitative picture

of the decomposition process. In a temperature-ramped TGA measurement (**Figure 6.2c**), the $PyBIGH_2(CO_3)(H_2O)_4$ crystals lost 35.2% of their mass between 65 and 140 °C, and the MS analysis confirmed the simultaneous evolution of water and CO_2 (See Chapter 6 Appendix **Figure 6.7**). These measurements are consistent with the loss of one carbonate and two protons (as CO_2 and H_2O), and four additional water molecules, as expected from the crystal structure of $PyBIGH_2(CO_3)(H_2O)_4$ (35.1% theoretical mass loss). Similarly, the mass loss of the crystals heated in open air in the oven for one hour at 120 °C (**Figure 6.2b**) was 34.3%, and the FTIR and NMR spectroscopic analysis of the resulting solid confirmed the complete disappearance of the carbonate peak and the regeneration of the anhydrous PyBIG ligand (**Figure 6.2e,f**). The TGA-MS analysis showed no decomposition of the regenerated ligand up to 190 °C (**Figure 6.2c**), which provides a thermal stability window of at least 50 °C for ligand recovery. Isothermal TGA runs at 120 and 100 °C (**Figure 6.2d**) showed complete loss of carbon dioxide and water after 60 and 150 minutes, respectively, with no additional mass loss after 5 hours. On the other hand, at 80 °C the decomposition reached 77% completion after 300 minutes. This corresponds to about an order of magnitude reduction in the decomposition temperature compared to inorganic carbonates, such as Na_2CO_3 or $CaCO_3$ (decomposition *T* of 800-900 °C) involved in traditional DAC technologies.[6,7]

An alternative approach to DAC with PyBIG is to combine the crystallization of $PyBIGH_2(CO_3)(H_2O)_4$ with the well-established carbonate/bicarbonate CO_2 capture cycle[12,22-24] (**Figure 6.3**). In this approach, CO_2 sorption by an alkali carbonate solution

(Eq. 1) is followed by the reaction of the resulting bicarbonate with PyBIG to crystallize $PyBIGH_2(CO_3)(H_2O)_4$ and regenerate the carbonate sorbent (Eq.2). Finally, thermal decomposition of $PyBIGH_2(CO_3)(H_2O)_4$ regenerates the PyBIG ligand and releases the CO_2.

To demonstrate the feasibility of this approach, solid PyBIG (1 mol equiv) was suspended in a solution of 1 M $NaHCO_3$ (5-6 mol equiv) and the slurry was stirred at room temperature for four hours. The resulting mixture was filtered, and the separated crystalline solid was confirmed by PXRD (See Chapter 6 Appendix **Figure 6.8**) and FTIR (See Chapter 6 Appendix **Figure 6.9**) to be $PyBIGH_2(CO_3)(H_2O)_4$. Subsequent heating of the carbonate crystals in the oven for one hour at 120 °C regenerated the PyBIG solid (See Chapter 6 Appendix **Figure 6.10**), which was recycled back into the original sodium bicarbonate solution. The entire carbonate separation cycle was run three times, with observed yields for $PyBIGH_2(CO_3)(H_2O)_4$ crystallization of 99.0 ± 0.4%, 97.2 ± 0.6%, and 91.4 ± 0.4%, corresponding to the first, second, and third cycle, respectively. The regeneration of the PyBIG ligand was essentially quantitative in each cycle. The slight decrease in the crystallization yield observed in the later cycles is explained by the gradual increase in the solution alkalinity (initial pH 8.5, final pH 10.5) as a result of the increasing CO_3^{2-}/HCO_3^- ratio. As more bicarbonate is converted into carbonate in each subsequent cycle, according to Eq. 2, it is expected the pH of the solution should eventually become high enough to inhibit the protonation of PyBIG, thereby decreasing the driving force for the crystallization of $PyBIGH_2(CO_3)(H_2O)_4$. This is corroborated by

the FTIR analysis of the isolated solid, which showed preponderantly the carbonate phase after the first two cycles, but a mixture of carbonate and free PyBIG ligand after the third cycle (See Chapter 6 Appendix **Figure 6.9**).

The efficacy of the atmospheric CO_2 capture via crystallization of $PyBIGH_2(CO_3)(H_2O)_4$, and the ease of CO_2 release (compared to inorganic carbonate salts), can be attributed to a combination of factors. First, the guanidine groups of the PyBIG ligand are sufficiently basic to become protonated in moderately alkaline carbonate/bicarbonate solutions (pH 8.5-10.5), thereby driving the crystallization of the bis-guanidinium carbonate salt. Second, the very low aqueous solubility of crystalline $PyBIGH_2(CO_3)(H_2O)_4$ facilitates its recovery from solution without the need of heating or evaporating water, which are energy intensive. Third, although the exact mechanism of $PyBIGH_2(CO_3)(H_2O)_4$ decomposition and CO_2 release has yet to be investigated, we surmise the close proximity of the carbonate and guanidinium groups, hydrogen-bonded within the crystal, facilitates proton transfer among them and the formation of H_2CO_3, which then decomposes into CO_2 and H_2O with the possible assistance of the included water molecules in the crystal.[25] Finally, as the PyBIG ligand can be quantitatively regenerated and recycled, the only chemical consumed in the overall CO_2 separation cycle is water, which could be easily recovered by condensation if desired. Furthermore, considering the relatively low temperature required for ligand regeneration is easily attainable using renewable energy such as concentrated solar power,[26] the overall separation process could be made energy

sustainable, offering good prospects for the development of economical DAC technologies.

6.2 References

1. D. S. Sholl, R. P. Lively, *Nature* **2016**, *532*, 435.
2. Lackner, K. S. *Science* **2003**, *300*, 1677.
3. D. M. Reiner, *Nature Energy* **2016**, *1*, 1.
4. D. W. Keith, *Science* **2016**, *325*, 1654.
5. K. S. Lackner, S. Brennan, J. M. Matter, A.-H. A. Park, A. Wright, B. van der Zwaan, *Proc. Natl. Acad. Sci.* **2012**, *109*, 13156.
6. E. S. Sanz-Perez, C. R. Murdock, S. A. Didas, C. W. Jones, *Chem. Rev.* **2016**, ***116*, 11840**.
7. Direct air capture of CO_2 with chemicals: A technology assessment for the APS Panel on Public Affairs. American Physical Society **2011**.
8. R. Baciocchi, G. Storti, M. Mazzotti, *Chem. Eng. Process.* **2006**, *45,* 1047.
9. F. Zeman, *Environ. Sci. Technol.* **2007**, *41*, 7558.
10. J. K. Stolaroff, D. W. Keith, G. V. Lowry, *Environ. Sci. Technol.* **2008**, *28*, 2728.
11. M. Mahmoudkhani, D. W. Keith, *Int. J. Greenhouse Gas Control* **2009**, *3,* 376.
12. T. Wang, K. S. Lackner, A. B. Wright, *Environ. Sci. Technol*. **2011***, 45*, 6670.
13. S. Choi, M. L. Gray, C. W. Jones, *ChemSusChem* **2011**, *4,* 628.
14. Choi, S., Drese, J. H., Eisenberger, P. M. & Jones, C. W. *Environ. Sci. Technol.* **2011**, *45*, 2420.
15. C. Gebald, J. A. Wurzbacher, P. Tingaut, T. Zimmermann, A. Steinfeld, *Environ. Sci. Technol.* **2011**, *45*, 9101.

16. A. Goeppert, M. Czaun, R. B. May, G. K. Surya Prakash, G. A. Olah, S. R. Narayanan, *J. Am. Chem. Soc.* **2011**, *133*, 20164.
17. T. M. McDonald, W. R. Lee, J. A. Mason, B. M. Wiers, C. S. Hong, J. R. Long, *J. Am. Chem. Soc.* **2012**, *134,* 7056.
18. A. Kumar, D. G. Madden, M. Lusi, K.-J. Chen, E. A. Daniels, T. Curtin, J. J. Perry IV, M. J. Zaworotko, *Angew. Chem. Int. Ed.* **2015**, *54,* 14372.
19. P. M. Bhatt, Y. Belmabkhout, A. Cadiau, K. Adil, O. Shekhah, A. Shkurenko, L. J. Barbour, M. Eddaoudi, *J. Am. Chem. Soc.* **2016**, *138,* 9301.
20. R. Custelcean, N. J. Williams, C. A. Seipp, *Angew. Chem. Int. Ed.* **2015**, *54,* 10525.
21. R. Custelcean, N. J. Williams, C. A. Seipp, A. S. Ivanov, V. S. Bryantsev, *Chem. Eur. J.* **2016**, *22,* 1997.
22. T. Wang, K. S. Lackner, A. B. Wright, *Phys. Chem. Chem. Phys.* **2013**, *15,* 504.
23. X. Shi, H. Xiao, K. S. Lackner, X. Chen, *Angew. Chem. Int. Ed.,* **2016**, *55,* 4026.
24. K. A. Mumford, K. H. Smith, C. J. Anderson, S. Shen, W. Tao, Y. A. Suryaputradinata, A. Qader, B. Hooper, R. A. Innocenzi, S. E. Kentish, G. W. Stevens, *Energy & Fuels* **2012**, *26*, 138.
25. C. S. Tautermann, A. F. Voegele, T. Loerting, I. Kohl, A. Hallbruker, E. Mayer, K. R. Liedl, *Chem. Eur. J.* **2002**, *8,* 66.
26. V. Nikulshina, C. Gebald, A. Steinfeld, *Chem. Eng. J.* **2009**, *146,* 244.

6.3 Appendix 6A Supplemental Information for Chapter 6

General Information: All reagents were purchased from commercial sources and used with no further purification. Unless otherwise noted, all water used was distilled/deionized water. Fourier-transform infrared (FTIR) spectra were collected on a Digilab FTS 7000 Series Infrared Spectrometer using a diamond ATR setup. UV-Vis spectra were measured in 10 mm path length quartz glass cuvettes using a Cary Varian 5000 spectrometer. NMR spectra were collected on a Bruker Avance III 400 using either a 5mm PABBI or PABBI probe. Powder X-ray diffraction (PXRD) measurements were done with a Panalytical Empyrean diffractometer using Cu Kα radiation (λ = 1.5418 Å). Single-crystal X-ray data were collected on a Bruker SMART APEX CCD diffractometer with fine-focus Mo Kα radiation (λ = 0.71073 Å), operated at 50 kV and 30 mA. Thermogravimetric analysis (TGA) was conducted on a TA Instruments Q5000 IR equipped via inline with a heated capillary to a Pfeiffer OminStar GSD 320 Mass spectrometer to analyze evolved gases. pH measurements were conducted with a Thermoscientific Orion Star A211 pH meter (using a five point calibration curve) and with Millipore MColorphast pH 7.5 - 14 strips.

Synthesis of PyBIG. 2,6-pyridinedicarboxaldehyde (3.8 g, 28 mmol) was dissolved in 70 mL of ethanol, and aminoguanidinium chloride (7.5 g, 68 mmol) was added to the solution. The round bottom flask was sealed, and the suspension was stirred overnight at 60 °C. Subsequently, the solution was placed into a freezer and allowed to sit at 0 °C for 24 hours. Vacuum filtration followed by subsequent rinsing with cold ethanol yielded 6.7 g of

the crude PyBIG product as the hydrochloride salt (PyBIG-Cl). This product was used as obtained in the next step in a portion-wise manner. 1.12 g of the obtained PyBIGCl was dissolved in a minimal amount of water (~30 mL), and NaOH (50 mL, 2 M) was added in one portion. The resulting solution became deep goldenrod yellow and was stirred at room temperature until a creamy precipitate appeared and no more precipitate could be observed forming (usually between 4 and 12 hours). The product was isolated by vacuum filtration, rinsed with water, and allowed to dry to give 650 mg (75% yield) of pure PyBIG · $2.5H_2O$. ^{1}H NMR (400 MHz, DMSO-d_6): δ 7.923 (2H, s), 7.869 (2H, d), 7.591 (1H, t), 6.047 (4H, bs), 5.723 (4H, bs). ^{13}C NMR (100 MHz, DMSO-d_6): δ 161.85, 155.69, 143.80, 136.18, 118.06. FTIR (cm^{-1}): 3345br, 3306br, 3077br, 1647w, 1582m, 1520vs, 1445s, 1420m, 1358w, 1328w, 1279w, 1156s, 1060w, 1004w, 989w, 959w, 938w, 910w, 812w, 748br, 737w, 687w. Elemental analysis: Anal. Calcd for $C_9H_{18}N_9O_{2.5}$: C, 36.98; H, 6.21; N, 43.13. Found: C, 37.10; H, 6.19; N, 43.52.

CO2 capture from air using aqueous PyBIG. An aqueous solution of PyBIG (5 mL, 9.58 mM) was placed in a 20 mL scintillation vial and left open to ambient air for one week. Within two days, small crystals formed on the surface of the liquid as well as within clouds of fine precipitate floating in the solution. After one week the solution was filtered, rinsed with water, and allowed to dry. Yield 9.2 mg, 0.024 mmol (50.3% ± 0.4%) of $PyBIGH_2(CO_3)(H_2O)_4$. FT-IR (cm^{-1}): 1692m, 1619m, 1566w, 1485w, 1447 w, 1357bs, 1327s, 1286w, 1232w, 1156s, 999w, 929s, 876w, 808w, 753b, 687w. Elemental analysis:

Anal. Calcd for $C_{10}H_{23}N_9O_7$: C, 31.50; H, 6.08; N, 33.06. Found: C, 31.59; H, 6.01; N, 33.32.

Crystallization of PyBIGH2(CO3)(H2O)4 from NaHCO3 solution. All observed and theoretical yields are reported in the format “observed yield mg/mmol (theory mg/mmol)”. PyBIG·2.5H_2O (502 mg, 1.72 mmol) was added to an aqueous solution of sodium bicarbonate (10 mL, 1M, pH 8.45). The resulting slurry was shaken at 1000 rpm on a vortex mixer for 4 hours, and the resulting white-cream solid was vacuum-filtered and washed with 1-2 mL of water. The remaining bicarbonate solution had a pH between 9 and 9.5 (measured with a pH strip). The solid was dried under vacuum, to yield 650 mg /1.70 mmol (655 mg/1.72 mmol) of PyBIG$H_2(CO_3)(H_2O)_4$ salt. This solid was placed in a vial and heated in the oven at 120 °C for one hour to give 420 mg/1.70 mmol (421 mg/1.70 mmol) of recovered PyBIG. The recovered ligand was added back to the original bicarbonate solution and allowed to vortex for another four hours, then it was filtered and dried to give 632 mg/1.66 mmol (647 mg/1.70 mmol) of PyBIG$H_2(CO_3)(H_2O)_4$ salt. Heating the carbonate salt for one hour at 120 °C gave 420 mg/1.70 mmol (410 mg/1.66 mmol) of the recovered PyBIG. The recovered ligand was added to the original bicarbonate solution once more, and allowed to vortex for four hours to give 590 mg/1.55 mmol (647 mg/1.70 mmol) of PyBIG$H_2(CO_3)(H_2O)_4$ salt. The final bicarbonate solution had a pH between 10.3 and 10.6 (measured with the pH meter).

PyBIG Regeneration. $PyBIGH_2(CO_3)(H_2O)_4$ crystals (35.0 mg, 0.09 mmol) were placed on a microscope slide and heated in the oven at 120 °C. After one hour, the slide was removed from the oven, allowed to cool to room temperature, and weighed. Yield 23.0 mg (0.09 mmol) of PyBIG (theory: 22.6 mg, 0.09 mmol). ^{1}H NMR (400 MHz, DMSO-d_6): δ 7.912 (2H, s), 7.869 (2H, d), 7.591 (1H, t), 6.035 (4H, bs), 5.685 (4H, bs). FTIR (cm^{-1}): 3105bw, 1660 w, 1599m, 1523s, 1444s, 1433w, 1325w, 1279w, 1148m, 1079w, 974w, 920w, 806w, 737w, 662w, 633w.

Solubility measurements. The solubility of PyBIGH2(CO3)(H2O)4 was determined by UV-Vis spectroscopy using the same methodology as previously described.[21] Saturated solutions were prepared by suspending excess of the crystalline solid in 10 mL of H2O inside 15 mL polypropylene centrifuge tubes, and mixing the suspensions on a rotating wheel for 72 hours at 60 rpm inside an incubator set at 25 ºC. The pH of the equilibrated solutions (measured with the pH meter) were in the range of 8.33–8.37. The measurements were done in duplicate, and the obtained average solubility was 1.35 ± 0.20 Å~ 10^{-3} M. Thus, considering the pK_a of HCO^{3-} of 10.32, and the average pH of the saturated solution of 8.35, the concentration of the carbonate anion [CO_3^{2-}] was determined to be 1.4 ± 0.2 Å~ 10^{-5} M. The solubility product of $PyBIGH_2(CO_3)(H_2O)_4$ was calculated using the following formula, where the activity coefficients (γ ±) were estimated at 0.74 using the Debye-Huckel limiting law:

$K_{sp} = (\gamma\pm)^2[PyBIGH_2^{2+}][CO_3^{2-}] = (0.74)^2$ [1.35 Å~ 10^{-3}][1.4 Å~ 10^{-5}] = 1.0 ± 0.4 Å~ 10^{-8}

TGA Measurements. The TGA-MS was conducted under an argon atmosphere at 25

mL/min flow rate. The sample was held at ambient temperature for 1.5 min, then ramped at 5 °C/min to 300 °C and held for 0.5 min. The mass spectrometer collected the evolved gases under scanning mode of 2-200 amu, with the SEM detector at a speed of 200 ms/amu. For the isothermal runs, samples were first held at ambient temperature for 1.5 min, then jumped to the desired temperature (80, 100 or 120 °C) and held for 300 min.

Single crystal X-ray diffraction. Single crystals of PyBIG·2.5H_2O were obtained by slow evaporation of an aqueous ethanol solution of PyBIG. Single crystals of PyBIG$H_2(CO_3)(H_2O)_4$ were obtained by leaving an aqueous solution of PyBIG in open air for a few days, or by mixing it with an excess aqueous solution of $NaHCO_3$. The structures were solved by direct methods and refined on F^2 using the SHELXTL software package (Bruker AXS, Inc., Madison, WI, 1997). Absorption corrections were applied using SADABS, part of the SHELXTL package. All non-hydrogen atoms were refined anisotropically.

6.4 Appendix 6B Figures and Tables for Chapter 6

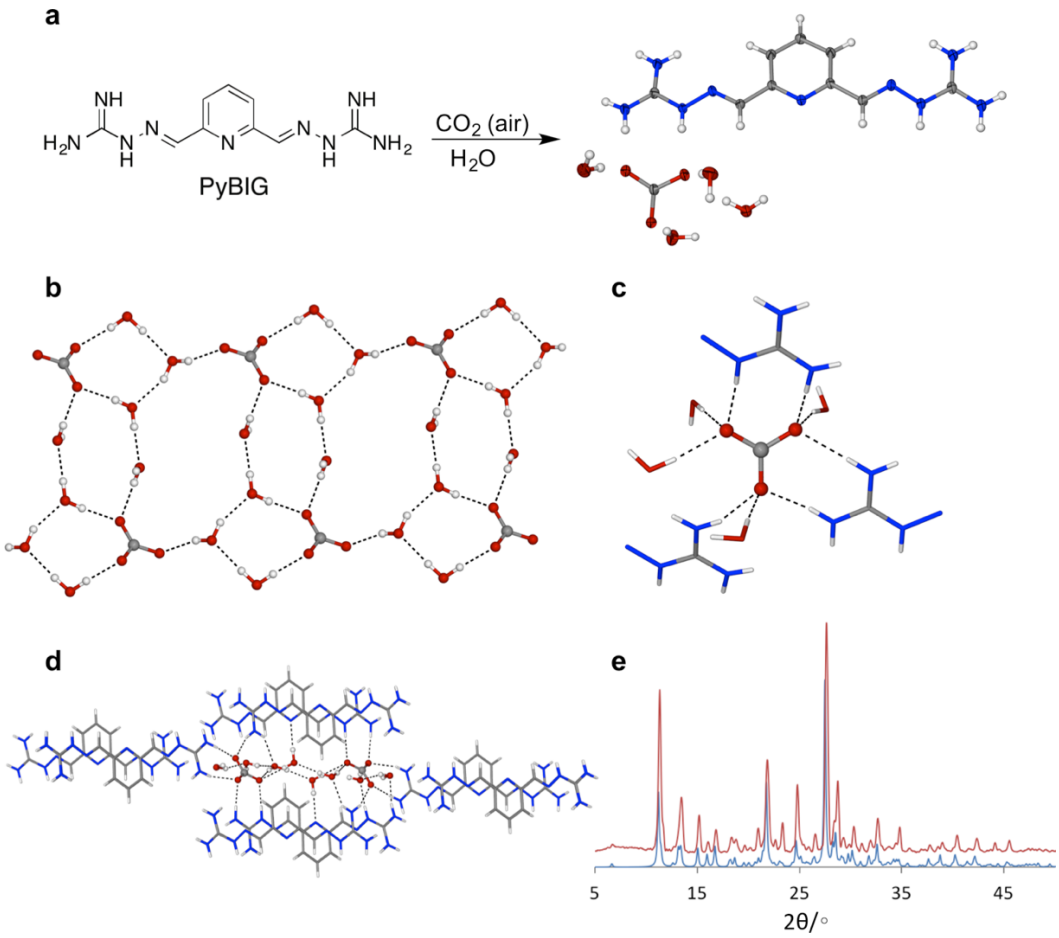

Figure 6.1. Atmospheric CO_2 capture via crystalline $PyBIGH_2(CO_3)(H_2O)_4$. a) Reaction of aqueous PyBIG (ChemDraw structure on the left) with CO_2 to form $PyBIGH_2(CO_3)(H_2O)_4$ (X-ray crystal structure on the right). b) Hydrogen-bonded $[CO_3(H_2O)_4^{2-}]_n$ cluster formed in the crystal. c) CO_3^{2-} binding site, with the anion accepting 4 water and 5 guanidinium hydrogen bonds. d) Hydrogen bonding of the $[CO_3(H_2O)_4^{2-}]_n$ cluster by the cationic stacks. e) Overlay of the experimental PXRD pattern of the bulk crystalline product (red) and the simulated PXRD pattern from the single-crystal X-ray data (blue).

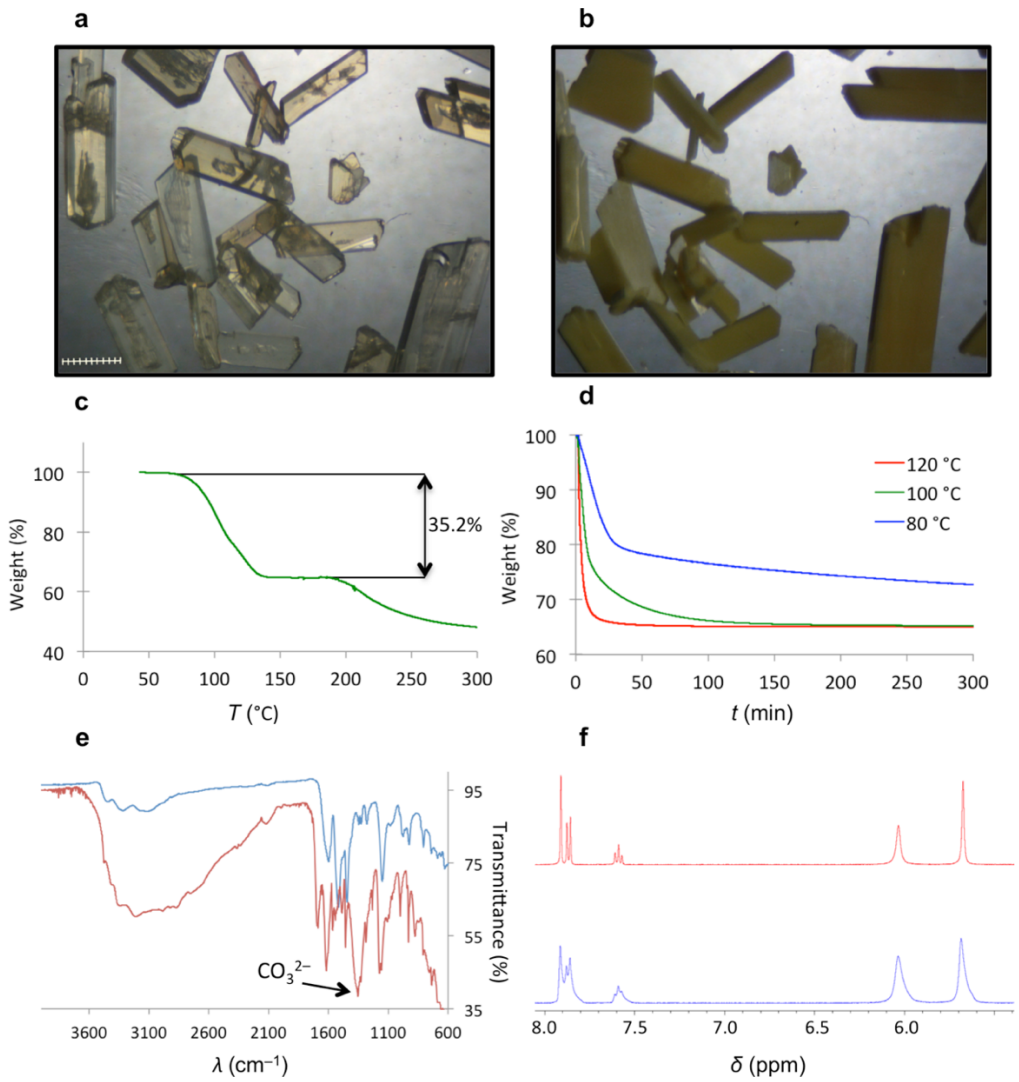

Figure 6.2. Thermal decomposition of $PyBIGH_2(CO_3)(H_2O)_4$ crystals and regeneration of the PyBIG sorbent. a), b) Micrographs of the initial crystals (a) and after heating in air at 120 °C for one hour (b); scale bar: 100 μm. c), d) TGA plots from temperature-ramped (c) and isothermal (d) measurements. e) Overlaid FTIR spectra of the carbonate crystals red) and the recovered PyBIG ligand (blue). f) ^{1}H NMR spectra (in DMSO-d_6) of the initial (red) and regenerated (blue) PyBIG.

$$CO_3^{2-} + CO_2 + H_2O \longrightarrow 2\,HCO_3^- \quad (\textbf{Eq. 1})$$

$$PyBIG_{(s)} + 2\,HCO_3^- + 4\,H_2O \longrightarrow PyBIGH_2(CO_3)(H_2O)_{4(s)} + CO_3^{2-} \quad (\textbf{Eq. 2})$$

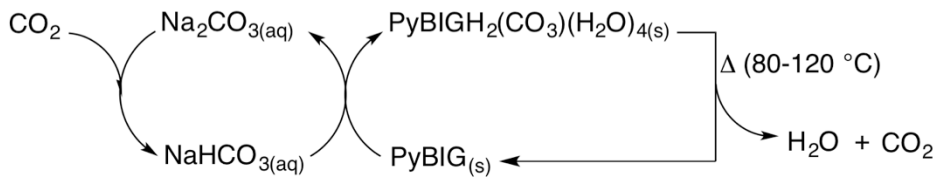

Figure 6.3. Atmospheric CO_2 capture combining CO_2 sorption by an alkali carbonate solution (Eq. 1) and carbonate crystallization with PyBIG (Eq. 2). The overall CO_2 separation cycle is shown in the schematic diagram.

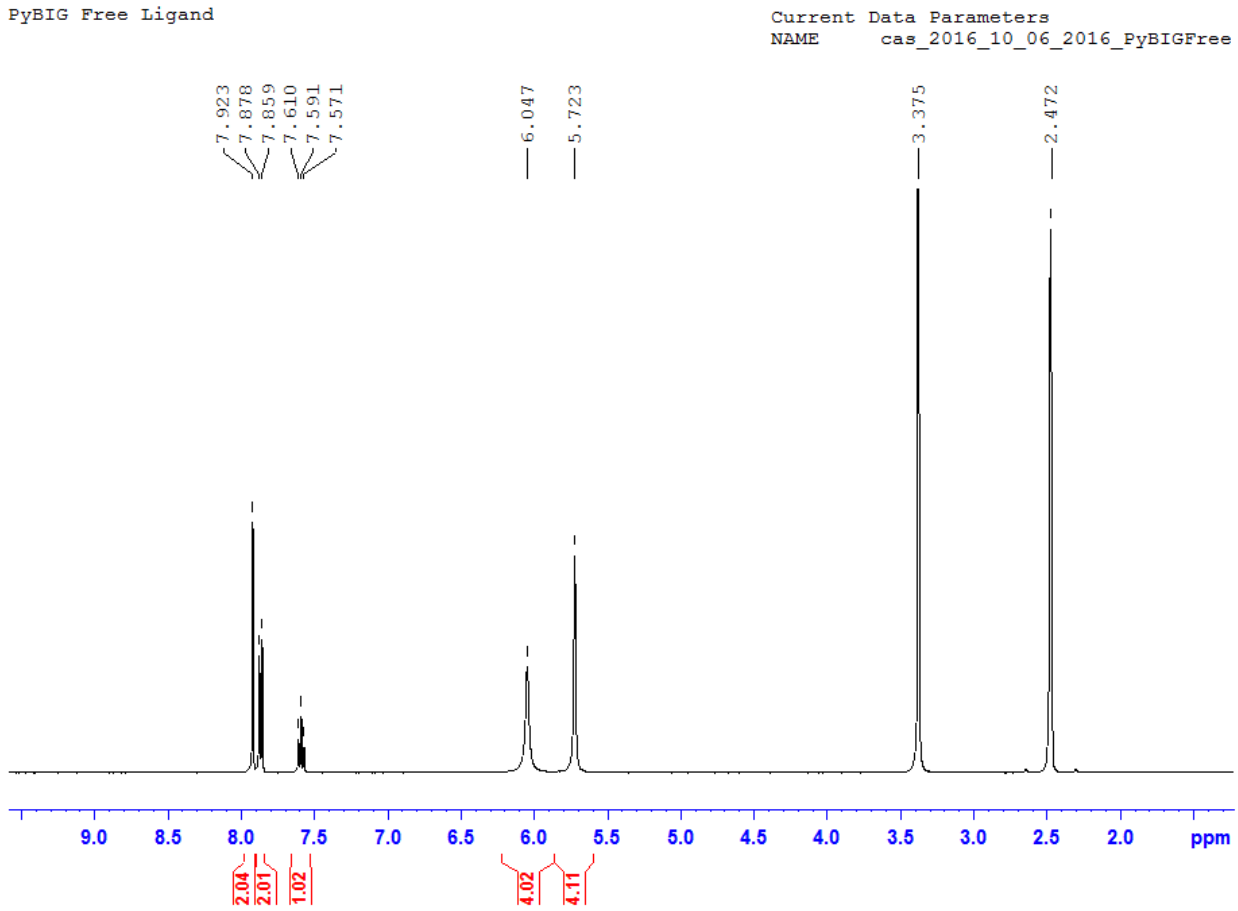

Figure 6.4. ^{1}H-NMR Spectrum of PyBIG in DMSO-d_6.

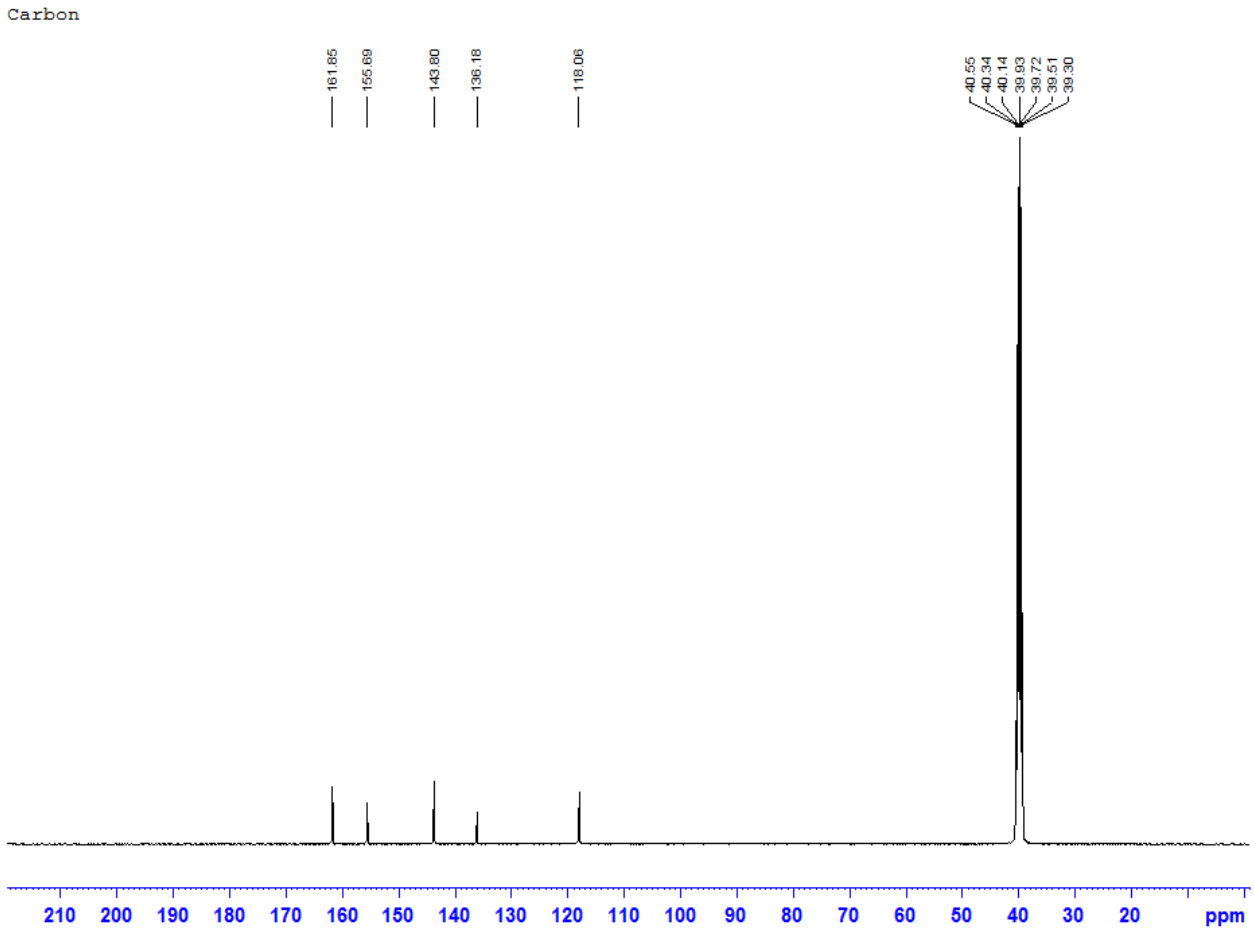

Figure 6.5. ^{13}C-NMR Spectrum of PyBIG in DMSO-d_6.

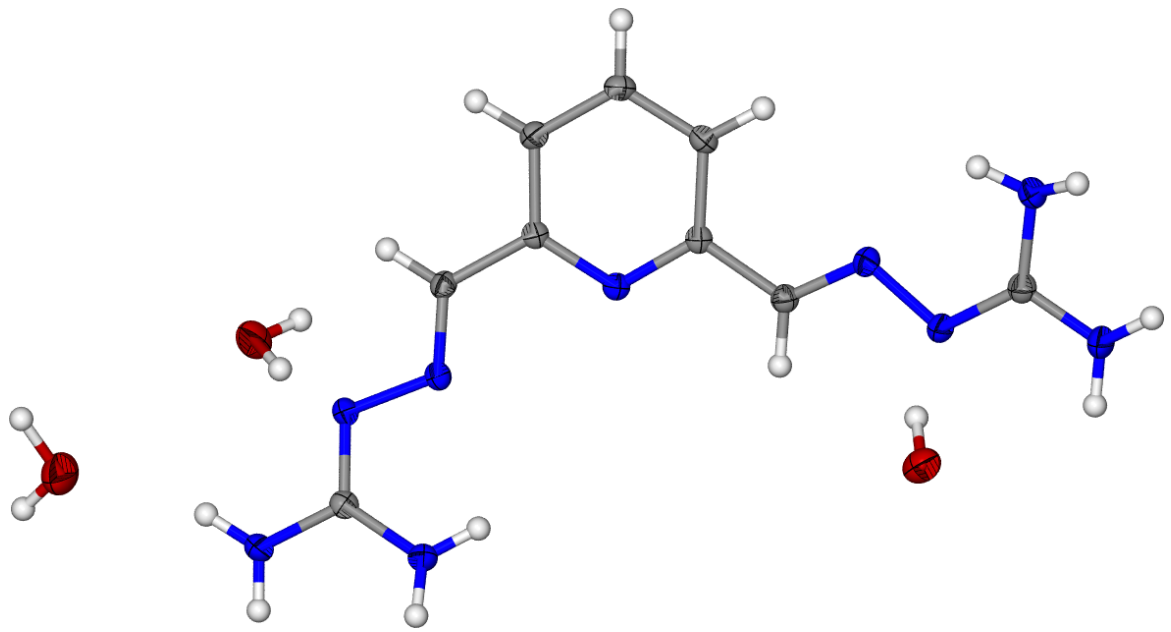

Figure 6.6. Single-crystal X-ray structure of PyBIG.2.5H_2O.

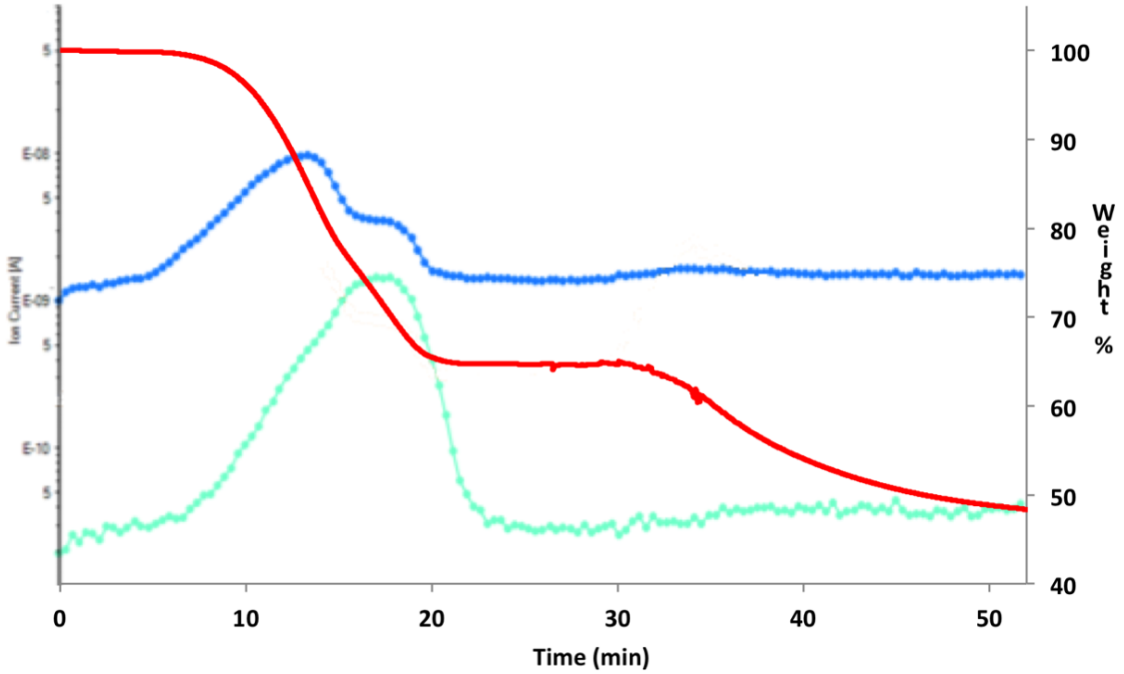

Figure 6.7. TGA-MS of PyBIGH2(CO3)(H2O)4. Overlay of the molecular peaks in the MS, corresponding to CO2 (m/z 44, teal) and H2O (m/z 18, blue), and the weight loss from the TGA (red), as a function of time. Fragmentation peaks in the MS are omitted for clarity.

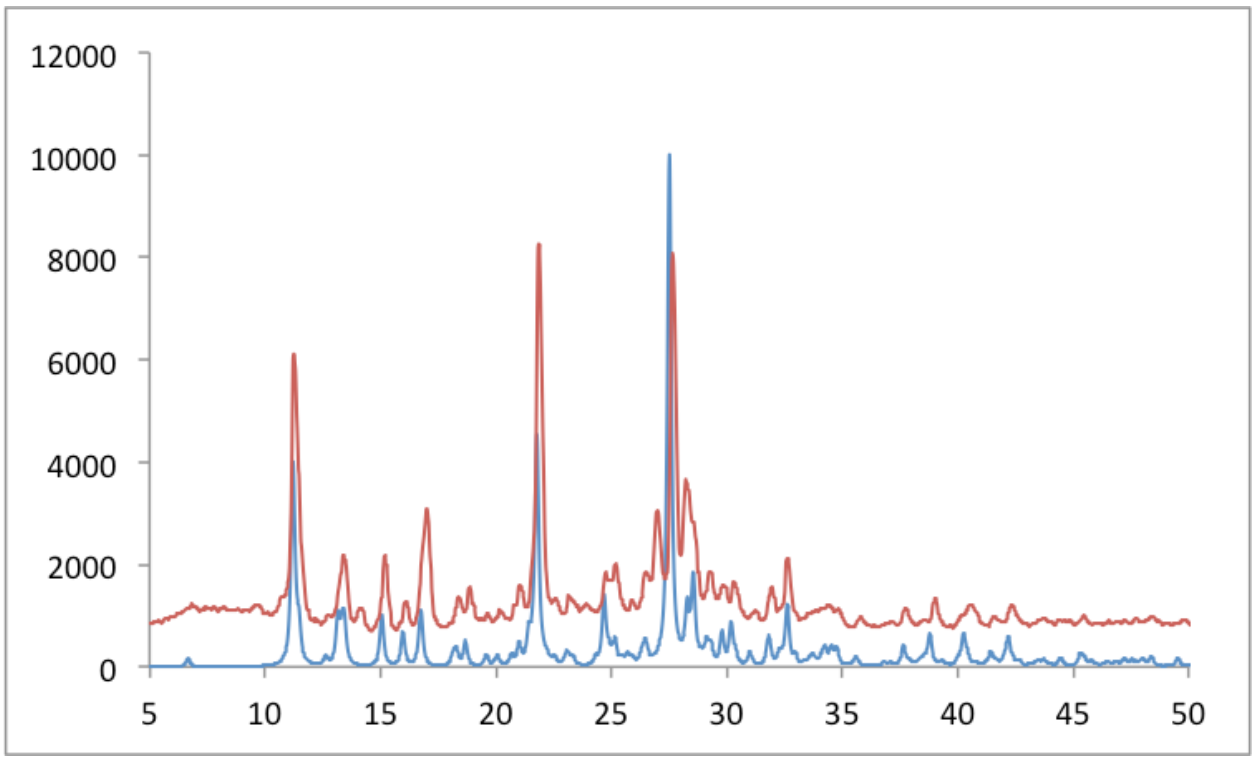

Figure 6.8. PXRD pattern of crystalline solid isolated from the slurry reaction of PyBIG with aqueous sodium bicarbonate (red) overlaid over the simulated PXRD pattern from the single-crystal X-ray structure of $PyBIGH_2(CO_3)(H_2O)_4$ (blue).

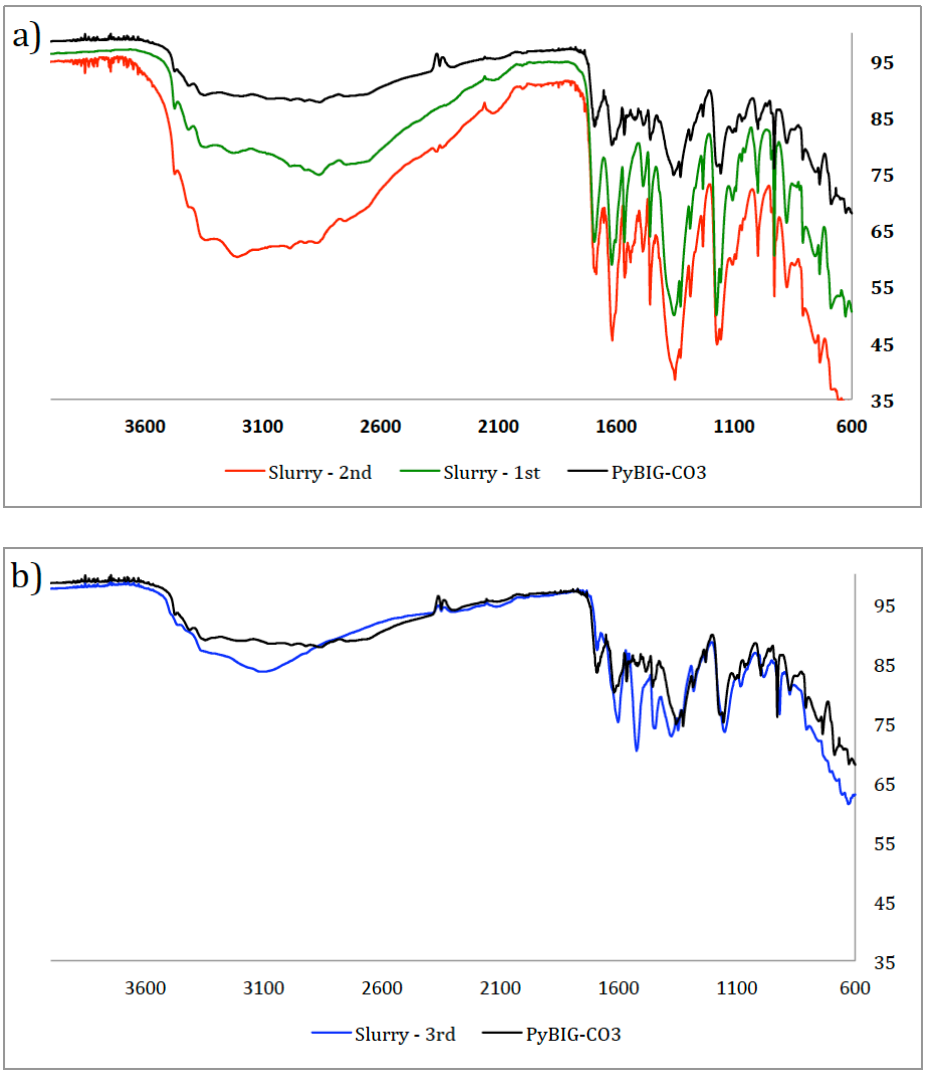

Figure 6.9. Comparative FTIR spectra of the solids isolated from the slurry reaction of PyBIG with aqueous sodium bicarbonate. a) Products from the first two cycles (green, red) overlaid over the reference spectrum of $PyBIGH_2(CO_3)(H_2O)_4$ (black); virtually no PyBIG ligand is observed. b) Product from the third cycle (blue), overlaid over the reference spectrum of $PyBIGH_2(CO_3)(H_2O)_4$ (black), indicating a mixture of carbonate and PyBIG.

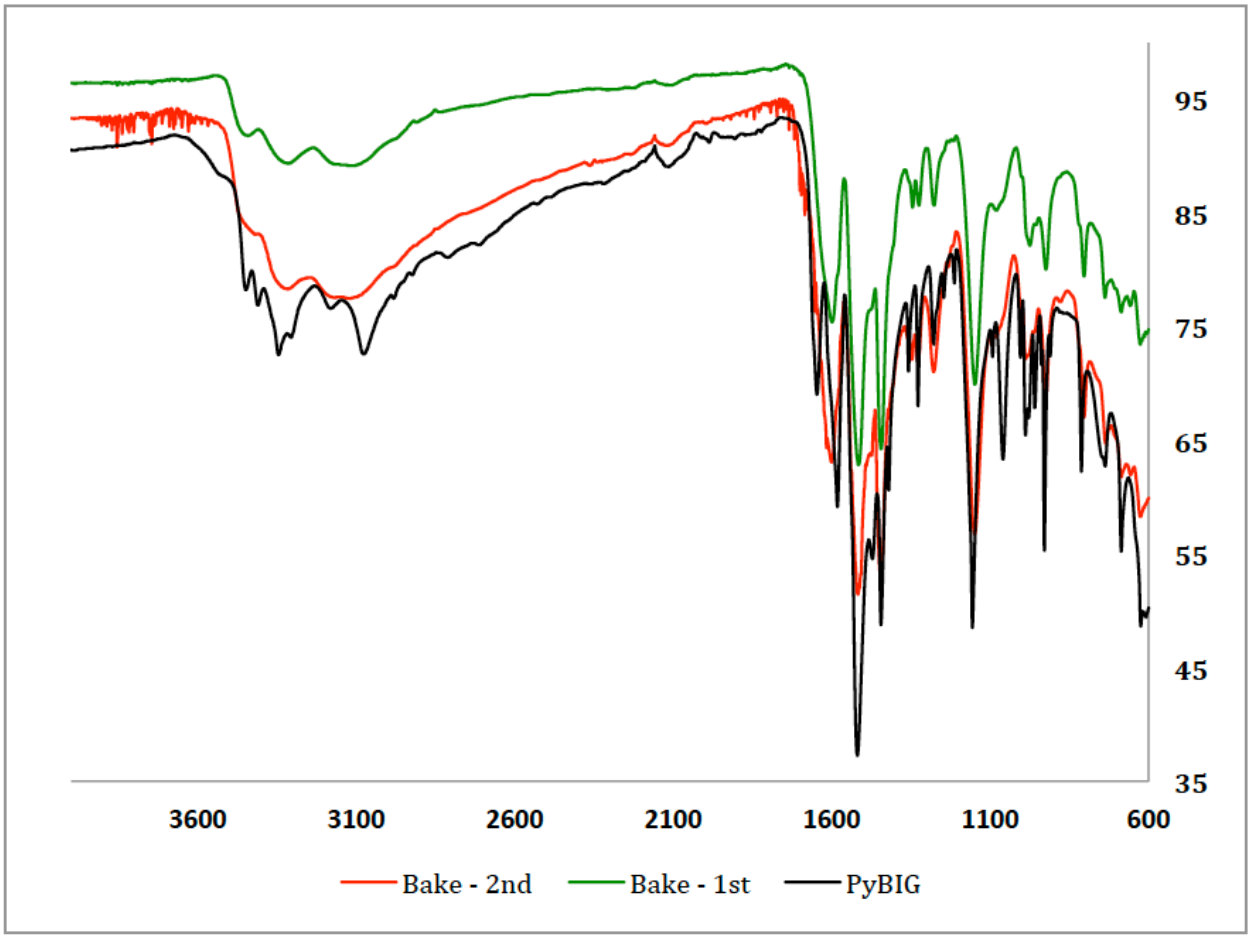

Figure 6.10. Comparative FTIR spectra of the recovered PyBIG ligand from the slurry reaction with aqueous sodium bicarbonate. The regenerated ligand matches the spectra of the as synthesized PyBIG. The only difference is the water peaks in the 3100-3600 region (O–H stretch) and at 1640 (H–O–H bend), present in the as synthesized PyBIG.2.5H_2O (black), and absent in the recovered anhydrous PyBIG (green, red).

Chapter 7 : Extraction of lanthanides using 1-hydroxy-6-N-octylcarboxamido-2(1H)-pyridinone as an extractant via competitive ligand complexations between aqueous and organic phases

Publication Statement for Chapter 7

Reference for Original Article:

Williams N.J.; Do-Thanh, C-L.; Stankovich, J.J.; Luo, H.; Dai, S. "Extraction of lanthanides using 1-hydroxy-6-N-octylcarboxamido-2(1H)-pyridinone as an extractant via competitive ligand complexations between aqueous and organic phases." *RCS Adv.* **2015**, 5, 129, 107054–107057.

Individual Author Contribution(s):

Williams, N. J. –Synthesis of ligands, radiochemistry experimentation, Ran ICP-MS and analyized data, and wrote and edited the article

Do-Thanh, C-L – Synthesized compounds and edited the article

Stankovich, J.J. – Ran ICP-MS

Luo, H. – Prepared solutions, ran extractions, edited the article

Dai, S. – Conceptualized the use of octyl-HOPO in TALSPEAK systems and wrote and edited the article

Journals Policy/Permission/Agreement for Reproduction of Article

Extraction of lanthanides using 1-hydroxy-6-***N***-octylcarboxamido-2(1***H***)-pyridinone as an extractant ***via*** competitive ligand complexations between aqueous and organic phases

N. J. Williams, C. Do-Thanh, J. J. Stankovich, H. Luo and S. Dai, *RSC Adv.*, 2015, **5**, 107054

DOI: 10.1039/C5RA23443C

If you are not the author of this article and you wish to reproduce material from it in a third party non-RSC publication you must formally request permission using RightsLink. Go to our Instructions for using RightsLink page for details.

Authors contributing to RSC publications (journal articles, books or book chapters) do not need to formally request permission to reproduce material contained in this article provided that the correct acknowledgement is given with the reproduced material.

Reproduced material should be attributed as follows:

- For reproduction of material from NJC:
  Reproduced from Ref. XX with permission from the Centre National de la Recherche Scientifique (CNRS) and The Royal Society of Chemistry.
- For reproduction of material from PCCP:
  Reproduced from Ref. XX with permission from the PCCP Owner Societies.
- For reproduction of material from PPS:
  Reproduced from Ref. XX with permission from the European Society for Photobiology, the European Photochemistry Association, and The Royal Society of Chemistry.

A version of this chapter was originally published by Neil J. Williams, Chi-Lihn Do-Thanh, Joseph J. Stankovich, Huimin Luo, and Sheng Dai in *RSC Advances*

Williams N.J.; Do-Thanh, C-L.; Stankovich, J.J.; Luo, H.; Dai, S. "Extraction of lanthanides using 1-hydroxy-6-N-octylcarboxamido-2(1H)-pyridinone as an extractant via competitive ligand complexations between aqueous and organic phases." *RCS Adv.* **2015**, 5, 129, 107054–107057.

The article used as Chapter 7 was modified in the following manner; the formatting was adapted to fit the formatting required by the University of Tennessee Knoxville, the figures and tables were renumbered to make all figures in the ensuing document contiguous. The work/research of the done by the student in the articles is as follows conducted experiments to measure the selectivity of the ligand across the lanthanide series, conducted radiochemical experiments to determine selectivity for lanthanides over minor actinides, wrote much of the publication and electronic supplemental information.

Abstract

The ability to selectively extract lanthanides is crucial in hydrometallurgy and the nuclear fuel cycle. The capabilities of 1-hydroxy-6-*N*-octylcarboxamido-2(1*H*)-pyridinone (octyl-HOPO) as an extractant for the separation of lanthanides and actinides was studied for the first time. Octyl-HOPO greatly outperformed the traditional ligand di-2-ethylhexyl phosphoric acid (DEHPA).

7.1 Introduction

Rare earth elements (REEs) are ubiquitous and indispensable in many modern-day scientific applications.[1,2] They are used extensively in green energy technologies, modern electronics, and advanced weapon systems. With continuous implementation and integration of new technologies in modern society, the demand for REEs will continue growing, making it necessary to develop more efficient means of producing and enriching large quantities of lanthanides.[3-5] The development of new methods for the selective separation of rare earth elements such as the lanthanides (Ln) from other metal ions as well as specific lanthanides has been a topic of great interest in the separation sciences.[6-13] The ability to selectively separate lanthanides from other metals has additional application in the nuclear fuel cycle as it could further improve the separation of trivalent Ln from trivalent actinides (An), specifically americium(III). The separation processes for the rare-earth fission products from trivalent actinides are arduous due to the similarities in their charge state and size. Traditional solvent extraction (SX) methods are not highly selective for lanthanides, meaning numerous extraction stages are necessary to effectively extract Ln, making processes very inefficient and cost-prohibitive.

The trivalent actinide–lanthanide separations by phosphorous-reagent extraction from aqueous complexes (TALSPEAK) process was developed 50 years ago.[14,15] The aim of the TALSPEAK process was to enhance the selectivity toward lanthanides over transuranics present in the post TRUEX waste stream.[16-19] The essence of TALSPEAK lies in utilizing a common ligand, diethylenetriamine pentaacetic acid (DTPA), as a

holdback reagent to complex more favourably with actinides over lanthanides. The selectivity of DTPA for actinides in the presence of lanthanides makes it possible to separate Ln from An by extracting the Ln using solvent extraction in combination with high concentrations of organophosphate ligand DEHPA present in the organic solvent diisopropylbenzene (DIPB). This competitive complexation by DTPA in the aqueous phase and by DEHPA in the organic phase is the key to breaking the linear dependence of the extraction efficiency on 1/r(REE radius) and achieving the selective extraction of Ln over An. Some of the major disadvantages associated with the TALSPEAK process are (a) low extraction efficiency, (b) high concentrations of DEHPA, (c) susceptibility to a third phase formation, and (d) loss of buffering reagents to the organic phase. All of these drawbacks in the TALSPEAK process are interconnected. For example, the low extraction efficiency demands the use of the higher DEHPA concentrations in the solvent. The increased concentrations of DEHPA can lead to the formation of a third phase during extraction. To overcome these drawbacks that have become associated with traditional TALSPEAK based on DEHPA, we herein report a new variant of the TALSPEAK process which utilizes the highly selective ligand 1-hydroxy-6-*N*-octylcarboxamido-2(1*H*)-pyridinone (octyl-HOPO), which serves as a replacement for DEHPA. The core of octyl-HOPO, 1,2–HOPO has been studied extensively over the course of the past two decades.[20-23] However, much of this research was focused on its use in chelation therapy for the removal of uranium and other actinides from biological systems.[23-25] More complex ligands utilizing multiple 1,2-HOPO cores that have been linked together have been synthesized for possible MRI imaging agents and sequestering agents.[25-29] Octyl-HOPO

has many advantages over DEHPA, some of which include an increased selectivity and stronger binding to Ln. The increase in binding strength allows for a marked decrease in the concentration of the extractant needed to achieve the desired separation, making the new TALSPEAK process more effective for the separation of the Ln and An.

Octyl-HOPO has been demonstrated as an effective ligand and extractant for the selective complexation of lanthanides in traditional solvent extraction processes.[27, 29,30] Herein we report the first investigation and use of octyl-HOPO as a replacement for DEPHA in a TALSPEAK system for the separation of lanthanides. Non-TALSPEAK conditions (e.g. both with and without holdback reagents and/or buffers) were used to directly compare the extraction properties of octyl-HOPO across the lanthanide series.

Octyl-HOPO (**Figure 7.2**) was synthesized according to the modified literature procedure[29, 30] and characterized by nuclear magnetic resonance (NMR) and mass spectrometry (MS) (see Chapter 7 Appendix).

The results shown in **Figure 7.3** and **Table 7.1** confirm that octyl-HOPO is a stronger complexant for lanthanides compared to DEHPA. From the large distribution ratios for the lanthanides shown in **Table 7.1**, it is possible to stipulate that only a very small quantity of the ligand is needed to efficiently extract the lanthanides in a process. This extraction behavior will minimize the extraction stages needed to achieve the desired separation, possibly lowering the costs of a process dramatically. Decreasing the concentration of the

ligand will have additional benefits such as lowering the probability of forming a third–phase. The solubility of the ligand at lower concentrations also removes the need for a modifier, improving the hydraulics of the system and simplifying the system.

When non-TALSPEAK conditions (no holdback reagent) were used, the previous trend seen in **Figure 7.3** for octyl-HOPO was no longer observed. Extraction of Ln(III) using the ligand develops a trend typical of extractants for the Ln(III), which is directly related to the size and acidity of the metal. The increased extraction efficiency of Ln with the octyl-HOPO over DEHPA can clearly be observed in **Figure 7.4**.

Once the extraction behavior of the lanthanides with octyl-HOPO was determined, the ligand's ability to separate Eu(III) from Am(III) was investigated with a direct comparison to DEHPA. The concentrations of DEHPA and the ligand used in the experiments were kept equivalent so that a direct comparison could be made. The aqueous phase with four different DTPA concentrations was used respectively during the experiment to study the effect of the holdback reagent (DTPA) would have on the extraction behavior of the octyl-HOPO and DEHPA. The extraction of Eu and Am were monitored using radiotracers Eu-152/154 and Am-241. The results from these experiments are shown in **Table 7.2**. The ligand has higher affinity for both Eu and Am compared to DEHPA at all four DTPA concentrations. There is a noticable decrease in the extraction of the Am(III) by octyl-HOPO as the concentration of DTPA is increased, resulting in a 40-fold decrease in the extraction of Am(III). The dramatic decrease in the extraction of the Am(III) compared to

Eu(III) is the main reason for the increased separation factor (SF) between the two. The SF for DEHPA is the inverse of octyl-HOPO with large SFs at low concentrations of holdback reagents that decrease as the DTPA concentration is increased. Although the DEHPA has a large SF at 0.005 M DTPA, this result is most likely due to DEHPA's inability to compete with the holdback reagent. The statement is supported by the fact that the distribution ratios for both Eu and Am decrease dramatically as the DTPA concentration increased.

In summary, these results lead us to conclude that octyl-HOPO has great versatility for the separation of lanthanides and is a viable replacement for DEHPA in the TALSPEAK process. The extraction efficiency of octyl-HOPO is considerably higher than that of DEHPA under the TALSPEAK conditions. Presently, we are synthesizing more lipophilic HOPO ligands possessing either longer alkyl groups that are branched or multiple alkyl chains of the amide (e.g. di-*n*-octyl). Further studies are currently underway to determine the extraction properties of octyl-HOPO in less common organic diluents (e.g. ionic liquids). We feel that these experimental results reported and discussed in this work represent class of extractants for REEs that function as cation exchangers and are stronger than DEHPA and other commonly used phosphorous-based extractants.

7.2 References

1. R. F. Service, *Science*, 2010, **327**, 1596-1597.
2. A. Cho, *Science*, 2013, **340**, 914-918.
3. P. D. Schumacher, N. A. Woods, J. O. Schenk and S. B. Clark, *Anal Chem*, 2010, **82**, 5663-5668.
4. Z. Varga, R. Katona, Z. Stefanka, M. Wallenius, K. Mayer and A. Nicholl, *Talanta*, 2010, **80**, 1744-1749.
5. Y. Hasegawa, S. Tamaki, H. Yajima, B. Hashimoto and T. Yaita, *Talanta*, 2011, **85**, 1543-1548.
6. D. Kim, L. E. Powell, L. H. Delmau, E. S. Peterson, J. Herchenroeder and R. R. Bhave, *Environmental Science & Technology*, 2015, **49**, 9452-9459.
7. X. Q. Sun, H. M. Luo and S. Dai, *Chemical Reviews*, 2012, **112**, 2100–2128.
8. K. Binnemans and P. T. Jones, *Journal of Rare Earths*, 2014, **32**, 195-200.
9. A. Rout and K. Binnemans, *Industrial & Engineering Chemistry Research*, 2014, **53**, 6500-6508.
10. A. Rout and K. Binnemans, *Dalton Transactions*, 2014, **43**, 3186-3195.
11. Y. Baba, A. Fukami, F. Kubota, N. Kamiya and M. Goto, *RSC Adv.*, 2014, **4**, 50726-50730.
12. K. Nakashima, F. Kubota, T. Maruyama and M. Goto, *Industrial & Engineering Chemistry Research*, 2005, **44**, 4368-4372.
13. X. Q. Sun, Y. M. Dong, Y. L. Wang and Y. J. Chai, *RSC Adv.*, 2015, **5**, 49500-49507.

14. B. Weaver and F. A. Kappelmann, *Journal of Inorganic and Nuclear Chemistry*, 1968, **30**, 263-272.

15. B. a. K. Weaver, F.A., *TALSPEAK: A New Method Of Separating Americium and Curium From The Lanthanides By Extraction From An Aqueous Solution Of An Aminopolyacetic Acid Complex With A Monoacidic Organophosphate Or Phosphate*, C. T. Division Report ORNL-3559, Oak Ridge National Laboratory, Oak Ridge, TN, 1964.

16. M. Nilsson and K. L. Nash, *Solvent Extraction and Ion Exchange*, 2007, **25**, 665-701.

17. M. Nilsson and K. L. Nash, *Solvent Extraction and Ion Exchange*, 2009, **27**, 354-377.

18. K. L. Nash, *Solvent Extr. Ion Exch.*, 2015, **33**, 1-55.

19. C. J. Leggett, G. Liu and M. P. Jensen, *Solvent Extraction and Ion Exchange*, 2010, **28**, 313-334.

20. P. E. Riley, K. Abu-Dari and K. N. Raymond, *Inorganic Chemistry*, 1983, **22**, 3940-3944.

21. Y. J. Li and A. E. Martell, *Inorganica Chimica Acta*, 1993, **214**, 103-111.

22. P. W. Durbin, B. Kullgren, J. Xu and K. N. Raymond, *Int. J. Radiat. Biol.*, 2000, **76**, 199-214.

23. A. E. V. Gorden, J. Xu, K. N. Raymond and P. Durbin, *Chem Rev*, 2003, **103**, 4207-4282.

24. A. Leydier, D. Lecerclé, S. Pellet-Rostaing, A. Favre-Réguillon, F. Taran and M. Lemaire, *Tetrahedron*, 2008, **64**, 11319-11324.

25. C. Ni, D. K. Shuh and K. N. Raymond, *Chem Commun (Camb)*, 2011, **47**, 6392-6394.

26. E. J. Werner, J. Kozhukh, M. Botta, E. G. Moore, S. Avedano, S. Aime and K. N. Raymond, *Inorganic Chemistry*, 2009, **48**, 277.

27. E. G. Moore, J. Xu, C. J. Jocher, I. Castro-Rodriguez and K. N. Raymond, *Inorg Chem*, 2008, **47**, 3105-3118.

28. A. D'Aleo, E. G. Moore, J. Xu, L. J. Daumann and K. N. Raymond, *Inorg Chem*, 2015, **54**, 6807-6820.

29. US Pat., US8557601(B2), 2013.

30. V. V. Romanovski, D. J. White, J. Xu, D. C. Hoffman and K. N. Raymond, *Solvent Extr. Ion Exch.*, 1999, **17**, 55-71.

7.3 Appendix 7A Supplemental Information for Chapter 7

7.3.1 Experimental Details

Solvents, reagents, and chemicals were purchased from commercial vendors and used without further purification. ^{1}H and ^{13}C NMR spectra were recorded at ambient temperature on a Varian VNMRS 500 MHz narrow-bore broadband system. ^{1}H and ^{13}C NMR chemical shifts were referenced to the residual solvent. Mass spectrometry analyses were performed using a JEOL AccuTOF-D time-of-flight (TOF) mass spectrometer with a DART (direct analysis in real time) ionization source from JEOL USA, Inc. (Peabody, MA).

Synthesis of 6-carboxy-1-hydroxy-2(1H)-pyridinone (1). This compound was prepared following a reported procedure.[1] A mixture of acetic anhydride (30 mL) and a 30% aqueous hydrogen peroxide solution (10 mL) was stirred in an ice bath for 4 h to form a peracetic acid solution. A separate solution was prepared by dissolving 6-hydroxypicolinic acid (5.03 g, 35.10 mmol) in a mixture of trifluoroacetic acid (30 mL) and glacial acetic acid (10 mL). After stirring at room temperature for 10 min, this 6-hydroxypicolinic acid solution was added to the peracetic acid solution. The reaction mixture was then stirred at 80 °C overnight, yielding a white precipitate after cooling to room temperature. The precipitate was filtered, washed with cold methanol, and dried under vacuum. A 10% w/w aqueous KOH solution (90 mL) was then added to the precipitate, and the mixture was stirred at 70 °C overnight. After cooling to room temperature, the mixture was cooled in an ice bath, and the product was precipitated by adding cold concentrated HCl (30 mL).

The precipitate was filtered and washed with a 0.1 M aqueous HCl solution, cold methanol, and cold water in succession. The product was dried under vacuum to yield an off-white solid (2.54 g, 47%). ^{1}H NMR (DMSO-d_6, 500 MHz) δ 11.33 (s, 1H), 7.45 (dd, J = 9.0, 7.0 Hz, 1H), 6.73 (dd, J = 9.0, 1.5 Hz, 1H), 6.65 (dd, J = 7.0, 1.5 Hz, 1H). ^{13}C NMR (DMSO-d_6, 126 MHz) δ 161.9, 157.2, 139.0, 136.8, 120.3, 106.4. HRMS (DART-TOF) m/z: $[M-H]^-$ calcd for $C_6H_4NO_4$: 154.0140; found: 154.0142.

Synthesis of 1-hydroxy-6-N-octylcarboxamido-2(1H)-pyridinone (octyl-HOPO) (2). This compound was synthesized according to a modified literature procedure.[2] 6-Carboxy-1-hydroxy-2(1H)-pyridinone (1) (1.01 g, 6.51 mmol) and N,N′-carbonyl diimidazole (CDI) (1.27 g, 7.81 mmol) were stirred in dry DMF (40 mL) at room temperature under N_2 for 2 h. Then, *n*-octylamine (1.18 mL, 7.17 mmol) was added, and the mixture continued stirring at room temperature under N_2 overnight. Afterwards, the solvent was removed by rotary evaporation, and the crude residue was taken up in dichloromethane (50 mL). The solution was extracted with 0.1 M NaOH (2 Å~ 25 mL), and the combined aqueous layers were reduced to about 20 mL in volume by rotary evaporation. The concentrated aqueous solution was acidified with 2 M HCl to pH 2, upon which white precipitates formed. The solids were collected by filtration, washed with cold water, and dried under vacuum to give the product as an off-white solid (1.16 g, 67%). ^{1}H NMR ($CDCl_3$, 500 MHz) δ 9.56 (s, 1H), 7.62 (d, J = 7.8 Hz, 1H), 7.49–7.43 (m, 1H), 7.03 (d, J = 8.6 Hz, 1H), 3.51–3.44 (m, 2H), 1.68–1.60 (m, 2H), 1.43–1.35 (m, 2H), 1.35–1.22 (m, 8H), 0.87 (t, J = 7.0 Hz, 3H). ^{13}C NMR (CDCl3, 126 MHz) δ 158.8, 156.6, 137.2, 133.2, 115.2, 114.0, 40.3, 32.0, 29.4,

27.2, 22.8, 14.3. HRMS (DART-TOF) m/z: $[M+H]^+$ calcd for $C_{14}H_{23}N_2O_3$: 267.1709; found: 267.1706.

Materials for Distribution studies: Extraction studies were carried out using 1,3-diisopropylbenzene obtained from Sigma Aldrich and was used as received without further purification. Aqueous phases solutions used distilled, deionized water from a Millipore filtration system (resistivity 18.2 MΩ cm^{-1}). The $^{152/154}Eu$ radioisotope was obtained from Isotope Products, Burbank, CA and the Radiochemical and Engineering Research Center of Oak Ridge National Laboratory provided the 241Am radioisotope. The lanthanides were obtained as 10,000 ppm (4% HNO_3) standardized solutions from High-Purity Standards, Charleston, SC. The DTPA used was obtained as the penta-sodium salt from Acros Organics as a 40% w/w aqueous solution. All other chemicals were obtained from Fisher Scientific and were used as received without further purification.

Distribution Studies. The extraction experiments of the lanthanides and europium/americium(Eu/Am) separation experiments were carried out in a similar manner. The aqueous solutions for both sets of experiments were the same with the exception that the Eu/Am experiments were spiked with a small quantity of a $^{152/154}Eu/^{241}Am$ radiotracer mixture prior to mixing. An aqueous solution containing 0.7 mmol of each lanthanide (with the exception of Pm) was made using analytical ICP standards. To this mixture was added one or more of the following; Citric Acid and/or

DTPA at the concentrations indicated in **Table 7.2** article. For the studies involving Eu/Am separation the citric acid was replaced with lactic acid to allow for a direct comparison to the initial work done by Boyd and Weaver.[3] The octyl-HOPO and DEHPA were dissolved in 1,3-diisopropylbenzene (DIPB) at the concentrations indicated. Extraction studies were preformed by pipetting 0.500 mL of the organic phase and 0.500 mL of the aqueous phase in a 2 mL eppendorf centrifuge tube. The solutions were mixed using a rugged rotating wheel set at 60 rpm in a temperature controlled air–box (25 ± 0.2 °C) for 3 hrs. After 3 hrs, the tubes were centrifuged at 3000 rom for 5 mins to ensure complete phase disengagement. A this point the two types of experiments utilized different methods for determining the distribution ratios (or values) (*D*), the D values were determined using Eq. 1.

$$D_{Ln} = \frac{[Ln]_{org}}{[Ln]_{aq}} \quad \textbf{(1)}$$

To determine the D_{Ln} for the adjacent lanthanide separations the organic phase was removed via pipette then the aqueous phase was subsampled and diluted 10x, then was diluted further 901x prior to injecting the sample into the inductively–coupled plasma mass spectrometer (ICP–MS). The concentrations of the lanthanides in the samples determined via ICP–MS were subtracted from the initial concentrations of the lanthanides, which were also determined by ICP–MS, to determine the concentrations of each lanthanide in the organic phase. Eq. 2 was used to determine the organic phase concentration. In Eq. 2 the initial aqueous [Ln] is subtracted from the experimentally determined [Ln] post mixing, this equation assumes that there was on film or third phase formations.

$$[Ln]_{org} = [Ln]_{aq(init.)} - [Ln]_{aq(mixed)} \quad \textbf{(2)}$$

The experiments used to determine the separation of Eu/Am utilizing radiotracers were simpler compared to the adjacent lanthanide separation experiments. Both organic and aqueous phases were subsampled by 0.250 mL for each phase and placing them in polypropylene culture tubes that were sealed and placed in a germanium spectrometer. The germanium spectrometer is used to measure the amount of disintegrations/counts in each sample over a set time period. The total amount of counts over a time period is normalized to give CPM, which is then used to determine the D value using CPM in each phase in place of concentration. The D values of the ^{152}Eu and ^{241}Am are used in Eq. 3 to calculate the separation factor (*SF*).

$$SF_{Eu/Am} = \frac{D_{Eu}}{D_{Am}} \quad \textbf{(3)}$$

Instrumentation: The $^{152/154}$Eu and ^{241}Am in the organic and aqueous solutions were counted using Canberra Analyst pure Ge Gamma counter. The counting times were of a sufficient duration to ensure that the counting error would not affect the precision of the distribution ratios, when combined the volumetric, replicate and counting errors would be less then ±5%. The lanthanide concentrations in the aqueous solutions were measured using a Thermo Scientific XSeries II ICP-MS. The ICP-MS method and instrument set up are the same as previously reported in the literature.[4]

7.4 Appendix References

1. N. Yasarawan, K. Thipyapong, S. Sirichai and V. Ruangpornvisuti, Journal of Molecular Structure, 2013, **1031**, 144-151.

2. V. V. Romanovski, D. J. White, J. Xu, D. C. Hoffman and K. N. Raymond, Solvent Extraction and Ion Exchange, 1999, **17**, 55-71.

3. B. Weaver and F. A. Kappelmann, TALSPEAK: A New Method of Separating Americium and Curium From the Lanthanides by Extraction From an Aqueous Solution of an Aminopolyacetic Acid Complex with a Monoacidic Organophosphate or Phosphate, C. T. Division Report ORNL-3559, Oak Ridge National Laboratory, Oak Ridge, 1964.

4. J. Kim, Y. Oyola, C. Tsouris, C. R. Hexel, R. T. Mayes, C. J. Janke and S. Dai, Industrial & Engineering Chemistry Research, 2013, 52, 9433-9440.

7.5 Appendix 7B Figures and Tables for Chapter 7

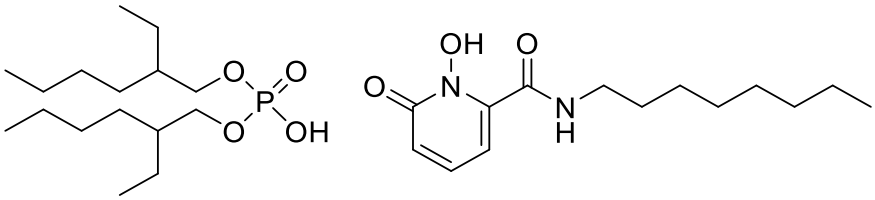

DEHPA Octyl-HOPO

Figure 7.1. Structure of DEHPA and its proposed replacement octyl-HOPO.

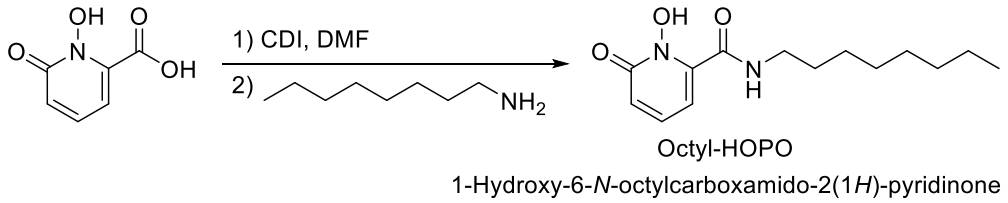

Figure 7.2. Reaction scheme for 1-Hydroxy-6-N-octylcarboxamido-2(1H)-pyridinone (Octyl-HOPO).

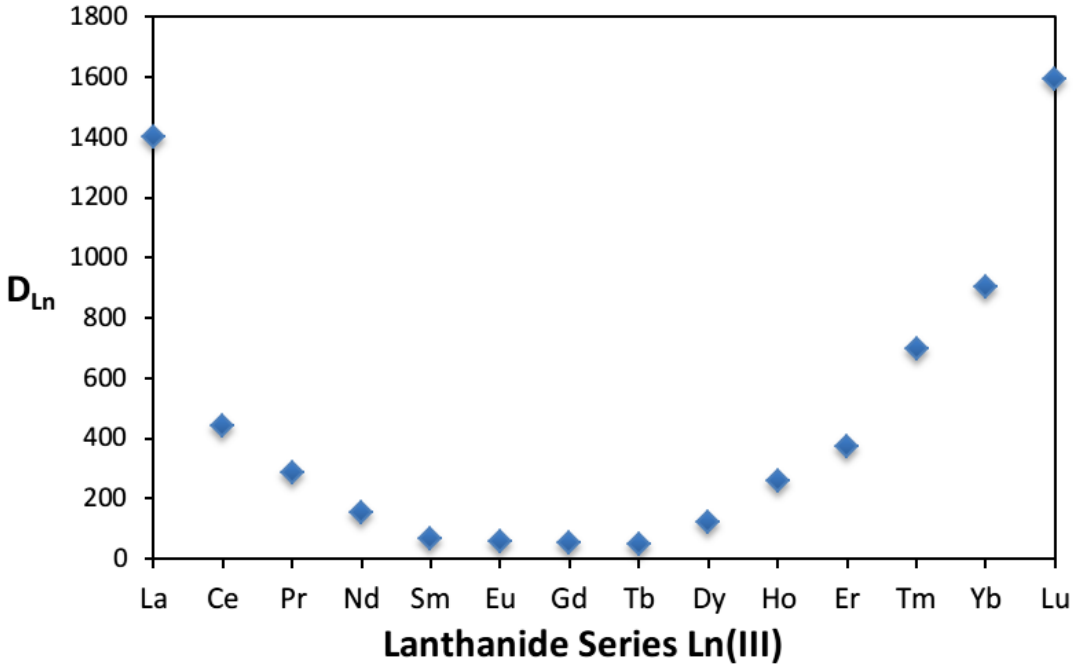

Figure 7.3. Extraction results of the solvent extractions under TALSPEAK conditions (DTPA holdback and citric acid buffer). For extraction 20 mmol of octyl-HOPO was dissolved in diisopropylbenzene (DIPB). An organic–to–aqueous phase ratio (O:A) of 1 was used and the samples were mixed for 3 hrs. at 25 °C.

Table 7.1. Comparison of distribution ratios for octyl-HOPO (HOPO) and DEHPA utilizing TALSPEAK conditions.

Ln(III)	HOPO	DEHPA
La	1.40×10^{3}	4.44×10^{-2}
Ce	4.42×10^{2}	7.02×10^{-2}
Pr	2.87×10^{2}	9.80×10^{-2}
Nd	1.53×10^{2}	1.11×10^{-1}
Sm	67.8	1.13×10^{-1}
Eu	56.9	1.14×10^{-1}
Gd	53.6	1.06×10^{-1}
Tb	46.3	1.08×10^{-1}
Dy	1.21×10^{2}	9.80×10^{-2}
Ho	2.58×10^{2}	7.16×10^{-2}
Er	3.72×10^{2}	5.40×10^{-2}
Tm	6.99×10^{2}	5.44×10^{-1}
Yb	9.05×10^{2}	3.89
Lu	1.59×10^{3}	7.39

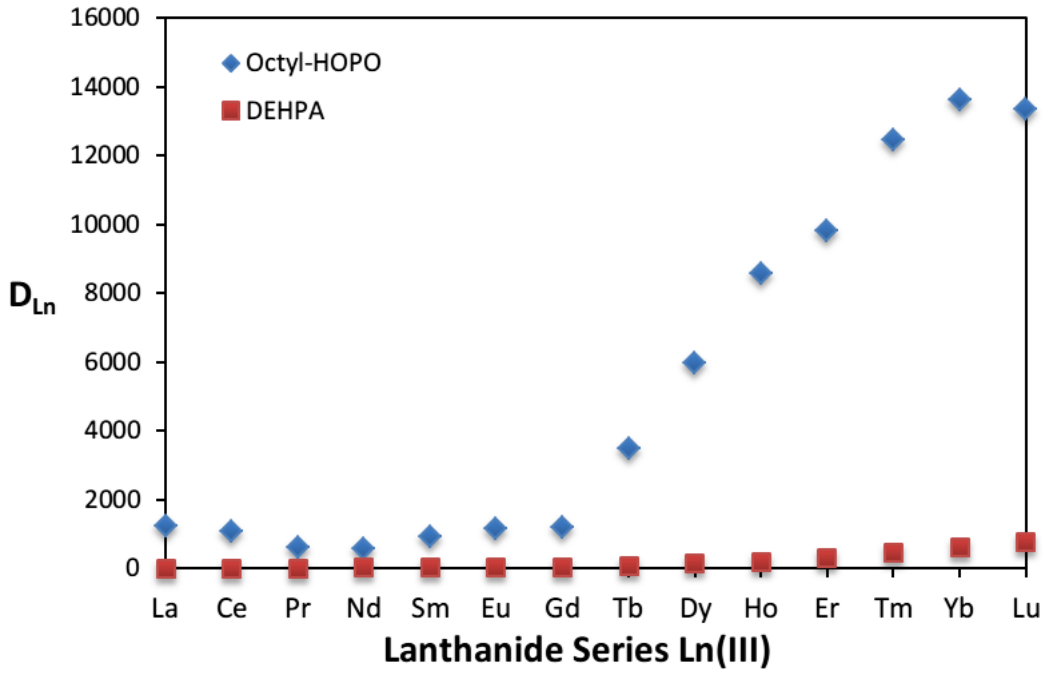

Figure 7.4. Extraction results for the lanthanides in a citric acid buffer in the absence of the DTPA holdback reagent. For the extraction experiments 20 mmol of either octyl-HOPO or DEHPA dissolved in DIPB was used. An O:A of 1 was used and samples were mixed for 3 hrs. at 25 °C.

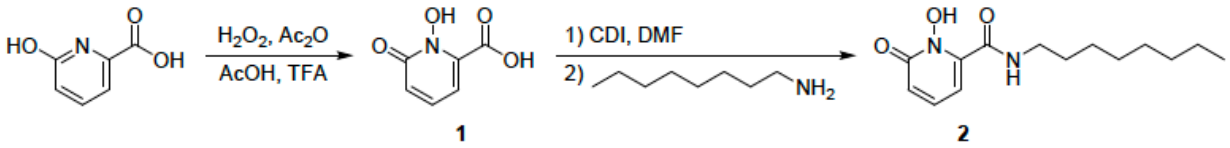

Figure 7.5. Synthesis scheme for 1-hydroxy-6-N-octylcarboxamido-2(1H)-pyridinone (octyl-HOPO, **2**).

Chapter 8 : Selective Separation of Americium from Europium Using 2,9-Bis(triazine)-1,10-phenanthrolines in Ionic Liquids: A New Twist on an Old Story

Publication Statement for Chapter 8

Reference for Original Article:

Williams N. J.; Dehaudt, J.; Bryantsev, V. S.; Luo, H.; Abney, C. W.; Dai, S. "Selective Separation of Americium from Europium Using 2,9-Bis(triazine)-1,10-phenanthrolines in Ionic Liquids: A New Twist on an Old Story." *Chem. Comm., 2017*, **53**, 2744-2748.

Individual Author Contribution(s):

Williams, N. J. – Co-conceptualized the use of BTPhens in ILs, radiochemistry experimentation, ran ion chromatography and analyzed data, prepared EXAFS samples and co-wrote and edited the article

Dehaudt, J. – Co-conceptualized the use of BTPhens in ILs, synthesized compounds and edited the article

Bryantsev, V.S. – Computational modeling and calculations for theoretical EXAFS fits and DFT

Luo, H. – Prepared solutions and edited the article

Abney, C. W. – Ran EXAFS of solutions, fit the data and co-wrote the article

Dai, S. – Edited the article

Journals Policy/Permission/Agreement for Reproduction of Article

Selective separation of americium from europium using 2,9-bis(triazine)-1,10-phenanthrolines in ionic liquids: a new twist on an old story

N. J. Williams, J. Dehaudt, V. S. Bryantsev, H. Luo, C. W. Abney and S. Dai, *Chem. Commun.*, 2017, **53**, 2744
DOI: 10.1039/C6CC09823A

If you are not the author of this article and you wish to reproduce material from it in a third party non-RSC publication you must formally request permission using RightsLink. Go to our Instructions for using RightsLink page for details.

Authors contributing to RSC publications (journal articles, books or book chapters) do not need to formally request permission to reproduce material contained in this article provided that the correct acknowledgement is given with the reproduced material.

Reproduced material should be attributed as follows:

- For reproduction of material from NJC:
  Reproduced from Ref. XX with permission from the Centre National de la Recherche Scientifique (CNRS) and The Royal Society of Chemistry.
- For reproduction of material from PCCP:
  Reproduced from Ref. XX with permission from the PCCP Owner Societies.
- For reproduction of material from PPS:
  Reproduced from Ref. XX with permission from the European Society for Photobiology, the European Photochemistry Association, and The Royal Society of Chemistry.

A version of this chapter was originally published by Neil J. Williams, Jérémy Dehaudt, Vyacheslav S. Bryantsev, Huimin Luo, Carter W. Abney, and Sheng Dai

Williams N. J.; Dehaudt, J.; Bryantsev, V. S.; Luo, H.; Abney, C. W.; Dai, S. "Selective Separation of Americium from Europium Using 2,9-Bis(triazine)-1,10-phenanthrolines in Ionic Liquids: A New Twist on an Old Story." *Chem. Comm., 2017*, **53**, 2744-2748.

The article used as Chapter 8 was modified in the following manner; the formatting was adapted to fit the formatting required by the University of Tennessee Knoxville, the figures and tables were renumbered to make all figures in the ensuing document contiguous. The work/research of the done by the student in the articles is as follows co-conceptualized the idea of using BTPhens in ILs with Jérémy Dehaudt, conducted radiochemical experiments to determine selectivity for minor actinides over lanthanides, prepared the solutions for EXAFs, co-wrote the article with Carter Abney.

Abstract

Bis-triazine phenanthrolines have shown great promise for f-block metal separations, attributable to their highly preorganized structure, nitrogen donors, and more enhanced covalent bonding with actinides over lanthanides. However, their limited solubility in traditional solvents remains a technological bottleneck. Herein we report our recent work using a simple 2,9-bis(triazine)-1,10-phenanthroline (Me-BTPhen) dissolved in an ionic liquid (IL), demonstrating the efficacy of IL extraction systems for the selective separation

of americium from europium, achieving separation factors in excess of 7500 and selectively removing up to 99% of the americium. Characterization of the coordination environment was performed using a combination of X-ray absorption fine structure spectroscopy (XAFS) and density functional theory (DFT) calculations.

8.1 Introduction

A growing global population combined with rapid development of emerging economies and a universal desire for improved standards of living drives an increasing demand for clean, renewable, and affordable sources of energy.[1,2] Although great effort has been devoted toward the development and deployment of renewable energy sources, e.g. solar and wind power, such technologies are inherently intermittent, requiring either extensive over-building to account for day-to-day variabilities, or installation of infrastructure to store power for increased delivery during times of high demand.[3] In contrast, nuclear energy remains the only mature, carbon neutral technology capable of sustained base-load power generation. Although comprising only 15% of the global power production portfolio,4 their use in place of coal-fired power plants has nevertheless afforded dramatic environmental and public health benefits; over the past three decades, nuclear power has prevented the generation of 64 Gt CO2-equivalent greenhouse gases and more than 1.84 million air pollution-related deaths.[4,5]

One major criticism of nuclear power is the generation of spent nuclear fuel, for which few (if any) long-term disposal solutions are available, and the volume of which should be

minimized for the sake of safety, proliferation resistance, and economics. Efficient separation of fission products and other spent fuel constituents is necessary to enable various disposal or recycle options. The minor actinides (An(III)), such as americium (Am(III)), are an example of such undesirable spent nuclear fuel constituents, as they undergo alpha decay6 and are deleterious to the stability of borosilicate glass wasteforms. Unfortunately, the selective separation of Am(III) is challenging due to their similar chemical reactivity and physical properties as lanthanides (Ln(III)) which are also present as fission products in spent nuclear fuel.

The comparatively recent discovery and development of bis(3,4-dimethyltriazine)-pyridines (Me-BTPs),[7,8] shown in **Figure 8.1**, dramatically improved the selectivity for minor actinides over other fission products. It was determined that highly preorganized ligands possessing electron-donating substitutents on a rigid 1,10-phenathroline backbone greatly increased recovery of Am(III) from acidic waste media.[9-13] Unfortunately, the 2,9-bis(3,4-diemthyltriazine)-1,10-phenathrolines (Me-BTPhens) are insoluble in the traditional organic solvents utilized in separations processes, requiring the addition of alcohol modifiers or use of expensive fluorinated solvents.[9,14] While more synthetically complex BTPhens have been made in an attempt to improve solubility,[14,15] only modest improvements in performance have been achieved in common hydrocarbons due to the disfavored energeics of forming highly charged metal-ligand complexes in nonpolar solvents. Preservation of charge balance either requires the undesirable co-extraction of counterions or addition of an organic-soluble cation exchanger. While

BTPhen ligands display vast potential for Am(III)/Ln(III) separations, there remains tremendous need for fundamental breakthroughs in how they can be practically and efficiently deployed.

One way to alleviate the problems discussed above is to substitute ionic liquids (ILs) in place of traditional molecular solvents. ILs have a proven track record in metal ion separations[16-18] and are capable of dissolving otherwise insoluble compounds,[19,20] can readily accommodate highly charged metal-ligand complexes, and can achieve charge balance through exchange of cationic imidazolium moieties into the aqueous phase.[21,22] Earlier studies have reported BTPs dissolved in ILs can achieve remarkable Am(III)/Ln(III) separation factors (SFAm/Eu > 3000),[23,24] suggesting that if ILs could serve as a solubilizing system for BTPhens, significant improvements in separation performance could be achieved. Herein, we report the efficacy of Me-BTPhen dissolved in ILs for the separation of Am(III) from Eu(III) in nitric acid media, as well as an investigation of the resulting metal-ligand complex through application of X-ray absorption fine structure (XAFS) spectroscopy and density functional theory (DFT) calculations.

2,9-bis(3,4-dimethyl-1,2,5-triazin-3-yl)-1,10-phenanthroline (Me-BTPhen) was made following previously reported synthetic methods.[9,14] Liquid-liquid extraction studies were done using the radioisotopes ^{241}Am(III) and $^{152/154}$Eu(III) to track and quantify the removal of each cation by the Me-BTPhen. Procedures for both synthesis and extraction experiments are provided in the appendix of Chapter 8.

The performance of Me-BTPhen for An(III)/Ln(III) separation was investigated in three different solvents: the IL solvent chloroform (CHCl3), trifluoromethylphenyl sulfone (known as FS-13), and the IL 1-butyl-3-methylimidazolium bis(trifluoromethylsulfonyl)imide (hereafter referred to as [C4mim][NTf2]). Although Me-BTPhen dissolved into each solvent at 4 mM, when mixed with the nitric acid solution only the [C4mim][NTf2] system was able to achieve an effective extraction of the radioisotopes. In $CHCl_3$, the Me_2-BTPhen would first complex then subsequently partition back into the aqueous phase. In FS-13 the ligands would complex and then precipitate at the aqueous-organic interface. The poor performance of Me-BTPhen in these molecular solvents is most likely due inability to achieve charge balance in the organic phase without extraction of three nitrate anions, and the poor solubility of the resulting highly polar metal-ligand-nitrate complex in the organic solvent.

When $[C_4mim][NTf_2]$ was used, the recovery of Am(III) was found to be nearly complete at $\geq$ 99.0 % removal at pH = 1, while the amount of Eu removed was $\leq$ 1.19 %. This affords a separation factor greater than 7500, which exceeds the next best separation factor reported with triazine ligand by 2.5×.23 When the concentration of the nitric acid increased, separation factors decreased drastically due to marked suppression of the amount of Am(III) extracted, while the uptake of Eu(III) increased slightly. This result is most likely due to the increasing ionic strength of the aqueous phase which retards the cation-exchange mechanism and thus prevents charge balance in the organic

solution.25, 26 The effective removal of Am(III) and Eu(III), corresponding separation factors, and percent efficiency for recovery of the Am and Eu are listed in **Table 8.1**.

Additional experiments were performed to investigate the structure of the ligand-metal complexes formed upon extraction into [C_4mim][NTf_2], in an effort to rationalize the remarkably high efficiency for Am removal. Speciation plots were developed using a 152/154Eu radiotracer to determine the stoichiometry of ligand-metal complex. The ligation of the metal species can be determined from the slope of the line in the plots, revealing the Me-BTPhen forms a 2-to-1 complex (**Figure 8.6**), as reported previously in the literature.[24,27] While clearly demonstrating the number of ligands bound to each metal, there remained uncertainty as to whether the IL solvent could also be participating in the extraction through direct interaction with the metal cation in the inner coordination sphere. In an effort to determine the complete structure of the complex in solution, we applied high level DFT calculations complemented by XAFS spectroscopy.

Eu(III) was chosen as an Am(III) surrogate for XAFS investigations due to possessing similar size and chemical reactivity while not presenting a radiological concern. Therefore, DFT calculations were performed on a series of Eu-Me-BTPhen complexes using the Gaussian 09.28 Selected calculations were also performed on the corresponding complexes with Am. The potential Eu complexes investigated consisted of 2 Me-BTPhen molecules and NO^{3-}, NTf_2^-, H_2O, OH^-, or no anion in the first coordination shell of the

metal ion. A figure displaying the geometrically optimized structures is given in **Figure 8.2**.

The coordination environment of the Eu-BTPhen complex in $[C_4mim][NTf_2]$ was also investigated through XAFS spectroscopy. XAFS data were collected at the Eu L(III)-edge (6977 eV) on beamline 11-2 at Stanford Synchrotron Radiation Lightsource, Data were processed and analyzed using open source fitting software.[29-31] Further details regarding data collection and processing are provided in the appendix for Chapter 8.

Principal component analysis of the nine normalized absorption datasets resulted in identification of only one mathematical component at the > 99.9% confidence level (**Figure 8.8**). This statistical approach reveals there is only one solution component contributing to the spectral response. DFT-optimized complexes (**Figure 8.2**) were used to prepare structure models for fitting to the EXAFS data. Reasonable preliminary fits were obtained for $[Eu(Me\text{-}BTPhen)_2]^{3+}$, $[Eu(Me\text{-}BTPhen)_2(H_2O)]^{3+}$, $[Eu(Me\text{-}BTPhen)_2(NO_3)]^{2+}$, and monodentate $[Eu(Me\text{-}BTPhen)_2(NTf_2)]^{2+}$. Similar to EXAFS spectra collected on $[Eu(CyMeBTPhen)_2(H_2O)](NO_3)_3$ crystals or the solvated compound in cyclohexanone,24 a shoulder is apparent at 1.5 Å in the Fourier transformed data, albeit more pronounced for the IL spectrum, and best resolved by inclusion of a tightly coordinating water molecule. Similar spectral contributions cannot be reasonably achieved with a chelating NO^{3-} due to bond length considerations (**Figure 8.11**). This is further supported by a constant NO^{3-} concentration post-extraction, also indicating charge

balance is achieved by exchange of 3 cationic $[C_4mim]^+$ per Eu^{3+} rather than extraction of a $Eu(NO_3)_3$ complex. While the spectroscopic feature could be resolved with a monodentate-bound NTf_2^-, the sterics of this putatively coordinating ligand are unlikely to accommodate the short interatomic distance necessary. Importantly, a deprotonated $[Eu(BTPhen)(OH)]^{2+}$ model system also failed to provide an adequate fit of the data due to the commensurate lengthening of the first shell bond lengths for the BTPhen ligand (**Figure 8.12**). The aforementioned discarded fits are displayed in the SI, accompanied by their corresponding DFT-based model (**Figures 8.11-8.14**).

In contrast to complexes displaying inner sphere interactions between Eu and an anion, the comparatively simple 1:2 $[Eu(BTPhen)_2(H_2O)]^{3+}$ complex afforded a good fit of the EXAFS data in both first and second coordination spheres (**Figure 8.3**), as well as with regards to reasonable fitting parameters (**Table 8.2**). Efforts were made to improve the goodness of fit through inclusion of more multiple scattering paths, as well as through addition of a separate σ^2 for the tightly coordinating H_2O. However, application of the F-test revealed the apparent gains were not statistically significant.[32-34] Expansion of the data range and inclusion of distant scatterers was also attempted in an effort to fit the feature at 4 Å, but was ultimately unsuccessful. It is expected multiple scattering paths and scattering from distant atoms on Me-BTPhen ligands are convoluted with those from anions in the second coordination sphere, making definitive refinement of these features particularly challenging.

Based on the structural information obtained from DFT and EXAFS, we can speculate on the possible origin of enhanced Am(III) over Eu(III) selectivity in the IL solvent compared to traditional organic solvents. As nitrate anions are extracted together with the trivalent metal ions into the organic phase, present DFT calculations and crystallographic evidence[24] suggest that one nitrate can enter the inner sphere of the complex and adopt a chelate coordination mode. Substitution of bidentate nitrate in organic solvent by H_2O in $[C_4mim][NTf_2]$ leads to a shorter average metal ion-ligand bond distance and a stronger ligand binding, which could in turn lead to a higher selectivity for Am(III) over Eu(III).

8.2. Conclusions

In conclusion, we report the remarkable capability of a simple Me-BTPhen extractant to achieve highly efficient partitioning of Am(III) from Eu(III) upon dissolution in commercially available $[C_4mim][NTf_2]$. Effecting separation factors in excess of 7500, this constitutes the most efficient system reported to date for a single-strike separation, exceeding the previous best soft *N*-donor system by more than 2.5× and the current state-of-the-art organic system by 41×. Complementary characterization approaches including slope analysis, DFT calculations, and XAFS confirmed the formation of a 2:1 complex upon extraction into the IL phase, while fitting of the EXAFS spectrum confirmed a coordination number of 9 and supports the non-interaction of the anion in the first coordination sphere. Implementation of this technology in the processing of spent nuclear fuel could result in tremendous cost savings from reduction in facility footprint, diminished quantities of solvent, smaller volumes of final waste streams requiring long-term storage.

8.3 References

1. U.S. Energy Information Administration. International Energy Statistics, http://www.eia.gov/cfapps/ipdbproject/IEDIndex3.cfm, (accessed April 4, 2015, 2015).

2. BP, *Statistical Review of World Energy*, 2014.

3. C. J. Barnhart, M. Dale, A. R. Brandt and S. M. Benson, *Energy Environ. Sci.*, 2013, **6**, 2804-2810.

4. P. A. Kharecha and J. E. Hansen, *Environ. Sci. Technol.*, 2013, DOI: 10.1021/es3051197.

5. A. Markandya and P. Wilkinson, *The Lancet*, 2007, **370**, 979-990.

6. R. O'Brien and J. A. Katalenich, *Journal of Propulsion and Power*, 2011, **27**, 1131-1134.

7. Y. Wei, K. N. Sabharwal, M. Kumagai, T. Asakura, G. Uchiyama and S. Fujine, *Journal of Nuclear Science and Technology*, 2000, **37**, 1108-1110.

8. M. Hudson, M. Foreman, C. Hill, N. Huet and C. Madic, *Solvent Extraction and Ion Exchange*, 2003, **21**, 637-652.

9. F. W. Lewis, L. M. Harwood, M. J. Hudson, M. G. Drew, J. F. Desreux, G. Vidick, N. Bouslimani, G. Modolo, A. Wilden, M. Sypula, T. H. Vu and J. P. Simonin, *Journal of the American Chemical Society*, 2011, **133**, 13093-13102.

10. G. M. Cockrell, G. Zhang, D. G. VanDerveer, R. P. Thummel and R. D. Hancock, *Journal of the American Chemical Society*, 2008, **130**, 1420-1430.

11. R. D. Hancock, *Chem Soc Rev*, 2013, **42**, 1500-1524.

12. P. Kaufholz, G. Modolo, A. Wilden, F. Sadowski, D. Bosbach, C. Wagner, A. Geist, P. J. Panak, F. W. Lewis and L. M. Harwood, *Solvent Extr. Ion Exch.*, 2016, **34**, 126-140.

13. M. D. Ogden, S. I. Sinkov, M. Nilson, G. J. Lumetta, R. D. Hancock and K. L. Nash, *J. Solution Chem.*, 2013, **42**, 211-225.

14. L. M. Harwood, D. M. Laventine, A. Afsar and M. J. Hudson, *Heterocycles*, 2012, **86**, 1419.

15. F. W. Lewis, L. M. Harwood, M. J. Hudson, A. Geist, V. N. Kozhevnikov, P. Distler and J. John, *Chem. Sci.*, 2015, **6**, 4812-4821.

16. J. Dehaudt, N. J. Williams, I. A. Shkrob, H. Luo and S. Dai, *Dalton. Trans.*, 2016, **45**, 11624-11627.

17. X. Sun, C.-L. Do-Thanh, H. Luo and S. Dai, *Chem. Eng. J.*, 2014, **239**, 392-398.

18. X. Sun, H. Luo and S. Dai, *Talanta*, 2012, **90**, 132-137.

19. X. Sun, H. Luo and S. Dai, *Chem Rev*, 2012, **112**, 2100-2128.

20. M. Atanassova and V. Kurteva, *RSC Adv.*, 2016, **6**, 11303-11324.

21. M. L. Dietz and D. C. Stepinski, *Talanta*, 2008, **75**, 598-603.

22. M. L. Dietz and J. A. Dzielawa, *Chem. Commun.*, 2001, DOI: 10.1039/B104349H, 2124-2125.

23. A. Bhattacharyya, S. A. Ansari, T. Gadly, S. K. Ghosh, M. Mohapatra and P. K. Mohapatra, *Dalton Trans*, 2015, **44**, 6193-6201.

24. D. M. Whittaker, T. L. Griffiths, M. Helliwell, A. N. Swinburne, L. S. Natrajan, F. W. Lewis, L. M. Harwood, S. A. Parry and C. A. Sharrad, *Inorg. Chem.*, 2013, **52**, 3429-3444.

25. H. Zhou, Y. Ao, J. Yuan, J. Peng, J. Li and M. Zhai, *RSC. Adv.*, 2014, **4**, 45612-45618.

26. X. Sun, J. R. Bell, H. Luo and S. Dai, *Dalton. Trans.*, 2011, **40**, 8019-8023.

27. A. Bremer, D. M. Whittaker, C. A. Sharrad, A. Geist and P. J. Panak, *Dalton. Trans.*, 2014, **43**, 2684-2694.

28. M. J. Frisch, et al., *Gaussian 09 Revision D.01; Gaussian, Inc.:*, Wallingford, CT, 2009.

29. S. M. Webb, *Phys. Scr.*, 2005, **2005**, 1011.

30. B. Ravel and M. Newville, *J. Synchrotron Radiat.*, 2005, **12**, 537-541.

31. J. J. Rehr and R. C. Albers, *Rev. Mod. Phys.*, 2000, **72**, 621-654.

32. L. Downward, C. H. Booth, W. W. Lukens and F. Bridges, *AIP Conf. Proc.*, 2007, **882**, 129-131.

33. W. C. Hamilton, *Acta Crystallographica*, 1965, **18**, 502-510.

34. S. Calvin, *XAFS for Everyone*, CRC Press, Boca Raton, FL, 2013.

8.4 APPENDIX 8A Supplemental Information for Chapter 8

8.4.1 Materials and Synthetic Methods

Materials. All reagents were obtained from Aldrich in their purest form and used without further purification. The solvent trifluoromethylphnyl sulfone (FS-13) was obtained from Marshallton Research Laboratories and used as received. The 1-alkyl-3-methylimidazolium bis[(trifluoromethyl)-sulfonyl]amide ([C_4mim][NTf_2]) ionic liquid was obtained from Sigma-Aldrich. Europium-152/154 was obtained from Isotope Products (presently owned by Eckert & Ziegler) and americium-241was produced at Oak Ridge National Laboratory.

Synthetic Methods. ^{1}H and ^{13}C NMR spectra were recorded using a Varian VNMRS 500 MHz spectrometer. The chemical shifts at 25°C (given in parts per million) were referenced to the residual protonated solvent. The mass peaks for protonated molecules were determined using DART (direct analysis in real time) at the Mass Spectrometry Center located in the Department of Chemistry at the University of Tennessee. The DART analyses were performed using a JEOL AccuTOF-D time-of-flight mass spectrometer with a DART ionization source from JEOL USA, Inc. (Peabody, MA).

Me-BTPhen was prepared according to a literature procedure[1] with a slight modification for the last step (Scheme 8.1). Neocuproine **1** was oxidized using selenium dioxide. The resulting dialdehyde **2** was treated with hydroxylaminehydrochloride. The dioxime **3** was

then converted to the dinitrile 4. The latter was reacted with hydrazine hydrate to give the dicarbohydrazonamide **5**. Me-BTPhen was obtained by reaction of **5** with diacetyl in presence of triethylamine. Synthetic details for the last step and NMR spectra of Me-BTPhen are given below.

To a suspension of 1,10-phenanthroline-2,9-dicarbohydrazonamide **5** (800 mg, 2.72 mmol) in THF (50 mL) was added diacetyl (0.5 mL, 5.75 mmol, 2.1 eq) and Et_3N (5 mL). The mixture was refluxed for 24h. After cooling, the solvent was removed under vacuum and the residue was washed with Et_2O. The crude product was purified by silica gel column chromatography (CH_2Cl_2/MeOH, 100:0 to 70:30 v/v) to give the desired compound as a yellow powder (660 mg, 62%). ^{1}H NMR (500 MHz, $CDCl_3$): δ 2.81 (s, 6H), 2.84 (s, 6H), 7.94 (s, 2H), 8.47 (dd, 2H, *J* = 8.4 Hz, 0.5 Hz), 8.99 (dd, 2H, *J* = 8.4 Hz, 0.5 Hz). ^{13}C NMR (126 MHz, $CDCl_3$): δ 19.7, 21.6, 123.0, 127.7, 130.1, 137.5, 146.4, 152.9, 157.5, 160.0, 161.3. HRMS: *m/z*: 395.1741 [M + H^+]. $C_{22}H_{19}N_8^+$ requires 395.1732.

8.4.2 Determination of distribution ratios.

The distribution ratio (D_M) for extraction of trivalent metal ions (M^{3+}) is defined by

$$D_M = \frac{C_{M,org}}{C_{M,aq}}$$

In this equation, $C_{m,aq}$ and $C_{m,org}$ represent the counts per a minute for the isotopes of $^{152/154}$Eu or ^{241}Am in either the organic or aqueous phases, respectively. A volume ratio is needed in the calculation of distribution ratios to account for the difference in volume

between the two immiscible phases. In all of our experiments, the volume ratio was close to 1:1 v/v. Separation factors SF for the metal ions *M* and *M'* are defined from:

$$SF_{M/M'} = D_M / D_{M'}$$

Eu/Am measurements. The distribution ratios for extraction using radiotracer techniques were calculated by measuring the amount of radioactivity of both aqueous and organic phases at equilibrium. Counting efficiency (^{241}Am or ^{152,154}Eu gamma ray absorption in solid scintillators) is identical for both phases; hence, the distribution ratio is defined by the ratio of specific radioactivity *S* (Bq/mL) of element *M* in the IL vs. aqueous phases.

$$D_M = \frac{C_{IL,f}}{C_{IL,f}} \propto \frac{S_{org,f}}{S_{aq,f}}$$

An equal volume of both IL (containing 4 mM complexant) and aqueous phases, 0.4 mL of each were used, respectively. Each sample was individually spiked with a 10 μL solution containing 1.85 × 10^6 Bq/mL (50 μCi/mL) of each radiotracer respectively. The solutions were mixed using a rotating wheel set at 60 rpm for 3 h at 25±0.2 °C. (Initial studies were performed at 1, 3, and 24 h, with samples contacted for 3 and 24 h observed to have the same *D* values. Due to this observation, it was assumed that the samples achieved equilibrium by the 3 h time point. Samples contacted/mixed for 1 h had lower *D* values than those at 3 h. For the sake of brevity and consistency, all samples were contacted for 3 h). After 3 h the samples were centrifuged at 3,000 rpm for 5 min at 25 °C to ensure the phases separated from each other. Then a 100 μL aliquots were subsampled from each phase and placed into polypropylene tubes that were sealed with a cap. These tubes were then placed in a Canberra Gamma Analyst germanium

spectrometer to determine the amounts of ^{241}Am and ^{152,154}Eu present in each sample. Prior to testing these samples, a quality assurance calibration was performed. The organic and aqueous samples were counted for a period of 30 min to ensure an accurate measurement. Additional blank samples (no isotopes present in solution) were run to ensure no background subtraction was necessary. Once the data was collected the total counts for each isotope in the samples was normalized to give the average counts per minute.

8.4.3 Slope Analysis

To determine the stoichiometry of the metal–ligand complex a slope analysis experiment was conducted. This experiment made use of the $^{152/154}$Eu radiotracer employing similar techniques to those discussed in the above section discussing use of Eu and Am radiotracers. In this experiment the concentration of the Me-BTPhen was varied in [C_4mim][NTf_2]; the concentrations were as follows: 1.0, 3.0, 10.0, and 30.0 mM. The IL solutions were then contacted with 0.1 M HNO_3 which had been spiked with a 10 μL solution containing 50 μCi/mL of the Eu radiotracer.

From **Figure 8.7** above, the trend line associated with the D_{Eu} for Me-BTPhen has a slope of two indicating that the ligand-metal complex is likely 2-to-1 during the extraction process. These results correlate with the solutions structural data presented and discussed in the manuscript. Additionally the 2-to-1 structure has been shown to exist in crystal structures in the previous reported examples in the literature.[2]

8.4.4 Quantification of Extracted Nitrate

The amount of nitrate extracted was determined by Ion Chromatography (IC) using conductivity detection. The IC used was a Dionex ICS-5000+ Reagent-Free High-Pressure IC system, the detector was a conductivity detector, the columns used were a Thermo Scientific Dionex IonPac AS11-HC Hydroxide-Selective Anion-Exchange Column (4 x 250 mm) with a IonPac AG11-HC Guard Column (4 x 50 mm). The program used to run the instrument and process the data is Chromeleon version 6.2. The eluent used in the IC for the samples was 30 mM KOH, using a flow rate of 1.5 mL/min with the conductivity set at 112 mA. A calibration curve was made by dilution a purchased 1000 ppm nitrate standard purchased from Inorganic Ventures.

8.4.5 Computational Methods

DFT calculations were performed on a series of Eu-Me-BTPhen and Am- Me-BTPhen complexes using the Gaussian 09,[3] Revision D01, software package at the B3LYP[4, 5] level of theory. A standard 6-311+G** basis sets were used for all light atoms. F-elements were modelled using the large-core (LC) relativistic effective core potential (RECP) and the associated (7s6p5d2f) /[5s4p3d2f][6, 7] basis sets. Since LC RECP calculations include the 4f electrons in the core, they were performed on a pseudo singlet state configuration. Solvent corrections we included as single-point energies using a generic ionic liquid implicit solvation model, SMD-GIL,[8] with generic values of solvent descriptors. Cartesian coordinates of all the ligand-metal ion complexes accompanied by their electronic

energies obtained at the B3LYP/LC(7s6p5d2f)/[5s4p3d2f]/6-311+G** level are given in Section S5.

Comparison of the relative stability of 2:1 ligand-metal ion complexes with monodentate and chelate coordination of NTf_2^- indicated that the chelate form with Eu^{3+} and Am^{3+} was 0.13−2.3 kcal/mol more stable than the monodentate form in the gas phase, but it was 5.4−5.7 kcal/mol less stable in the presence of implicit solvent. With the NO_3^- anion, we could locate only the Eu(III) and Am(III) complexes in the chelate mode, whereas the complex in the monodentate mode were not a stationary point on the potential energy surface, which converged to the chelating species during the geometry optimization. Eu/Am-ligand bond distances for the DFT optimized 2:1 ligand-metal ion complexes are listed in **Table 8.3**

8.4.6 X-ray Absorption Fine Structure Spectroscopy

Data Collection and Processing. XAFS samples were prepared by mixing 2 mL of a 15 mM Me-BTPhen dissolved in $[C_4mim][NTf_2]$ with an equal volume of an aqueous solution of 15 mM $Eu(NO_3)_3$. The samples were mixed, then centrifuged to separate the two phases, then the top aqueous layer was removed by pipette and a fresh solution of $Eu(NO_3)_3$ was added to the IL solution and the process was repeated once more. The sample was contacted twice to ensure complete loading of the Me-BTPhen. After the second contact, 1.5 mL of Eu-loaded ionic liquid solution was pipetted into a screw-cap sample vial.

X-ray absorption data were collected at beamline 11-2 at Stanford Synchrotron Radiation Lightsource. Samples were inserted into a plexiglass sample box which was purged with He throughout the duration of the experiment. Spectra were collected at ambient temperature and pressures at the europium L_3-edge (6.977 keV) with fluorescence detection afforded by a Canberra 100-pixel Ge solid-state monolith detector. Sollar slits were used to decrease noise from x-ray scattering. Signal intensity was investigated both with and without use of a Cr-filter, with superior signal afforded when the filter was not used. A $Eu(NO_3)_3$ reference sample was measured simultaneously for energy calibration and data alignment. Samples were positioned on the beam to maximize fluorescence signal. The beam dimensions were 2 × 5 mm for all scans. Data were collected over four regions: -230 to -30 eV (10 eV step size, dwell time of 0.25 seconds), -30 to -5 eV (5 eV step size, dwell time of 0.5 seconds), -5 to 30 eV (1 eV step size), 3 $Å^{-1}$ to 13 $Å^{-1}$ (0.05 $Å^{-1}$ step size), with dwell time increasing as a function of k from 2 seconds at 3 $Å^{-1}$ to 16 seconds at 13 $Å^{-1}$. Data were not collected further in k-space due to the occurrence of the Eu L_{II}-edge (7.617 keV, 12.95 $Å^{-1}$). Nine scans were collected.

The data were reformatted using SixPack[9] then processed and analyzed using the Athena and Artemis programs of the IFEFFIT package based on FEFF 6.[10, 11] Reference foil data were aligned to the first zero-crossing of the second derivative of the normalized μ(E) data, which was subsequently calibrated to the literature E_0 for the europium L_{III}-edge (6.977 keV). Any contributions from the Eu L_{II}-pre-edge were removed by truncating all data sets at 7.578 keV. Spectra were averaged in μ(E) prior to normalization. The

background was removed and the data were assigned an Rbkg value of 1.1, less than one-half the value of the half-path length for the nearest scattering element, prior to normalizing to obtain a unit edge step.

EXAFS Analysis. The processed data set was initially qualitatively compared against scattering paths generated from DFT-derived potential structure models, as displayed in **Figure 8.9**. Inspection of the simulated direct scattering paths reveals all models display reasonable scattering paths for the majority of features, but that with the exception of $[Eu(Me\text{-}BTPhen)_2(OH)]^{2+}$, none are immediately capable of adequately fitting the shoulder observed at 1.5 Å. Of the remaining structure models, Eu-bound H_2O and monodentate-bound NTf_2^- both possess a single scattering path capable of shifting to fit this shoulder without inducing physically unreasonable distortions in the Me-BTPhen coordinating ligands. Accordingly, structure models generated from chelating NO_3^- and NTf_2^- were discarded. Notably, both of these discarded models also would require a first coordination shell of 10 atoms. The final model was intended to interrogate whether the large feature at 4 Å could be attributed to formation of dimeric Eu species. A search of the CCDC database reveald that while no 4:2 Me-BTPhen:M complexes had been reported, several related 4:2 phenanthroline (Phen):Eu complexes were known. However, inspection of the Eu-Eu scattering path (3.73 Å) for this complex (plotted in red in **Figure 8.9**) was not located in a position that would beneficially contribute to a fit of the experimental spectrum. Additionally, as BTPhen possesses more *N*-donor atoms than

Phen it would completely or (near completely) fill the Eu first coordination sphere, discouraging the prospects of forming a dimeric species.

8.4.7 Principal Component Analysis

The EXAFS data was initially fit with k-weighting of 1,2, and 3, then finalized with k^2-weighting in R-space. Structural parameters that were determined by the fits were the change in R_{eff} (ΔR_i), the relative mean square displacement of the scattering element (σ^2_i), the passive electron reduction factor (S_0^2), and the energy shift of the photoelectron, (ΔE_0). The data range used for fitting was 1.15 – 3.4 Å in R-space and 3 – 10.3 $Å^{-1}$ in k-space, affording 10 independent points, with the range identified to minimize truncation effects in k-space and avoid spectral contributions from the artifact of the Fourier transform at approximately 0.8 Å in R-space. The number of variables was not permitted to exceed 2/3 the number of independent points in keeping with the Nyquist criterion.[12, 13]

Preliminary models were constructed from all first and second shell single scattering paths, as well as all multiple scattering paths providing at least 15% of the contribution of the most intense single scattering peak and with half-path length less than 3.7 Å. We asserted any changes in half path length would be attributable to translation of the Me-BTPhen with respect to Eu, rather than distortion of bond lengths within the rigid and electronically delocalized ligand. Therefore, scattering path lengths were fitted with only two parameters (one for translation of the phenanthroline portion, the second for

translation of the triazine), while different mean square relative deviation parameters (σ^2) were afforded for each of the first two shells of coordinating atoms (**Figure 8.10**).

8.5 Appendix References

1. Laventine D. M., Afsar A., Hudson M. J. and H. L. M., *Heterocycles*, 2012, **86**, 1419-1429.

2. H. Zhou, Y. Ao, J. Yuan, J. Peng, J. Li and M. Zhai, *RSC. Adv.*, 2014, **4**, 45612-45618.

3. M. J. Frisch and e. al., *Journal*, 2009.

4. A. D. Becke, *J. Chem. Phys.*, 1993, **98**, 5648-5652.

5. C. Lee, W. Yang and R. G. Parr, *Phys. Rev. [Sect.] B*, 1988, **37**, 785-789.

6. M. Dolg, H. Stoll, A. Savin and H. Preuss, *Theor. Chim. Acta.*, 1989, **75**, 173-194.

7. A. Moritz, X. Cao and M. Dolg, *Theoretical Chemistry Accounts*, 2006, **117**, 473-481.

8. V. S. Bernales, A. V. Marenich, R. Contreras, C. J. Cramer and D. G. Truhlar, *J Phys Chem B*, 2012, **116**, 9122-9129.

9. S. M. Webb, *Phys. Scr.*, 2005, **2005**, 1011.

10. B. Ravel and M. Newville, *J. Synchrotron Radiat.*, 2005, **12**, 537-541.

11. J. J. Rehr and R. C. Albers, *Rev. Mod. Phys.*, 2000, **72**, 621-654.

12. S. D. Kelly, K. M. Kemner, J. B. Fein, D. A. Fowle, M. I. Boyanov, B. A. Bunker and N. Yee, *Geochim. Cosmochim. Acta*, 2002, **66**, 3855-3871.

13. S. Calvin, *XAFS for Everyone*, CRC Press, Boca Raton, FL, 2013.

8.6 Appendix 8B Figures and Tables for Chapter 8

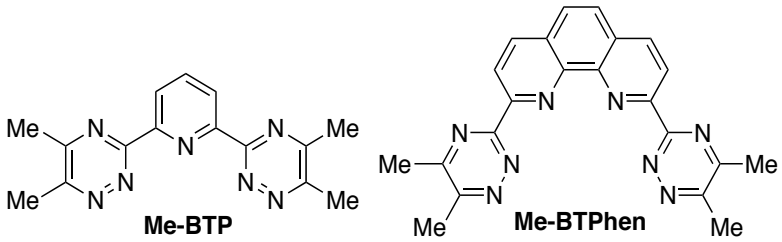

Figure 8.1. Structures of bis-triazine heterocycles.

Table 8.1. Extraction values (*D*), separation factors (*SF*), and percent recovery of Am and Eu by 4 mM Me-BTPhen for various nitric acid concentrations.

$[NO_3^-]$	D_{Am}	D_{Eu}	$SF_{Am/Eu}$	%Am	%Eu
0.1	94.9	0.0120	7857.1	99.0	1.19
0.5	3.25	0.132	24.6	76.47	11.67
1.0	1.07	0.152	7.0	51.57	13.21

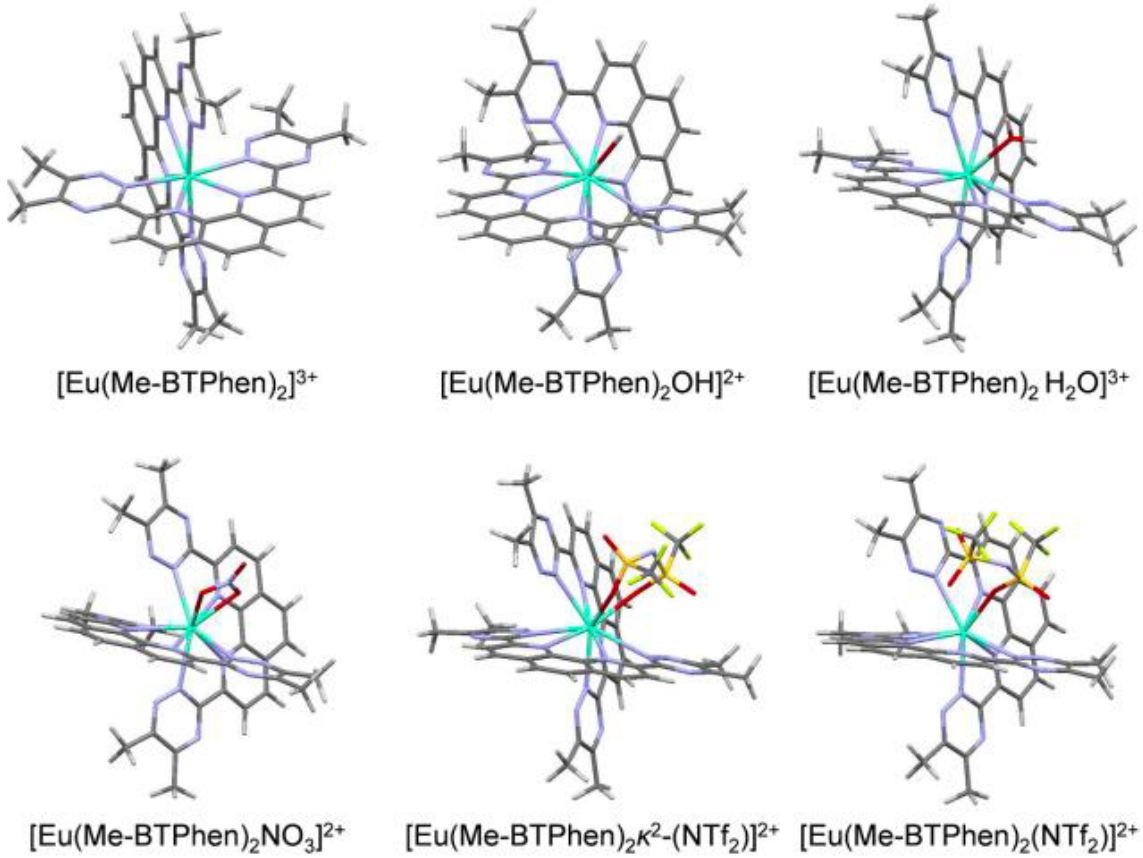

Figure 8.2. Geometry optimized Eu-Me-BTPhen complexes obtained from DFT calculations. The name of the complex is provided below the corresponding structure. Eu is turquoise, C grey, O red, S yellow, and H white.

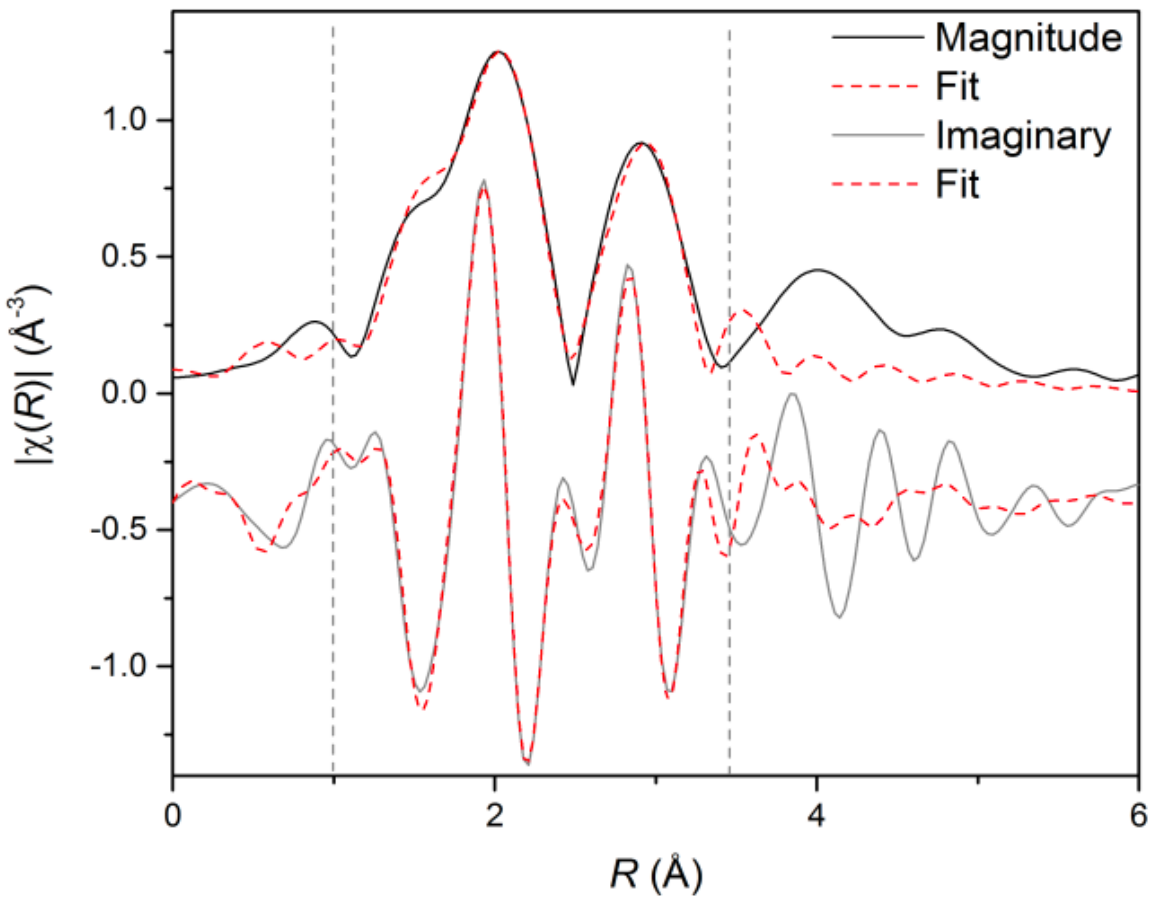

Figure 8.3. Fourier transform of the Eu LIII-edge EXAFS spectrum in *R*-space (black line), with accompanying fit afforded by the $[Eu(BTPhen)_2(H_2O)]^{2+}$ model. The imaginary component (grey line) and fit are offset beneath. Grey dashed lines denote the fit window.

Table 8.2. Data for EXAFS fit with $[Eu(Me\text{-}BTPhen)_2(H_2O)]^{2+}$ Structure Model.

Path	Coord. No.	Bond Length (Å)	σ^2 $(\times 10^{-3}\ \text{Å}^2)$
$Eu \rightarrow OH_2$	1	1.93 ± 0.02	4.9 ± 0.09
$Eu \rightarrow N_{phen}$	4	2.53 ± 0.02	4.9 ± 0.09
$Eu \rightarrow N_{azine(1)}$	4	2.55 ± 0.01	4.9 ± 0.09
$Eu \rightarrow C_{phen}$	4	3.39 ± 0.02	2 ± 0.1
$Eu \rightarrow N_{azine(2)}$	4	3.43 ± 0.01	2 ± 0.1
$Eu \rightarrow C_{azine}$	8	3.44 ± 0.01	2 ± 0.1
$Eu \rightarrow N_{phen} \rightarrow C_{phen}$	24	3.64 ± 0.02	7 ± 0.1
$E_0 = 9.5 \pm 0.8$		$R = 0.96\%$	${\chi_\nu}^2 = 32.7$

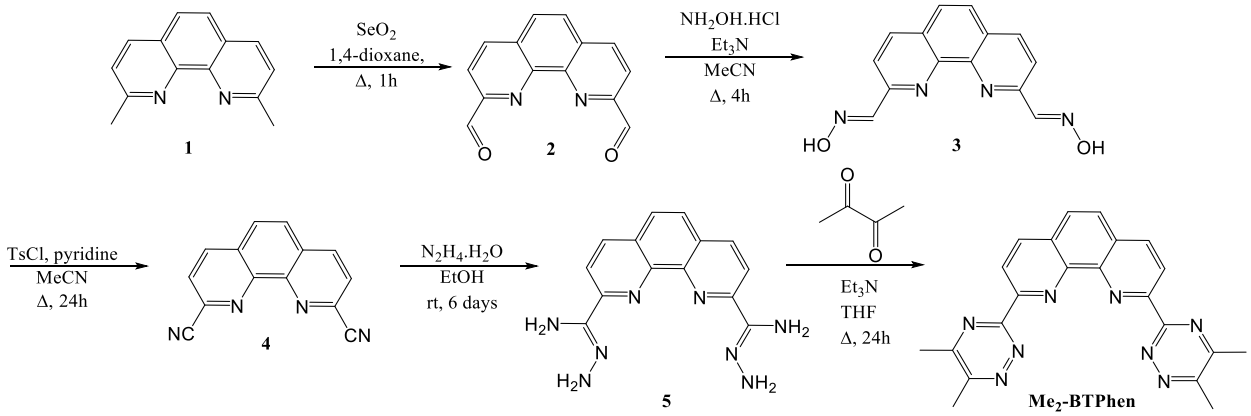

Figure 8.4. Synthetic route for the preparation of Me$_2$-BTPhen.

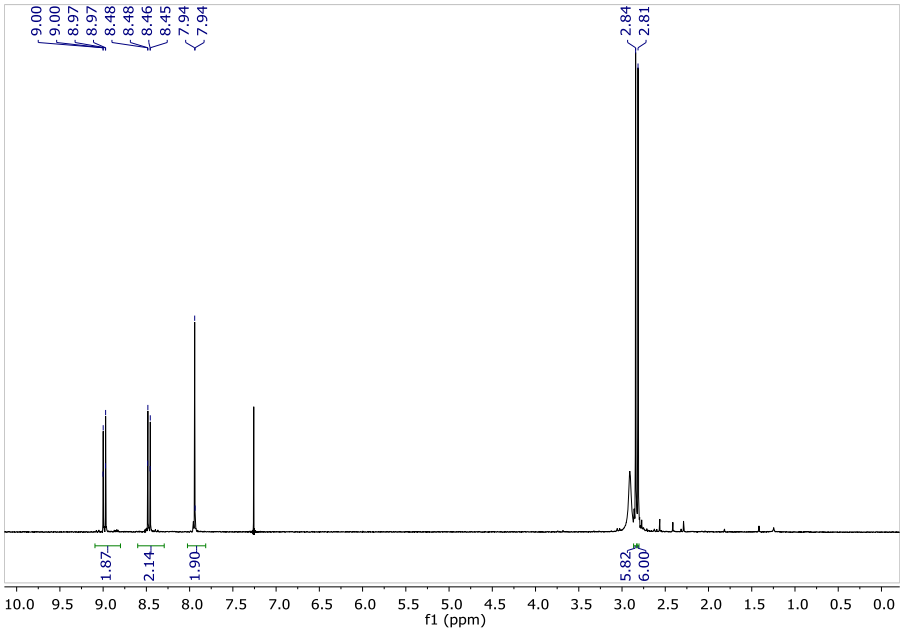

Figure 8.5. ^{1}H NMR of Me_2-BTPHen in $CDCl_3$

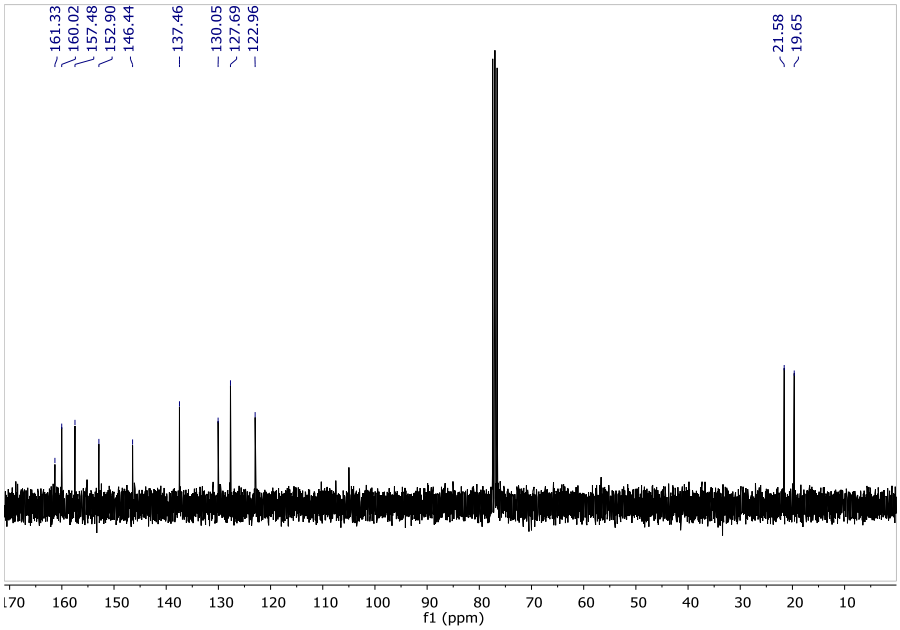

Figure 8.6. ^{13}C NMR of Me_2-BTPhen in $CDCl_3$.

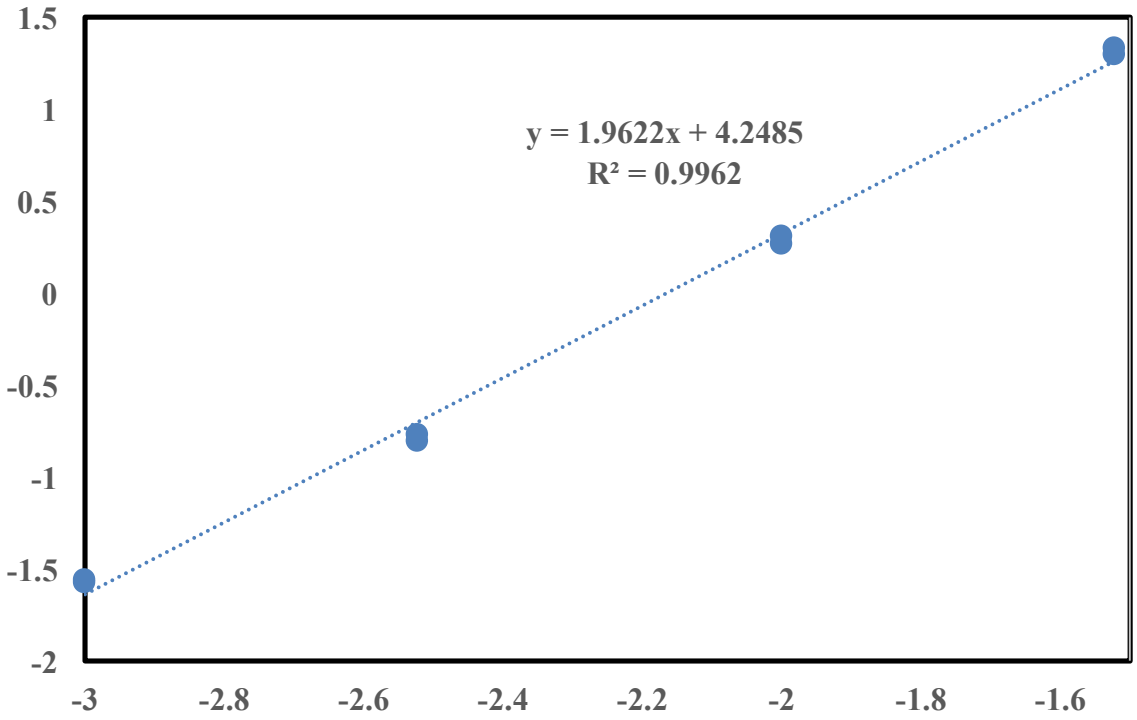

Figure 8.7. Slope Analysis of Me-BTPhen with Eu extracted from 0.1 M HNO_3. The y-axis represents the logD_{Eu} and the x-axis is the log[Me-BTPhen].

Table 8.3. Eu/Am-Ligand Bond Distances in Å for Geometrically Optimized Molecules as Determined by DFT Calculations.

	No Anion	OH^-	H_2O	NTf_2^- (mono)	NO_3^- (chelate)	NTf_2^- (chelate)
$O_{Anion-1}$	---	2.126/2.194	2.570/2.692	2.436/2.492	2.537/2.584	2.551/2.602
$O_{Anion-2}$	---	---	---	---	2.539/2.587	2.568/2.614
N_{Phen-1}	2.563/2.634	2.637/2.696	2.571/2.635	2.582/2.645	2.633/2.698	2.630/2.667
N_{Phen-2}	2.564/2.634	2.638/2.697	2.594/2.636	2.591/2.655	2.637/2.699	2.667/2.691
N_{Phen-3}	2.564/2.634	2.640/2.706	2.595/2.661	2.593/2.659	2.637/2.718	2.605/2.714
N_{Phen-4}	2.564/2.635	2.646/2.711	2.611/2.662	2.599/2.664	2.663/2.719	2.659/2.721
$N_{Azide-1}$	2.587/2.635	2.703/2.738	2.611/2.656	2.636/2.680	2.652/2.695	2.658/2.700
$N_{Azide-2}$	2.587/2.636	2.706/2.748	2.646/2.657	2.640/2.686	2.652/2.695	2.684/2.726
$N_{Azide-3}$	2.588/2.636	2.712/2.752	2.657/2.702	2.656/2.700	2.684/2.729	2.705/2.737
$N_{Azide-4}$	2.588/2.637	2.714/2.758	2.657/2.703	2.656/2.701	2.685/2.730	2.713/2.746
Average Coord. #	*2.576/2.635* *8*	*2.614/2.667* *9*	*2.599/2.667* *9*	*2.599/2.654* *9*	*2.635/2.685* *10*	*2.644/2.692* *10*

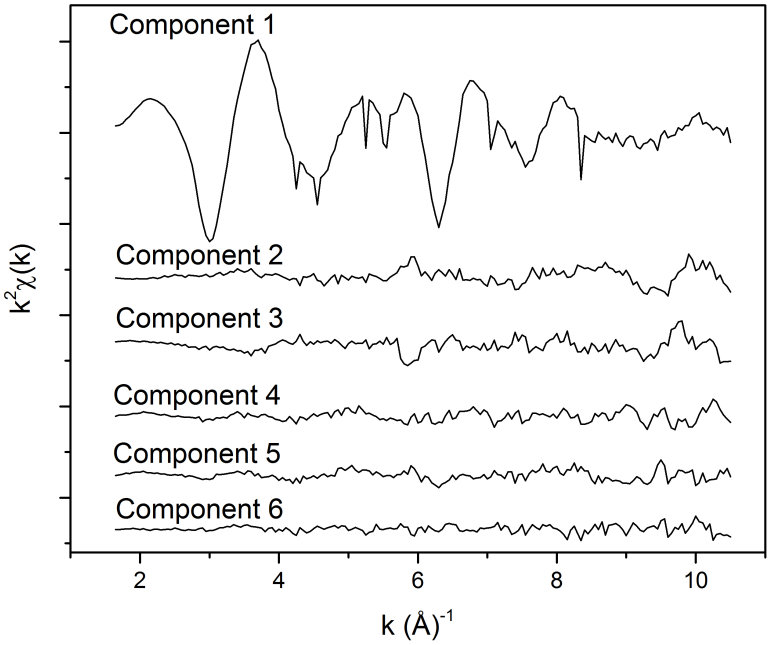

Figure 8.8. The first six principal components derived from nine Eu L_{III}-edge k^2-weighted EXAFS spectra of a Eu solution with 7.5 mM Me-BTPhen in an ionic liquid solvent. Components 7-9 (not shown) are similar to components 2 – 6. These data reveal only one mathematical component in the EXAFS spectra, indicating an adequate fit should be achievable from a single appropriate structure model.

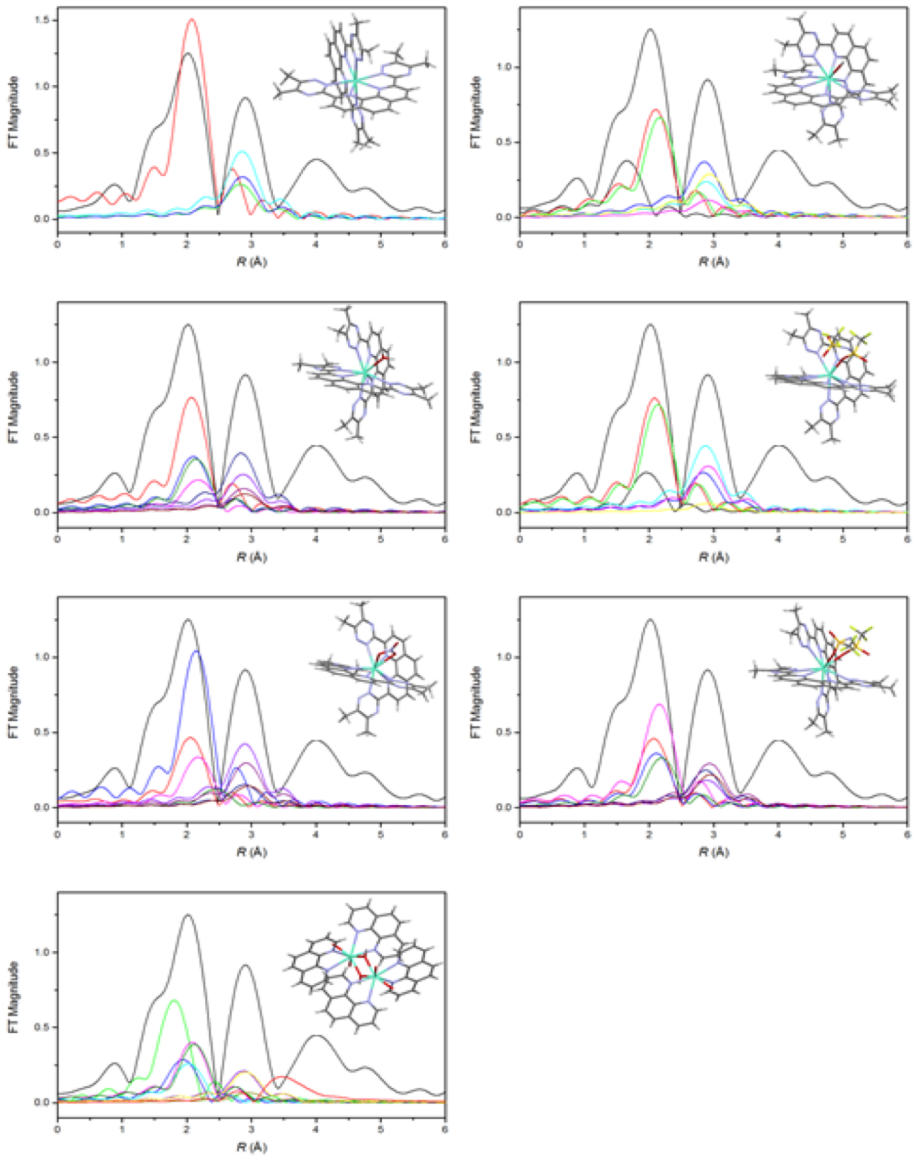

Figure 8.9. Single scattering paths for potential structure models compared against experimental EXAFS data, ordered by increasing coordination number and first-shell bond length. Representative DFT-calculated structures are provided in the upper corner of their corresponding spectrum. Top row, left to right: No anion, H^-; second row, left to right: H_2O, NTf_2 (monodentate); third row, left to right: NO_3 (chelate), NTf_2 (chelate); bottom row: $Eu_2(Phen)_2(OH)_2$ dimer.

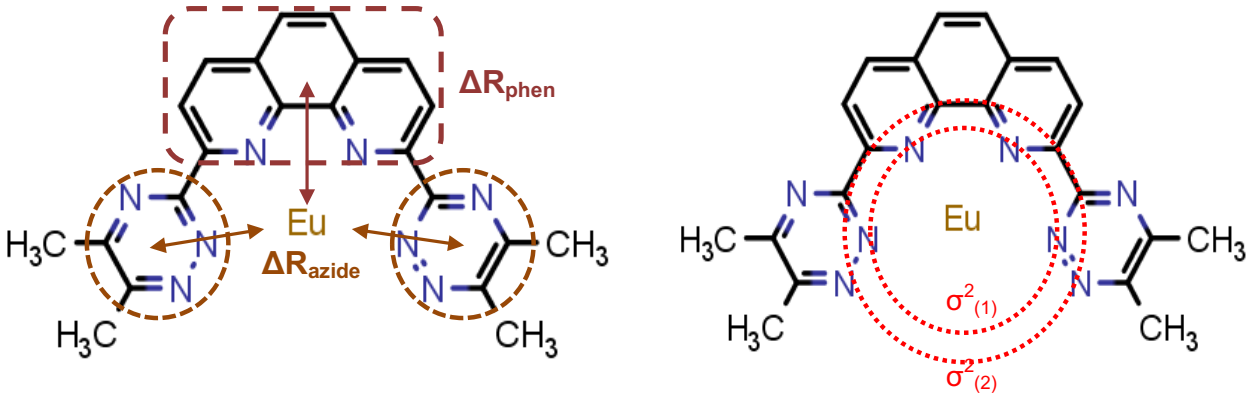

Figure 8.10. Assignment of ΔR and σ^2 parameters for the Me-BTPhen ligands.

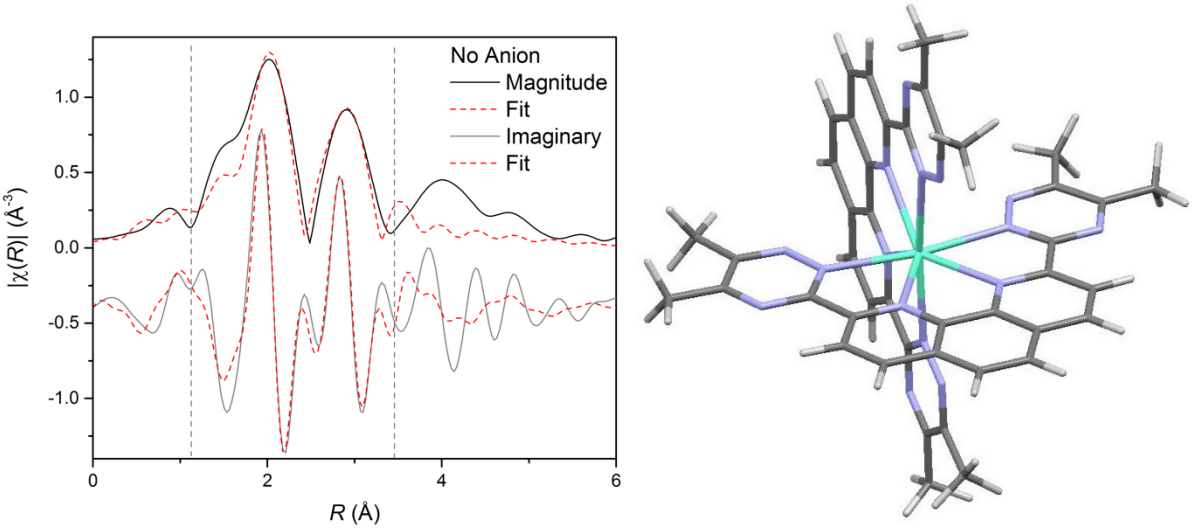

Figure 8.11. (Left) Rejected XAFS fit from structure model $[Eu(Me\text{-}BTPhen)_2]^{3+}$. (Right) DFT-optimized structure model used for preparation of the structure model.

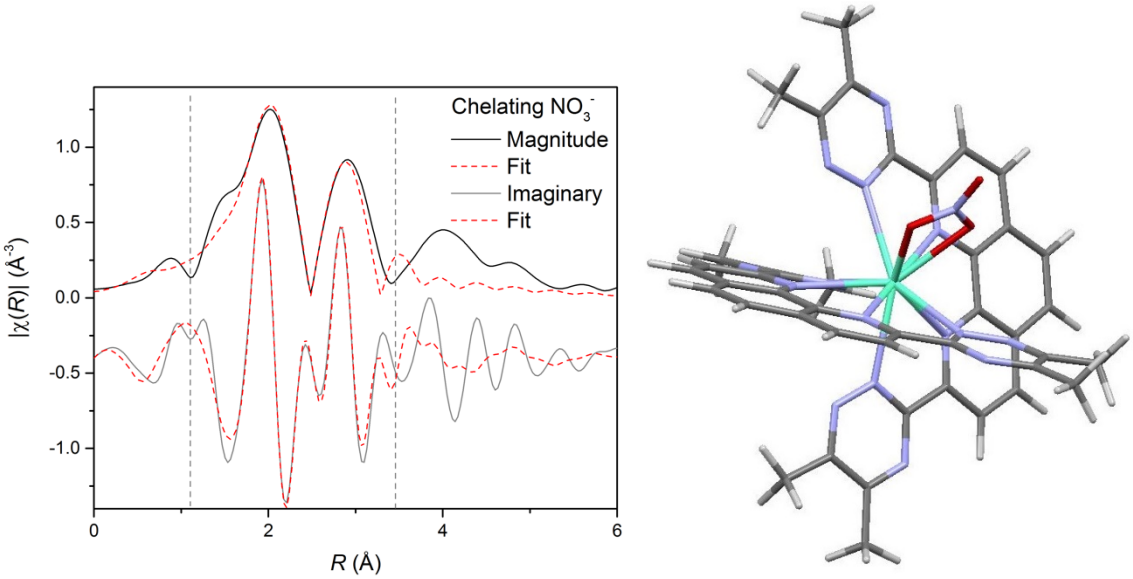

Figure 8.12. (Left) Rejected XAFS fit from structure model $[Eu(Me\text{-}BTPhen)_2NO_3]^{2+}$. (Right) DFT-optimized structure model used for preparation of the structure model.

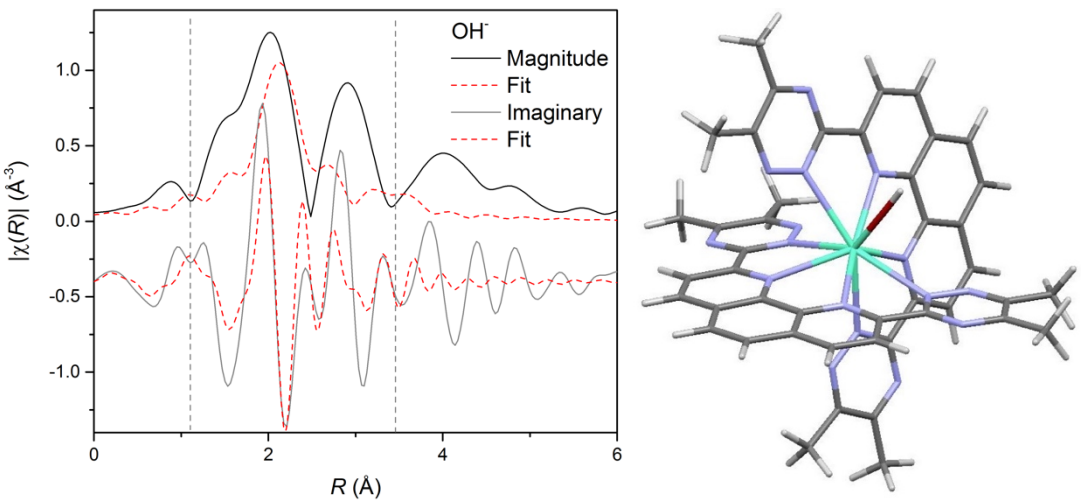

Figure 8.13. (Left) Rejected XAFS fit from structure model $[Eu(Me\text{-}BTPhen)_2OH]^{2+}$. (Right) DFT-optimized structure model used for preparation of the structure model.

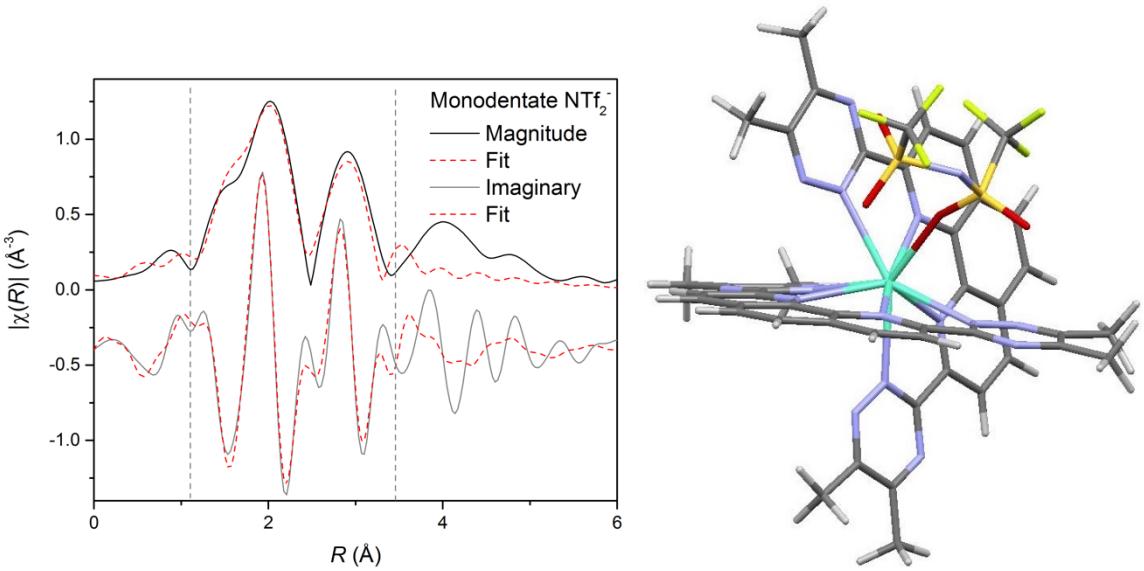

Figure 8.14. (Left) Rejected XAFS fit from structure model $[Eu(Me\text{-}BTPhen)_2NTf_2]^{2+}$. (Right) DFT-optimized structure model used for preparation of the structure model.

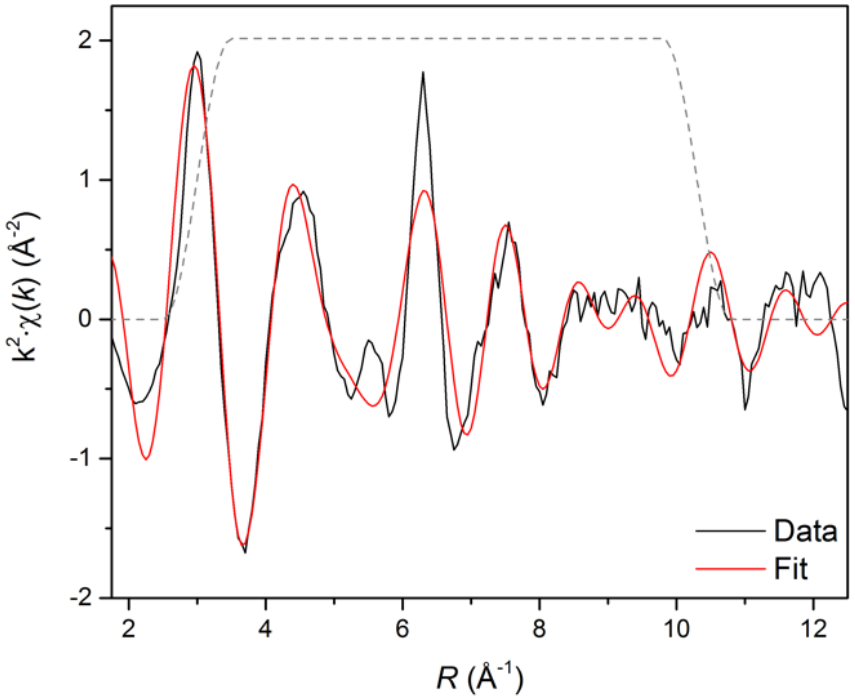

Figure 8.15. k^2-weighted $\chi(k)$ EXAFS data and fit for $[Eu(Me\text{-}BTPhen)_2(H_2O)]^{3+}$.

Chapter 9 : Selective separation of trivalent f-ions using 1,10-phenanthroline-2,9-dicarboxamide ligands in ionic liquids

Publication Statement for Chapter 9

Reference for Original Article:

Dehaudt, J.; Williams N.J.; Skrob, I.A.; Luo, H.; Dai, S. "Selective separation of trivalent f-ions using 1,10-phenanthroline-2,9-dicarboxamide ligands in ionic liquids." *Dalton Trans.* **2016**, 45, 11624-11627.

Individual Author Contribution(s):

Dehaudt, J. – Co-conceptualized the use of task-specific ILs for Eu/Am separations, synthesized compounds and edited the article

Williams, N. J. – Radiochemistry experimentation, ran ICP-MS and analyzed data, and edited the article

Skrob, I.A. – Computational modeling and calculations and wrote the article

Luo, H. – Prepared solutions and edited the article

Dai, S. – Co-conceptualized the use of task-specific ILs for Eu/Am separations, edited the article

Journals Policy/Permission/Agreement for Reproduction of Article

Selective separation of trivalent f-ions using 1,10-phenanthroline-2,9-dicarboxamide ligands in ionic liquids

J. Dehaudt, N. J. Williams, I. A. Shkrob, H. Luo and S. Dai, *Dalton Trans.*, 2016, **45**, 11624

DOI: 10.1039/C6DT01800A

If you are not the author of this article and you wish to reproduce material from it in a third party non-RSC publication you must formally request permission using RightsLink. Go to our Instructions for using RightsLink page for details.

Authors contributing to RSC publications (journal articles, books or book chapters) do not need to formally request permission to reproduce material contained in this article provided that the correct acknowledgement is given with the reproduced material.

Reproduced material should be attributed as follows:

- For reproduction of material from NJC:
  Reproduced from Ref. XX with permission from the Centre National de la Recherche Scientifique (CNRS) and The Royal Society of Chemistry.
- For reproduction of material from PCCP:
  Reproduced from Ref. XX with permission from the PCCP Owner Societies.
- For reproduction of material from PPS:
  Reproduced from Ref. XX with permission from the European Society for Photobiology, the European Photochemistry Association, and The Royal Society of Chemistry.

A version of this chapter was originally published by Jérémy Dehaudt, Neil J. Williams, Ilya A. Shkrob, Huimin Luo, and Sheng Dai in *Dalton Transactions*

Dehaudt, J.; Williams N.J.; Skrob, I.A.; Luo, H.; Dai, S. “Selective separation of trivalent f-ions using 1,10-phenanthroline-2,9-dicarboxamide ligands in ionic liquids.” *Dalton Trans.* **2016**, 45, 11624-11627.

The article used as Chapter 9 was modified in the following manner; the formatting was adapted to fit the formatting required by the University of Tennessee Knoxville, the figures and tables were renumbered to make all figures in the ensuing document contiguous. The work/research of the done by the student in the articles is as follows ran the inductively couple plasma mass spec experiments to determine the selectivity of the phenanthroline based TS-IL for specific lanthanides, conducted radiochemical experiments to determine selectivity for minor actinides over lanthanides, assisted in the writing of the electronic supplemental information section and editing of the main article.

Abstract

1,10-Phenanthroline-2,9-dicarboxamide complexants decorated with alkyl chains and imidazolium cations have been studied for extraction of trivalent f-ions into imidazolium ionic liquids. The dicationic complexants are shown to extract Am over Eu with separation factors >50 and high extraction efficiencies. The different size selectivities

for lanthanide ions were observed for these two types of complexants, highlighting the importance of the positive charge in controlling both extraction efficiencies and extraction selectivities.

9.1 Introduction

A major concern in the nuclear fuel cycle is long-term radiotoxicity resulting from the slow decay of plutonium and minor actinides (Am and Cm). While plutonium can be removed and recycled into fuels using the conventional PUREX process,[1] the further separation and removal of minor actinides (An) from fission products such as lanthanides (Ln) can reduce the quantity of radioactive wastes that must be placed in long-term storage. This can lead to improved options for underground disposal or transmutation. Apart from the above separation need for lanthanides, advanced separation technologies targeted to lanthanides are essential to the efficient recycling of lanthanides that are critical materials with growing demand in applications such as artificial lighting, wind energetics, and electronics.[2]

Separations of trivalent An and Ln ions by means of liquid–liquid extraction is a challenging task due to the similarity of their properties. This task can be achieved by taking advantage of mixing of the extended 5*f* orbitals with 6*d* orbitals in An(III) ions as compared to the inner shell 4*f* orbitals in Ln(III) ions.[3] Therefore, soft-atom donor ligands are increasingly considered, as they form complexes with a more covalent character for An(III) than Ln(III) ions.[4] Separation factors over several hundreds have been observed

using polyazine extractants like TPTZ,[5] BTP,[6] or BTPhen.[6,7] Another approach was to balance soft-atom (N) and hard-atom (O) interactions, in order to improve chemical stability of the complexants and extend their range to strongly acidic feeds (which typically contain 1 M nitric acid), so no denitrification of the feed is required. This strategy has been applied to a variety of polynitrogen aromatic ligands such as 2,2′-bipyridine,[8] 1,10-phenanthroline,[9] 2,2′:6′,2″-terpyridine,[10] 2,6-dipyridyl-1,3,5-triazine[11] that were functionalized by amide moieties.[12]

Parallel to this effort, ionic liquids (IL) have found increased use in nuclear separations.[13,14] Such diluents exhibit low vapour pressure and low flammability, high thermal stability[15] and radiation hardness[16,17] that make them attractive for such applications. Extraction in ILs frequently involves cation exchange pathway in competition with neutral complex extraction,[18,19] and this exchange needs to be suppressed to achieve high ion selectivity, which is key in nuclear separations. Most of the extracting agents used in IL studies have been developed for use in conventional solvents (e.g., hydrocarbon diluents), and they are suboptimal for ILs. One approach to improving their performance has been coupling the neutral ligand with structural ions in ILs (thereby turning the ligand into a taskspecific ionic liquid extractant).[20–25] This is the approach that we are pursuing in this present study.

Recently, soft-N triazinyl ligands have been studied for the Ln/An separations in IL. Separation factors ($SF_{Am/Eu}$) exceeding 3000 have been reported.[26] These new and

unexpected results encouraged us to examine An/Ln separations using soft-N/hard-O 1,10-phenanthroline-2,9-dicarboxamide ligands (L) in hydrophobic ILs consisting of 1-(n-alkyl)-3-methylimidazolium cations ($C_n mim^+$, n = 4–8 carbons) and bis[(trifluoromethyl)sulfonyl] imide anion (NTf_2^-). To this end, we examined two types of such ligands: (i) the traditional design with long alkyl arms (1 and 2 in **Figure 9.1**) and (ii) imidazolium cation-conjugated ligands (3 and 4 in **Figure 9.1**). The synthetic details are given in the appendix for the chapter.

Below we demonstrate that these synthetically accessible and chemically stable extractants can efficiently separate Am(III) from Eu(III) in 1 M nitric acid without the use of the additional solvent modifiers and synergists.

As **2** was found to be poorly soluble in ILs, only neutral ligand **1**, and dicationic ligands **3** and **4** are examined below. Three imidazolium based ILs ($[C_n mim][NTf_2]$ with n = 4, 6, and 8) were evaluated as diluents for 1 : 1 v/v extraction of Eu(III) and An(III) ions from 0.1 M and 1 M aqueous nitric acid solutions. These data are summarized in **Table 9.1** (see **Table 9.2** in the appendix of the chapter). **Table 9.1** gives the distribution ratios (D_{Am} and D_{Eu}) for partitioning of the respective ions between the IL and the aqueous phase. Also given in this table are the separation factors $SF_{Am/Eu} = D_{Am}/D_{Eu}$. Dicationic ligands **3** and **4** consistently demonstrated superior performance to neutral ligand **1**, yielding greater distribution ratios and separation factors. In 0.1 M HNO_3 solution (chapter appendix, **Table 9.2**), D_{Am} ~ 130 was observed for **4**. The distribution ratios strongly decreased with

the increasing acidity of the raffinate due to protonation of the extractants in strong acid (chapter appendix, **Table 9.2**). The nature of the IL diluent was also important: as the alkyl chain of the imidazolium cation became longer, distribution ratios for Eu(III) and Am(III) ions decreased considerably (**Table 9.1** and **Figure 9.1**). This dependence indicates the occurrence of cation exchange as one of the competing extraction pathways since the increasing hydrophobicity of the IL cation impedes its migration into the aqueous phase (to compensate the transfer of the metal ion complex into IL), decreasing the extraction efficiency.

Regardless of this interference, $SF_{Am/Eu}$ ~ 50 was obtained for both **3** and **4** in [C_6mim][NTf_2] (**Table 9.1**). While such SFs have previously been reported for 1 and 2 in molecular solvents,[12,27] D_{Am} was considerably higher in ILs. As seen from **Table 9.1** and **Figure 9.2**, due to this increase, all three conditions that are required for efficient Am/Eu separation have been satisfied for **3** and **4** in [C_6mim][NTf_2] for extraction from 1M nitric acid.[28] $SF_{Am/Eu} > 10$ and $D_{Am} > 1 > D_{Eu}$ (see **Figure 9.2**).

To gain more mechanistic insight, solvent extraction was carried out using aqueous solutions containing 35 μM each Ln(III) nitrate (pH 3.25) and IL solutions containing 4 mM **1** or **3**. As the ionic radius decreases across the 4*f* period, this changes the thermodynamics of metal ion complexation giving rise to size-selective Ln(III) ion extraction that is pivotal to achieve group An/Ln separations. The results of these experiments are shown in **Figure 9.1** (chapter appendix, **Table 9.2** and **9.3** and **Figure 9.7**). For **1** in n-dodecane, distribution ratios D_{Ln} were low (<0.05), and no size selectivity

was observed, whereas in the imidazolium ILs the extraction was both efficient and selective. Interestingly, opposite trends were obtained for **1** and **3** (**Figure 9.3**). Neutral ligand **1** selectively extracts heavy lanthanides (with small ionic radii) over light lanthanides (with large ionic radii) with the separation factor $SF_{Lu/La}$ ~ 240 (**Figure 9.3**). In contrast, **3** selectively extracts light lanthanides over heavy lanthanides with $SF_{Ce/Dy}$ ~ 150 (**Figure 9.3**). The nature of the IL cation exerts strong influence on Ln partitioning (in see appendix for chapter, **Figure 9.7**). The distribution ratios D_{Ln} were particularly high for **3** in $[C_6mim][NTf_2]$ (D_{Pr} ~ 3×10^5 and $D_{Ln} > 5 \times 10^3$; see appendix for chapter, **Figure 9.7**, panel b[†]). The sigmoid dependence of D_{Ln} on the atomic number for **3** hints at the complexity of the extraction mechanisms that we proceed to discuss. From previous studies[6,9,27,29] it is known that phenanthroline based ligands (L) tend to form 1 : 2 complexes (with the coordination number of 8 or 10), which can include an additional nitrate anion ligand. In an ionic liquid, the extracted complexes would be $[Ln^{III}L_2(NO^{3-})_x](A^-)_y$, where x = 0 or 1, and the compensating outer sphere anions A^- can be either NO^{3-} or NTf_2^-.

We have modelled these species using computational approach described in the appendix for the chapter and the resulting structures are shown in **Figure 9.4** and **9.5**. Our calculations indicate strong H-bonding (occurring both in **3** and **4**) between the amide hydrogen and a sulfuryl group in NTf_2^- anions paired with the imidazolium cations of the same ligand. In the resulting Ln(III) complexes, these H-bound anions neatly fit in between the imidazolium and phenanthroline rings, compensating the positive charge of

the central Ln(III) ion (**Figure 9.5** and **Figure 9.8** in the appendix). Both types of the complex formation (x = 0 and x = 1) are possible for **3** and **4**, with the x = 0 species having D_2 symmetry (**Figure 9.5**) and the x = 1 having C_2 symmetry (**Figure 9.5b**). The corresponding Ln–X (X = O or N) bond distances systematically increase with the ion radius; these distances are only slightly (~50 pm) greater for x = 1 complexes as compared to x = 0 complexes (in the appendix, **Figure 9.9**), indicating the ease of accommodating the nitrate ligand.

In the chapter appendix, **Figure 9.10(a)** the electronic energy is computed as a function of the Ln–N distance along the reaction coordinate (for the nitrate anion). For all lanthanide ions, there is a minimum on the potential surface at r(Ln–N) ≈ 4.1 Å, which corresponds to the nitrate trapped between two imidazolium cations belonging to two different ligands **3** in a helix shaped complex (**Figure 9.5a, b** and in the appendix, **Figure 9.10(b)**). The reaction barrier for the nitrate addition significantly increases with the ionic radius of Ln(III) ion, reaching ~20 kcal mol^{-1} by the middle of the lanthanide period, suggesting that this addition is energetically prohibitive for heavy lanthanides even though the enthalpy of this addition would be negative. In contrast, the addition of nitrate to **1** (and, more generally, the complexes with neutral ligands) does not exhibit such a barrier, as there are no outer sphere cation groups electrostatically interacting with the nitrate anion. We, therefore, suggest that the complicated shape of D_{Ln} dependence shown in **Figure 9.3** for **3** is due to the switchover in the geometry of the extracted complex that does not occur for **1**.

Recently, it has been observed[29] that precisely such switchover between x = 1 and x = 0 complexes for, respectively, Am(III) and Eu(III) ions bound to soft-N triazinyl ligands is responsible for large SFs observed in soft-N systems; previously this selectivity was believed to arise exclusively through the strength of Ln–N interactions in the structurally similar complexes.[6] The inclusion of the nitrate ligand into the first coordination sphere can improve solubility of the complexes in ILs, accounting for the trends observed. Therefore, there could be a close connection between the complexity of the D_{Ln} curve for **3** in IL (shown in **Figure 9.3**) and the efficient Am/Eu separations in this system, in contradiction to the simplicity of this curve for **1** and the lower Am/Eu selectivity observed for this neutral ligand. This hypothesis can be potentially tested through a systematic X-ray absorption study of the solution complexes, as suggested by the simulated spectra shown in the appendix for the chapter, **Figure 9.9**.

9.2. Conclusions

In summary, 1,10-phenanthroline-2,9-dicarboxamides bis conjugated to imidazolium cations (**Figure 9.1**) have been recognized as selective and efficient agents for extracting trivalent ions of minor actinides over lanthanides into imidazolium ionic liquid diluents under the conditions that are relevant to nuclear cycle separations. These remarkable extractants (which can be alternatively considered as task-specific ionic liquids) can also be used for the group separation of light over heavy lanthanides, whereas the corresponding neutral ligand exhibits the opposite trend. While clearly more work is needed to rationalize these observations, the striking differences observed between the

neutral and dicationic soft-N/hard-O ligands in ILs strongly imply tuning of the metal–ligand coordination through Coulomb interactions in the outer sphere, and we suggest nitrate ligand addition as a possible cause for the observed trends, including the complex ion size dependence of the distribution ratios across the lanthanide period and the uncommonly high Am/Eu selectivity.

9.3 References

1. U.S. Energy Information Administration. International Energy Statistics, http://www.eia.gov/cfapps/ipdbproject/IEDIndex3.cfm, (accessed April 4, 2015, 2015).

2. BP, *Statistical Review of World Energy*, 2014.

3. Barnhart C. J., Dale, M., Brandt A. R., Benson, S. M. *Energy Environ. Sci.*, 2013, **6**, 2804-2810.

4. Kharecha, P. A., Hansen, J. E., *Environ. Sci. Technol.*, 2013, DOI: 10.1021/es3051197.

5. A. Markandya and P. Wilkinson, *The Lancet*, 2007, **370**, 979-990.

6. R. O'Brien and J. A. Katalenich, *Journal of Propulsion and Power*, 2011, **27**, 1131-1134.

7. Y. Wei, K. N. Sabharwal, M. Kumagai, T. Asakura, G. Uchiyama and S. Fujine, *Journal of Nuclear Science and Technology*, 2000, **37**, 1108-1110.

8. M. Hudson, M. Foreman, C. Hill, N. Huet and C. Madic, *Solvent Extraction and Ion Exchange*, 2003, **21**, 637-652.

9. F. W. Lewis, L. M. Harwood, M. J. Hudson, M. G. Drew, J. F. Desreux, G. Vidick, N. Bouslimani, G. Modolo, A. Wilden, M. Sypula, T. H. Vu and J. P. Simonin, *Journal of the American Chemical Society*, 2011, **133**, 13093-13102.

10. G. M. Cockrell, G. Zhang, D. G. VanDerveer, R. P. Thummel and R. D. Hancock, *Journal of the American Chemical Society*, 2008, **130**, 1420-1430.

11. R. D. Hancock, *Chem Soc Rev*, 2013, **42**, 1500-1524.

12. P. Kaufholz, G. Modolo, A. Wilden, F. Sadowski, D. Bosbach, C. Wagner, A. Geist, P. J. Panak, F. W. Lewis and L. M. Harwood, *Solvent Extr. Ion Exch.*, 2016, **34**, 126-140.

13. M. D. Ogden, S. I. Sinkov, M. Nilson, G. J. Lumetta, R. D. Hancock and K. L. Nash, *J. Solution Chem.*, 2013, **42**, 211-225.

14. L. M. Harwood, D. M. Laventine, A. Afsar and M. J. Hudson, *Heterocycles*, 2012, **86**, 1419.

15. F. W. Lewis, L. M. Harwood, M. J. Hudson, A. Geist, V. N. Kozhevnikov, P. Distler and J. John, *Chem. Sci.*, 2015, **6**, 4812-4821.

16. J. Dehaudt, N. J. Williams, I. A. Shkrob, H. Luo and S. Dai, *Dalton. Trans.*, 2016, **45**, 11624-11627.

17. X. Sun, C.-L. Do-Thanh, H. Luo and S. Dai, *Chem. Eng. J.*, 2014, **239**, 392-398.

18. X. Sun, H. Luo and S. Dai, *Talanta*, 2012, **90**, 132-137.

19. X. Sun, H. Luo and S. Dai, *Chem Rev*, 2012, **112**, 2100-2128.

20. M. Atanassova and V. Kurteva, *RSC Adv.*, 2016, **6**, 11303-11324.

21. M. L. Dietz and D. C. Stepinski, *Talanta*, 2008, **75**, 598-603.

22. M. L. Dietz and J. A. Dzielawa, *Chem. Commun.*, 2001, DOI: 10.1039/B104349H, 2124-2125.

23. A. Bhattacharyya, S. A. Ansari, T. Gadly, S. K. Ghosh, M. Mohapatra and P. K. Mohapatra, *Dalton Trans*, 2015, **44**, 6193-6201.

24. D. M. Whittaker, T. L. Griffiths, M. Helliwell, A. N. Swinburne, L. S. Natrajan, F. W. Lewis, L. M. Harwood, S. A. Parry and C. A. Sharrad, *Inorg. Chem.*, 2013, **52**, 3429-3444.

25. H. Zhou, Y. Ao, J. Yuan, J. Peng, J. Li and M. Zhai, *RSC. Adv.*, 2014, **4**, 45612-45618.

26. X. Sun, J. R. Bell, H. Luo and S. Dai, *Dalton. Trans.*, 2011, **40**, 8019-8023.

27. A. Bremer, D. M. Whittaker, C. A. Sharrad, A. Geist and P. J. Panak, *Dalton. Trans.*, 2014, **43**, 2684-2694.

28. M. J. Frisch, et al., *Gaussian 09 Revision D.01; Gaussian, Inc.:*, Wallingford, CT, 2009.

29. S. M. Webb, *Phys. Scr.*, 2005, **2005**, 1011.

30. B. Ravel and M. Newville, *J. Synchrotron Radiat.*, 2005, **12**, 537-541.

31. J. J. Rehr and R. C. Albers, *Rev. Mod. Phys.*, 2000, **72**, 621-654.

32. L. Downward, C. H. Booth, W. W. Lukens and F. Bridges, *AIP Conf. Proc.*, 2007, **882**, 129-131.

33. W. C. Hamilton, *Acta Crystallographica*, 1965, **18**, 502-510.

9.4 Appendix 9A Supplemental Information for Chapter 9

9.4.1 Materials and synthetic methods.

Solvents. All reagents were obtained from Aldrich in their purest form and used without further purification. 1-alkyl-3-methylimidazolium bis[(trifluoromethyl)-sulfonyl]amide ([$C_n$mim] [NTf_2]) ionic liquids (*n*=4, 6, and 8), were synthesized using modified procedures from[1,2].

Extractants: synthetic strategy and analytical detail. The synthesis of extractants **1** to **4** followed **Figure 9.6**. Phenanthroline dicarboxamide ligands were prepared from phenanthroline dicarboxylic acid **7** obtained by oxidation of neocuproine **5** [3,4]. Ligands **1** and 2 were obtained by converting the dicarboxylic acid **7** into diacyl chloride that was reacted with N,N-dioctylamine and N-octylamine, respectively. Compounds **8** and **9** were obtained by peptide conjugation of **7** with N-(3-aminopropyl)-imidazole using carbonyldiimidazole (CDI) as a coupling reagent. Imidazole moieties were quarternized in presence of 1-butylbromide to yield **10** and **11**. Finally, the bromide metathesis was performed using $LiNTf_2$ to obtain **3** and **4**. Below we give the synthetic procedures, ^{1}H and ^{13}C nuclear magnetic resonance spectra (see **Figures 9.12 to 9.19** and **Figures 9.20 to 9.27**, respectively) and high resolution mass spectra (HRMS) or electrospray ionization mass spectra (ESI/MS) for these compounds.

^{1}H and ^{13}C NMR spectra were recorded using a Varian Mercury 300 MHz or a Varian VNMRS 500 MHz spectrometers. The chemical shifts at 25 °C (given in parts per million) were referenced to the residual protonated solvent. The mass peaks for protonated molecules were determined using DART (direct analysis in real time) for neutral compounds (as protonated molecules) or ESI/MS for charged species. All mass spectrometry analyses were conducted at the Mass Spectrometry Center located in the Department of Chemistry at the University of Tennessee. The DART analyses were performed using a JEOL AccuTOF-D time-of-flight mass spectrometer with a DART ionization source from JEOL USA, Inc. (Peabody, MA). The ESI/MS analyses were performed using a QSTAR Elite quadrupole time-of-flight (QTOF) mass spectrometer with an electrospray ionization source from AB Sciex (Concord, Ontario, Canada).

2,9-bis(N,N-dioctylaminocarbonyl)-1,10-phenanthroline (1). Phenanthroline dicarboxylic acid (429 mg, 1.6 mmol) was refluxed in thionyl chloride (10 mL) for 6 h. $SOCl_2$ was removed under vacuum. The crude diacyl chloride was dissolved in dichloromethane. A solution of N,N-diisopropylethylamine (DIPEA, 0.58 mL, 3.5 mmol) and di-N,N-octylamine (1.06 mL, 3.5 mmol) in dichloromethane (75 mL) was added dropwise at 0°C. The mixture was refluxed for 6 h. After cooling, the organic layer was separated and washed with 1 M HCl (2X 30 mL) and water (6X 10 mL), dried over $MgSO_4$, and reduced in vacuum. The yellow residue was purified by silica gel flash chromatography (hexanes/ethyl acetate, 100:0 to 70:30 v/v) to yield the title compound as a white powder. Yield: 670 mg (59%).

^{1}H NMR (300 MHz, $CDCl_3$): δ 0.73 (t, 6H, ^3J = 7.1 Hz), 0.89 (t, 6H, ^3J = 7.1 Hz), 0.93-1.10 (m, 20H), 1.24-1.46 (m, 20H), 1.63 (p, 4H, ^3J = 7.2 Hz), 1.76 (p, 4H, ^3J = 7.2 Hz), 3.56 (t, 4H, ^3J =7.6 Hz), 3.75 (t, 4H, ^3J = 7.6 Hz), 7.83 (s, 2H), 8.01 (d, 2H, ^3J = 8.3 Hz), 8.31 (d, 2H, ^3J = 8.3 Hz); 13C NMR (75 MHz, CDCl3): δ 14.0, 14.1, 22.5, 22.7, 26.7, 27.3, 27.8, 29.0, 29.1, 29.3, 29.5, 31.6, 31.9, 47.0, 49.1, 123.4, 127.1, 128.8, 136.7, 144.2, 154.7, 168.3; HRMS: m/z: 715.5899. [M + H^+]. $C_{46}H_{75}N_4O_2^+$ requires 715.5890.

2,9-bis(N-octylaminocarbonyl)-1,10-phenanthroline (2). Phenanthroline dicarboxylic acid 7 (429 mg, 1.6 mmol) was refluxed in thionyl chloride (10 mL) for 6 h. $SOCl_2$ was removed under vacuum. The crude diacyl chloride was dissolved in CH_2Cl_2. A solution of DIPEA (0.58 mL, 3.5 mmol) and N-octylamine (0.58 mL, 3.5 mmol) was added dropwise at 0 °C. After cooling, the organic layer was washed with 1 M HCl (2X 30 mL) and with water (6X 10 mL), dried over $MgSO_4$ and reduced in vacuum. The residue was purified by silica gel flash chromatography (95:5 v/v CH_2Cl_2/MeOH) to yield the title compound as a pale yellow powder. Yield: 361 mg (46%).

1H NMR (300 MHz, $CDCl_3$): δ 0.84 (t, 6H, ^3J = 7.0 Hz), 1.17-1.38 (m, 20H), 1.38-1.63 (m, 4H) 3.19-3.44 (m, 4H), 7.92 (s, 2H), 8.44 (d, 2H, ^3J = 8.3 Hz), 8.61 (d, 2H, ^3J = 8.3 Hz), 8.65-8.73 (m, 2H); ^{13}C NMR (75 MHz, $CDCl_3$): δ 14.1, 22.6, 27.1, 29.2, 29.3, 29.8, 31.8, 39.7, 127.7, 127.7, 130.5, 137.9, 144.1, 150.1, 164.0; HRMS: m/z: 491.3389 [M + H^+]. $C_{30}H_{43}N_4O_2^+$ requires 491.3386.

2,9-bis(N-(1-(3-butylimidazolium))propylaminocarbonyl)-1,10-phenanthroline di[bis(trifluoromethylsulfonyl)imide)] (3). To a solution of 10 (1.62 g, 2.14 mmol) in acetonitrile (20 mL) was added dropwise a solution of lithium bis(trifluoromethane sulfonyl)imide ($LiNTf_2$, 3.07 g, 10.7 mmol) in acetonitrile (15 mL). The mixture was stirred at room temperature for 2 days. The solvent was removed in vacuum and the residue was washed with water, diethyl ether, and dichloromethane. The highly viscous oil was dried in vacuum for 5 h. Yield: 2.10 g (85%)

^{1}H NMR (300 MHz, DMSO-d_6): δ 0.88 (t, 6H, ^3J = 7.3 Hz), 1.18-130 (m, 4H), 1.69-1.79 (m, 4H), 2.19-2.30 (m,4H), 3.53 (q, 4H, ^3J = 6.5 Hz), 4.14 (t, 4H, ^3J = 7.2 Hz), 4.33 (t, 4H, ^3J =6.8 Hz), 7.80 (s, 2H), 7.87 (s, 2H), 8.49 (d, 2H, ^3J = 8.3 Hz), 8.77 (d, 2H, ^3J = 8.77 Hz), 9.24 (s, 2H), 9.53 (s, 2H, ^3J = 6.1 Hz); ^{13}C NMR (126 MHz, DMSO-d_6): δ 13.6, 19.2, 30.4, 31.7, 36.5, 47.5, 49.1, 118.6, 121.2, 122.3, 128.4, 130.8, 136.6, 136.7, 139.4, 141.1, 150.0, 164.8; HRMS: ESI$^+$ m/z: 298.1797. $C_{34}H_{44}N_8O_2^{2+}$ requires 298.1794; ESI- m/z: 279.9174. NTf_2^- requires 279.9173.

2,9-bis(N-(1-(3-butyl-2-methyl-imidazolium))propylaminocarbonyl)-1,10-phenanthroline di[bis(trifluoromethylsulfonyl)imide)] (4). To a solution of 11 (255 mg, 0.325 mmol) in acetonitrile (10 mL) was added dropwise a solution of $LiNTf_2$ (467 mg, 1.62 mmol) in acetonitrile (3 mL). Further synthesis proceeded as explained above for 3. Yield: 340 mg (88%).

^{1}H NMR (300 MHz, DMSO-d_6): δ 0.74 – 0.89 (m, 6H), 1.10-1.24 (m, 4H), 1.55 (m, 4H), 2.64 (s,6H), 3.52 (m, 4H), 3.98 (t, 4H, ^3J = 7.5 Hz), 4.26 (t, 4H, ^3J = 7.5 Hz), 7.64 (d, 2H, ^3J = 2.1 Hz), 7.79 (d, 2H, ^3J = 2.1 Hz),8.19 (s, 2H), 8.44 (d, 2H, ^3J = 8.3 Hz), 8.74 (d, 2H, ^3J = 8.3 Hz), 9.46 (t, 2H, ^3J =6.1 Hz); ^{13}C NMR (126 MHz, DMSO-d6): δ 9.7, 13.7, 19.3, 29.3, 31.4, 36.8, 46.2, 47.7, 116.1, 118.6, 121.2, 121.6, 121.7, 128.4, 130.8, 138.7, 144.3, 150.0, 167.7; HRMS: ESI$^+$ m/z: 312.1955. $C_{36}H_{48}N_8O_2^{2+}$ requires 312.1950; ESI$^-$ m/z: 279.9172. NTf_2^- requires 279.9173.

2,9-bis(N-(1-imidazolyl)propylaminocarbonyl)-1,10-phenanthroline (8). A solution of 1,10-phenanthroline-2,9-dicarboxylic acid **7** (1.8 g, 6.71 mmol) in N,N-dimethylformamide (DMF, 35 mL) was heated to 45 °C. CDI (3.41 g, 21.0 mmol) was added in several portions. The mixture was heated at 45 °C for 2 h. After cooling to 20 °C, N-(3-aminopropyl)-imidazole (1.72 mL, 14.4 mmol) was added dropwise. The mixture was stirred at room temperature for 4 days. Water was added and DMF was removed in vacuum. A solution of Na_2CO_3 (1 M, 100 mL) was added to the residue. After standing overnight at 5 °C, the yellow precipitate was filtered, washed with water and diethyl ether. Yield: 1.90 g (59%).

^{1}H NMR (300MHz, DMSO-d_6): δ 2.09 (p, 4H, ^3J = 7.0 Hz), 3.46 (q, 4H, ^3J = 6.7 Hz), 4.08 (t, 4H, ^3J = 6.8 Hz), 6.90 (s, 2H), 7.24 (s, 2H), 7.71 (s, 2H), 8.21 (s, 2H), 8.46 (d, 2H, ^3J = 8.3 Hz), 8.73 (d, 2H, ^3J = 8.3 Hz), 9.52 (t, 2H, ^3J = 8.3 Hz); ^{13}C NMR (75 MHz, DMSO-

d_6): δ 31.0, 36.5, 43.9, 119.4, 121.1, 127.9, 128.4, 130.3, 137.4, 138.2, 143.7, 149.7, 164.1; HRMS: m/z: 483.2253 [M + H^+]. $C_{26}H^{27}N_8O_2^+$ requires 483.2257.

2,9-bis(N-(1-(2-methylimidazolyl)propylaminocarbonyl)-1,10-phenanthroline (9). A solution of 1,10-phenanthroline-2,9-dicarboxylic acid 7 (0.714 g, 2.66 mmol) in DMF (15 mL) was heated to 45 °C. The carbonyldiimidazole (CDI, 1.5 g, 8.33 mmol) was added in several portions. The mixture was heated at 45°C for 2 h. After cooling of this reaction mixture to 20 °C, N-(3-aminopropyl)-2-methyl-imidazole (0.98 mL, 7.18 mmol) was added dropwise. The mixture was stirred at room temperature for 4 days. Water was added (10 mL) and DMF was removed in vacuum. A solution of Na_2CO_3 (1 M, 75 mL) was added to the residue. After standing at 5 °C overnight, the yellow precipitate was filtered and washed with water and diethyl ether. Yield: 620 mg (46%)

^{1}H NMR (300 MHz, DMSO-d_6): δ 2.02 (p, 4H, ^3J = 7.0 Hz), 2.26 (s, 6H), 3.62 (m, 4H), 3.94 (t, 4H, ^3J = 7.0 Hz), 6.73 (s, 2H), 7.11 (s, 2H), 8.14 (s, 2H), 8.44 (d, 2H, ^3J =8.3 Hz), 8.70 (d, 2H, ^3J =8.3 Hz), 9.48 (d, 2H, ^3J = 6.2 Hz); ^{13}C NMR (75 MHz, DMSO-d_6): δ 13.0, 30.7, 37.0, 43.4, 120.1, 121.6, 126.6, 128.4, 130.7, 138.7, 144.1, 150.1, 164.5, 208.2; HRMS: m/z: 511.2561 [M + H^+]. $C_{28}H_{31}N_8O_2^+$ requires 511.2570.

2,9-bis(N-(1-(3-butylimidazolium)propylaminocarbonyl))-1,10-phenanthroline dibromide (10). 1-bromobutane (0.21 mL, 1.96 mmol) was added dropwise to a solution of 8 (390 mg, 0.81 mmol) in acetonitrile (20 mL) at 0 °C. The mixture was stirred at 20 °C for 12 h

and then at 85 °C for 2 days. The solvent was removed in vacuum. The resulting yellow residue was washed with hexanes. The yellow powder was dried in vacuum. Yield: 543 mg (89%).

^{1}H NMR (300 MHz, $CDCl_3$): δ 0.81 (t, 6H, ^3J = 7.2 Hz), 1.15-1.28 (m, 4H), 1.68-1.79 (m, 4H), 2.39-2.55 (m, 4H), 3.71-3.75 (m, 4H), 4.18 (t, 4H, ^3J = 7.2 Hz), 4.58 (t, 4H, ^3J = 6.5 Hz), 7.40 (s, 2H), 7.84 (d, 2H, ^3J = 10.3 Hz), 8.34 (d, 2H, ^3J = 8.2 Hz), 8.43(d, 2H, ^3J = 8.2 Hz), 9.84 (t, 2H, ^3J = 5.9Hz), 10.21 (s, 2H); ^{13}C NMR (75 MHz, CDCl3): δ 13.5, 19.5, 30.3, 32.0, 36.8, 48.2, 49.9, 122.0, 123.2, 127.9, 130.5, 136.8, 137.8, 144.6, 150.6, 165.6; ESI$^+$ m/z: 298.1794. $C_{34}H_{44}N_8O_2^{2+}$ requires 298.1794; ESI$^-$: m/z: 78.9182. Br^- requires 78.9183.

2,9-bis(N-(1-(3-butyl-2-methyl-imidazolium))propylaminocarbonyl)-1,10-phenanthroline dibromide (11). 1-bromobutane (0.084 mL, 0.784 mmol) was added dropwise to a solution of 9 (204 mg, 0.81mmol) in acetonitrile (15 mL) at 0 °C. The mixture was stirred at 20 °C for 12 h then at 85 °C for 2 days. The solvent was removed in vacuum. The resulting yellow residue was washed with hexanes. The yellow powder was dried in vacuum. Yield: 231 mg (90%).

^{1}H NMR (300 MHz, DMSO-d_6): δ 0.82 (t, 4H, ^3J = 7.3 Hz), 1.18 (m, 4H), 1.57 (p, 4H, ^3J = 7.3Hz), 2.22 (t, 4H, ^3J = 6.4 Hz), 2.67 (s, 6H), 3.56 (d, 4H, ^3J = 6.4 Hz), 4.01 (t, 4H, ^3J = 7.4 Hz),4.28 (m, 4H), 7.68 (d, 2H, ^3J = 2.1 Hz), 7.84 (d, 2H, ^3J = 2.1 Hz), 8.21 (s, 2H),

8.45 (d, 2H, ^3J = 8.4 Hz), 8.76 (d, 2H, ^3J = 8.4 Hz), 9.49 (t, 2H, ^3J = 6.1 Hz); ^{13}C NMR (126 MHz, DMSO-d_6): δ 10.0, 13.8, 19.3, 29.3, 31.4, 36.9, 46.2, 47.7, 121.6, 121.8, 128.4, 130.8, 138.7, 144.2, 144.3, 150.1, 164.7; ESI$^+$ m/z: 312.1961. $C_{36}H_{48}N_8O_2^{2+}$ requires 312.1950; ESI$^-$: m/z: 78.9177 Br^- requires 78.9183.

9.4.2 Determination of distribution ratios.

Caution! ^{152,154}Eu and ^{241}Am are radioactive. All radiotracer experiments were carried out in radiochemical laboratories equipped for handling these isotopes.

The distribution ratio (DM) for extraction of trivalent metal ions (M^{3+}) is defined by

$$D_M = \frac{(C_{aq,i} - C_{aq,f})}{(C_{aq,f})} \times \frac{Volume\ of\ aqueous\ phase}{Volume\ of\ IL\ phase} \quad \text{(S1)}$$

In this equation, $C_{aq,i}$ and $C_{aq,f}$ represent the initial and final (equilibrium) concentrations of the metal ions in the aqueous phase, respectively. Although the value of DM depends on the concentration of free extractant, the trends reflected in DM should be the same as for the corresponding equilibrium constants for a given extractant concentration. A volume ratio is needed in the calculation of distribution ratios to account for the difference in volume between the two immiscible phases. In all of our experiments, the volume ratio was close to 1:1 v/v. Separation factors SF for the metal ions M and M' are defined from

$$SF_{M/M^1} = \frac{D_M}{D_{M^1}} \quad \text{(S2)}$$

Eu/Am measurements. The distribution ratios for extraction using radiotracer techniques were calculated by measuring the amount of radioactivity of both aqueous and organic

phases at equilibrium. Counting efficiency (^{241}Am or ^{152,154}Eu gamma ray absorption in solid scintillators) is identical for both phases; hence, the distribution ratio is defined by the ratio of specific radioactivity S (Bq/mL) of element M in the IL vs. aqueous phases

$$D_M = \frac{C_{IL,f}}{C_{aq,f}} \propto \frac{S_{org,f}}{S_{aq,f}} \quad \text{(S3)}$$

Europium-152/154 was obtained from Isotope Products (presently owned by Eckert & Ziegler) and americium-241was produced at Oak Ridge National Laboratory. An equal volume of both IL (containing 4 mM extractant) and aqueous phases, 0.4 mL of each were used, respectively. Each sample was individually spiked with a 10 μL solution containing 50 μCi/mL of each radiotracer respectively. The solutions were mixed using a rotating wheel set at 60 rpm for 3 h at 25±0.2 °C. After 3 h the samples were centrifuged at 3,000 rpm for 5 min at 25 °C to ensure the phases separated from each other. Then 100 μL aliquots were subsampled from each phase and placed into polypropylene tubes that were sealed with a cap. These tubes were then placed in a Canberra Gamma Analyst germanium spectrometer to determine the amounts of ^{241}Am and ^{152,154}Eu present in each sample. Prior to testing these samples, a quality assurance calibration was performed. The organic and aqueous samples were counted for a period of 30 min to ensure an accurate measurement. Additional blank samples (no isotopes present in solution) were run to ensure no background subtraction was necessary. Once the data was collected the total counts for each isotope in the samples was normalized to give the average counts per minute.

Lanthanide series. Extraction experiments were performed by contacting 0.5 mL of IL containing 4 mM of extractant 1 or 3 with 0.5 mL of aqueous phase (pH 3.25) containing ~35 μM of each lanthanide nitrate hydrate for elements given in **Table 9.2** and **9.3**. The aqueous solutions were prepared in deionized water (with a specific resistance 18 MΩ-cm or greater). These solutions were mixed in a vibrating mixer for 3 h and then stirred for a day at 25 °C; this treatment was followed by centrifugation for 5 min at 3,000 rpm to separate the two phases. The upper (aqueous) phase was separated, and metal ion concentrations were determined using inductively coupled plasma - mass spectrometry (Thermo X-series ICP-MS). The values of D_{Ln} were obtained in triplicate with an uncertainty less than 5%, and the average values are given in this Communication.

9.4.3 Computational approach

The structures and energetics for Ln complexes in the gas phase were estimated using Sparkle/RM1 semiempirical method developed by Simas and co-workers[5,6] from MOPAC2016 suit.[7,8] The method typically gives ~ 50 pm accuracy in Ln-X distances for X=O, N, S and P atoms.[5] In this method, the lanthanide ion is replaced with a “sparkle”: a ghost atom with +3 charge and a set of parameterized Gaussian orbitals centered on this ion. According to the method developers, “the principle behind the Sparkle Model was that the 4*f* electrons do not participate in the chemical bond because they are shielded from the coordination polyhedron by the more diffuse 5s and 5p closed shells, rendering the coordination bond essentially electrostatic.”[5] Therefore, the covalent character of Ln-

X bonds is entirely neglected in this model. All other bonds are treated at the RM1 (Recife Model 1) semiempirical level.[9]

In our calculations, no solvent was included, and the molecular symmetry was externally imposed. To calculate the energetics of nitrate addition, all degrees of freedom except for the Ln-N distance in the nitrate ligand were optimized. X-ray absorption spectra were calculated for the gas phase geometry optimized structures using program FEFF 8.2.[10,11]

9.5 Appendix References

1. H. M. Luo, S. Dai, P. V. Bonnesen, T. J. Haverlock, B. A. Moyer and A. C. Buchanan, Solvent Extr. Ion Exch., 2006, 24, 19-31.

2. P. Bonhote, A. P. Dias, N. Papageorgiou, K. Kalyanasundaram and M. Gratzel, Inorg. Chem., 1996, 35, 1168–1178.

3. C. J. Chandler, L. W. Deady and J. A. Reiss, J. Heterocyclic Chem., 1981, 18, 599-601.

4. A. De Cian, E. DeLemos, J.-L. Mergny, M.-P. Teulade-Fichou and D. Monchaud, J. Am. Chem. Soc., 2007, 129, 1856-1857.

5. M. A. M. Filho, J. D. L. Dutra, G. B. Rocha, R. O. Freirea and A. M. Simas, RSC Adv., 2013, 3, 16747-16755.

6. M. A. M. Filho, J. D. L. Dutra, G. B. Rocha, A. M. Simas and R. O. Freire, PLoS ONE, 2014, 9, e86376.

7. J. J. P. Stewart, 2016, MOPAC2016.

8. J. D. C. Maia, G. A. U. Carvalho, J. Mangueira , C. P. , S. R. Santana, L. A. F. Cabral and G. B. Rocha, J. Chem. Theory Comput., 2012, 8, 3072-3081.

9. G. B. Rocha, R. O. Freire, A. M. Simas and J. J. P. Stewart., J. Comp. Chem., 2006, 27, 1101-1111.

10. A. L. Ankudinov, C. Bouldin, J. J. Rehr, J. Sims and H. Hung, Phys. Rev. B, 2002, 65, 104107

11. A. L. Ankudinov, B. Ravel, J. J. Rehr and S. D. Conradson, Phys. Rev. B, 1998, 58, 7565-7576.

9.6 Appendix 9B Figures and Tables for Chapter 9

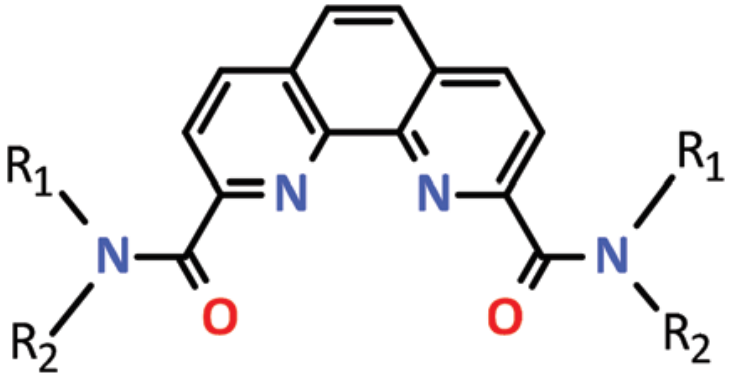

1: $R_1 = R_2 =$ *n*-octyl

2: $R_1 = H$; $R_2 =$ *n*-octyl

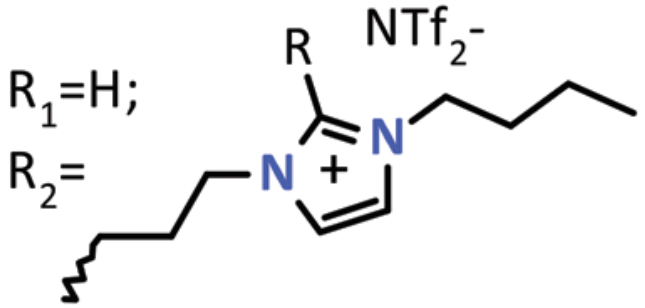

3: R = H

4: R = Me

Figure 9.1. Chemical structures for 1,10-phenanthroline-2,9-dicarboxamidecomplexants **1** to **4**.

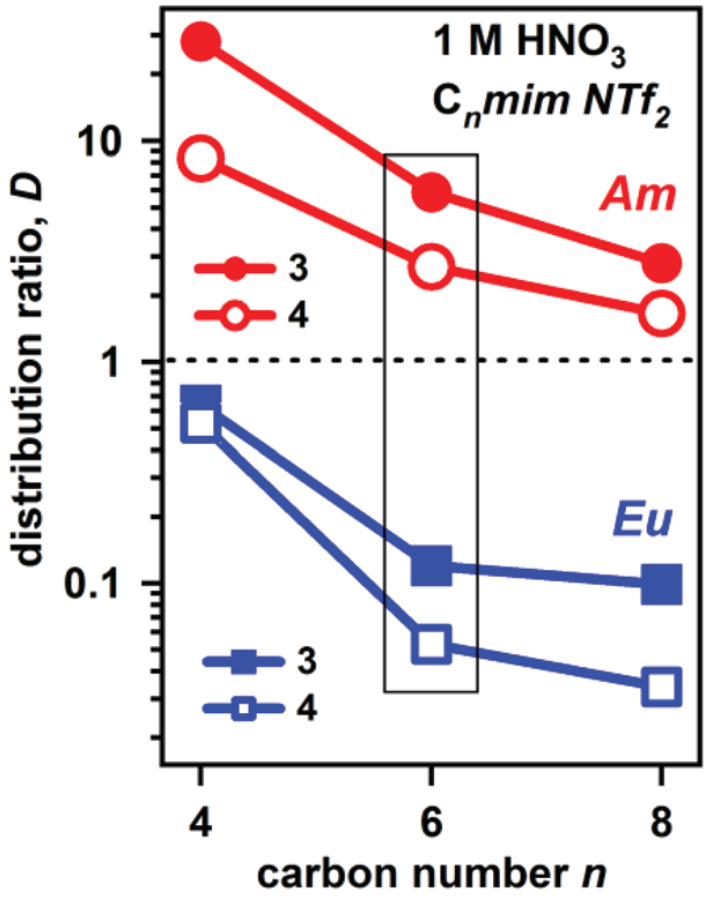

Figure 9.2. Influence of the alkyl chain length in IL cation on the distribution ratios for Eu(III) (squares) and Am(III) (circles) ions in 1 M nitric acid (4 mM **3** or **4** in Cnmim NTf_2). For $[C_6mim][NTf_2]$, the conditions are optimum for efficient Am/Eu separations.

Table 9.1. Distribution ratios (*D*) between IL and aqueous phases and separation factors ($SF_{Am/Eu}$) for Am(III) and Eu(III) ions in 1 M nitric acid solutions. The extractant concentration in $[C_n mim][NTf_2]$ was 4 mM (1 : 1 v/v extraction)

Ligand	$[C_n mim][NTf_2]_n$	D_{Am}	D_{Eu}	$SF_{Am/Eu}$
1	4	0.17	0.0065	26.2
	6	0.11	0.011	10.0
	8	0.053	0.0023	23.0
3	4	28.2	0.64	44.0
	6	5.9	0.12	48.9
	8	2.8	0.10	28.3
4	4	8.3	0.53	15.7
	6	2.7	0.053	50.9
	8	1.7	0.034	48.8

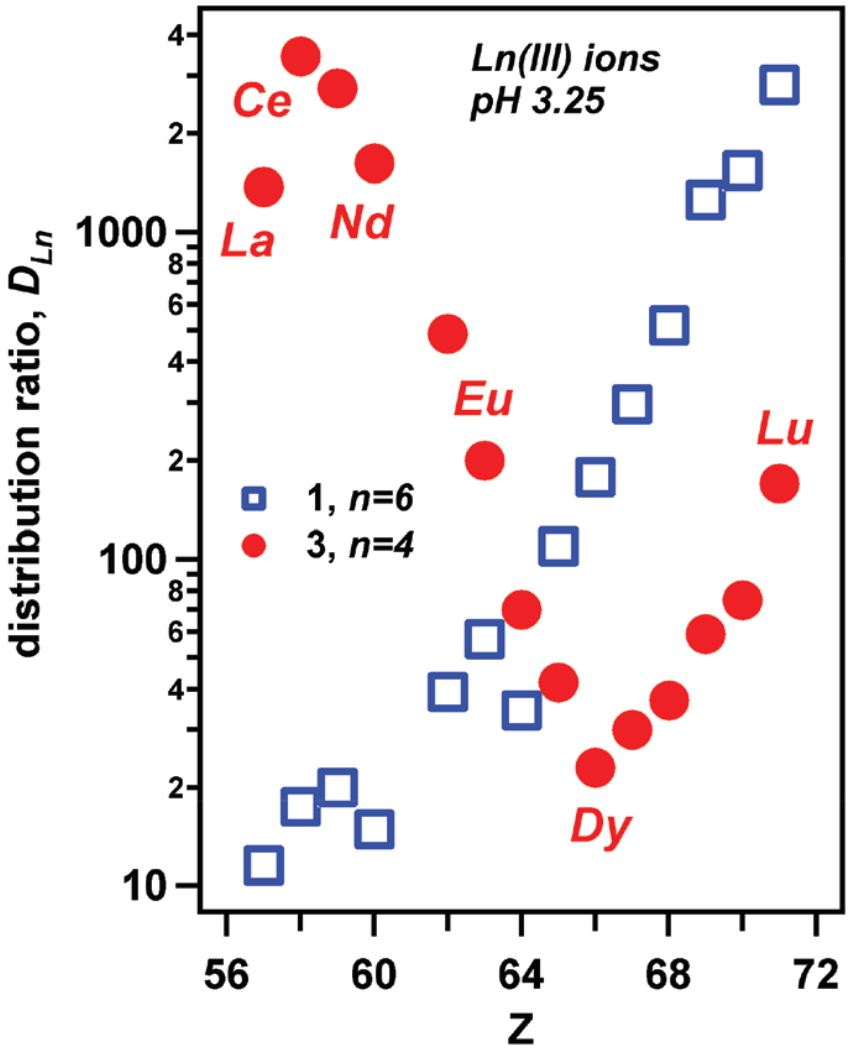

Figure 9.3. Distribution ratios D_{Ln} for Ln(III) ions across the lanthanide period for 4 mM **1** in [C_6mim][NTf_2] (open squares) and 4 mM **3** in [C_4mim][NTf_2] (filled circles). D_{Ln} are plotted vs. the atomic number *Z* of the lanthanide.

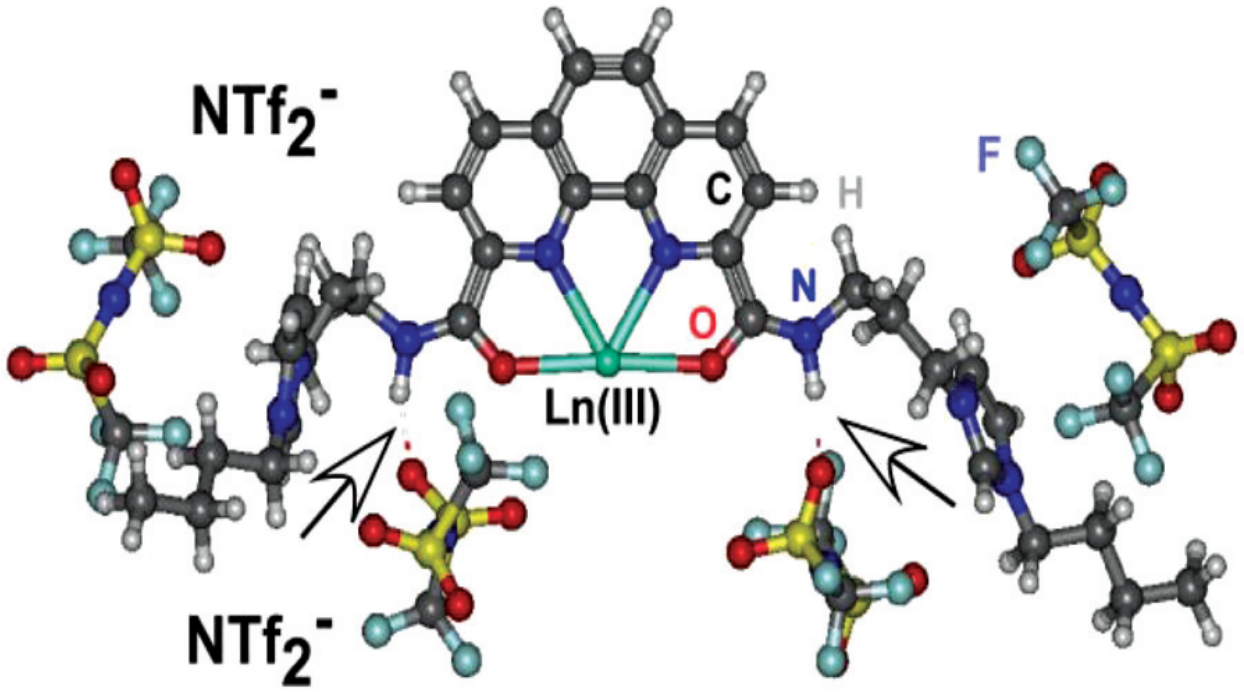

Figure 9.4. Molecular structure of **3** interacting with four NTf_2^- anions (taken from the optimized geometry gas phase $[Gd^{III}L_2](NTf_2^-)_8$ complex shown in **Figure 9.5**). The arrows indicate hydrogen bonds between the amide group in **3** and the sulfuryl groups in the IL anion.

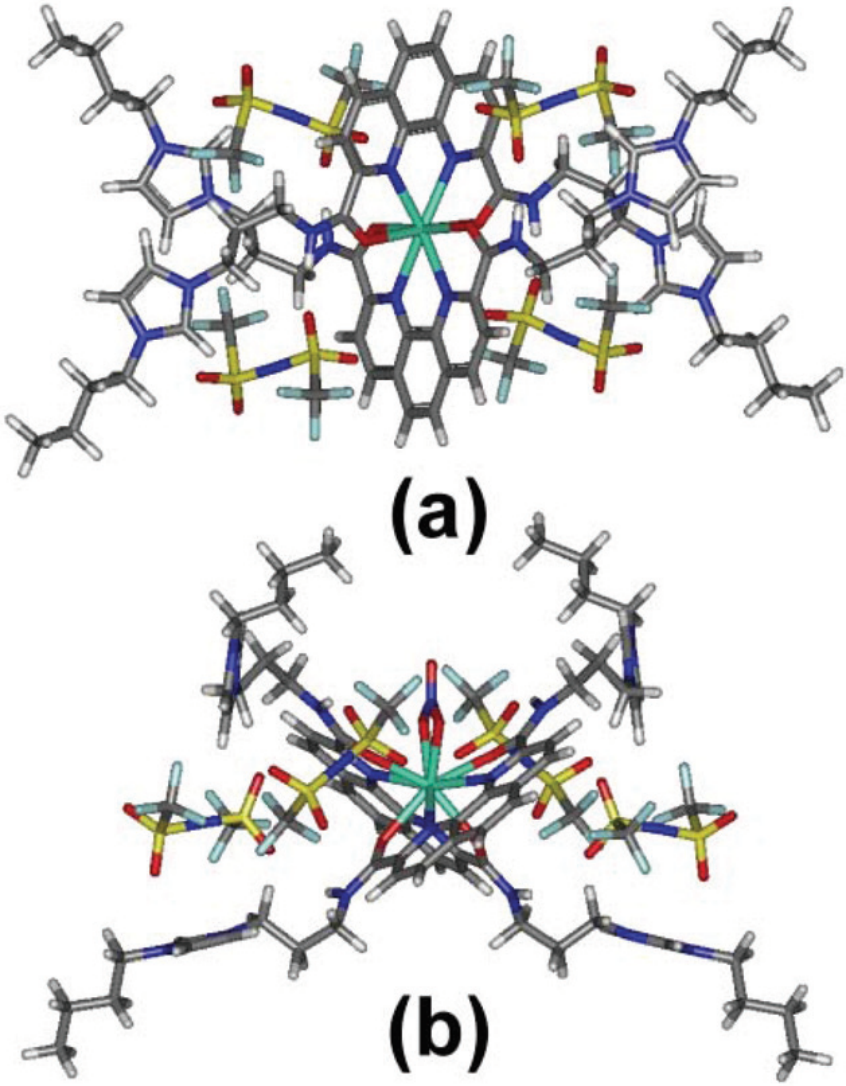

Figure 9.5. Optimized geometry $[Gd^{III}L_2(NO_3^-)_x](NTf_2^-)_8$ complexes for ligand **3** with (a) x = 0 and (b) x = 1 (the outer anions not shown).

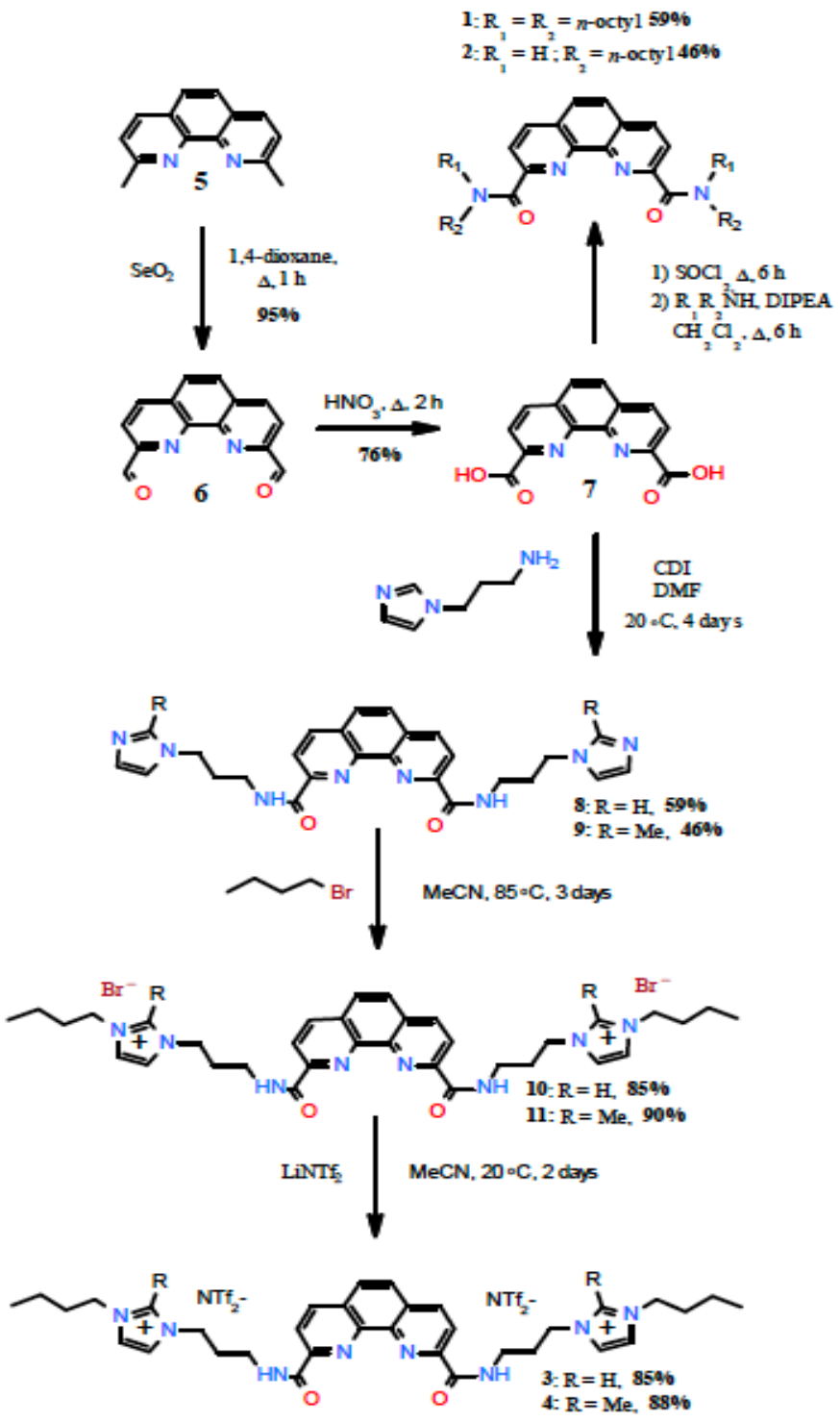

Figure 9.6. Synthetic scheme for extractants **1** to **4**.

Table 9.2. Distribution ratios (DAm and DEu) and separation factors (SFAm/Eu) for Am(III) and Eu(III) ions in nitric acid solutions. The extractant (L) concentration in [Cnmim] [NTf2] was 4 mM (1:1 v/v extraction).

L	$[C_n mim][NTf_2]$ *n*	0.1 M HNO_3			1.0 M HNO_3		
		D_{Am}	D_{Eu}	$SF_{Am/Eu}$	D_{Am}	D_{Eu}	$SF_{Am/Eu}$
1	4	12.7	0.7	19.0	0.17	0.0065	26.2
	6	1.7	1.0	1.7	0.11	0.011	10.0
	8	0.95	0.1	9.5	0.053	0.0023	23.0
3	4	97	31	3.1	28	0.64	44.0
	6	16.4	6.1	2.7	5.9	0.12	48.9
	8	1.5	1.1	1.3	2.8	0.01	28.3
4	4	130	3.5	37.6	8.3	0.53	15.7
	6	2.1	0.2	8.7	2.7	0.053	50.9
	8	1.8	0.09	20.2	1.7	0.034	48.8

Table 9.3. Distribution ratios DLn for Ln(III) ions for extraction from aqueous solution (pH 3.25) using 4 mM **1** in different imidazolium ILs (n is the carbon number for the alkyl arm of the IL cation) and *n*-dodecane.

Ln	$[C_n mim][NTf_2]$				*n*-dodecane
	2	4	6	8	
La	96	97	12	0.41	0.034
Ce	100	110	17	0.58	0.038
Pr	78	88	20	1.1	0.031
Nd	36	41	15	0.82	0.037
Sm	11	14	39	2.3	0.036
Eu	6.7	11	57	3.0	0.040
Gd	4.2	73	34	2.0	0.031
Tb	8.6	17	110	5.6	0.024
Dy	13	27	180	6.0	0.028
Ho	14	74	300	8.8	0.033
Er	90	160	520	15	0.031
Tm	180	310	1300	42	0.029
Yb	150	270	1600	85	0.045
Lu	190	220	2800	180	0.039

Table 9.4. Distribution ratios DLn for Ln(III) ions for extraction from aqueous solution (pH 3.25) using 4 mM **3** in different imidazolium ILs (n is the carbon number for the alkyl arm of the IL cation).

Ln	$[C_n mim][NTf_2]$		
	2	4	6
x	10^3	1	10^3
La	14	1400	250
Ce	–	3400	–
Pr	30	2750	300
Nd	21	1600	170
Sm	13	490	130
Eu	5.2	200	42
Gd	1.8	70	23
Tb	1.0	42	6.8
Dy	0.32	23	83
Ho	0.30	30	73
Er	0.28	37	54
Tm	0.30	59	22
Yb	0.23	75	92
Lu	0.32	170	100

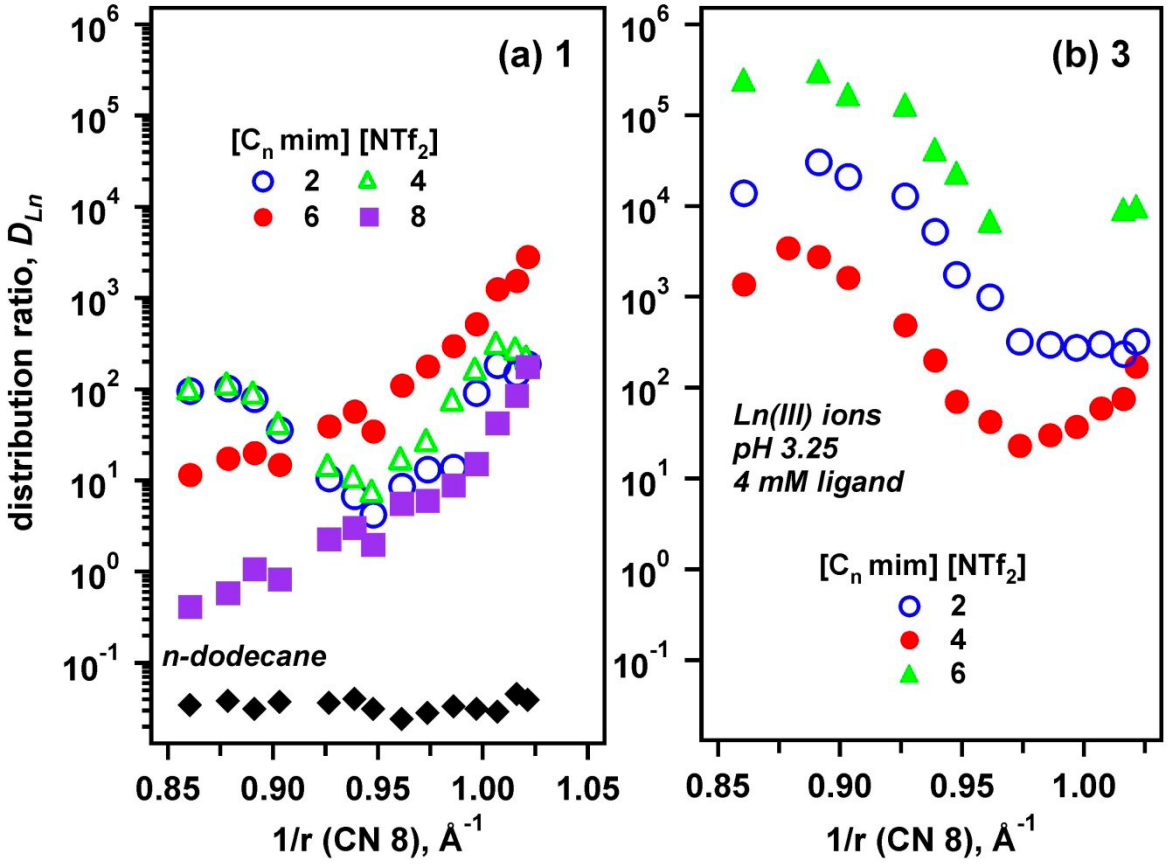

Figure 9.7. Extraction of Ln(III) ions from 1 mM nitric acid using 4 mM **1** (a) or **3** (b) for different imidazolium ILs ([Cnmim] [NTf_2], *n*=2-8) and *n*-dodecane (in panel a). The distribution ratios D_{Ln} are plotted vs. 1/*r*, where *r* is the ionic radius for coordination number 8. In panel a, the complex dependencies observed for [C_2mim] [NTf_2] and [C_4mim] [NTf_2] are likely to arise due to interference of cation exchange, which is entirely suppressed for more hydrophobic cations.

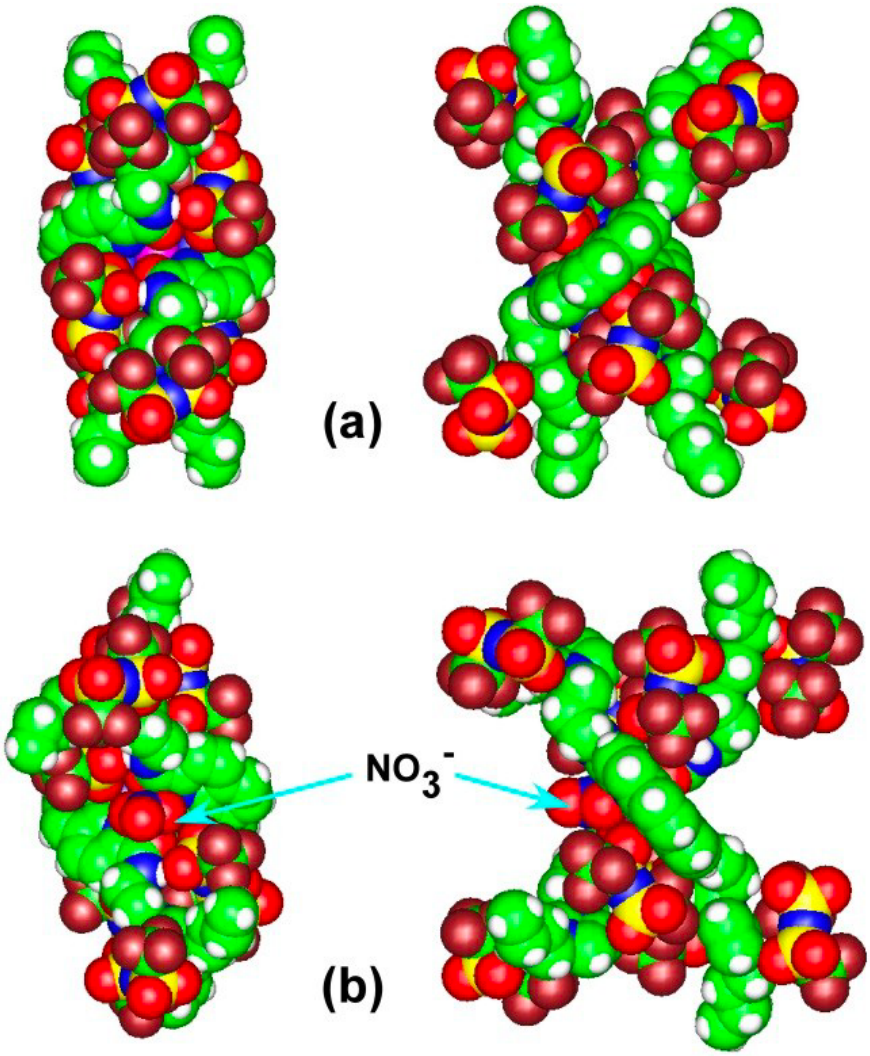

Figure 9.8. Space filling renditions of optimized geometry axisymmetric $[Gd^{III}L_2(NO_3^-)_x](NTf_2)_8$ complexes for ligand 3: (a) x=0 and (b) x=1 complexes. The arrows indicate the nitrate ligand. Top views and side views of these helical complexes are given side by side.

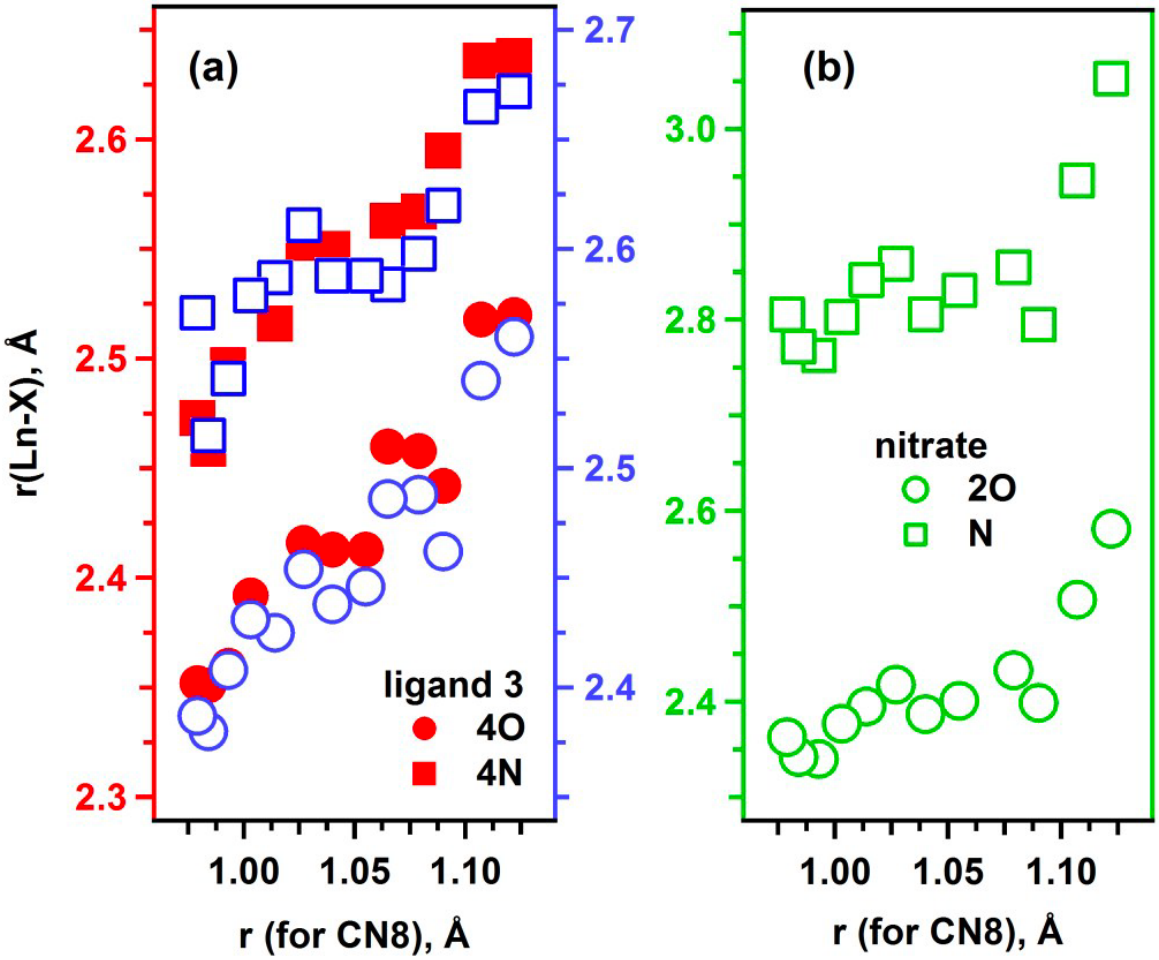

Figure 9.9. Ionic radius dependences for Ln-X distances in optimized geometry $[Ln^{III}L_2(NO_3)_x](NTf_2^-)_8$ complexes for ligand **3** assuming x=0 (filled symbols) and x=1 (open symbols). Panel a is for O and N atoms in ligand **3**, panel b is for the nitrate ligand. X=O corresponds to the circles and X=N corresponds to the squares. The ionic radii (across the lanthanide period) are for the coordination number of eight. As the ionic radius increases for lighter lanthanide ions, the ligands move away from the metal ion, making it more accessible to nitrate addition.

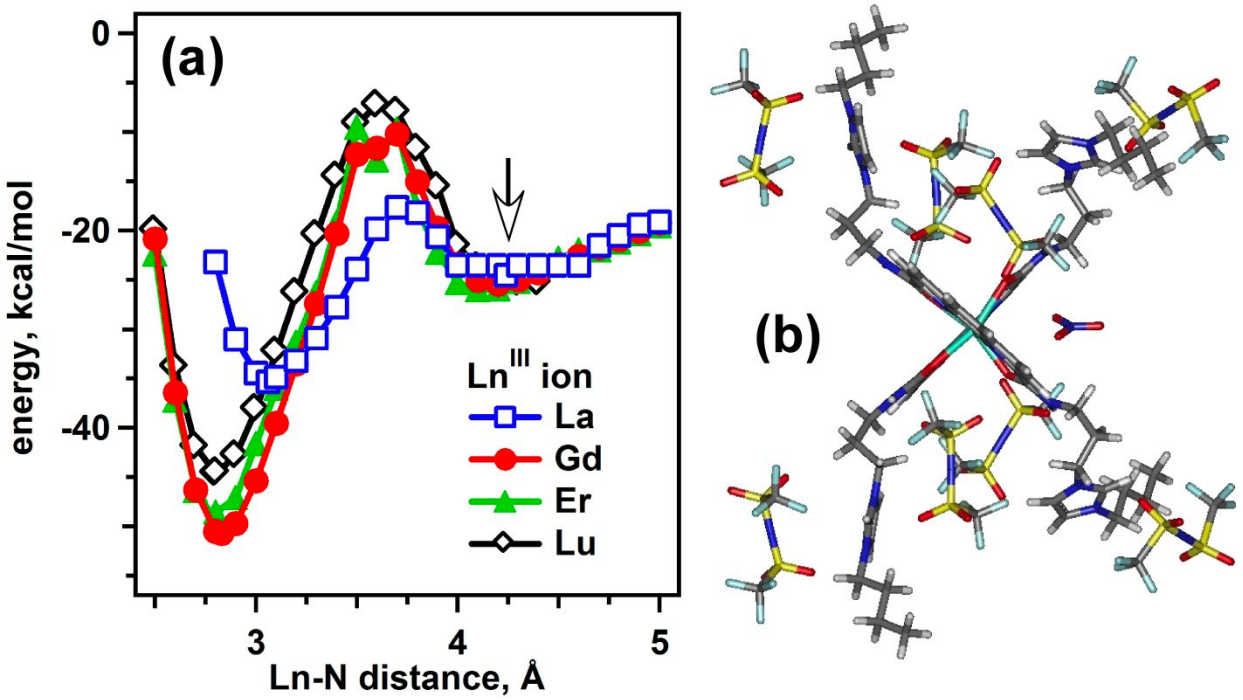

Figure 9.10. (a) Energy profile for the axisymmetric $[Ln^{III}L_2(NO_3^-)](NTf_2^-)_8$ complex (for La, Gd, Er and Lu) as a function of Ln-N distance for the NO_3^- nitrogen (all other degrees of freedom optimized). The arrow indicates a local potential minimum for the nitrate anion in between the two imidazolium cations in this complex, as shown in panel b. As the ionic radius increases, the energy barrier to NO_3^- addition systematically decreases, and so does the enthalpy of this addition. Zero energy corresponds to the nitrate anion removed from the complex.

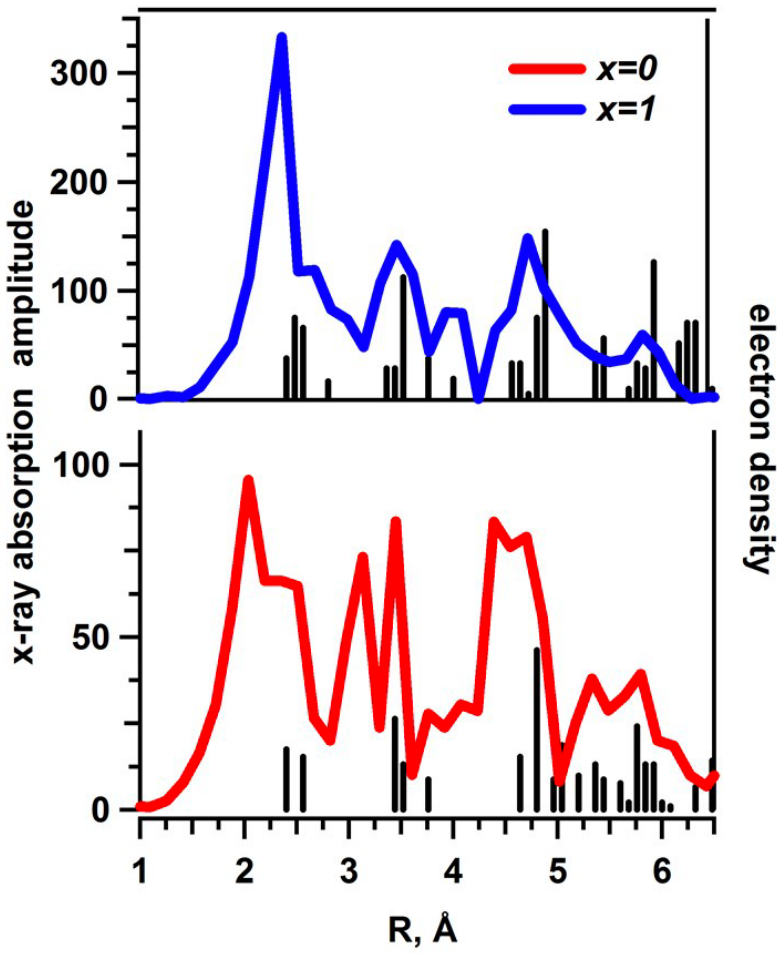

Figure 9.11. Simulated R-space k3-weighted EXAFS (extended X-ray absorption fine structure) patterns for $[Gd^{III}L_2(NO_3^-)_x](NTf_2^-)_8$ complexes for x=0 and x=1 (see the legend in the plot) juxtaposed onto the electron density distribution in these two complexes. The large amplitude in the first peak due to the presence of the bound nitrate ligand makes it easy to quantify the degree of nitrate involvement by means of X-ray absorption spectroscopy.

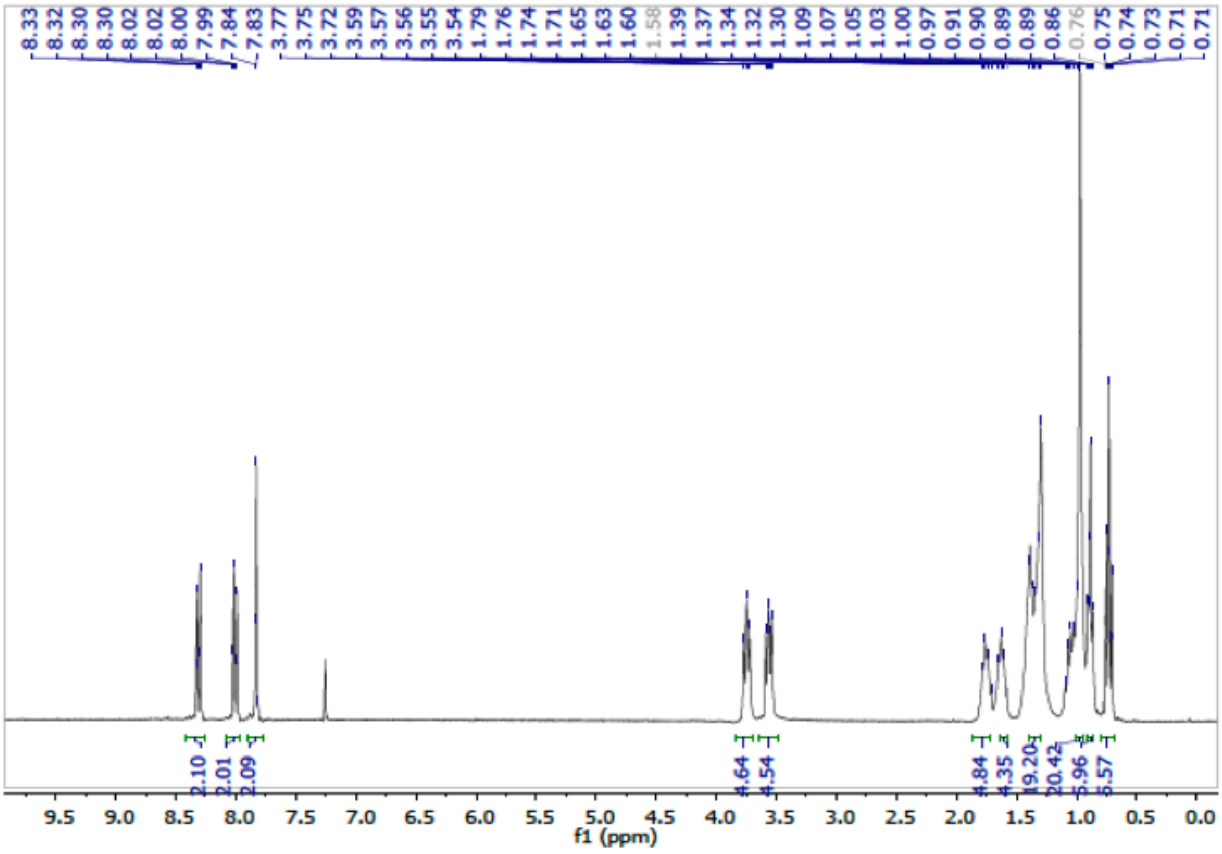

Figure 9.12. ^{1}H NMR of compound **1** in $CDCl_3$.

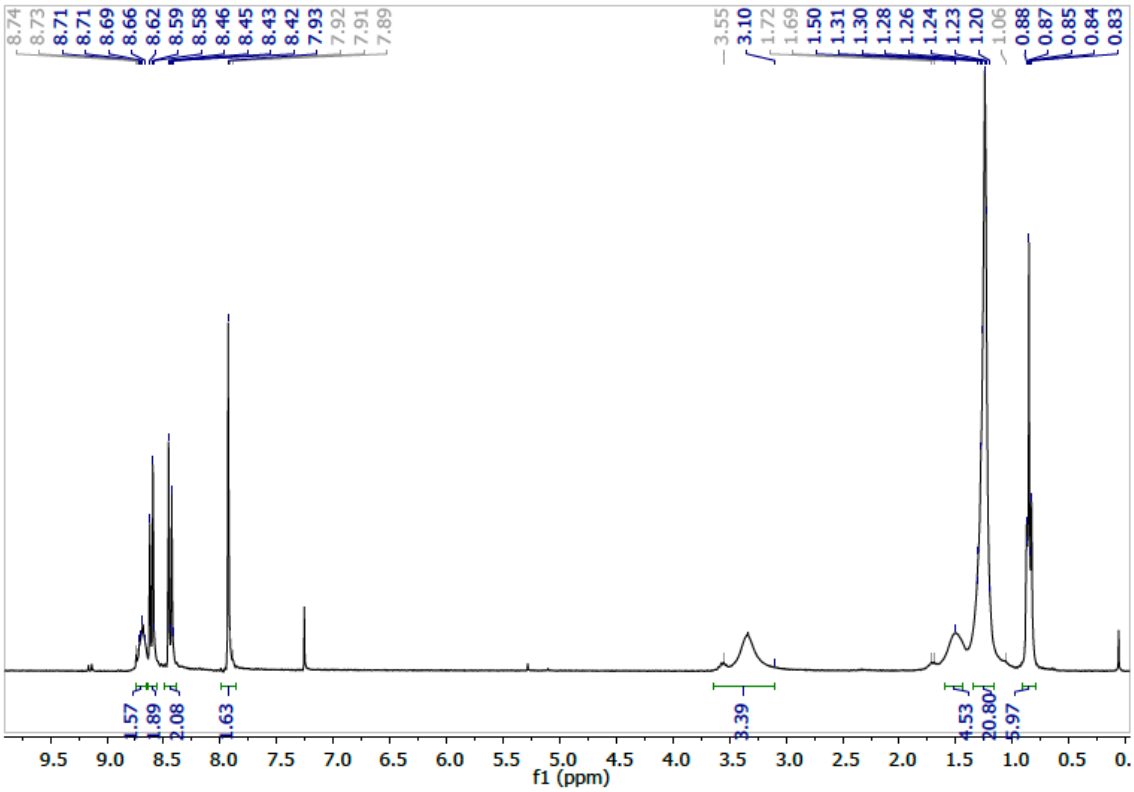

Figure 9.13. ^{1}H NMR of compound **1** in $CDCl_3$.

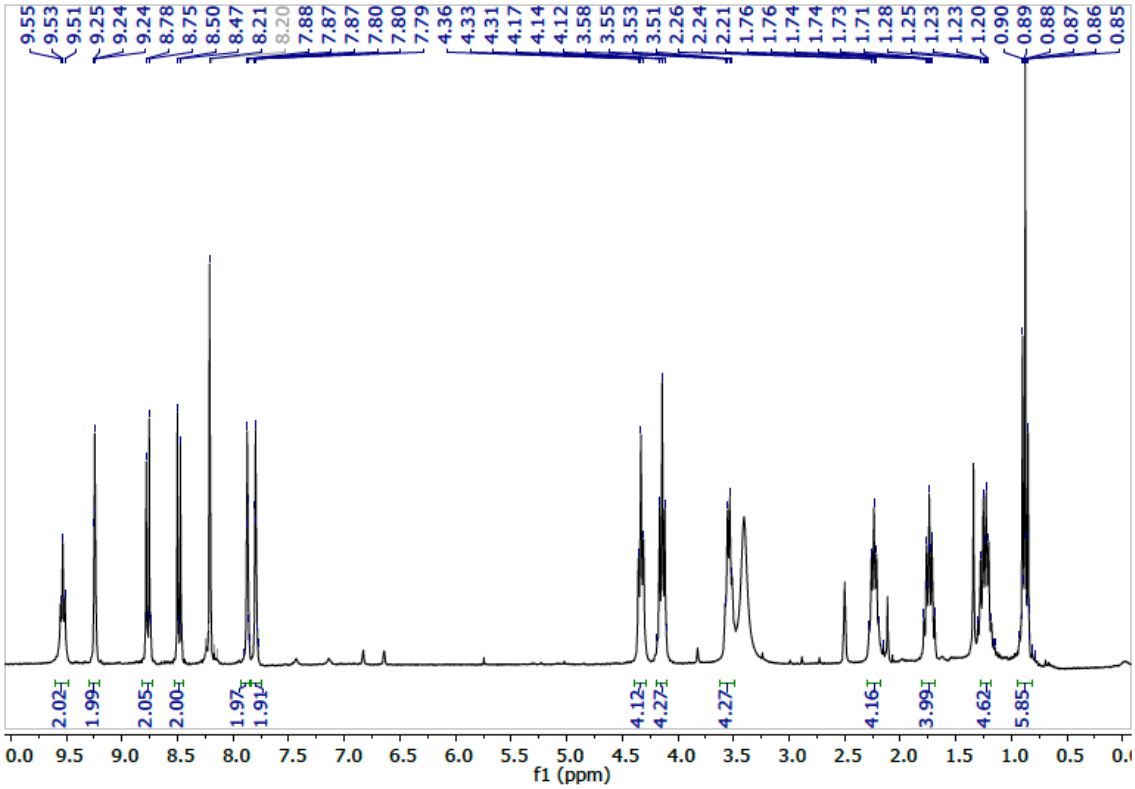

Figure 9.14. ^{1}H NMR of compound **3** in DMSO-d_6.

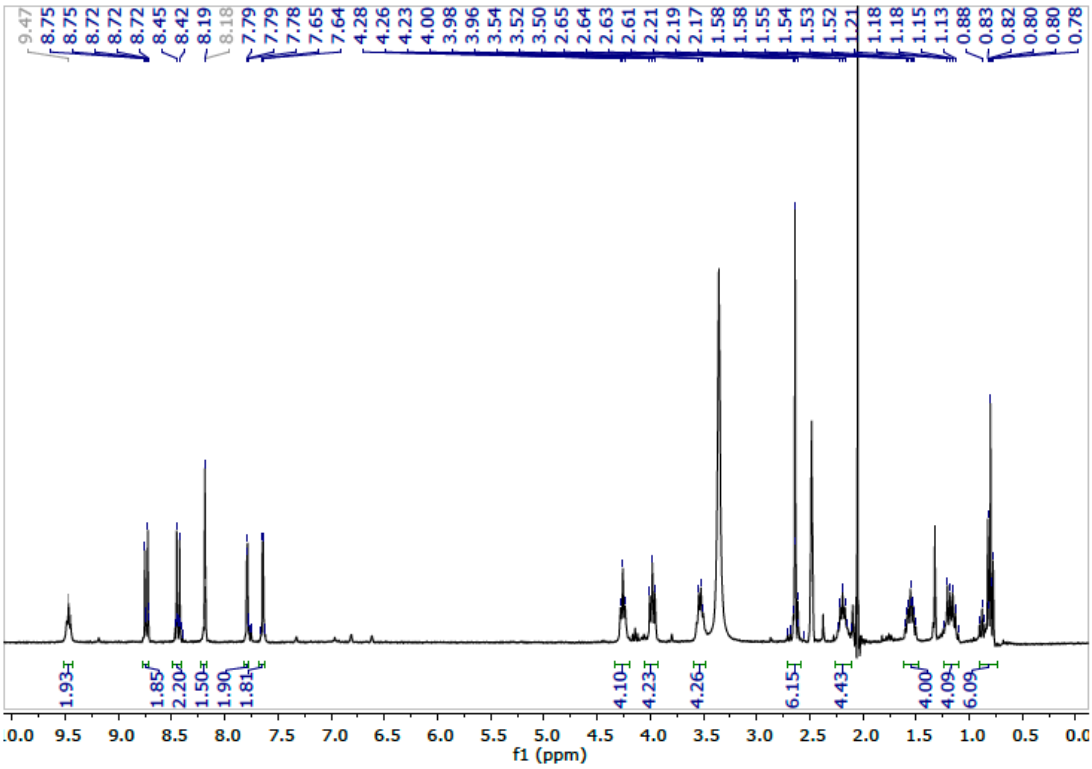

Figure 9.15. ^{1}H NMR of compound **4** in DMSO-d_6.

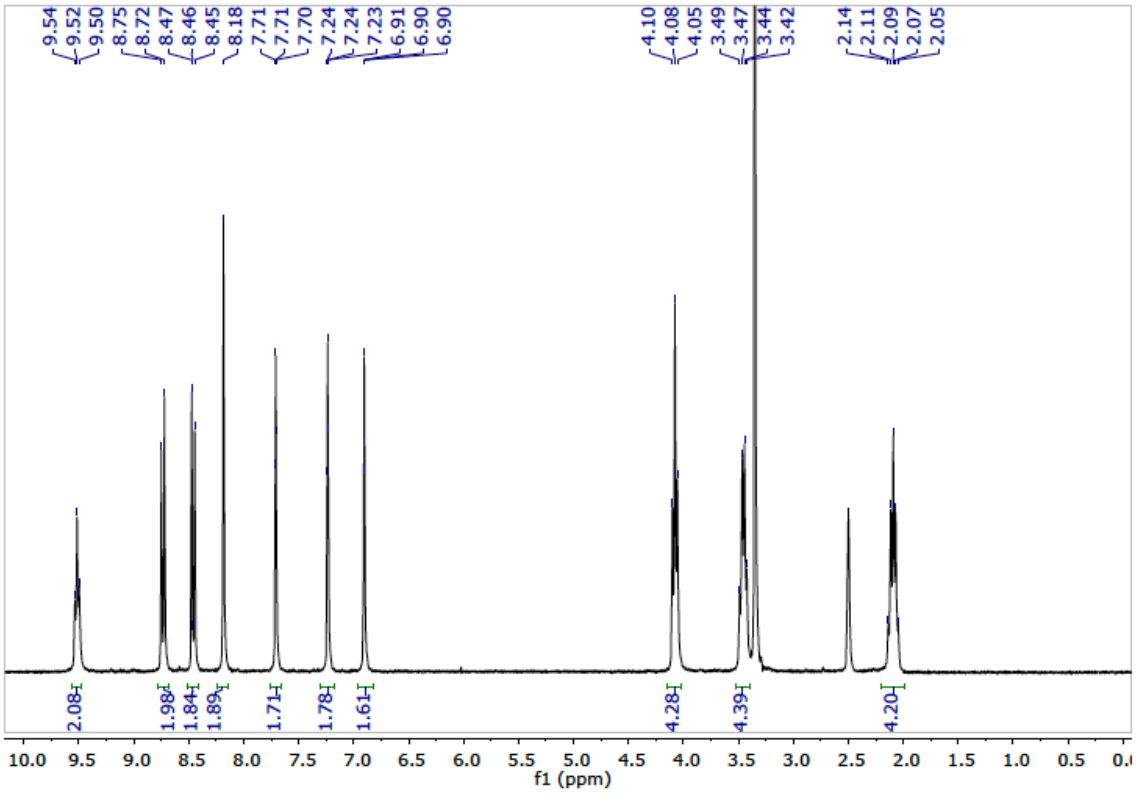

Figure 9.16. ^{1}H NMR of compound **8** in DMSO-d_6.

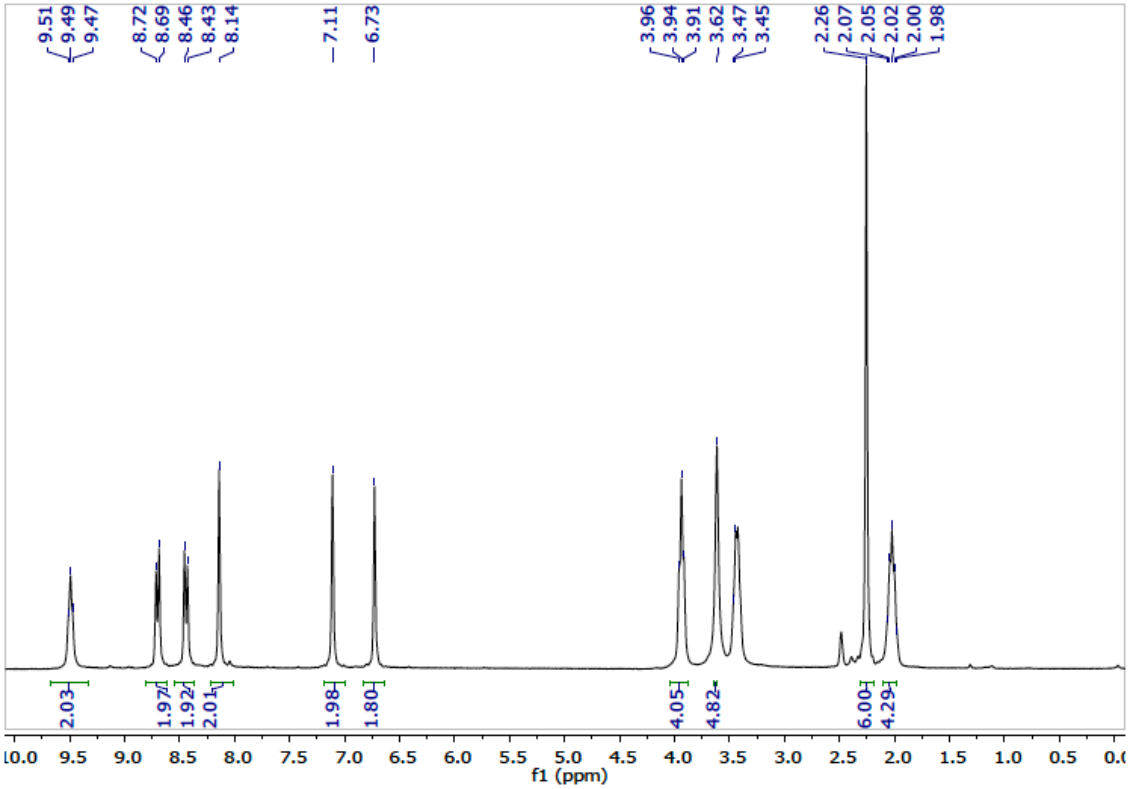

Figure 9.17. ^{1}H NMR of compound **9** in DMSO-d_6.

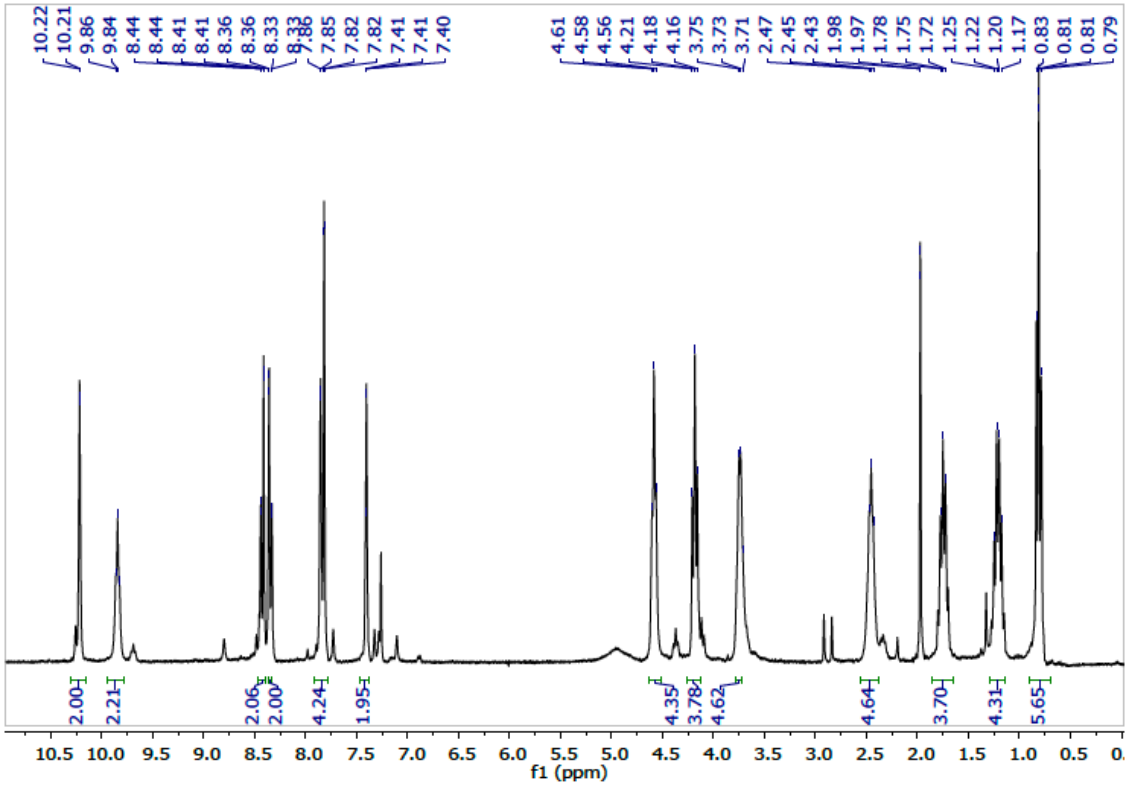

Figure 9.18. ^{1}H NMR of compound 10 in $CDCl_3$.

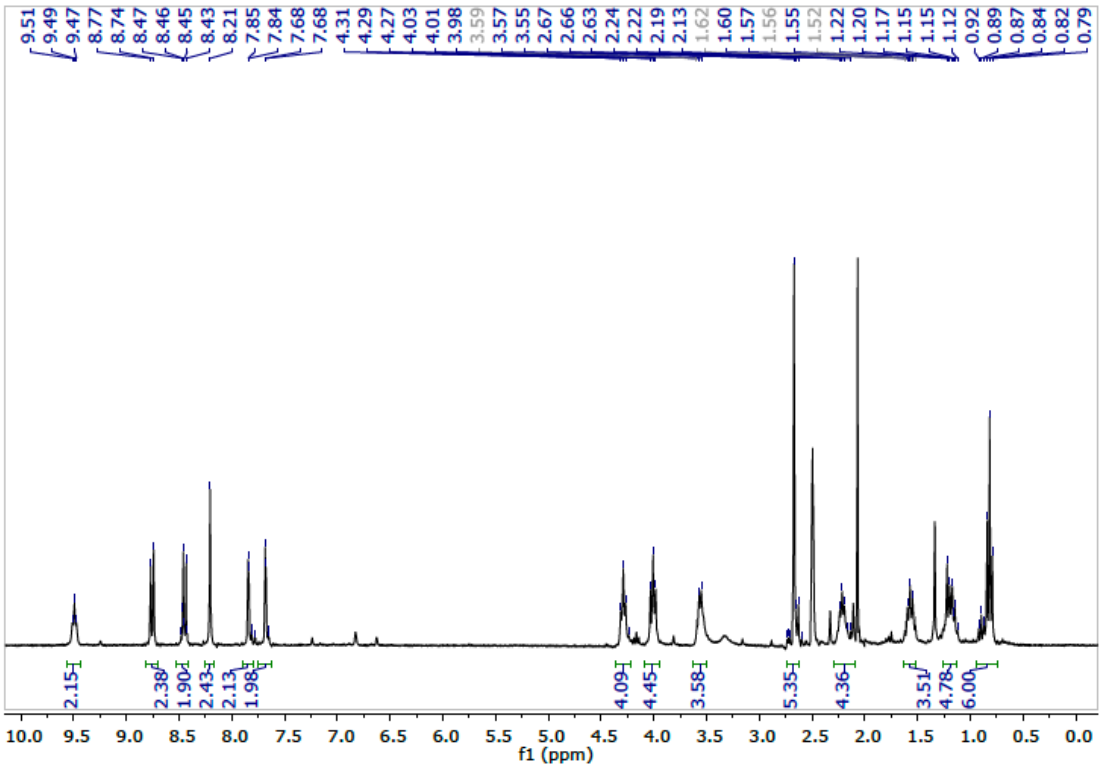

Figure 9.19. ^{1}H NMR of compound **11** in DMSO-d_6.

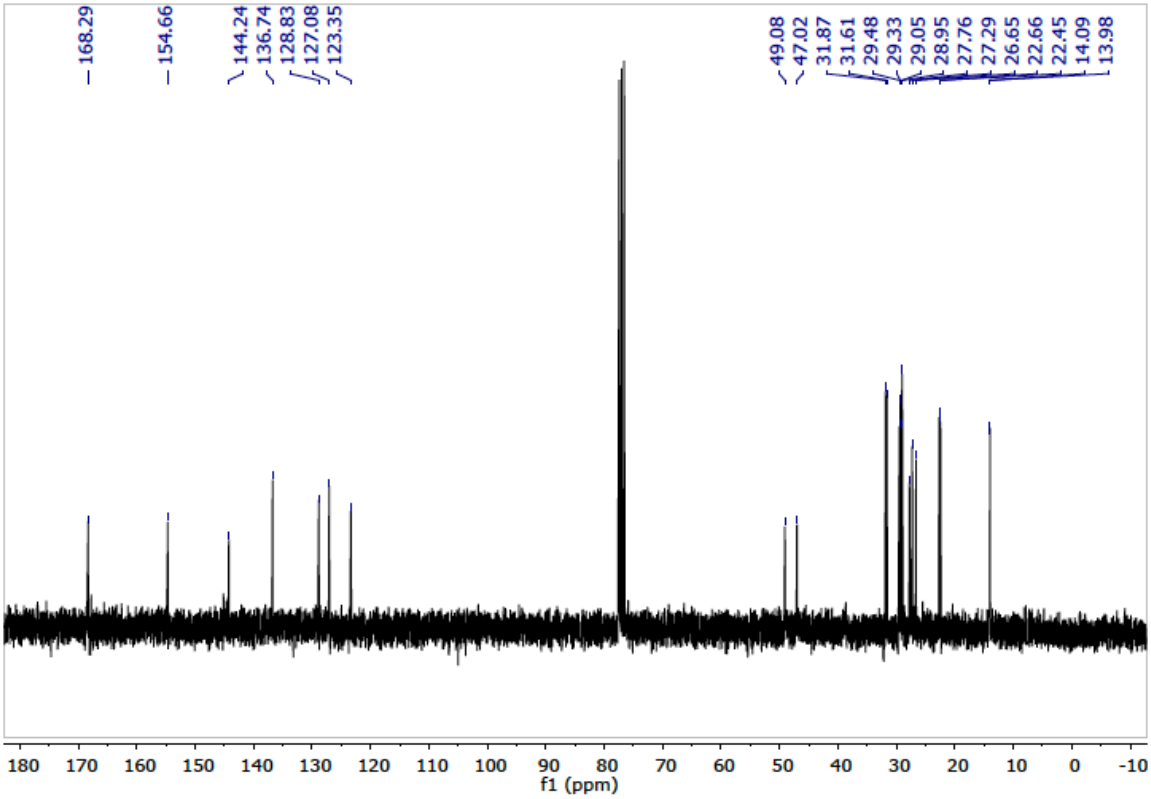

Figure 9.20. ^{13}C NMR of compound **1** in $CDCl_3$.

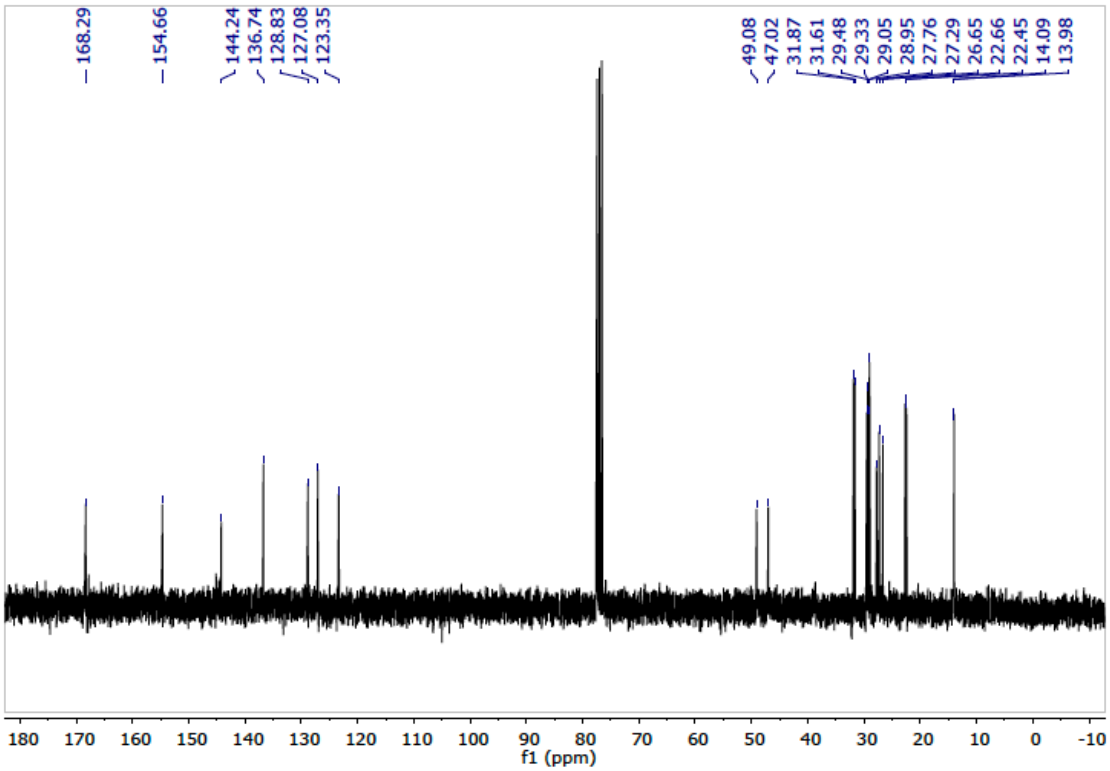

Figure 9.21. ^{13}C NMR of compound **2** in $CDCl_3$.

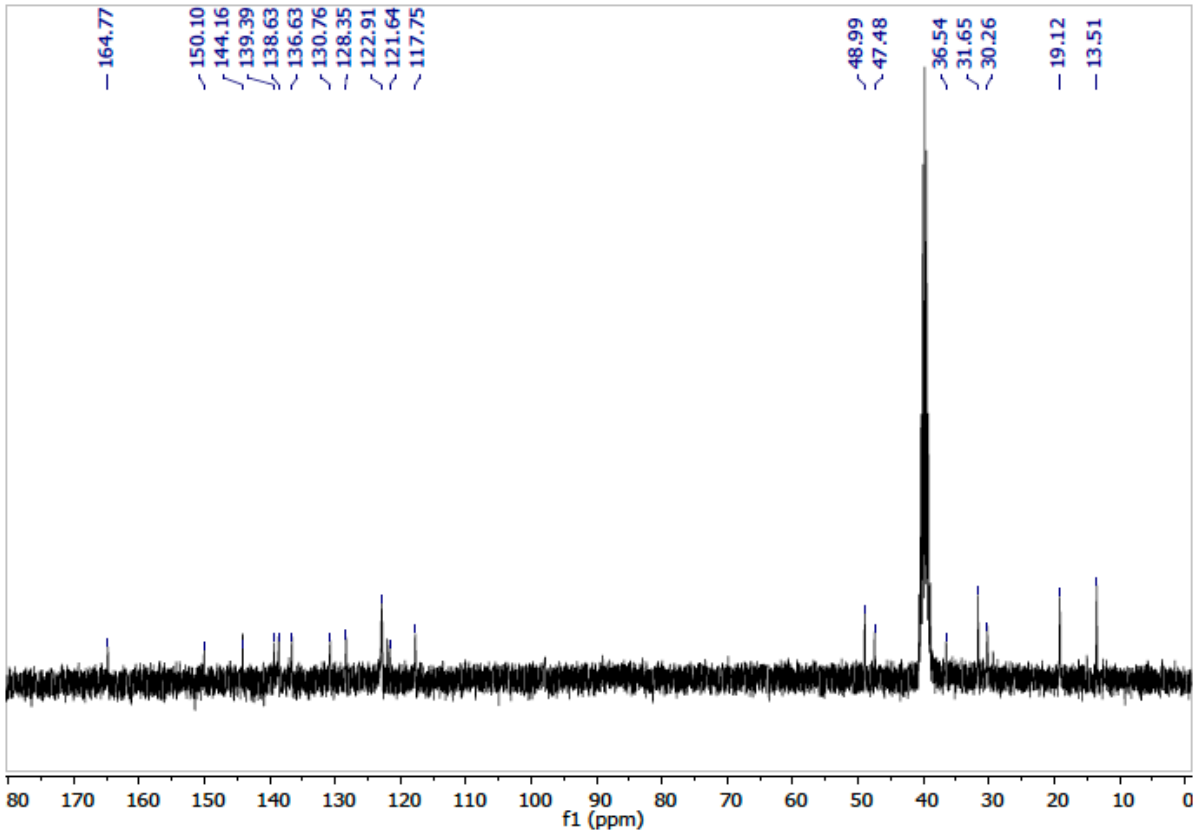

Figure 9.22. ^{13}C NMR of compound **3** in DMSO-d_6.

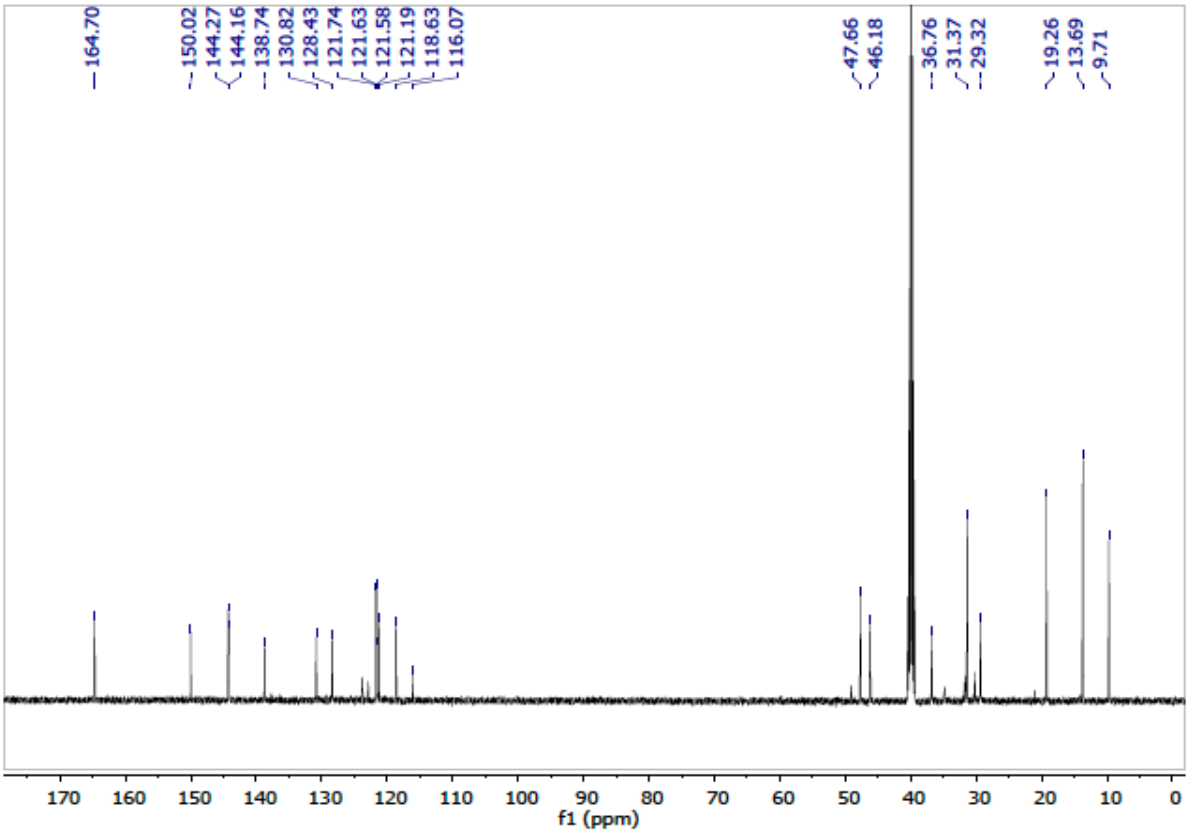

Figure 9.23. ^{13}C NMR of compound **4** in DMSO-d_6.

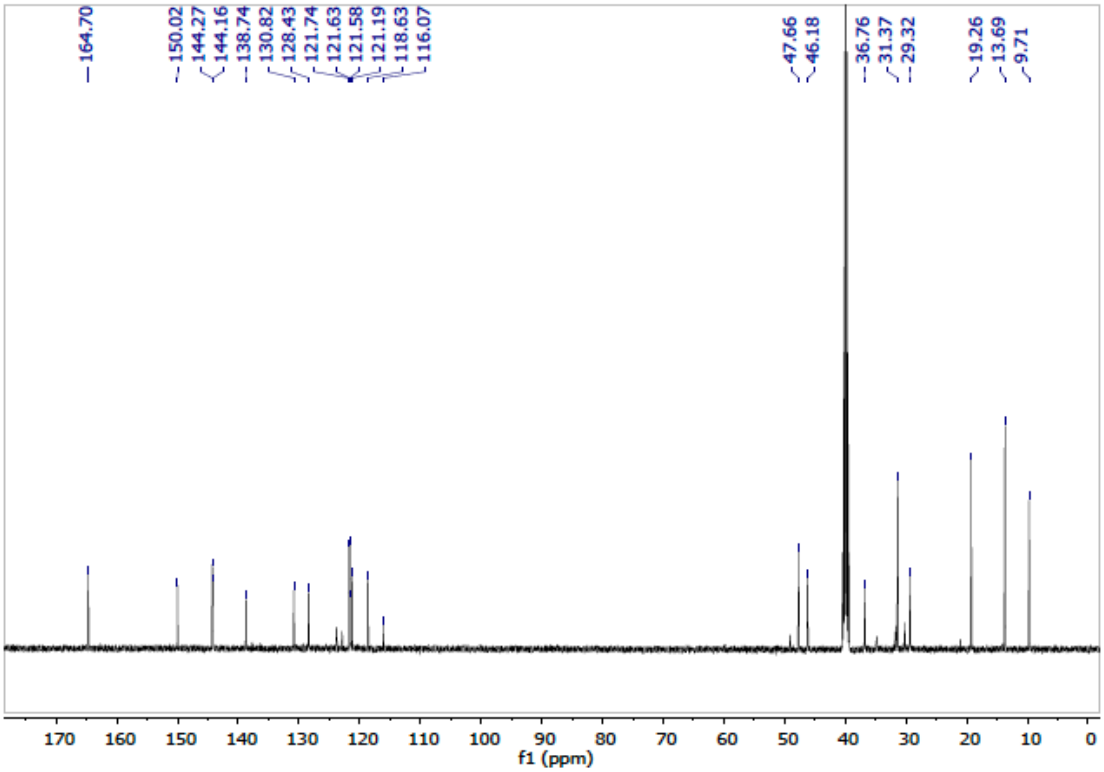

Figure 9.24. ^{13}C NMR of compound **8** in DMSO-d_6.

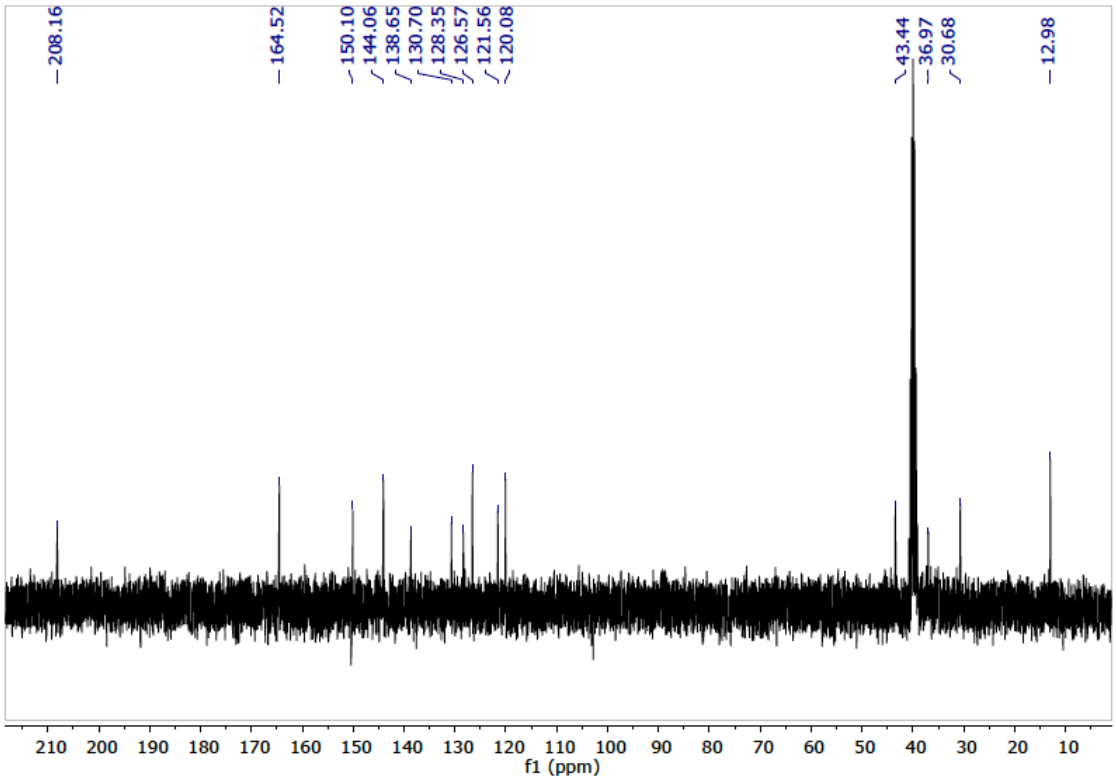

Figure 9.25. ^{13}C NMR of compound **9** in DMSO-d_6.

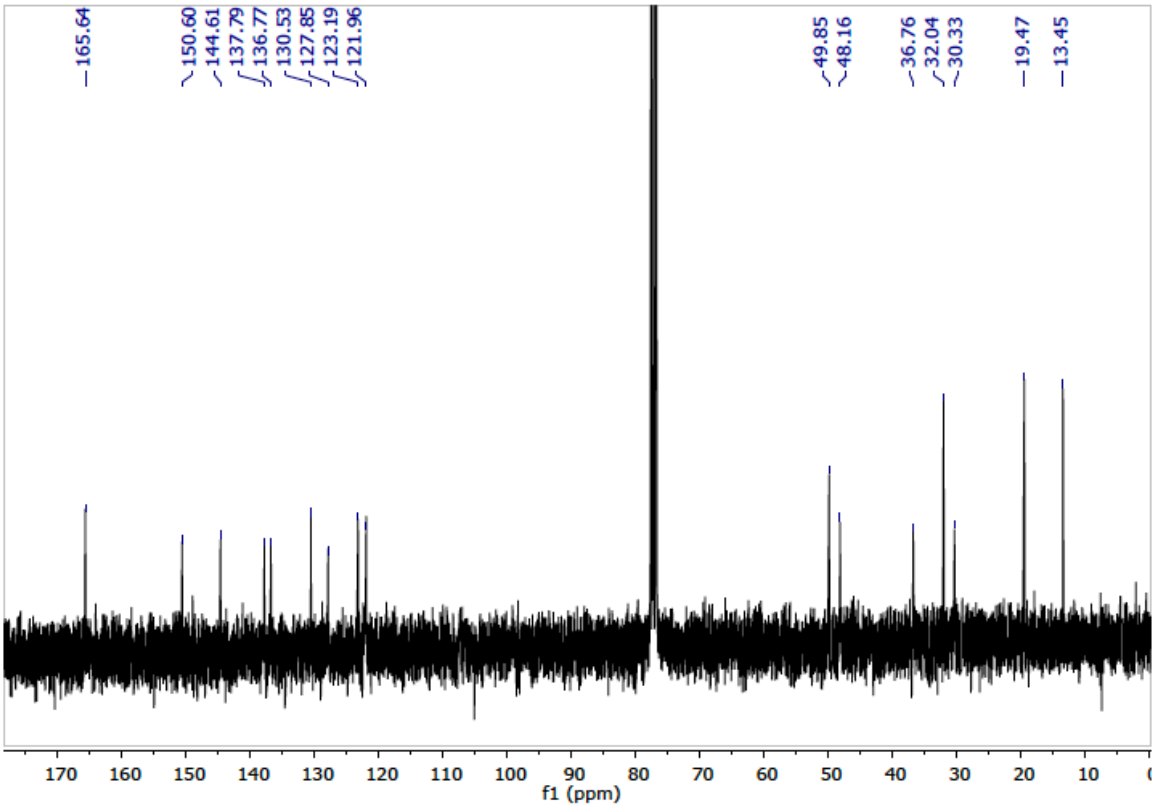

Figure 9.26. ^{13}C NMR of compound **10** in $CDCl_3$**.**

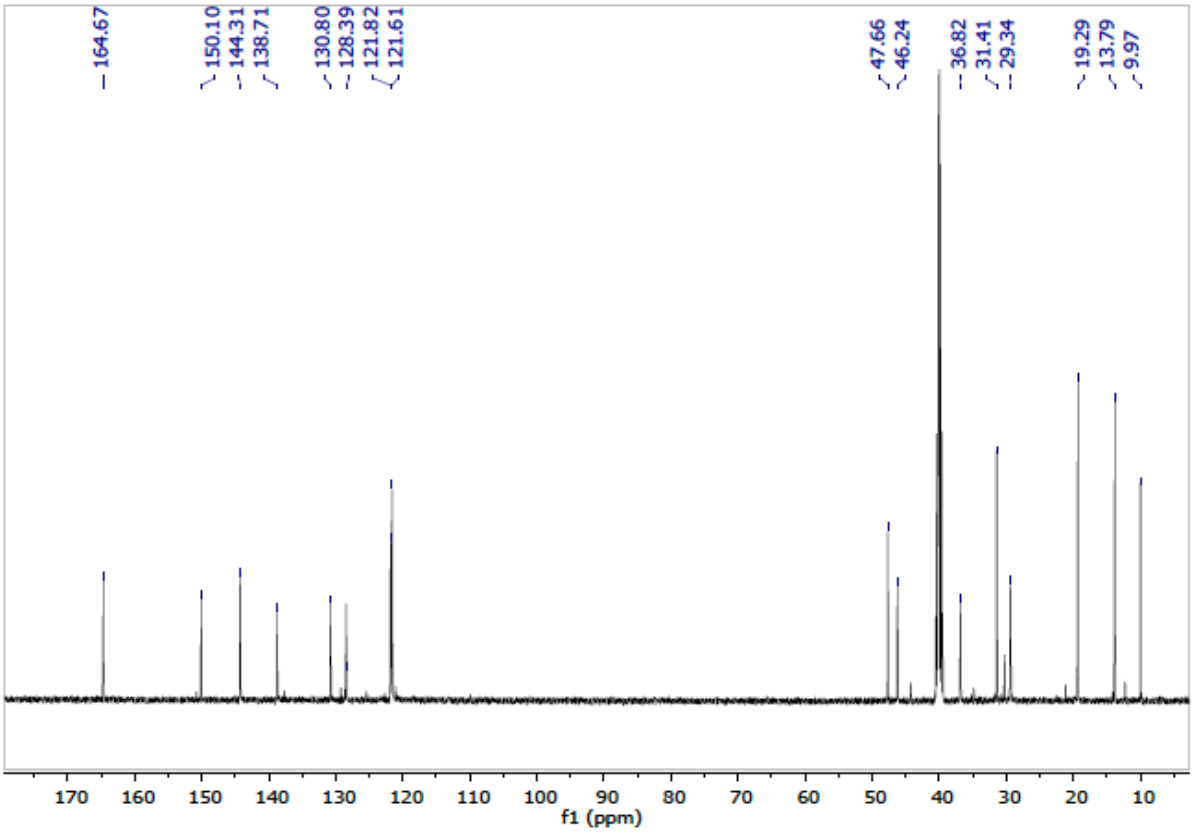

Figure 9.27. ^{13}C NMR of compound **11** in DMSO-d_6.

Chapter 10 : Conclusion

Improving the ability of receptors and ligands to selectively separate ions both cationic or anionic from solutions has a major impact throughout the world. Achieving a selective separation of specific ions makes it possible for governments and industries to deal with pollution and further prevent the spread of contaminations in the form of harmful compounds which are release for industrial processes. The development of material and process which can successfully remove harmful radioactive cations particularly the minor actinides from waste allows for the closing of the nuclear fuel cycle. Material that can remove nitrate, phosphate, sulfate and even be used for carbon capture can have a major effect on the surrounding ecosystems. In this work, the two major goals were first the development of materials/receptor that could remove oxoanions via solvent extraction or crystallization. The second goal was to use and improve the solubility of ligands for use in the separation of *f*-block elements by solvent extraction processes.

In **Chapters 2** and **3**, the development, synthesis, and testing of new anion receptors were presented and discussed. These new receptors were designed and developed for used in solvent extraction test to determine if it was possible to remove anions by encapsulating them in microenvironment more favorable for extraction. In

, we looked at a modified calix[4]pyrrole which has additional alkyl groups added at the *meso* positions of the receptor with the hope of increasing the solubility of the receptor in organic solvents. This modification was somewhat successful at improving the solubility in some organic solvents although the increase in solubility was not enough to make this

receptor ideal for further development in a solvent extraction process. In **Chapter 3**, a new simple di-iminoguanidinium receptor was designed, synthesized and tested for sulfate extraction. This new receptor known as TABEDIG was easy to synthesis in relatively high yields, using cheap reagents in simple reactions. TABEDIG proved to be an extremely soluble in common organic solvents (e.g.1,2-DCE, toluene, etc…) used for the initially testing of extractants. More impressive was the solubility of TABEDIG (≥ 1.0 M) in Isopar L (C-12 branched hydrocarbon) which is commonly used industrial solvent extraction processes. No other ionic species is known to be soluble on its' own in this solvent. The ability to extract sulfate into all of the solvents that were tested for sulfate separations was an unexpected result, leading to additional characterization and testing using SAXS and Karl Fischer titrations to elucidate what occurs during extraction to make TABEDIG such an effect receptor.

In **Chapters 4**, **5**, and **6**, the use of new oxoanion bis-iminoguanidinums (BIGs) receptors were discussed and their use to selectively separated oxoanions from aqueous solutions via crystallization was investigated. The first generation of these BIGs (GBIGs) were introduced in **Chapter 4**. These GBIGs were formed in-situ on aqueous solutions and then would selective crystallize with oxoanions thereby removing them from solutions. Additionally, once the GBIG-sulfate crystals were formed they were found to be relatively insoluble with a K_{sp} similar to that of $SrSO_4$. The second generation of BIGs (BBIGs) was discussed in-depth in **Chapter 5**, these were found to form complexes with sulfate that were even less soluble that than the first generation (GBIGs). The solubility of these

BBIGs with sulfate was found to be similar to the K_{sp} of $BaSO_4$. Additional testing of the BBIGs found that they were able to remove almost all of the sulfate from seawater via precipitation using only a slight excess of BBIGs. The BBIGs were 99.99% effective at removing sulfate from the seawater. The third generation of BIGs (PyBIGs) discussed in **Chapter 6**, represented a slight departure from the first and second generation of BIGs (GBIGs and BBIGs). Instead of sulfate, we looked at this generations remarkable ability to do direct capture of CO_2 for the air. This generation (PyBIGs) was found to form insoluble salts with carbonate when they were dissolved in water in their neutral guanidine form in slightly basic solutions. The PyBIGs were form insoluble complexes with carbonate in aqueous solution by removing a proton from the bicarbonate. What makes this discovery more remarkable was the fact that it was possible to use a simple method for direct air-capture of CO_2, with a following step heating the PyBIG to regenerate the starting guanidine by heating to 120 °C. This regeneration step is the most interesting part of the story of PyBIG because it is possible to keep reusing this receptor over continuous cycles to capture more CO_2 without having to heat it to high temperatures typically used with the conventional calcium hydroxide methods using for direct air capture and trapping of CO_2.

In **Chapters 7**, **8**, and **9**, the focus shifted from looking at the removal of anions and oxoanions to cations and the selective separation of actinides from lanthanides. In **Chapter 7**, the ligand octyl-1,2-HOPO was made and it's possible use in modified TALSPEAK processes was investigated. Octyl-1,2-HOPO was found to be more effective

than the current organic soluble ligand (DEHPA) used in the TALSPEAK. With octyl-1,2-HOPO it was possible to increase the extraction of europium for aqueous solutions using significantly less of the organic ligand compounds. In **Chapter 8**, ionic liquids were used to improve the solubility and effectiveness of a 2,9-bis(triazine)-1,10-phenathroline (BTPhens) for the selective removal of americium (^{241}Am) over europium. In ionic liquids the BTPhens were able to effectively remove 99.999% of the americium while simultaneously rejecting the europium. This result is the highest currently reported separation faction between americium and europium (~7000). In **Chapter 9**, a new class of task-specific ionic liquids (TS-ILs) were introduced and tested for minor actinides separations. This new class of TS-ILs were found to be effective for the separation of americium from europium. Although the separation factor for these compounds were not as great as BTPhen their synthesis is less expensive and time consuming making them more attractive for further study and development as ligands/extractants for minor actinide separations.

VITA

Neil J. Williams was born in Virginia Beach, Virginia to Twoey and Kent Williams. He has one brother Alexander and one sister Jenny. He grew up in Northern Virginia and later in Raleigh, North Carolina. He graduated from Wakefield High School in 2004. He later attended the University of North Carolina Wilmington and graduated in 2008 with a Bachelors of Science in Biology and a Bachelors of Arts in Chemistry. After graduating with his Bachelors degrees he continued at the University of North Carolina Wilmington for his Masters of Science in Chemistry and graduated in 2010. After obtaining his Masters he moved to Knoxville, Tennessee and start working at Oak Ridge National Laboratory as a Post Masters Researcher. He works on the development of an improved solvent extraction system for the clean-up of cold war legacy nuclear waste stored at the Savannah River Site in South Carolina. In the spring of 2014, he started at the University of Tennessee-Knoxville on is doctorate degree. During his time in the PhD program, Neil published 12 peer-reviewed papers, four of which were featured as covers for the issues, has two patents pending, attended multiple conferences, and presented his research to members of Congress at one of the National Laboratory Science Days on Capitol Hill.